

Analysis of Individual Enzyme Molecules in Large Arrays of Femtoliter-Sized Reaction Chambers



DISSERTATION ZUR ERLANGUNG DES DOKTORGRADES DER
NATURWISSENSCHAFTEN (DR. RER. NAT.) DER FAKULTÄT
CHEMIE UND PHARMAZIE DER UNIVERSITÄT REGENSBURG

vorgelegt von

Raphaela Barbara Liebherr

aus Sonthofen (Allgäu)

im Jahr 2015

Diese Doktorarbeit entstand in der Zeit von Oktober 2011 bis April 2015 am Institut für Analytische Chemie, Chemo- und Biosensorik an der Universität Regensburg.

Die Arbeit wurde durchgeführt bei Prof. Dr. Joachim Wegener unter Anleitung von PD Dr. Hans-Heiner Gorris.

Promotionsgesuch eingereicht:	April 2015
Kolloquiumstermin:	12.06.2015
Prüfungsausschuss:	
Vorsitzender:	Prof. Dr. Frank-Michael Matysik
Erstgutachter:	Prof. Dr. Joachim Wegener
Zweitgutachter:	PD Dr. Hans-Heiner Gorris
Drittprüfer:	Prof. Dr. Burkhard König

Table of Contents

1. Introduction and Theoretical Background	1
1.1. Single Enzyme Molecule Analysis.....	1
1.1.1. Single Molecule Enzymology in Modern Bioanalytical Research	1
1.1.2. Enzyme Kinetics from a Single Molecule Point of View.....	4
1.2. Fluorescence Microscopy - Method of Choice in Single Molecule Analysis ..	7
1.2.1. Basic Principles of Fluorescence.....	7
1.2.2. Theoretical Aspects of Fluorescence Microscopy.....	12
1.2.3. Limitations of Fluorescence Microscopy in Single Molecule Enzymology ...	16
1.3. Single Molecule Technologies	17
1.3.1. Femtoliter Arrays on Optical Fiber Bundles	23
1.3.2. Femtoliter Arrays Molded in PDMS.....	28
1.3.3. Femtoliter Arrays Fabricated in Glass Slides.....	31
1.3.4. Single Enzyme Molecule Analysis in Femtoliter Arrays.....	34
1.4. Motivation and Aim of Work.....	36
1.5. References	38
2. Design and Development of Femtoliter Arrays for the Highly Parallel Analysis of Single Enzyme Molecules.....	51
2.1. Introduction	51
2.2. Results and Discussion.....	54
2.2.1. Femtoliter Array Microfabrication and Characterization.....	54
2.2.2. Optimization of the Single Molecule Detection Platform.....	58
2.2.3. β -Galactosidase Single Molecule Measurements.....	66
2.2.4. Features of Fused Silica and PDMS Femtoliter Arrays.....	71
2.3. Materials and Methods.....	73

2.3.1. Femtoliter Array Microfabrication and Characterization	73
2.3.2. Optimizing Single Molecule Detection in Femtoliter Arrays	77
2.3.3. Experiments on Enzyme Kinetics	80
2.4. Conclusion	85
2.5. References	86
3. A Single Molecular Perspective on the Functional Diversity of Wild-Type and <i>in Vitro</i> Evolved β-Glucuronidase.....	91
3.1. Introduction	91
3.2. Results and Discussion	95
3.2.1. Single Molecule Analysis of Wild-Type β -Glucuronidase	95
3.2.2. Molecular Evolution from a Single Molecule Perspective	102
3.2.3. Circular Dichroism Analysis	111
3.3. Materials and Methods.....	114
3.3.1. General Preparatory and Analytical Methods	114
3.3.2. Protein Expression and Purification.....	115
3.3.3. Experiments on Enzyme Kinetics	118
3.3.4. Circular Dichroism Experiments	119
3.4. Conclusion	120
3.5. References	122
4. Femtoliter Arrays for Concentration Analysis.....	127
4.1. Introduction	127
4.2. Results and Discussion	130
4.3. Materials and Methods.....	135
4.4. Conclusion	136
4.5. References	137

5.	Array Functionalization for Application in Concentration Analysis...	139
5.1.	Introduction	139
5.2.	Results and Discussion	143
5.2.1.	Array Functionalization Using Click Chemistry	143
5.2.2.	Biocompatible Click Chemistry	154
5.2.3.	Introduction of Enzymes by Click Chemistry – An Example.....	160
5.2.4.	Immobilization of Antibodies via Peptide Chemistry	164
5.3.	Materials and Methods.....	168
5.3.1.	General Specifications	168
5.3.2.	Introduction of Peptides using Click Chemistry.....	170
5.3.3.	HRP Modification for Application in Click Reactions	179
5.3.5.	Immobilization of Antibodies via Peptide Chemistry	181
5.4.	Conclusion	183
5.5.	References	184
6.	Summary	191
6.1.	In English.....	191
6.2.	In German	193
7.	Appendix.....	197
7.1.	Analysis of Single β -Galactosidase in Femtoliter Arrays.....	197
7.2.	Single Molecule Perspective on Evolution.....	204
7.3.	Femtoliter Arrays for Concentration Analysis.....	213
7.4.	References	228
7.5.	Lab Course on Single Enzyme Analysis in PDMS Femtoliter Arrays.....	229
7.6.	Abbreviations	240

8.	Curriculum Vitae	243
9.	List of Publications and Presentations	245
9.1.	Master Thesis	245
9.2.	Papers	245
9.3.	Abstracts for Posters and Talks	246
10.	Acknowledgment.....	247
11.	Declaration.....	251

1. Introduction and Theoretical Background

The introductory chapter was in parts adopted from the review article “Enzyme Molecules in Solitary Confinement”, Liebherr R.B. and H.H. Gorriss, *Molecules*, **2014** (19): 14417. [1]

1.1. Single Enzyme Molecule Analysis

1.1.1. Single Molecule Enzymology in Modern Bioanalytical Research

Catalysts influence the kinetics of chemical reactions with the objective of the initiation of a reaction, an increase in reaction speed or an impact on the selectivity of a chemical reaction. The first catalytic technical process applied by humans is considered to be the alcoholic fermentation of sugar, primarily used several thousand years before Christ. [2, 3] The main catalyst involved in this process is called alcohol dehydrogenase and belongs to the special group of catalysts that take center stage in this thesis, called enzymes.

Enzymes are omnipresent catalysts of biochemical reactions. They are complex protein constructs defined by a specific amino acid sequence and folding structure that determine their functionality. Enzyme catalysis enables the execution of extensive biochemical reactions upon which depends the existence of life. Detailed studies of enzymes and their catalytic activity have provided us with a global understanding of enzyme structure and functionality. Currently, our knowledge about enzyme kinetics mainly relies on bulk-phase experiments, [4-6] in which the activity of a large number of molecules – in the range of 10^{12} - 10^{18} or higher – is measured and the kinetic

parameters are averaged over the whole population. Therefore, no information about the contribution of individual enzyme molecules can be gained.

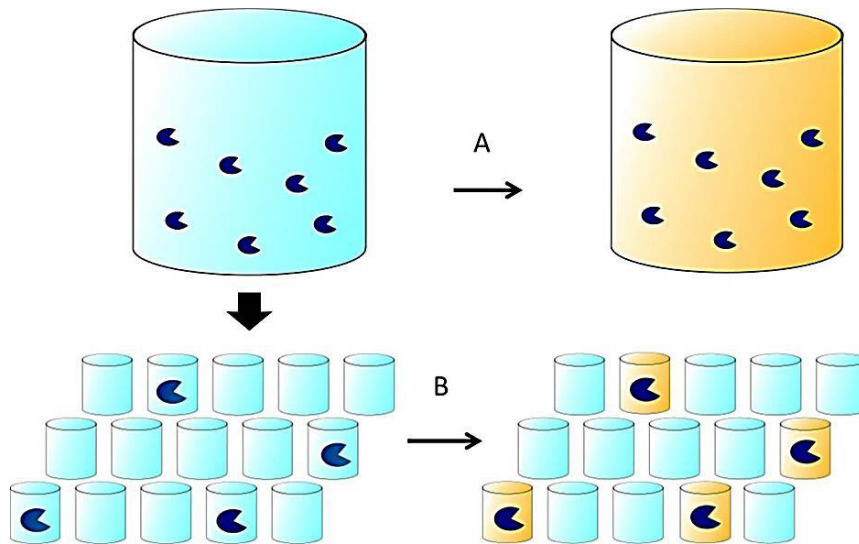


Figure 1.1 Enzyme reactions are often monitored by conversion of a fluorogenic substrate (light blue) to a fluorescent product (yellow). (A) In traditional ensemble experiments the average activity of an entire enzyme population is recorded. (B) When isolated in the wells of a femtoliter array, the individual substrate turnover rates of many single enzyme molecules can be investigated simultaneously.

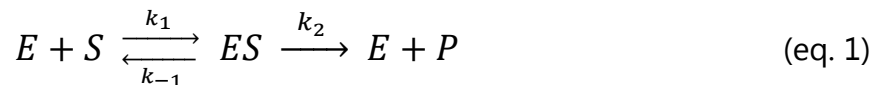
The development of single molecule technologies (Figure 1.1) has provided new insights into enzyme catalysis that were previously hidden in bulk reactions. [7, 8] On the microscopic level the substrate turnover of individual enzyme molecules could be visualized, unravelling broad activity distributions and dynamic fluctuations within enzyme populations. [9] Different conformational states of individual enzyme molecules entail dynamic fluctuations such as varying substrate turnover rates over time (dynamic heterogeneity) [10-13] or broad distributions of catalytic rates within an enzyme population (static heterogeneity). [14-16] A microscopic view on enzyme reactions has

disclosed differences between individual enzyme molecules in a population and provided us with a deeper understanding of enzyme-substrate interactions as well as enzyme kinetics.

Additionally, single molecule enzymology has uncovered enzymatic sub-populations hidden in bulk-phase experiments and enabled the assessment of cooperativity in oligomeric enzymes such as β -galactosidase. [17] Moreover, one could obtain information on the impact of external influences such as temperature, [18-22] pH, inhibitors [23, 24] or buffer additives [25] on enzymatic reactions. In summary, the development of more sensitive detection methods and new single molecule technologies has greatly extended our understanding of the fundamental biochemical processes of life.

1.1.2. Enzyme Kinetics from a Single Molecule Point of View

The single molecule approach to enzyme kinetics requires an adaption of the classical Michaelis-Menten equation. [4] A simple hydrolytic enzyme reaction is typically formulated as two subsequent elementary equations:



An enzyme (E) binds a substrate (S) to form a transient enzyme-substrate complex (ES) with a rate constant k_1 . ES can either dissociate with the rate constant k_{-1} or convert to the free enzyme (E) and product (P) in an irreversible step (k_2). The velocity (v) of an enzyme reaction is proportional to the concentration of the ES complex:

$$v = \frac{d[P]}{dt} = k_2[ES] \quad (\text{eq. 2})$$

[ES] cannot be easily determined in an enzyme reaction. In traditional enzymatic ensemble experiments [ES] is considered as constant during the initial phase of the enzyme reaction (steady-state assumption), as the substrate is present in large excess ($[S] \gg [E]$) [26] and the equilibrium of ES formation is typically faster than the catalytic step ($k_1 \approx k_{-1} > k_2$).

$$v = \frac{d[ES]}{dt} = k_1[E][S] - (k_{-1} + k_2)[ES] = 0 \quad (\text{eq. 3})$$

After considering the total enzyme concentration being $[E]_0 = [E] + [ES]$ and converting $(k_{-1}+k_2)/k_1$ into the rate constant K_M . Equation 3 can be rearranged and [ES] expressed in terms of experimentally defined quantities:

$$[ES] = \frac{[E]_0[S]}{K_M + [S]} \quad (\text{eq. 4})$$

Combination of equation 2 and 4 yields the Michaelis-Menten equation:

$$v = \frac{k_2[E]_0[S]}{K_M+[S]} = v_{max} \frac{[S]}{K_M+[S]} \quad (\text{eq. 5})$$

The velocity (v) of the enzyme reaction shows a characteristic hyperbolic dependency on $[S]$. v_{max} is the maximum enzymatic turnover rate at substrate saturation and K_M is the substrate concentration where the enzymatic velocity is half of v_{max} . K_M and v_{max} can be calculated by measuring v as a function of the substrate concentration.

In a single molecule experiment, however, the single enzyme molecule is either bound in the ES complex or is free. Consequently, it is meaningless to define $[ES]$. Instead, a stochastic approach is adopted to obtain a single molecule Michaelis-Menten equation, where $[ES]$ is replaced by ρ_{ES} , the probability of finding the enzyme molecule in its bound state. [8, 14, 27] In analogy to equation 4, ρ_{ES} can be expressed in terms of experimentally defined quantities, but without the restrictive condition of $[S] \gg [E]$:

$$\rho_{ES} = \frac{[S]}{K_M+[S]} \quad (\text{eq. 6})$$

The substrate turnover of a single enzyme molecule leads to the generation of fluorescent product over time, and the velocity (v_i) of an individual enzyme molecule is defined as:

$$v_i = \frac{d[P]}{dt} = k_2 \rho_{ES} \quad (\text{eq. 7})$$

And the single molecule equivalent of the Michaelis-Menten equation is given by:

$$v_i = \frac{k_2[S]}{K_M+[S]} = k_{cat} \frac{[S]}{K_M+[S]} \quad (\text{eq. 8})$$

Single enzyme molecule experiments in femtoliter arrays disclose the activity distribution between individual molecules within an enzyme population. The velocity (v_i) of many

individual enzyme molecules can be collected and displayed in a histogram, in which the occurrence of v_i follows a Gaussian distribution. The standard deviation ($\sigma(v_{i(1-n)})$) can be calculated for any substrate concentration and gives information about the degree of the activity distribution within the enzyme population. The mean ($\mu(v_{i(1-n)})$) is consistent with the activity of the bulk reaction (v_{bulk}), if the exact concentration of *active* enzyme in the sample solution is known. As it can be difficult to determine the exact amount of *active* enzyme in a bulk phase experiment, v_{bulk} may be lower than $\mu(v_{i(1-n)})$, where only active molecules are included.

Other expressions of the Michaelis-Menten equation have also been derived to account for the different observables in single enzyme molecule experiments. For example, the group of Xie [13, 28] observed the generation of individual product molecules in an enzyme reaction by monitoring the emission of fluorescent bursts originating from each substrate turnover event. The reaction rate of an individual enzyme was evaluated from the inverse of the mean waiting time $\langle\tau\rangle$ between two successive turnover events. In this case, the Michaelis-Menten equation was reformulated to:

$$\frac{1}{\langle\tau\rangle} = k_{cat} \frac{[S]}{K_M + [S]} \quad (\text{eq. 9})$$

1.2. Fluorescence Microscopy – Method of Choice in Single Molecule Analysis

Most modern single molecule experiments are based on fluorescence technologies. Fluorescence microscopy is a highly sensitive method, [29] because one fluorophore can emit up to 10^6 photons before it eventually photobleaches. Fluorescence microscopy has become an essential method for the non-invasive interrogation of biomolecules, invigorated by new methods to increase the optical resolution of microscopy beyond the diffraction limit of light. If a sensitive camera is employed and the background is reduced considerably (e.g. by total internal reflection microscopy (TIRF)) even single fluorophore molecules can be observed. Today, fluorescence microscopy is applied to study the motion and interaction of individual molecules, molecular cooperativity or protein folding.

1.2.1. Basic Principles of Fluorescence

A fluorophore is a molecule that exhibits the ability to absorb energy of a distinct wavelength and then re-emit energy at a different but equally distinct wavelength. The energy of the emitted light depends on both the fluorophore itself and its chemical environment. [30]

At room temperature, a given molecule resides in the electronic and vibrational ground state, according to the Boltzmann distribution. Upon irradiation, the molecule absorbs energy in form of photons, provided that the energy of the photon matches the energy gap between the electronic ground and excited states. Thereupon, in accordance with the Franck-Condon principle, [30, 31] an electron is transferred from the electronic

and vibrational ground state ($S_{0, v=0}$) to an excited electronic and vibrational state ($S_{1, v=n}$, $S_{2, v=n}$). Immediate vibrational relaxation in combination with internal conversion (IC) leads to the population of the excited state $S_{1, v=0}$. From this point several different transitions can occur, summarized in the Jablonski diagram (Figure 1.2).

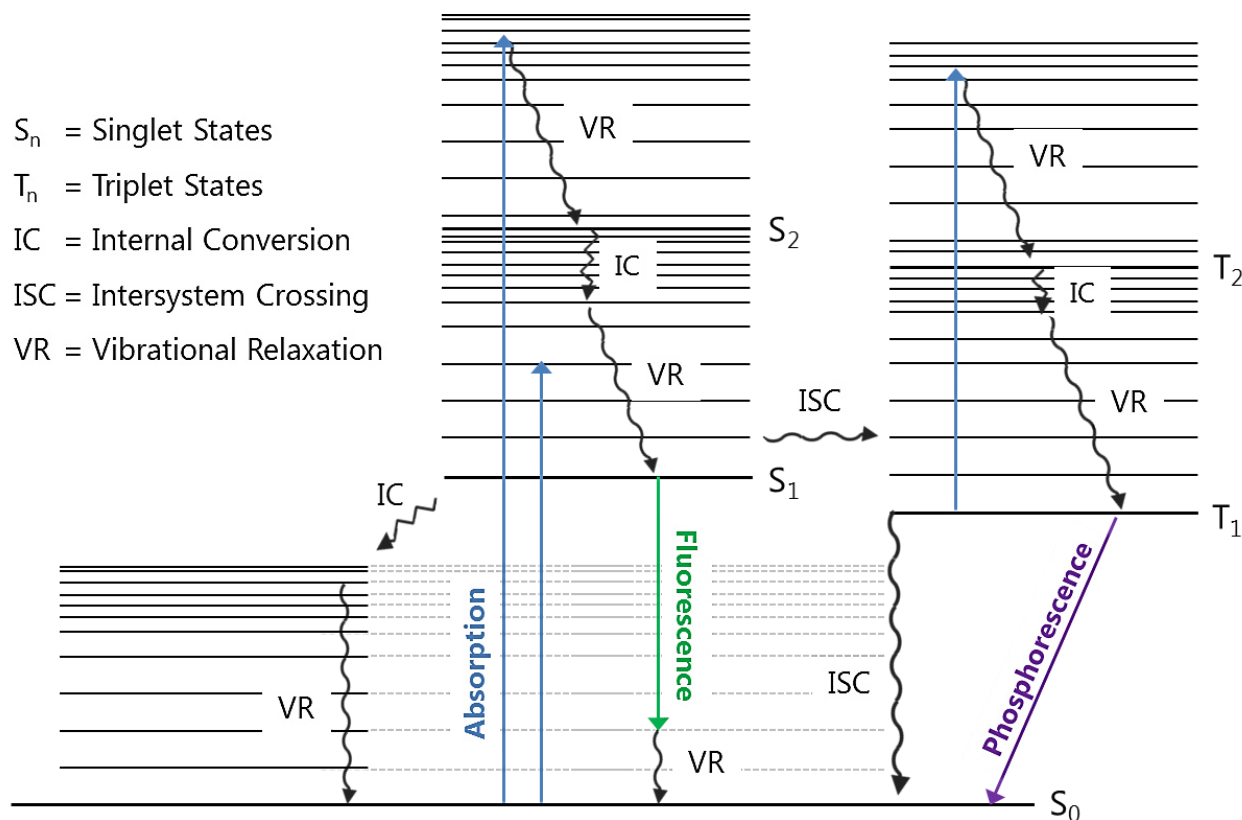


Figure 1.2 Jablonski Diagram indicating the electronic levels of any given organic molecule as well as possible radiative and non-radiative transitions between Singlet (S_n) and Triplet (T_n)-states. Each electronic state is subdivided in a number of vibrational levels (v_n).

The molecule might be excited into higher singlet states by absorption of a second photon ($S_1 \rightarrow S_n$). Otherwise, internal conversion followed by vibrational relaxation could lead to a non-radiative return to the ground state S_0 . The spin of the excited electron might also be reversed by intersystem crossing (ISC), leaving the molecule in the first

excited triplet state, T_1 . Equally to singlet states, triplet states can be excited into higher triplet states by absorption of a second photon. Depopulation of the T_1 triplet state can occur non-radiative via intersystem crossing or by radiative deactivation, called phosphorescence ($T_1 \rightarrow S_0$). Because triplet/singlet transitions are spin-forbidden, they are typically quite inefficient and implicate long triplet-state lifetimes (microseconds) compared to the short average lifetime of an excited singlet state (nanoseconds). [30-32] Depending on the molecular structure, depopulation of $S_{0, v=0}$ can also occur radiatively, by spontaneous emission of a photon, called fluorescence. According to the Franck-Condon principle, the radiative transition to the electronic ground state results in the population of higher excited vibrational states of S_0 . Afterwards, thermal equilibrium, in accordance with the Boltzmann distribution, is reached by vibrational relaxation. [30]

Due to the loss of vibrational energy in course of the cycle of absorbance and emission, fluorescence emission always occurs at a lower energy than excitation. This characteristic red-shift of emitted light is generally known under the term of "Stokes shift", named after the Irish physicist George G. Stokes. [30] The high sensitivity of fluorescence based technologies, compared to alternative spectroscopic methods, is based on the Stokes shift that enables an efficient suppression of excitation light (Rayleigh-scattering) and thus reduction of background noise by application of an appropriate filter system.

The luminescence intensity I of the light emitted from an excited sample can be calculated from Parker's law:

$$I = I_0 \Phi_f k \varepsilon c d \quad (\text{eq. 10})$$

where I_0 represents the intensity of the excitation light, Φ_f the quantum yield of the fluorophore, k the geometric factor of the experimental setup, ε the molar extinction

coefficient, d the distance of penetrated medium and c the concentration of the fluorophore. Just as the absorbance, the fluorescence intensity of an excited sample is linearly dependent on the concentration of the fluorophore.

The fluorescence quantum yield Φ_f of a fluorophore, included in equation 10, is defined as the ratio of fluorescence photons emitted from the molecule to photons absorbed. It can be expressed by two rate constants, the radiative decay constant p_r and the non-radiative decay constant p_{nr} that comprises all possible competing, non-radiative transitions from excited states including internal conversion, intersystem crossing and other quenching mechanisms.

$$\Phi_f = \frac{p_r}{p_r + p_{nr}} \quad (\text{eq. 11})$$

In addition to the fluorescence quantum yield, the fluorescence lifetime is a crucial selection criterion for fluorophores in single-molecule fluorescence spectroscopy. The fluorescence lifetime τ_f reflects the average time a molecule spends in its excited state S_1 , before it returns to the ground state via spontaneous emission. [33, 34] The connection of the time-dependent fluorescence intensity $I(t)$ with the fluorescence lifetime τ_f can be described by an exponential function, where I_0 refers to the initial luminescence intensity at time $t=0$.

$$I(t) = I_0 e^{-\frac{t}{\tau_f}} \quad (\text{eq. 12})$$

Next to the non-radiative, vibrational relaxation events described in the Jablonski diagram, other processes such as fluorescence quenching due to complex formation (static quenching) or collision (dynamic quenching) as well as photobleaching can decrease the fluorescence intensity of a fluorophore. [35, 36] Dynamic or collisional

quenching occurs when an excited fluorophore collides with a quencher molecule, such as oxygen or halogens, whereupon the fluorophore releases its energy and returns to the electronic ground state. The decrease in fluorescence intensity is described by the Stern-Volmer equation:

$$\frac{F_0}{F} = 1 + K_{SV}[Q] = 1 + k_q\tau_0[Q] \quad (\text{eq. 13})$$

K_{SV} represents the Stern-Volmer quenching constant, k_q the bimolecular quenching constant, τ_0 the unquenched lifetime and $[Q]$ the concentration of the quencher. Besides collisional quenching, other quenching processes occur, like static quenching originating from the formation of a non-fluorescent complex between fluorophore and quencher in the ground state.

Furthermore, photochemical processes proceeding during excitation, such as ionization after singlet-singlet-absorption, can permanently alter the molecular structure of a fluorophore resulting in a permanent loss of fluorescence. The rate of this so-called photobleaching is dependent on the intensity of the irradiation light and the molecular structure of the fluorophore.

1.2.2. Theoretical Aspects of Fluorescence Microscopy

In fluorescence microscopy, the photo-physical properties of fluorophores, described above, are utilized: The specimen of interest is irradiated with light of a specific wavelength, which is absorbed by the fluorophore. The emitted light of longer wavelengths is separated from the excitation light and collected in a detector (Figure 1.3).

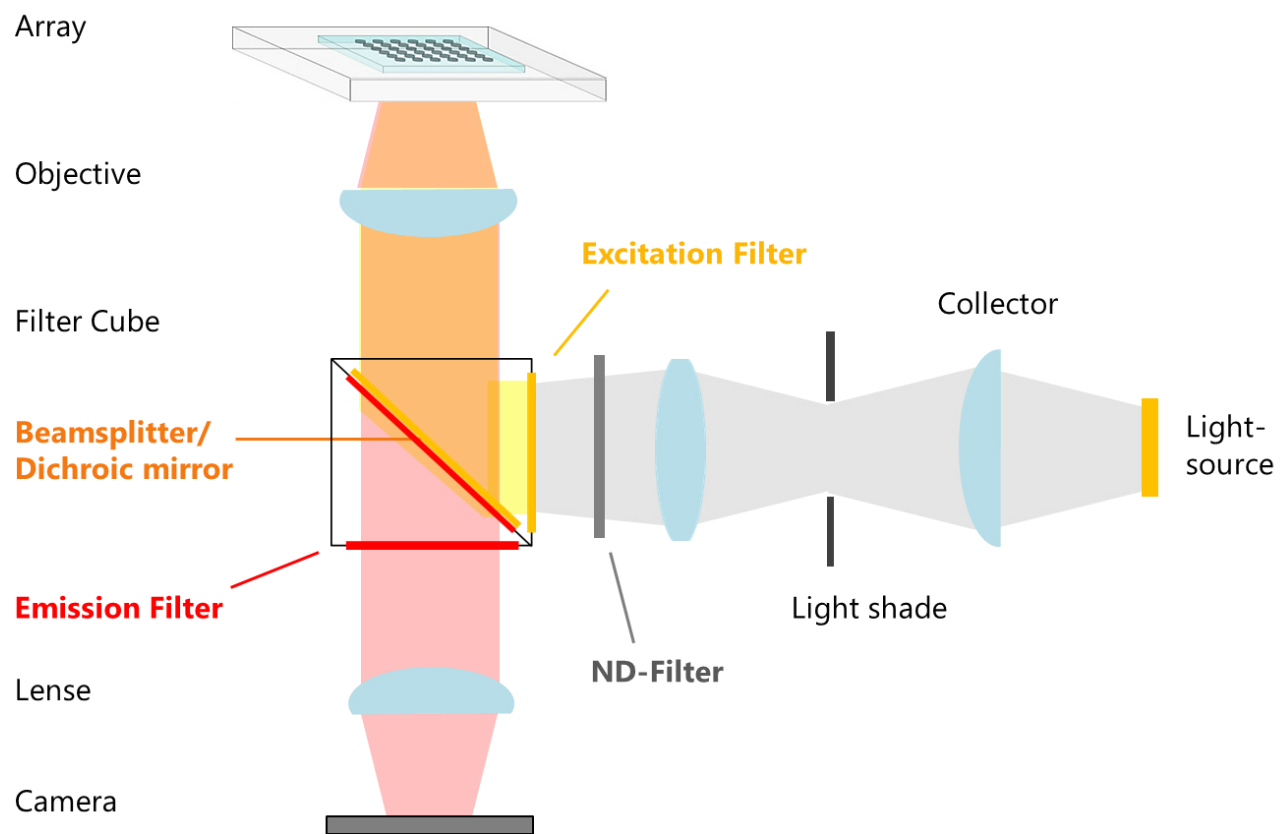


Figure 1.3 Schematic representation of the light path through an inverse epi-fluorescence microscope. In epi-fluorescence microscopes, the objective attends to both, focusing of excitation and emission light. The two light beams are separated in the filter cube.

As an individual enzyme molecule in any occupied reaction chamber produces hundreds of fluorescent product molecules per second, single enzyme molecule studies in femtoliter arrays do not require the detection of single fluorophores with highly sensitive technologies such as TIRF or confocal microscopy. Thus, a conventional wide-field microscope suffices to monitor the substrate turnover of individual enzyme molecules.

Figure 1.3 shows a schematic representation of the light-path through an inverse wide-field epi-fluorescence microscope as employed during this thesis. In contrast to an upright microscope, the specimen is located above the objective in an inverse microscope, offering an easy access to the analyzed sample. The array is placed on the microscope stage and irradiated from below through the objective lenses. Light from the excitation source is collected, concentrated and subsequently attenuated using neutral density (ND) filters before it enters the filter cube. ND filters are specified in units of optical density (OD_λ):

$$OD_\lambda = -\log_{10}\left(\frac{I}{I_0}\right) = \log_{10}\left(\frac{1}{T_\lambda}\right) \quad (\text{eq. 14})$$

In the equation 14, T_λ is defined as the intensity-ratio of transmitted light/incident light. The total density of a series of ND filters equals the sum of the individual filter densities. [37] Reduction of the incident light decreases photobleaching of the fluorophore.

The filter cube consists of three optical filters, which are specific for each type of fluorophore. The cube can be exchanged easily to investigate different fluorophores. Only wavelengths suitable for the excitation of the fluorophore pass through the excitation filter. The monochromatic light is then reflected to the object by a dichromatic mirror. Dichromatic mirrors, also called beam-splitters, are specified by their critical wavelength: light of shorter wavelength will be reflected from the mirror, while longer wavelengths pass through. The beam-splitter is chosen to have its critical wavelength between the maxima of excitation and emission. Consequently, the excitation light is

reflected and transmitted to the specimen, while the long-wave fluorescence light passes the mirror. The emitted light finally reaches the detector after passing the emission- or barrier filter and the ocular. The emission filter cuts out any remaining portion of excitation light, guaranteeing a thorough separation of excitation and emission light, which is mandatory to obtain a good microscopy image.

The objective is an essential part of an optical microscope. It has a crucial impact on the resolution of the specimen and the quality of the image. Additionally, the objective lenses, in combination with the ocular lenses, determine the magnification of the object. The numerical aperture (NA) of a microscope specifies the resolution of the objective. It is defined as:

$$NA = n \sin \alpha \quad (\text{eq. 15})$$

where α is the half-angle of aperture of the objective and n the refractive index of the medium. [38] The minimum resolvable distance between two object-points decreases with an increasing NA and the resolution limit (R) of an optical microscope is defined as:

$$R = \frac{\lambda}{2 NA} \quad (\text{eq. 16})$$

The numerical aperture of an objective and thus the resolution of an optical microscope can be altered by oil immersion. In this approach, both the specimen and the objective lens are immersed in a transparent oil of high refractive index ($n \approx 1.515$). [39] Thereby, the NA of the objective lens is increased, resulting in an enhanced resolution.

To improve the quality of a microscope image several corrections have been applied to objective lenses in order to reduce common aberrations that would result in a distorted image: [40] (1) Spherical aberration: The refraction of incident light on spherical lenses varies between different locations on the lens surface, resulting in a blurred image of the object. By application of objective lenses with an aspherical lens surface this

defect can be eliminated. (2) Chromatic aberration: The refractive index depends on the wavelength of the incident light. With increasing wavelength, the refractive index gradually decreases. Consequently, light of different wavelengths does not intersect in one convergent point. An objective with integrated correction of chromatic aberration (achromatic lens) consists of two individual lenses made from glass with different refractive indices. This way two different wavelengths (e.g. red and blue) are brought into focus in the same plane. (3) Curvature of field: This aberration generates a curved image of the object. Thus, only a small part of the image can be focused. The aberration can readily be corrected by applying flat-field objectives.

For the investigation of single enzyme molecules by fluorescence microscopy, a plan-achromatic objective lens was applied, that is corrected for curvature of field, spherical and chromatic aberration.

1.2.3. Limitations of Fluorescence Microscopy in Single Molecule Enzymology

As stated above, fluorescence microscopy is most frequently employed for single molecule studies due to its high sensitivity and broad applicability. However, the limited availability of suitable fluorogenic substrates, which are stable and non-fluorescent in their native form, but become highly fluorescent after enzyme catalysis, poses a great challenge on single enzyme molecule analysis. The generation of new, stable fluorogenic substrates or the development of alternative readout schemes is therefore essential.

Another problem of fluorogenic substrates relates to their mode of conversion. Many fluorogenic substrates contain two enzymatically cleavable bonds conjugated to one fluorophore. Consequently, the enzymatic catalysis proceeds in two steps. For example, fluorescein-di- β -D-galactopyranoside (FDG) is frequently used as a model substrate for monitoring the activity of single β -galactosidase molecules in fL volumes. The quantum yield of the mono-substituted fluorescein intermediate, however is very low and strongly depends on the substituent. [41-44] The two-step reaction results in sigmoidal kinetic curves that are very difficult to analyze. Consequently, resorufin- β -D-galactopyranoside that contains only a single cleavage site for β -galactosidase greatly simplifies the kinetic analysis. Similarly, there are two cleavage sites in most fluorogenic substrates for proteases that catalyze the hydrolysis of peptide bonds. [45] To circumvent this limitation, Terentyeva *et al.* [46] developed fluorogenic substrates for α -chymotrypsin containing only one cleavable peptide bond and compared their hydrolysis with conventional substrates containing two cleavage sites. The study revealed that the double-substituted substrate analogues yield kinetic parameters that are significantly different from those obtained from mono-substituted substrate analogues. In summary, progress in single molecule analysis relies on the systematic development of new long-lasting, preferably mono-substituted fluorogenic substrates.

1.3. Single Molecule Technologies

Biological systems have been studied by using a broad range of single molecule techniques that have emerged over the last twenty years. Generally, two fundamentally different forms of single molecule experiments can be distinguished. The first type is based on the detection of single fluorophore molecules to monitor single molecule dynamics, [47-49] single molecule trajectories [50] and conformational changes. [51-53] A wide range of such single fluorophore detection techniques [54-58] allow for studying structural and behavioral diversities between individual biomolecules. For example, single enzymatic turnover events can be observed by recording bursts of fluorophores released in subsequent catalytic cycles. [13] For detecting single fluorophore molecules, however, it is necessary to minimize the high background fluorescence originating from inelastic (Raman) and elastic (Rayleigh) scattering of surrounding molecules and fluorescent contaminations. [59] The key to background reduction is to keep the excitation or detection volume as small as manageable, for example by using total internal reflection fluorescence (TIRF) microscopy [60-62] or confocal microscopy. [8-11, 13, 63-67] There are many excellent reviews on single molecule experiments that rely on the detection of single turnover events. [30, 68-74]

This thesis is concerned with the second type of single enzyme molecule experiments that investigate the catalytic activity of individual enzyme molecules without the need for detecting single fluorophore molecules. In traditional bulk experiments, the activity of enzymes is usually determined from the increase of product concentration over time. This principle can also be applied to single molecule experiments. An individual enzyme molecule is isolated with a fluorogenic substrate in a defined volume and the accumulation of the fluorescent product can be monitored over time. Owing to

the small reaction volume (usually between 10 to 1000 fL) a small amount of accumulated fluorescent product is sufficient to exceed the limit of detection.

Single enzyme molecules can be isolated and investigated free in solution by using capillary electrophoresis in combination with laser-induced fluorescence (CE-LIF) (Figure 1.4)

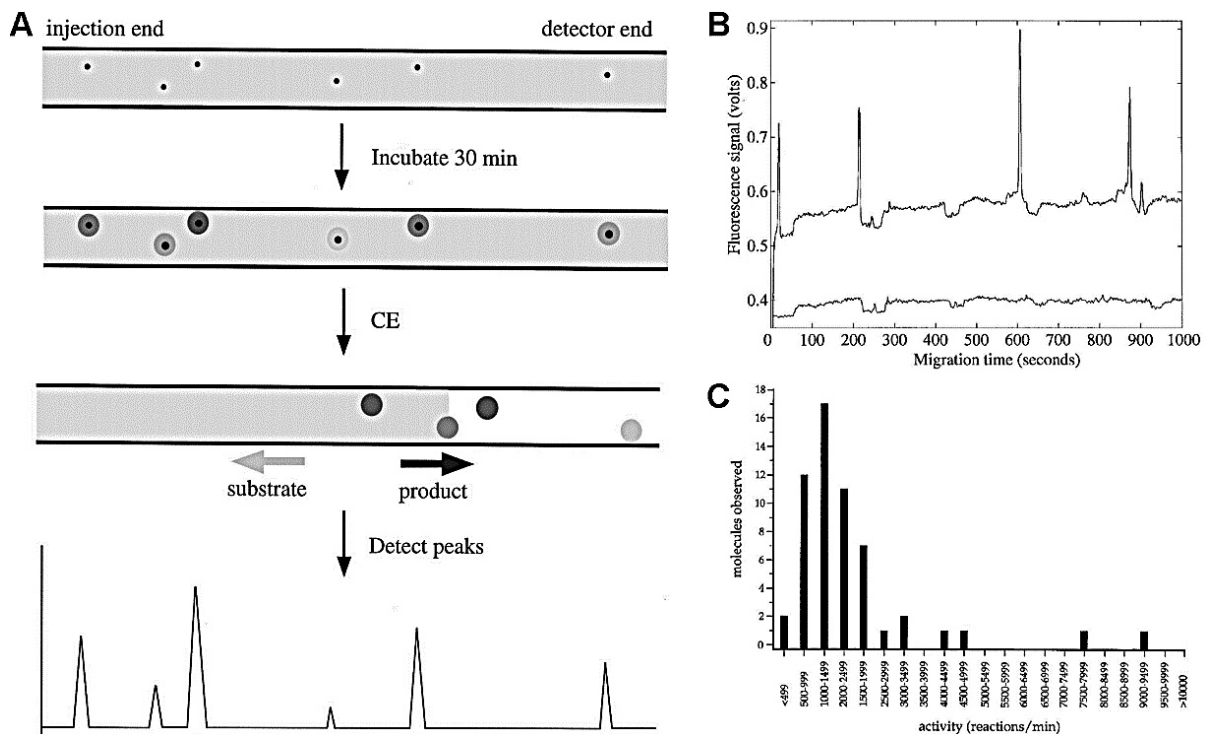


Figure 1.4 Single molecule enzymology by capillary electrophoresis. (A) The capillary is filled with a solution of substrate (grey) and highly diluted enzyme (black dots). After incubation the product accumulates in the vicinity of the enzyme molecules. When an electric field is applied, the substrate migrates towards the injection-end whereas the product migrates towards the detector, generating peaks in the electropherogram; (B) electropherogram of the single molecule β -galactosidase assay; (C) the resorufin- β -D-galactopyranoside turnover distribution of single β -galactosidase molecules indicates a broad conformational heterogeneity. Modified schematic representation reprinted with permission from [75], © 1998, Canadian Science Publishing.

CE enables the separation of substrate and product of an enzymatic reaction based on their different electrophoretic mobility. Thus, the formation of a fluorescent product and the decrease of the substrate concentration can be monitored in parallel. A very dilute enzyme solution is filled into a narrow capillary together with the fluorogenic substrate. At low enzyme concentrations, each enzyme molecule is separated by several centimeters such that the diffusion zones of the individual enzyme molecules do not overlap. The local accumulation of fluorescent product can be attributed to the substrate turnover of a single enzyme molecule. Each product zone migrates to the detector, where it is monitored. The product concentration can be determined from the area under the peaks of the electropherogram. CE-LIF for single enzyme molecule analysis was first introduced by Xue and Yeung in 1995 [15] and further developed in the groups of Dovichi and Craig. [75] The technique has been successfully applied for detecting and analyzing individual molecules of β -galactosidase, [20, 76-82] alkaline phosphatase [21, 83] and lactate dehydrogenase. [15] CE confines a volume in only two directions but is open in the flow direction. Therefore, it is usually not suitable for time-resolved measurements.

The three-dimensional isolation of individual enzyme molecules in separate compartments allows for performing time-resolved measurements to investigate single enzyme molecule dynamics. The first isolation of individual enzyme molecules and their substrate in a confined volume was performed by Rotman *et al.*, [18] who enclosed individual β -galactosidase molecules in droplets of a water-in-oil emulsion (Figure 1.5). To date, individual biomolecules have been isolated by using various types of emulsion-defined femtoliter droplets. [16, 84-91] To avoid the generation of multi-enzyme droplets, the enzyme is highly diluted before the emulsion is generated. As the volume of droplets prepared by standard emulsification techniques is broadly distributed,

additional steps have frequently been used to exclude larger droplets from data analysis. [92]

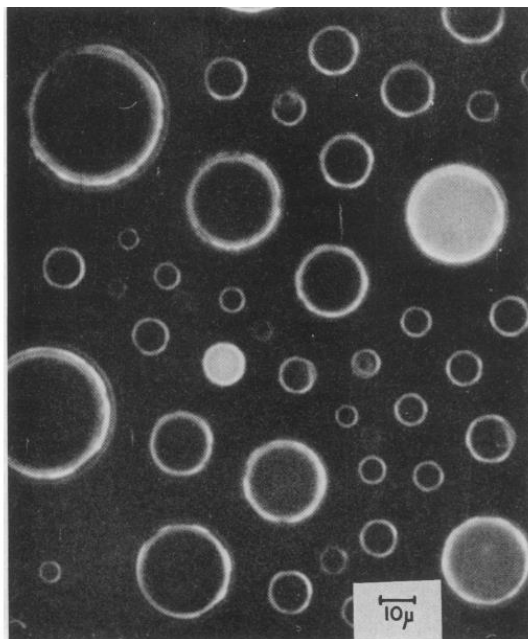


Figure 1.5 Photograph of the first single enzyme molecule experiment performed by Rotman *et al.* in water in oil emulsion droplets. Individual molecules of β -galactosidase together with a fluorogenic substrate are enclosed in the water droplets. The enzymatic substrate turnover of single enzyme molecules is monitored by the generation of fluorescent product, which appears white in the image. Image reprinted with permission from [18].

Other ultra-small reaction chambers such as lipid vesicles, virus capsids or even living cells have also been successfully applied for the confinement of individual biomolecules. Liposomes or lipid vesicles define a small reaction volume enclosed by lipid membranes, where both bulk phase and vesicle content are aqueous solutions (Figure 1.6 A). [93-95] There are a broad range of methods for preparing liposomes as reviewed by Jesorka and colleagues. [96] Liposomes can confine volumes similar in size as bacterial cells and are thus well suited for the investigation of biological processes. [97]

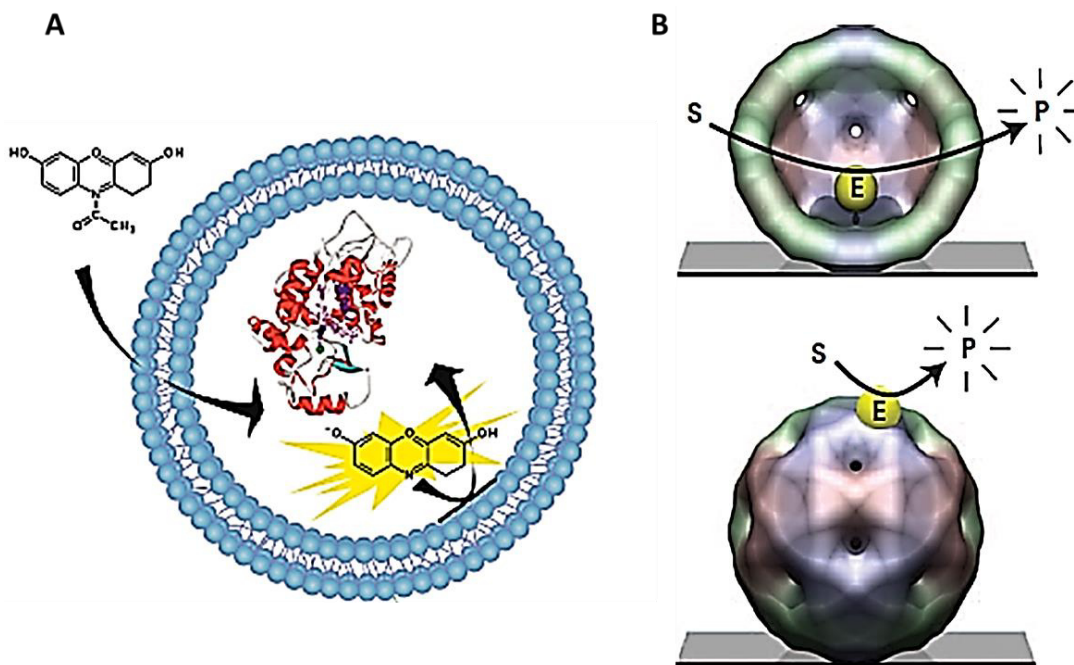


Figure 1.6 Enclosure of individual enzyme molecules in ultra-small, self-assembled reaction chambers. (A) An individual HRP molecule is encapsulated within a large unilamellar vesicle. The externally added substrate Amplex Red diffuses into the vesicle and is oxidized by HRP to the fluorescent product resorufin, which remains trapped in the vesicle interior; (B) A single HRP molecule (E) is confined in an icosahedral virus capsid. The fluorogenic substrate (S) penetrates the capsid where it is converted to fluorescent product (P). The accumulated product is monitored by fluorescence microscopy before it finally diffuses out through the capsid pores. Modified schematic representation reprinted with permission from [94] © 2012 and from [98] Macmillan Publishers, © 2007.

For enclosing single enzyme molecules in virus capsids, usually the cowpea chlorotic mottle virus (CCMV) has been employed that provides a small reaction chamber in form of an icosahedral protein capsid (Figure 1.6 B). [98-100] Virus capsids have an inner diameter of several nm, defining a volume of a few zeptoliter (zL). To overcome the limitations of the ultra-small confinement, a single enzyme molecule is enclosed inside the virus capsid, whereas substrate and product can pass by diffusion due to the size-selective permeability of the protein cage. [100] Similar as liposomes or virus capsids, living cells can confine single biomolecules. [101] Single molecule studies in living cells

can provide new insights into fundamental biochemical processes in a physiological environment. [102-104]

Spatial confinement of enzyme molecules in small reaction containers avoids the need for immobilizing the enzyme on a surface, which can lead to steric hindrance, partial inactivation or disturbance of the original enzyme activity. [9] Self-assembled micro-vessels for single enzyme molecule analysis (bottom-up approach) [105, 106] such as water droplets in oil, lipid vesicles or virus capsids can have variable sizes and need to be surface immobilized for long-time monitoring. These problems can be avoided by the systematic structuring of surfaces (top-down approach) [105, 106] to generate large arrays of thousands of reaction chambers with uniform size and defined position.

1.3.1. Femtoliter Arrays on Optical Fiber Bundles

Microwell arrays in optical-fiber bundles were first developed in the mid 1990's in the laboratory of David Walt. [107] Over the years the arrays were optimized and employed for various bioanalytical applications. Optical-fiber bundles consist of hundreds to several thousands of individual glass fibers that are bundled, melted and fused into one unity. [108] Each fiber is composed of two different types of glass with different refractive indices. A core with diameters between 2 and 20 μm is surrounded by a common cladding material of lower refractive index than the core material (Figure 1.7). Light that enters the waveguide within a critical angle α is transmitted along the fiber by total internal reflection over long distances without severe attenuation. [108]

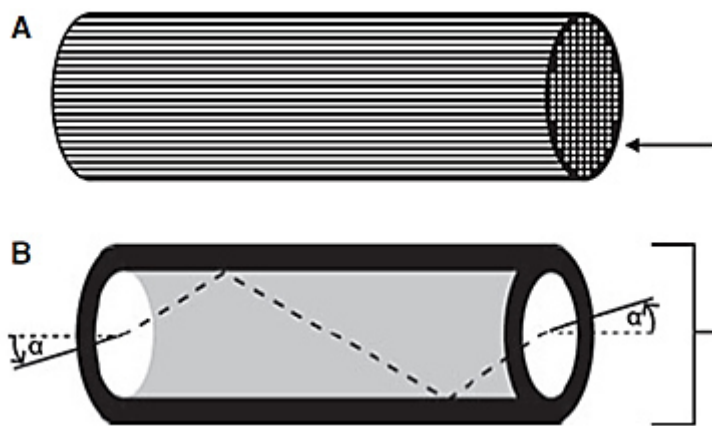


Figure 1.7 Femtoliter array on an optical-fiber bundle. (A) An optical-fiber bundle typically consists of several thousands of individually addressable fibers that are fused into a common cladding material. (B) Due to the different refractive indices of cladding material and core, light propagates along the entire fiber length by total internal reflection. Schematic representation reprinted from [109] with permission from John Wiley and Sons, © (2007).

The core material of the fibers can be etched selectively to form arrays of homogenous fL reaction chambers. The microwells are arranged in very high density arrays of about

25 000 mm^{-2} . The fL-sized reaction vessels on one end of the optical-fiber bundle are loaded with a fluorescent sample. The other end is connected to an epi-fluorescence microscope where the incoming light is filtered and detected by a sensitive CCD camera. Excitation light is launched into the entire array. The emission light is transmitted through individual cores at the bottom face of the microwells. Each fiber provides the signal from the reaction chamber to which it is linked. In this way, a multitude of individual reaction vessels can be investigated in parallel. [109] Typical optical-fiber bundles applied in single molecule enzymology contain about 50 000 fibers with an overall diameter of 1.5 mm. [105, 106]

A crucial disadvantage of femtoliter arrays fabricated in optical-fiber bundles represents the reduced signal acquisition by the fiber cores. Only light that enters the fiber cores within the acceptance cone is transmitted via total internal reflection. The angle of the acceptance cone depends of the refractive indices of fiber core and cladding. However, it is typically distinctly lower than the numerical aperture of a high-resolution microscopy objective lens. Furthermore, the long light path in combination with the specific dopants of the fiber materials leads to straylight and autofluorescence.

Optical-fiber bundle arrays were applied in multiple single molecule enzymology studies. In a proof of principle experiment, individual molecules of β -galactosidase were enclosed in a homogeneous fiber bundle array together with an excess of resorufin- β -D-galactopyranoside (RGP). [14] Monitoring of a large population of β -galactosidase molecules revealed discrete and long-lived substrate turnover rates for individual β -galactosidase molecules. The broad activity distribution within an enzyme population (static heterogeneity) can be attributed to different conformational states and is consistent with previous single molecule studies. [75, 110, 111] β -Galactosidase was further employed for the first single molecule investigation of competitive enzyme inhibition in optical-fiber bundle arrays. [23] Binding and release rates of the slow-

binding inhibitor D-galactal from single β -galactosidase molecules were observed. The work was further expanded [24] by comparing the activity of β -galactosidase in the presence of D-galactal and N-p-bromobenzylamino-hydroxymethyl-cyclopentanetriol (NpBHC). The inhibitor-release kinetics of the inhibitors was fundamentally different: While D-galactal release from individual molecule of β -galactosidase was cooperative, [23] NpBHC was released sequentially from the four enzyme subunits.

Recently, the Walt group investigated heating effects on the activity of β -galactosidase in optical-fiber bundles. [112] Upon heating the individual enzyme molecules switched between different activity-states resulting from conformational changes. The activity changes were random and did not correlate with the enzyme's original activity. Consequently, the static heterogeneity within an enzyme population is related to the presence of different stable conformations and individual β -galactosidase molecules possess numerous stable activity states that can be interconverted upon exposure to thermal energy.

Single enzyme molecule experiments of horseradish peroxidase (HRP) enclosed in optical-fiber bundle arrays revealed a ten times lower substrate turnover rate for HRP at the single-molecule level compared to the bulk experiment. [113] This phenomenon was explained by the complex redox mechanism of HRP catalysis that involves two separate steps of product formation and the generation of radical intermediates. The high surface to volume ratio for experiments performed in fL-arrays increases the probability of potential side reactions of the highly active radical intermediates.

Evaporation of water from microwells is a significant problem when working with arrays of ultra-small reaction vessels. [114-116] Instead of sealing the fiber bundle arrays mechanically by a silicone gasket, oil-sealing of the fL-sized reaction chambers was successfully explored to ensure a tight enclosure and avoid evaporation of the aqueous solution. [117]

In addition to basic research, the enzymatic turnover of single enzyme molecules in optical-fiber bundle arrays has also been employed for implementing a single molecule ELISA. [118, 119] In this case, the enzyme is used as a reporter for the detection of other analyte molecules. The analyte concentration can be determined by counting the chambers that light up if a single reporter enzyme molecule turns over the fluorogenic substrate (for details see chapter 4.1). The enzymatic signal amplification enables the detection of analytes with high sensitivity. In a proof of principle experiment, single molecules of streptavidin-labeled β -galactosidase were bound to a biotin-derivatized reaction vessel surface. [120] After sealing, the single enzyme molecules were detected by monitoring the accumulation of fluorescent product. This technique has been further developed to enable the detection of varying biological analytes such as proteins [120] or DNA [121]. The single-molecule ELISA has been commercialized by Quanterix Corporation for detecting proteins in blood at femtomolar or even subfemtomolar concentrations. [122-125]

The fiber bundle microarrays have recently been replaced by fL-arrays integrated in an enclosed microfluidic device fabricated in a thermoplastic cyclic olefin polymer (COP). [126] The polymer arrays were oil-sealed in an integrated microfluidic device that facilitated the isolation of single beads in the fL-wells and provided further advantages such as low-cost manufacturing, or the possibility to establish fully automated single-molecule array systems.

In analytical applications such as single molecule ELISAs, one has to consider that even a large array can hold only a limited amount of probe volume. For example, femtoliter arrays of 100 000 wells, each defining a volume of 50 fL, can only hold a probe volume of 5 nL. Consequently, a pre-concentration step is essential to probe a larger volume. This can typically be achieved by implementing bead-based microwell arrays. [74, 107, 108] Furthermore, to make single enzyme analysis applicable in clinical studies,

multiple targets need to be measured in parallel in one sample. Recently, Rissin *et al.* [127] reported the successful operation of multiplexing in bead microwell arrays. Introduction of multiplexing is an important step towards the implementation of single molecule analysis as a standard method in biomedical applications.

Besides single enzyme molecule analysis, the Walt group has also employed optical-fiber bundles for establishing DNA arrays. [128-130] For example, optically encoded microspheres confined in fiber-optic arrays were applied for the simultaneous detection of six biological warfare agents. [128] In a similar way, chromosomal DNA from *Salmonella spp.* and ribosomal RNA from several harmful algal bloom species could be detected. [129, 130] Optical-fiber bundle arrays were further applied to isolate and investigate individual cells: Yeast, [131] bacteria [132-134] and mammalian cells [135, 136] have been enclosed separately in the wells of an optical-fiber bundle array together with a solution of the required nutrients. The single-cell studies provided new details regarding cellular processes and enabled the functional screening of biochemically active reagents. Recently, Vajrala *et al.* [137] investigated individual mitochondria in the wells of an optical-fiber bundle array. Utilizing the fluorescence of NADH, the metabolic status of individual mitochondria at varying respiratory states was monitored by fluorescence microscopy.

1.3.2. Femtoliter Arrays Molded in PDMS

Soft lithography is another established method for the fabrication of arrays of femtoliter-sized reaction containers. Soft lithography is a low-cost and effective method based on replica molding for the generation of microstructures. [138, 139] A master mold is applied as a template to cast complementary structures in elastomers such as polyurethanes, polyimides and most commonly poly(dimethylsiloxane) (PDMS).

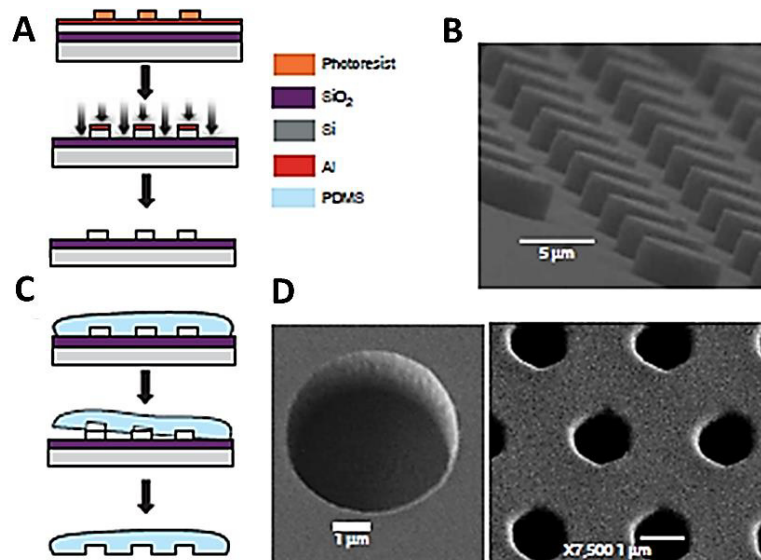


Figure 1.8 Femtoliter array molded in PDMS. (A) Fabrication of the template: a silicon wafer is covered with an aluminum mask and patterned by photolithography. (B) Scanning electron microscopy (SEM) image of the silicon template demonstrating the regular array of homogeneous cylindrical shapes. (C) Liquid PDMS was poured on the Teflon-coated mold, polymerized at high temperature and finally peeled off. (D) SEM images of the PDMS fL-array. Schematic representation reprinted with permission from Macmillan Publishers Ltd: Nature Biotechnology [115] © (2005).

PDMS is well-suited for the fabrication of bioanalytical assay systems as it is nontoxic and oxygen-permeable. Furthermore, it is transparent and can be easily patterned into minute structures. For example, Rettig *et al.* [140] and Sasuga *et al.* [141] isolated

individual cancer cells in thousands of PDMS microwells defining a picoliter (pL) volume. They used fluorescence imaging to test the cells for vitality [140] or to determine intracellular protein concentrations and enzymatic activities. [141]

Single enzyme molecules were first analyzed in fL arrays of PDMS by Rondelez and colleagues. [115] A silicon master stamp patterned by photolithography was used to mold series of identical PDMS sheets with integrated arrays of 30 fL reaction containers (Figure 1.8). The containers were sealed via PDMS adhesion to a glass coverslip under mechanical pressure. In a proof of principle experiment, the hydrolysis of fluorescein-di- β -D-galactopyranoside (FDG) by single molecules of β -galactosidase was monitored using wide-field fluorescence microscopy. The PDMS array was further applied in several studies to investigate the biomechanical processes involved in ATP synthesis and hydrolysis, catalyzed by the enzymes F_1 -ATPase and F_0F_1 -ATP synthase. [142-145]

Arata *et al.* [146] developed a PDMS fL-array combined with an integrated on-chip microreactor and microheater that enabled the measurement of enzymatic activity at high temperatures. The on-chip microheater PDMS array system was applied to investigate the temperature dependency of the β -galactosidase activity. β -Galactosidase survived short-time exposure to high temperatures. Additionally, the enzyme activity was found to be about four times higher at 60 °C than at room temperature. Temperature effects on the activity of single β -galactosidase molecules were further explored in optical-fiber bundle arrays as described in the previous chapter. [112]

Single α -chymotrypsin molecules were isolated and investigated in arrays of 4.2-fL reaction chambers molded in PDMS. [147] The protease activity of individual α -chymotrypsin molecules was monitored using a protein-dye conjugate consisting of casein labeled with a large number of self-quenched fluorophores. After proteolysis by chymotrypsin, the fluorophores were spatially separated, which led to a 50- to 100-fold increase of the fluorescence signal. Consistent with other studies on single enzyme

molecules, individual α -chymotrypsin molecules exposed a heterogeneous activity within the enzyme population.

Microfluidic methods play an important role in delivering fluids to fL wells. Jung *et al.* [148] combined an array of homogeneous PDMS microwells (4.4 μm diameter and 6.5 μm height, defining a volume of 100 fL) with a microfluidic device, to control the initiation of the enzymatic reaction. [148] In a proof of principle experiment, the reactants β -galactosidase and resorufin- β -D-galactopyranoside were introduced from separate inlets and combined in less than 100 ms in a mixing channel. The homogeneous enzyme-substrate mixture was then enclosed in the wells of the PDMS fL array by using a glass coverslip under hydraulic pressure. In this microfluidic system, single enzyme molecule kinetics could be monitored within milliseconds after mixing enzyme and substrate. Another method to generate high-density fL arrays within microfluidic channels in PDMS was presented by Ota *et al.* [149] Many small reaction chambers (5 μm in diameter and 6 μm in depth) were formed in the walls of a main channel by PDMS molding. When aqueous solutions and organic solvents were subsequently infused into the channel, aqueous droplets were confined in the chambers by the organic solvent. β -Galactosidase in the droplets catalyzed the hydrolysis of fluorescein-di- β -D-galactopyranoside (FDG) to fluorescent fluorescein, which was monitored in parallel in about 300 reaction chambers by fluorescence microscopy.

Microfluidic PDMS systems have not only been applied to investigate single enzyme molecules. Recently, Fowlkes and colleagues [150] studied the mobility of individual fluorescent molecules in a microfluidic device with sealable fL-volume reaction chambers by fluorescence correlation spectroscopy.

1.3.3. Femtoliter Arrays Fabricated in Glass Slides

Fabrication of planar femtoliter arrays in hard materials such as glass coverslips avoids the limitations of optical-fiber bundles, such as limited signal acquisition, increased straylight and autofluorescence, and thus enables an increase in sensitivity. Topographically patterned surfaces in glass slides are usually fabricated by photolithography or particle beam lithography. [151]

Tan and colleagues [110] applied photolithography to microfabricate large arrays of homogeneous fL-wells into the surface of fused silica slides. A very thin fused silica coverslip was used to seal the liquid-filled reaction chambers. In this array format the enzymatic redox activity of single molecules of lactate dehydrogenase (LDH-1) was monitored over time. [110] The enzyme-catalyzed redox-process was compared to the Os^{III} -catalyzed redox reaction of Ce^{IV} and As^{III} to fluorescent Ce^{III} and As^{V} . The activity distribution observed for single metal ions was considerably narrower than for individual enzyme molecules. The broad activity distribution within the LDH-1 population was attributed to varying protein conformations which distinguishes enzymatic catalysis from metal ion catalysis.

Recently, arrays of fL droplets were generated on a hydrophilic-in-hydrophobic micropatterned surface. [88, 152, 153] A hydrophobic carbon-fluorine polymer was spin-coated on a clean coverglass. Photolithography and reactive ion etching was conducted subsequently to expose the hydrophilic SiO_2 surface. The hydrophilic-in-hydrophobic micro-patterned coverglass was covered with an aqueous solution. Fluorinated oil, which has a higher density than water, was then flowed into the aqueous solution near the micro-patterned surface. The hydrophobic surface was covered with oil, while the hydrophilic glass surface retained the aqueous solution in the form of many homogeneous droplets. In this way, more than 10^6 dome-shaped droplets were prepared

simultaneously. Individual β -galactosidase molecules were enclosed in the droplets together with the fluorogenic substrate fluorescein-di- β -D-galactopyranoside to measure the activity of single enzyme molecules. The fluorescence images of the droplets were recorded on a confocal microscope.

In connection with previous experiments conducted in PDMS arrays, [142-144] Noji and colleagues [88] investigated the kinetic parameters of the rotary motor protein F_1 -ATPase in the hydrophilic-in-hydrophobic array system.

In our group, we have prepared homogeneous arrays of 62 500 femtoliter-sized reaction vessels etched into the surface of fused silica slides to enclose single enzymes molecules (see chapter 2.2.1). Amongst others, we applied the fused silica fL-array to investigate the oxidation of the fluorogenic substrate Amplex Red to fluorescent resorufin by hundreds of individual horseradish peroxidase (HRP) molecules. [154] We demonstrated the presence of distinct, long-lived kinetic states of individual HRP molecules. Additionally, we have found that the signal generation of horseradish peroxidase enclosed in a femtoliter well was ten times lower than in bulk reaction. [113, 154] This can be explained by a two-step reaction mechanism which leads to the formation of a radical intermediate that can also react with the well surface instead of forming the fluorescent product.

As a basic principle, in single molecule analysis, it is essential to address possible surface reactions, which are a consequence of the large surface to volume ratio in femtoliter wells. For example, non-specific protein binding can be avoided by adding an excess of blocking reagents that are not involved in the reaction. [14] In general, new solution additives and surface chemistries for surface passivation are needed to reduce non-specific protein binding.

Femtoliter arrays in glass slides have not only been used for single molecule enzymology. Iino *et al.* [155, 156] applied the design of the fL-droplet array for the

development of a single-cell drug efflux assay in individual cells of *Escherichia coli*. Additionally, single-molecule investigations on DNA-hybridization have been conducted in fL-arrays fabricated in fused silica coverslips. [116] The so-called “Dimple Machine” consists of a fused silica coverslip containing multiple arrays of nanofabricated circular drops or dimples fabricated by electron-beam lithography. The dimples were loaded with a solution containing two strands of fluorescently labeled single-stranded DNA molecules and reversibly sealed with a pneumatically actuated, structured PDMS lid. DNA hybridization was monitored by co-localization and fluorescence resonance energy transfer (FRET). [116]

1.3.4. Single Enzyme Molecule Analysis in Femtoliter Arrays

As outlined above, homogeneous arrays of fL-sized reaction vessels can be fabricated in the surface of optical-fiber bundles, glass coverslips, poly(dimethylsiloxane) (PDMS) sheets or thermoplastics by using established microfabrication techniques. The microchambers usually define a volume of several femtoliters (fL) with a diameter between 3 μm and 10 μm and a depth between 200 nm and 5 μm . [108, 115, 116] Because of the small dimensions of the fL-containers, they can be arranged in very high density arrays. [157] For example, fL-arrays etched into the surface of a glass coverslip have a density of 10 000 mm^{-2} . [154] When these arrays are filled with an enzyme solution, thousands of individual molecules can be observed in parallel, enabling excellent statistical analysis and high quality data evaluation.

Enzyme molecules cannot be loaded individually into the fL-sized reaction vessels. Therefore, separation depends on the random distribution of the enzyme molecules in the wells of the array. The Poisson distribution is a simple statistical method to determine the optimal enzyme concentration to maximize the number of wells occupied with a single enzyme molecule. In general, Poisson statistics describes the probability of a rare event in a large number of trials. When applied to the distribution of enzyme molecules in the wells of a fL-array, the probability $P_{\mu}(x)$ that exactly x enzyme molecules are enclosed in a specific well can be calculated by equation (1), where μ is the mean number of enzyme molecules per well:

$$P_{\mu}(x) = \frac{e^{-\mu}\mu^x}{x!} \quad (\text{eq. 17})$$

For example, at a ratio of one enzyme molecule per 20 reaction chambers, 95% of the reaction vessels are empty, 5% are occupied with a single enzyme molecule and only 0.1% of the wells contain more than a single molecule. [14] In order to further decrease

the probability of multiple molecules per chamber, a stronger reduction of the enzyme concentration would be necessary resulting in an increasing number of empty wells. Consequently, when working with fL-arrays, a high degree of parallelization is mandatory. The large size of the array ensures that hundreds of enzyme molecules can be investigated in parallel even if only every twentieth reaction chamber is occupied.

Femtoliter chambers have an ideal size for single enzyme molecule investigation: They are small enough to isolate individual enzyme molecules and can accumulate a high number of product molecules in a short time. Additionally, they are big enough to hold a large excess of substrate molecules and ensure a constant substrate concentration over the whole course of the experiment. Only in this case the substrate turnover rate of individual enzyme molecules can be calculated accurately.

1.4. Motivation and Aim of Work

The confinement of bioanalytical reactions in arrays of uniform, fL-sized reaction chambers enables the disclosure of new mechanistical aspects of biochemical processes. [158] Details of biomolecular interactions, different conformational states and subpopulations of proteins and other biomolecules that are hidden in traditional bulk experiments can be unraveled. [159]

Many established single molecule experiments are limited by the low number of enzyme molecules that can be monitored in parallel in one measurement. By separating individual biomolecules in large arrays of homogeneous microcompartments, thousands of analytical measurements can be performed simultaneously. The highly parallel readout scheme provides excellent statistics on the activity distribution in an enzyme population and enables the recovery of new information about enzyme kinetics and conformational characteristics. [105, 106] Enclosing individual enzyme molecules in microwells does not require any surface immobilization steps and allows for the kinetic investigation of enzymes free in solution.

It was the aim of this thesis to develop an innovative and optimized setup for single enzyme analysis in femtoliter arrays that enables highly sensitive and accurate measurements. Two different types of femtoliter array systems in fused silica and PDMS should be tested and their application for single molecule enzymology improved in several steps. The effectiveness of the respective optimized setup should then be evaluated in the context of the investigation of individual molecules of the model enzyme β -galactosidase.

After the successful implementation and thorough verification of the designed setup, it should be further employed to gain detailed information on the enzyme kinetics of β -glucuronidase. In this context, the establishment of a novel, single molecule

perspective on the mechanisms that drive the evolution of a new enzyme activity was intended. For this purpose the kinetics of wild-type and *in vitro* evolved β -glucuronidase should be investigated at the single molecule level. From this study we expected new insights not only on the catalysis of enzymes but also on the processes that evolve new catalytic activities.

Finally, in a third project, the established femtoliter array platform was to be applied to break new ground on a different application of single enzyme molecule detection: Typically, femtoliter arrays are employed for fundamental research. However, they can also be applied for analytical measurements. [122, 160] Large arrays of fL-sized reaction chambers in combination with enzymatic signal amplification enable the digital readout of target concentrations in biological or environmental samples. In this work, fused silica femtoliter arrays should be modified, to enable their use in bioanalytical assays. The ambition was to introduce biomolecules such as peptides, antibodies or even whole enzymes on the surface of the wells of the femtoliter arrays, thus laying the basis for their future application in concentration analysis.

Fundamentally, the development of new fabrication techniques and sensitive detection methods drives the field of single molecule enzymology. It enables us to disclose new, fascinating details concerning enzyme interaction and kinetics, so we can further extend our understanding of the fundamental biochemical processes of life.

1.5. References

1. Liebherr, R.B. and H.H. Gorris, *Enzyme Molecules in Solitary Confinement*. *Molecules*, **2014** (19): 14417.
2. McGovern, P.E., J. Zhang, J. Tang, Z. Zhang, G.R. Hall, *et al.*, *Fermented beverages of pre- and proto-historic China*. *Proc. Natl. Acad. Sci. U. S. A.*, **2004** (101): 17593.
3. Cavalieri, D., P.E. McGovern, D.L. Hartl, R. Mortimer, and M. Polsinelli, *Evidence for *S. cerevisiae* fermentation in ancient wine*. *J. Mol. Evol.*, **2003** (57): 226.
4. Michaelis, L. and M.L. Menten, *Die Kinetik der Invertinwirkung*. *Biochem. Z.*, **1913** (49): 333.
5. Knowles, J.R., *To Build an Enzyme*. *Philos. Trans. R. Soc. London, B*, **1991** (332): 115.
6. Knowles, J.R., *Enzyme Catalysis - Not Different, Just Better*. *Nature*, **1991** (350): 121.
7. Engelkamp, H., N.S. Hatzakis, J. Hofkens, F.C. De Schryver, R.J. Nolte, and A.E. Rowan, *Do enzymes sleep and work?* *Chem. Commun.*, **2006**: 935.
8. Lu, H.P., L. Xun, and X.S. Xie, *Single-molecule enzymatic dynamics*. *Science*, **1998** (282): 1877.
9. Michalet, X., S. Weiss, and M. Jager, *Single-molecule fluorescence studies of protein folding and conformational dynamics*. *Chem. Rev.*, **2006** (106): 1785.
10. Velonia, K., O. Flomenbom, D. Loos, S. Masuo, M. Cotlet, *et al.*, *Single-enzyme kinetics of CALB-catalyzed hydrolysis*. *Angew. Chem. Int. Ed.*, **2005** (44): 560.
11. Flomenbom, O., K. Velonia, D. Loos, S. Masuo, M. Cotlet, *et al.*, *Stretched exponential decay and correlations in the catalytic activity of fluctuating single lipase molecules*. *Proc. Natl. Acad. Sci. U. S. A.*, **2005** (102): 2368.
12. van Oijen, A.M., P.C. Blainey, D.J. Crampton, C.C. Richardson, T. Ellenberger, and X.S. Xie, *Single-molecule kinetics of lambda exonuclease reveal base dependence and dynamic disorder*. *Science*, **2003** (301): 1235.
13. English, B.P., W. Min, A.M. van Oijen, K.T. Lee, G. Luo, *et al.*, *Ever-fluctuating single enzyme molecules: Michaelis-Menten equation revisited*. *Nat. Chem. Biol.*, **2006** (2): 87.
14. Rissin, D.M., H.H. Gorris, and D.R. Walt, *Distinct and long-lived activity states of single enzyme molecules*. *J. Am. Chem. Soc.*, **2008** (130): 5349.

15. Xue, Q. and E.S. Yeung, *Differences in the chemical reactivity of individual molecules of an enzyme*. Nature, **1995** (373): 681.
16. Lee, A.I. and J.P. Brody, *Single-molecule enzymology of chymotrypsin using water-in-oil emulsion*. Biophys. J., **2005** (88): 4303.
17. Gershenson, A., *Single molecule enzymology: watching the reaction*. Curr. Opin. Chem. Biol., **2009** (13): 436.
18. Rotman, B., *Measurement of activity of single molecules of beta-D-galactosidase*. Proc. Natl. Acad. Sci. U. S. A., **1961** (47): 1981.
19. Craig, D.B. and L.N. Chase, *Arrhenius Plot for a Reaction Catalyzed by a Single Molecule of beta-Galactosidase*. Anal. Chem., **2012** (84): 2044.
20. Craig, D.B., B. Bayaraa, D. Lee, and J. Charleton, *Effect of Induction Temperature and Partial Thermal Denaturation on the Catalytic and Electrophoretic Heterogeneity of Beta-Galactosidase from Two Escherichia Coli Strains*. J. Liq. Chromatogr. Relat. Technol., **2013** (36): 2944.
21. Craig, D.B., E.A. Arriaga, J.C.Y. Wong, H. Lu, and N.J. Dovichi, *Studies on single alkaline phosphatase molecules: Reaction rate and activation energy of a reaction catalyzed by a single molecule and the effect of thermal denaturation - The death of an enzyme*. J. Am. Chem. Soc., **1996** (118): 5245.
22. Dyck, A.C. and D.B. Craig, *Individual molecules of thermostable alkaline phosphatase support different catalytic rates at room temperature*. Luminescence, **2002** (17): 15.
23. Gorris, H.H., D.M. Rissin, and D.R. Walt, *Stochastic inhibitor release and binding from single-enzyme molecules*. Proc. Natl. Acad. Sci. U. S. A., **2007** (104): 17680.
24. Mogalasetti, P., H.H. Gorris, M.J. Rojek, and D.R. Walt, *Elucidating the Relationship between Substrate and Inhibitor Binding to the Active Sites of tetrameric Chem Sci*, **2014** (5): 4467.
25. Craig, D.B., T. Hall, and D.M. Goltz, *Escherichia coli beta-galactosidase is heterogeneous with respect to a requirement for magnesium*. BioMetals, **2000** (13): 223.
26. Segel, L.A., *On the Validity of the Steady-State Assumption of Enzyme-Kinetics*. B. Math. Biol., **1988** (50): 579.
27. Xie, S.N., *Single-molecule approach to enzymology*. Single Mol., **2001** (2): 229.
28. Kou, S.C., B.J. Cherayil, W. Min, B.P. English, and X.S. Xie, *Single-molecule Michaelis-Menten equations*. J. Phys. Chem. B, **2005** (109): 19068.

29. Alt, W., *An objective lens for efficient fluorescence detection of single atoms*. *Optik*, **2002** (113): 142.
30. Sauer, M., J. Hofkens, and J. Enderlein, *Handbook of Fluorescence Spectroscopy and Imaging*. 1st ed (**2011**): Wiley-VCH.
31. Lakowicz, J.R., *Principles of Fluorescence Spectroscopy*. 3rd ed (**2006**): Springer.
32. Lottspeich, F. and H. Zorbas, *Bioanalytik* (**1998**): Spektrum Akademischer Verlag.
33. Lakowicz, J.R., H. Szmazinski, K. Nowaczyk, K.W. Berndt, and M. Johnson, *Fluorescence Lifetime Imaging*. *Anal. Biochem.*, **1992** (202): 316.
34. Szmazinski, H., K. Nowaczyk, K. Berndt, and J.R. Lakowicz, *Fluorescence Lifetime Imaging*. *FASEB J.*, **1992** (6): A35.
35. Song, L.L., E.J. Hennink, I.T. Young, and H.J. Tanke, *Photobleaching Kinetics of Fluorescein in Quantitative Fluorescence Microscopy*. *Biophys. J.*, **1995** (68): 2588.
36. Song, L.L., I.T. Young, and H.J. Tanke, *Photobleaching Kinetics of Fluorescein in Quantitative Fluorescence Microscopy*. *Zool. Stud.*, **1995** (34): 111.
37. Murphy, D.B. and M.W. Davidson, *Fundamentals of Light Microscopy and Electronic Imaging*. (**2001**): Wiley-Blackwell.
38. Abramowitz, M., K.R. Spring, H.E. Keller, and M.W. Davidson, *Basic principles of microscope objectives*. *BioTechniques*, **2002** (33): 772.
39. Olympus. *Immersion Media*. 2015 [cited 2015 April 07]; Available from: <http://www.olympusmicro.com/primer/anatomy/immersion.html>.
40. Olympus. *Optical Aberrations*. 2015 [cited 2015 April 07]; Available from: <http://www.olympusmicro.com/primer/anatomy/aberrationhome.html>.
41. Melhado, L.L., S.W. Peltz, S.P. Leytus, and W.F. Mangel, *Para-Guanidinobenzoic Acid-Esters of Fluorescein as Active-Site Titrants of Serine Proteases*. *J. Am. Chem. Soc.*, **1982** (104): 7299.
42. Maeda, H., H. Matsuno, M. Ushida, K. Katayama, K. Saeki, and N. Itoh, *2,4-Dinitrobenzenesulfonyl fluoresceins as fluorescent alternatives to Ellman's reagent in thiol-quantification enzyme assays*. *Angew. Chem. Int. Ed.*, **2005** (44): 2922.
43. Burchak, O.N., L. Mugerli, F. Chatelain, and M.Y. Balakirev, *Fluorescein-based amino acids for solid phase synthesis of fluorogenic protease substrates*. *Bioorg. Med. Chem.*, **2006** (14): 2559.

44. Liu, B., S. Fletcher, M. Avadisman, P.T. Gunning, and C.C. Gradinaru, *A photostable, pH-invariant fluorescein derivative for single-molecule microscopy*. *J. Fluoresc.*, **2009** (19): 915.
45. Gorris, H.H., S. Bade, N. Rockendorf, E. Albers, M.A. Schmidt, M. Franek, and A. Frey, *Rapid profiling of peptide stability in proteolytic environments*. *Anal. Chem.*, **2009** (81): 1580.
46. Terentyeva, T.G., W. Van Rossom, M. Van der Auweraer, K. Blank, and J. Hofkens, *Morpholinecarbonyl-Rhodamine 110 based substrates for the determination of protease activity with accurate kinetic parameters*. *Bioconjugate Chem.*, **2011** (22): 1932.
47. Nettels, D., I.V. Gopich, A. Hoffmann, and B. Schuler, *Ultrafast dynamics of protein collapse from single-molecule photon statistics*. *Proc. Natl. Acad. Sci. U. S. A.*, **2007** (104): 2655.
48. Talaga, D.S., W.L. Lau, H. Roder, J.Y. Tang, Y.W. Jia, W.F. DeGrado, and R.M. Hochstrasser, *Dynamics and folding of single two-stranded coiled-coil peptides studied by fluorescent energy transfer confocal microscopy*. *Proc. Natl. Acad. Sci. U. S. A.*, **2000** (97): 13021.
49. Ha, T., A.Y. Ting, J. Liang, W.B. Caldwell, A.A. Deniz, *et al.*, *Single-molecule fluorescence spectroscopy of enzyme conformational dynamics and cleavage mechanism*. *Proc. Natl. Acad. Sci. U. S. A.*, **1999** (96): 893.
50. Manley, S., J.M. Gillette, G.H. Patterson, H. Shroff, H.F. Hess, E. Betzig, and J. Lippincott-Schwartz, *High-density mapping of single-molecule trajectories with photoactivated localization microscopy*. *Nat. Methods*, **2008** (5): 155.
51. Zhao, Y.F., D. Terry, L. Shi, H. Weinstein, S.C. Blanchard, and J.A. Javitch, *Single-molecule dynamics of gating in a neurotransmitter transporter homologue*. *Nature*, **2010** (465): 188.
52. Schuler, B., E.A. Lipman, and W.A. Eaton, *Probing the free-energy surface for protein folding with single-molecule fluorescence spectroscopy*. *Nature*, **2002** (419): 743.
53. Merchant, K.A., R.B. Best, J.M. Louis, I.V. Gopich, and W.A. Eaton, *Characterizing the unfolded states of proteins using single-molecule FRET spectroscopy and molecular simulations*. *Proc. Natl. Acad. Sci. U. S. A.*, **2007** (104): 1528.
54. Hess, S.T., T.P. Girirajan, and M.D. Mason, *Ultra-high resolution imaging by fluorescence photoactivation localization microscopy*. *Biophys. J.*, **2006** (91): 4258.
55. Ritter, J.G., R. Veith, A. Veenendaal, J.P. Siebrasse, and U. Kubitscheck, *Light sheet microscopy for single molecule tracking in living tissue*. *PLoS One*, **2010** (5): e11639.
56. Wang, Q., R.H. Goldsmith, Y. Jiang, S.D. Bockenhauer, and W.E. Moerner, *Probing single biomolecules in solution using the anti-Brownian electrokinetic (ABEL) trap*. *Acc. Chem. Res.*, **2012** (45): 1955.

57. Uchihashi, T., R. Iino, T. Ando, and H. Noji, *High-speed atomic force microscopy reveals rotary catalysis of rotorless F(1)-ATPase*. *Science*, **2011** (333): 755.
58. Jones, S.A., S.H. Shim, J. He, and X. Zhuang, *Fast, three-dimensional super-resolution imaging of live cells*. *Nat. Methods*, **2011** (8): 499.
59. Bohmer, M. and J. Enderlein, *Fluorescence spectroscopy of single molecules under ambient conditions: methodology and technology*. *ChemPhysChem*, **2003** (4): 793.
60. Ishijima, A., H. Kojima, T. Funatsu, M. Tokunaga, H. Higuchi, H. Tanaka, and T. Yanagida, *Simultaneous observation of individual ATPase and mechanical events by a single myosin molecule during interaction with actin*. *Cell*, **1998** (92): 161.
61. Funatsu, T., Y. Harada, M. Tokunaga, K. Saito, and T. Yanagida, *Imaging of single fluorescent molecules and individual ATP turnovers by single myosin molecules in aqueous solution*. *Nature*, **1995** (374): 555.
62. Adachi, K., K. Oiwa, T. Nishizaka, S. Furuike, H. Noji, *et al.*, *Coupling of rotation and catalysis in F(1)-ATPase revealed by single-molecule imaging and manipulation*. *Cell*, **2007** (130): 309.
63. Hatzakis, N.S., H. Engelkamp, K. Velonia, J. Hofkens, P.C. Christianen, *et al.*, *Synthesis and single enzyme activity of a clicked lipase-BSA hetero-dimer*. *Chem. Commun.*, **2006**: 2012.
64. Edman, L., Z. Foldes-Papp, S. Wennmalm, and R. Rigler, *The fluctuating enzyme: a single molecule approach*. *Chem. Phys.*, **1999** (247): 11.
65. De Cremer, G., M.B. Roeffaers, M. Baruah, M. Sliwa, B.F. Sels, J. Hofkens, and D.E. De Vos, *Dynamic disorder and stepwise deactivation in a chymotrypsin catalyzed hydrolysis reaction*. *J. Am. Chem. Soc.*, **2007** (129): 15458.
66. Kuznetsova, S., G. Zauner, T.J. Aartsma, H. Engelkamp, N. Hatzakis, *et al.*, *The enzyme mechanism of nitrite reductase studied at single-molecule level*. *Proc. Natl. Acad. Sci. U. S. A.*, **2008** (105): 3250.
67. Terentyeva, T.G., H. Engelkamp, A.E. Rowan, T. Komatsuzaki, J. Hofkens, C.B. Li, and K. Blank, *Dynamic disorder in single-enzyme experiments: facts and artifacts*. *ACS Nano*, **2012** (6): 346.
68. Moerner, W.E. and D.P. Fromm, *Methods of single-molecule fluorescence spectroscopy and microscopy*. *Rev. Sci. Instrum.*, **2003** (74): 3597.
69. Huang, B., *Super-resolution optical microscopy: multiple choices*. *Curr. Opin. Chem. Biol.*, **2010** (14): 10.

70. Huang, B., M. Bates, and X. Zhuang, *Super-resolution fluorescence microscopy*. Annu. Rev. Biochem., **2009** (78): 993.
71. Chen, Q., R. Groote, H. Schonherr, and G.J. Vancso, *Probing single enzyme kinetics in real-time*. Chem. Soc. Rev., **2009** (38): 2671.
72. Roeffaers, M.B., G. De Cremer, H. Uji-i, B. Muls, B.F. Sels, *et al.*, *Single-molecule fluorescence spectroscopy in (bio)catalysis*. Proc. Natl. Acad. Sci. U. S. A., **2007** (104): 12603.
73. Blank, K., G. De Cremer, and J. Hofkens, *Fluorescence-based analysis of enzymes at the single-molecule level*. Biotechnol. J., **2009** (4): 465.
74. Holzmeister, P., G.P. Acuna, D. Grohmann, and P. Tinnefeld, *Breaking the concentration limit of optical single-molecule detection*. Chem. Soc. Rev., **2014** (43): 1014.
75. Craig, D.B. and N.J. Dovichi, *Escherichia coli beta-galactosidase is heterogeneous with respect to the activity of individual molecules*. Can. J. Chem., **1998** (76): 623.
76. Craig, D., E.A. Arriaga, P. Banks, Y. Zhang, A. Renborg, M.M. Palcic, and N.J. Dovichi, *Fluorescence-Based Enzymatic Assay by Capillary Electrophoresis Laser-Induced Fluorescence Detection for the Determination of a Few Beta-Galactosidase Molecules*. Anal. Biochem., **1995** (226): 147.
77. Craig, D.B., *Heterogeneous Properties of Individual Molecules of beta-Galactosidase from the Thermophilic Bacteria Geobacillus stearothermophilus*. Protein J., **2010** (29): 55.
78. Craig, D.B., *A simple system for the measurement of the distribution of activities of individual molecules of E. coli beta-galactosidase*. Anal. Method., **2012** (4): 85.
79. Craig, D.B., A.M. Haslam, J.M.L. Coombs, and E.R. Nichols, *Kinetic studies of unmodified individual Escherichia coil beta-galactosidase molecules in free solution*. Biochem. Cell Biol., **2010** (88): 451.
80. Craig, D.B. and A. Henderson, *Electrophoretic heterogeneity limits the utility of streptavidin-beta-galactosidase as a probe in free zone capillary electrophoresis separations*. Protein J., **2013** (32): 81.
81. Craig, D.B., T.T. Morris, and C.M.Q. Ong-Justiniano, *Measurement of the Activity of Individual Subunits of Single Molecules of the Tetrameric Enzyme beta-Galactosidase*. Anal. Chem., **2012** (84): 4598.
82. Craig, D.B., T. Schwab, and R. Sterner, *Random mutagenesis suggests that sequence errors are not a major cause of variation in the activity of individual molecules of beta-galactosidase*. Biochem. Cell Biol., **2012** (90): 540.

83. Whisnant, A.R. and S.D. Gilman, *Studies of reversible inhibition, irreversible inhibition, and activation of alkaline phosphatase by capillary electrophoresis*. Anal. Biochem., **2002** (307): 226.
84. Margulies, M., M. Egholm, W.E. Altman, S. Attiya, J.S. Bader, *et al.*, *Genome sequencing in microfabricated high-density picolitre reactors*. Nature, **2005** (437): 376.
85. Mazutis, L., A.F. Araghi, O.J. Miller, J.C. Baret, L. Frenz, *et al.*, *Droplet-Based Microfluidic Systems for High-Throughput Single DNA Molecule Isothermal Amplification and Analysis*. Anal. Chem., **2009** (81): 4813.
86. Mazutis, L., J.C. Baret, P. Treacy, Y. Skhiri, A.F. Araghi, *et al.*, *Multi-step microfluidic droplet processing: kinetic analysis of an in vitro translated enzyme*. Lab Chip, **2009** (9): 2902.
87. Nakano, M., J. Komatsu, S. Matsuura, K. Takashima, S. Katsura, and A. Mizuno, *Single-molecule PCR using water-in-oil emulsion*. J. Biotechnol., **2003** (102): 117.
88. Sakakihara, S., S. Araki, R. Iino, and H. Noji, *A single-molecule enzymatic assay in a directly accessible femtoliter droplet array*. Lab Chip, **2010** (10): 3355.
89. Pekin, D., Y. Skhiri, J.C. Baret, D. Le Corre, L. Mazutis, *et al.*, *Quantitative and sensitive detection of rare mutations using droplet-based microfluidics*. Lab Chip, **2011** (11): 2156.
90. Kiss, M.M., L. Ortoleva-Donnelly, N.R. Beer, J. Warner, C.G. Bailey, *et al.*, *High-Throughput Quantitative Polymerase Chain Reaction in Picoliter Droplets*. Anal. Chem., **2008** (80): 8975.
91. Shim, J.U., R.T. Ranasinghe, C.A. Smith, S.M. Ibrahim, F. Hollfelder, *et al.*, *Ultraprapid generation of femtoliter microfluidic droplets for single-molecule-counting immunoassays*. ACS Nano, **2013** (7): 5955.
92. Becher, P., *Emulsions: Theory and Practice*. 3rd ed (**2001**): American Chemical Society.
93. Rhoades, E., E. Gussakovskiy, and G. Haran, *Watching proteins fold one molecule at a time*. Proc. Natl. Acad. Sci. U. S. A., **2003** (100): 3197.
94. Piwonski, H.M., M. Goomanovsky, D. Bensimon, A. Horovitz, and G. Haran, *Allosteric inhibition of individual enzyme molecules trapped in lipid vesicles*. Proc. Natl. Acad. Sci. U. S. A., **2012** (109): E1437.
95. Boukobza, E., A. Sonnenfeld, and G. Haran, *Immobilization in surface-tethered lipid vesicles as a new tool for single biomolecule spectroscopy*. J. Phys. Chem. B, **2001** (105): 12165.
96. Jesorka, A. and O. Orwar, *Liposomes: Technologies and Analytical Applications*. Annu. Rev. Anal. Chem., **2008** (1): 801.

97. Hsin, T.M. and E.S. Yeung, *Single-molecule reactions in liposomes*. *Angew. Chem. Int. Ed.*, **2007** (46): 8032.
98. Comellas-Aragones, M., H. Engelkamp, V.I. Claessen, N.A. Sommerdijk, A.E. Rowan, *et al.*, *A virus-based single-enzyme nanoreactor*. *Nat. Nanotechnol.*, **2007** (2): 635.
99. Comellas-Aragones, M., A. de la Escosura, A.J. Dirks, A. van der Ham, A. Fuste-Cune, J.J.L.M. Cornelissen, and R.J.M. Nolte, *Controlled Integration of Polymers into Viral Capsids*. *Biomacromolecules*, **2009** (10): 3141.
100. de la Escosura, A., R.J.M. Nolte, and J.J.L.M. Cornelissen, *Viruses and protein cages as nanocontainers and nanoreactors*. *J Mater Chem*, **2009** (19): 2274.
101. Xie, X.S., J. Yu, and W.Y. Yang, *Perspective - Living cells as test tubes*. *Science*, **2006** (312): 228.
102. Xie, X.S., P.J. Choi, G.W. Li, N.K. Lee, and G. Lia, *Single-molecule approach to molecular biology in living bacterial cells*. *Annu. Rev. Biophys.*, **2008** (37): 417.
103. Golding, I., J. Paulsson, S.M. Zawilski, and E.C. Cox, *Real-time kinetics of gene activity in individual bacteria*. *Cell*, **2005** (123): 1025.
104. Lemon, K.P. and A.D. Grossman, *Localization of bacterial DNA polymerase: evidence for a factory model of replication*. *Science*, **1998** (282): 1516.
105. Gorris, H.H. and D.R. Walt, *Analytical chemistry on the femtoliter scale*. *Angew. Chem. Int. Ed.*, **2010** (49): 3880.
106. Gorris, H.H. and D.R. Walt, *Analytische Chemie im Femtoliter*. *Angew. Chem.*, **2010** (122): 3970.
107. Walt, D.R., *Protein measurements in microwells*. *Lab Chip*, **2014** (14): 3195.
108. Walt, D.R., *Fibre optic microarrays*. *Chem. Soc. Rev.*, **2010** (39): 38.
109. Gorris, H.H., T.M. Blicharz, and D.R. Walt, *Optical-fiber bundles*. *FEBS J.*, **2007** (274): 5462.
110. Tan, W.H. and E.S. Yeung, *Monitoring the reactions of single enzyme molecules and single metal ions*. *Anal. Chem.*, **1997** (69): 4242.
111. Shoemaker, G.K., D.H. Juers, J.M. Coombs, B.W. Matthews, and D.B. Craig, *Crystallization of beta-galactosidase does not reduce the range of activity of individual molecules*. *Biochemistry*, **2003** (42): 1707.

112. Rojek, M.J. and D.R. Walt, *Observing single enzyme molecules interconvert between activity states upon heating*. PLoS One, **2014** (9): e86224.
113. Gorris, H.H. and D.R. Walt, *Mechanistic aspects of horseradish peroxidase elucidated through single-molecule studies*. J. Am. Chem. Soc., **2009** (131): 6277.
114. Heyries, K.A., C. Tropini, M. Vaninsberghe, C. Doolin, O.I. Petriv, *et al.*, *Megapixel digital PCR*. Nat. Methods, **2011** (8): 649.
115. Rondelez, Y., G. Tresset, K.V. Tabata, H. Arata, H. Fujita, S. Takeuchi, and H. Noji, *Microfabricated arrays of femtoliter chambers allow single molecule enzymology*. Nat. Biotechnol., **2005** (23): 361.
116. Shon, M.J. and A.E. Cohen, *Mass action at the single-molecule level*. J. Am. Chem. Soc., **2012** (134): 14618.
117. Zhang, H., S. Nie, C.M. Etson, R.M. Wang, and D.R. Walt, *Oil-sealed femtoliter fiber-optic arrays for single molecule analysis*. Lab Chip, **2012** (12): 2229.
118. Rissin, D.M. and D.R. Walt, *Digital concentration readout of single enzyme molecules using femtoliter arrays and Poisson statistics*. Nano Lett., **2006** (6): 520.
119. Ekins, R. and D. Kelso, *Single-molecule ELISA*. Clin. Chem., **2011** (57): 372.
120. Rissin, D.M. and D.R. Walt, *Duplexed sandwich immunoassays on a fiber-optic microarray*. Anal. Chim. Acta, **2006** (564): 34.
121. Li, Z., R.B. Hayman, and D.R. Walt, *Detection of single-molecule DNA hybridization using enzymatic amplification in an array of femtoliter-sized reaction vessels*. J. Am. Chem. Soc., **2008** (130): 12622.
122. Rissin, D.M., C.W. Kan, T.G. Campbell, S.C. Howes, D.R. Fournier, *et al.*, *Single-molecule enzyme-linked immunosorbent assay detects serum proteins at subfemtomolar concentrations*. Nat. Biotechnol., **2010** (28): 595.
123. Wilson, D.H., D.W. Hanlon, G.K. Provuncher, L. Chang, L. Song, *et al.*, *Fifth-generation digital immunoassay for prostate-specific antigen by single molecule array technology*. Clin. Chem., **2011** (57): 1712.
124. Song, L., D.W. Hanlon, L. Chang, G.K. Provuncher, C.W. Kan, *et al.*, *Single molecule measurements of tumor necrosis factor alpha and interleukin-6 in the plasma of patients with Crohn's disease*. J. Immunol. Methods, **2011** (372): 177.

125. Rissin, D.M., D.R. Fournier, T. Piech, C.W. Kan, T.G. Campbell, *et al.*, *Simultaneous Detection of Single Molecules and Singulated Ensembles of Molecules Enables Immunoassays with Broad Dynamic Range*. *Anal. Chem.*, **2011** (83): 2279.
126. Kan, C.W., A.J. Rivnak, T.G. Campbell, T. Piech, D.M. Rissin, *et al.*, *Isolation and detection of single molecules on paramagnetic beads using sequential fluid flows in microfabricated polymer array assemblies*. *Lab Chip*, **2012** (12): 977.
127. Rissin, D.M., C.W. Kan, L. Song, A.J. Rivnak, M.W. Fishburn, *et al.*, *Multiplexed single molecule immunoassays*. *Lab Chip*, **2013** (13): 2902.
128. Song, L.N., S. Ahn, and D.R. Walt, *Fiber-optic microsphere-based arrays for multiplexed biological warfare agent detection*. *Anal. Chem.*, **2006** (78): 1023.
129. Ahn, S., D.M. Kulis, D.L. Erdner, D.M. Anderson, and D.R. Walt, *Fiber-optic microarray for simultaneous detection of multiple harmful algal bloom species*. *Appl. Environ. Microbiol.*, **2006** (72): 5742.
130. Ahn, S. and D.R. Walt, *Detection of Salmonella spp. using microsphere-based, fiber-optic DNA microarrays*. *Anal. Chem.*, **2005** (77): 5041.
131. Whitaker, R.D. and D.R. Walt, *Fiber-based single cell analysis of reporter gene expression in yeast two-hybrid systems*. *Anal. Biochem.*, **2007** (360): 63.
132. Biran, I., D.M. Rissin, E.Z. Ron, and D.R. Walt, *Optical imaging fiber-based live bacterial cell array biosensor*. *Anal. Biochem.*, **2003** (315): 106.
133. Kuang, Y., I. Biran, and D.R. Walt, *Living bacterial cell array for genotoxin monitoring*. *Anal. Chem.*, **2004** (76): 2902.
134. Kuang, Y., I. Biran, and D.R. Walt, *Simultaneously monitoring gene expression kinetics and genetic noise in single cells by optical well arrays*. *Anal. Chem.*, **2004** (76): 6282.
135. Whitaker, R.D. and D.R. Walt, *Multianalyte single-cell analysis with multiple cell lines using a fiber-optic array*. *Anal. Chem.*, **2007** (79): 9045.
136. Taylor, L.C. and D.R. Walt, *Application of high-density optical microwell arrays in a live-cell biosensing system*. *Anal. Biochem.*, **2000** (278): 132.
137. Vajrala, V.S., E. Suraniti, P. Garrigue, B. Goudeau, M. Rigoulet, *et al.*, *Optical microwell array for large scale studies of single mitochondria metabolic responses*. *Anal. Bioanal. Chem.*, **2014** (406): 931.
138. Xia, Y.N. and G.M. Whitesides, *Soft lithography*. *Annu. Rev. Mater. Sci.*, **1998** (28): 153.

139. Xia, Y.N. and G.M. Whitesides, *Soft lithography*. *Angew. Chem. Int. Ed.*, **1998** (37): 551.
140. Rettig, J.R. and A. Folch, *Large-scale single-cell trapping and imaging using microwell arrays*. *Anal. Chem.*, **2005** (77): 5628.
141. Sasuga, Y., T. Iwasawa, K. Terada, Y. Oe, H. Sorimachi, O. Ohara, and Y. Harada, *Single-cell chemical lysis method for analyses of intracellular molecules using an array of picoliter-scale microwells*. *Anal. Chem.*, **2008** (80): 9141.
142. Rondelez, Y., G. Tresset, T. Nakashima, Y. Kato-Yamada, H. Fujita, S. Takeuchi, and H. Noji, *Highly coupled ATP synthesis by F1-ATPase single molecules*. *Nature*, **2005** (433): 773.
143. Iino, R., Y. Rondelez, M. Yoshida, and H. Noji, *Chemomechanical coupling in single-molecule F-type ATP synthase*. *J. Bioenerg. Biomembr.*, **2005** (37): 451.
144. Iino, R. and H. Noji, *F1-ATPase: a highly coupled reversible rotary motor*. *Biochem. Soc. Trans.*, **2006** (34): 993.
145. Okuno, D., R. Iino, and H. Noji, *Rotation and structure of FoF1-ATP synthase*. *J. Biochem.*, **2011** (149): 655.
146. Arata, H.F., Y. Rondelez, H. Noji, and H. Fujita, *Temperature alternation by an on-chip microheater to reveal enzymatic activity of beta-galactosidase at high temperatures*. *Anal. Chem.*, **2005** (77): 4810.
147. Chen, A.Y., A.S. Jani, L. Zheng, P.J. Burke, and J.P. Brody, *Microfabricated arrays of cylindrical wells facilitate single-molecule enzymology of alpha-chymotrypsin*. *Biotechnol. Prog.*, **2009** (25): 929.
148. Jung, S.Y., Y. Liu, and C.P. Collier, *Fast mixing and reaction initiation control of single-enzyme kinetics in confined volumes*. *Langmuir*, **2008** (24): 4439.
149. Ota, S., H. Kitagawa, and S. Takeuchi, *Generation of femtoliter reactor arrays within a microfluidic channel for biochemical analysis*. *Anal. Chem.*, **2012** (84): 6346.
150. Fowlkes, J.D. and C.P. Collier, *Single-molecule mobility in confined and crowded femtolitre chambers*. *Lab Chip*, **2013** (13): 877.
151. Gates, B.D., Q. Xu, M. Stewart, D. Ryan, C.G. Willson, and G.M. Whitesides, *New approaches to nanofabrication: molding, printing, and other techniques*. *Chem. Rev.*, **2005** (105): 1171.
152. Gau, H., S. Herminghaus, P. Lenz, and R. Lipowsky, *Liquid morphologies on structured surfaces: From microchannels to microchips*. *Science*, **1999** (283): 46.

153. Lenz, P. and R. Lipowsky, *Morphological transitions of wetting layers on structured surfaces*. Phys. Rev. Lett., **1998** (80): 1920.
154. Ehrl, B.N., R.B. Liebherr, and H.H. Gorris, *Single molecule kinetics of horseradish peroxidase exposed in large arrays of femtoliter-sized fused silica chambers*. Analyst, **2013** (138): 4260.
155. Iino, R., K. Hayama, H. Amezawa, S. Sakakihara, S.H. Kim, *et al.*, *A single-cell drug efflux assay in bacteria by using a directly accessible femtoliter droplet array*. Lab Chip, **2012** (12): 3923.
156. Iino, R., Y. Matsumoto, K. Nishino, A. Yamaguchi, and H. Noji, *Design of a large-scale femtoliter droplet array for single-cell analysis of drug-tolerant and drug-resistant bacteria*. Front. Microbiol., **2013** (4): 300.
157. LaFratta, C.N. and D.R. Walt, *Very high density sensing arrays*. Chem. Rev., **2008** (108): 614.
158. Collier, C.P. and M.L. Simpson, *Micro/nanofabricated environments for synthetic biology*. Curr. Opin. Biotechnol., **2011** (22): 516.
159. Claessen, V.I., H. Engelkamp, P.C. Christianen, J.C. Maan, R.J. Nolte, K. Blank, and A.E. Rowan, *Single-biomolecule kinetics: the art of studying a single enzyme*. Annu. Rev. Anal. Chem., **2010** (3): 319.
160. Rissin, D.M., D.R. Walt, and H.H. Gorris, *Methods and arrays for target analyte detection and determination of target analyte concentration in solution*. Tufts College USA (**2007**), Patent WO 2007/098148-A3.

2. Design and Development of Femtoliter Arrays for the Highly Parallel Analysis of Single Enzyme Molecules

This chapter is based upon the Journal Article "*Three-in-one enzyme assay based on single molecule detection in femtoliter arrays*", Liebherr R.B., A. Hutterer, M.J. Mickert, F.C. Vogl, A. Beutner, A. Lechner, H. Hummel and H.H. Gorris, **2015**, submitted.

2.1 Introduction

A profound insight into biochemical processes requires experimental settings that are comparable in size to the elementary structures of life. An *Escherichia coli* bacterial cell, for example, defines a volume of $1 \mu\text{m}^3$ (which equates 1 femtoliter). [1] The development of new technologies that enable investigation in femtoliter-sized volumes promotes our quest for an extensive comprehension of fundamental biochemical principles.

To date, varying forms of ultra-small reaction chambers such as lipid vesicles and liposomes, [2-5] virus capsids [6-8], droplets of water-in-oil emulsions [9-15] or even whole cells [16-18] have been applied for the isolation and investigation of single biomolecules (chapter 1.3). These self-assembled micro-vessels for single molecule enzymology can adopt variable sizes and usually need to be surface immobilized for long-time monitoring. In contrast, the systematic structuring of smooth surfaces with help of modern microfabrication techniques enables the generation of large arrays of thousands of reaction chambers with uniform size and defined position. Spatial confinement of individual enzyme molecules in the wells of such femtoliter arrays renders an artificial surface-immobilization superfluous. Thus, possible negative side

effects such as steric hindrance, partial inactivation or disturbance of the original enzyme activity are avoided.

For single molecule analysis the highly diluted enzyme solution is combined with an excess of a fluorogenic substrate and enclosed in the array. After loading, the wells are sealed thoroughly using a quartz coverslip, [19, 20] a PDMS seal, [21, 22] a droplet of oil [23] or a valve system. [24, 25] The enzyme activity is then investigated by monitoring the increase in fluorescent product concentration over time. Within the small dimensions of a femtoliter well, a single enzyme molecule can generate a high local concentration of fluorescent product, sufficient to exceed the limit of detection. The femtoliter wells are arranged in very high density arrays. Thus, thousands of individual molecules can be observed in parallel, enabling the analysis of a statistically representative enzyme population.

In our group we work with two different, complementary setups for single enzyme molecule investigation: The femtoliter arrays are fabricated either in fused silica slides or in poly(dimethylsiloxane) (PDMS) respectively and consist of 62 500 uniform reaction chambers that define a volume of approximately 40 femtoliter. In this chapter, the design and development of the two types of femtoliter arrays is presented. The gradual improvement of the experimental setup, regarding aspects such as array sealing, photobleaching, non-specific protein adsorption and signal readout, is discussed in detail.

Subsequently, the applicability of the two complementary femtoliter array systems, fabricated in fused silica or PDMS respectively, for single enzyme molecule analysis is evaluated. For this purpose, several hundred individual molecules of β -galactosidase were isolated in the femtoliter arrays and the individual substrate turnover rates investigated by fluorescence microscopy. Single enzyme measurements were

performed in both types of femtoliter arrays to verify the efficiency of the optimized detection schemes. The obtained results were compared and checked against previous reports. Besides, the two complementary array systems were contrasted to identify the benefits and drawbacks of the respective detection schemes regarding single molecule enzymology.

2.2 Results and Discussion

2.2.1 Femtoliter Array Microfabrication and Characterization

The femtoliter arrays were either fabricated in the surface of fused silica slides by photolithography and reactive ion etching or molded in PDMS. The feature structures of both types of femtoliter arrays were defined by a photolithographic chrome mask.

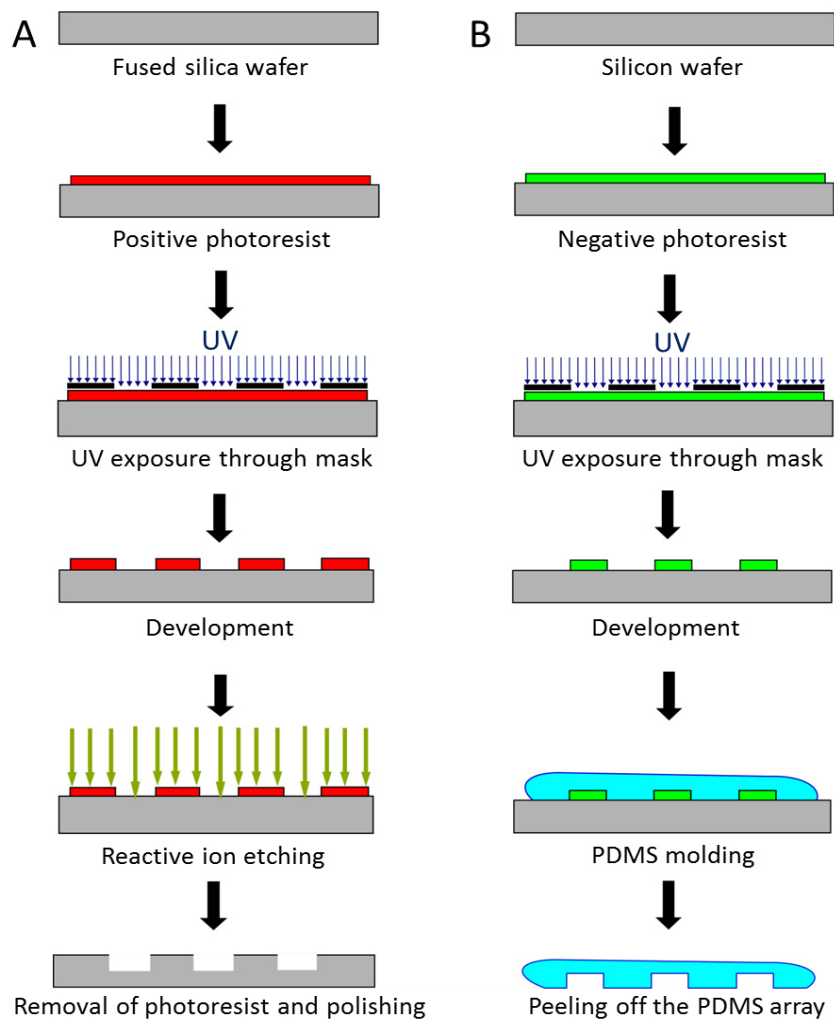


Figure 2.1 Schematic view of the femtoliter array fabrication process. Femtoliter arrays were either generated in the surface of fused silica slides by photolithography and reactive ion etching (A) or molded in PDMS using a silicon master template (B).

For fused silica array fabrication (Figure 2.1 A), a highly thermostable, positive photoresist was applied. A clean fused silica wafer was covered with the photoresist by spin-coating and the chrome mask was vacuum contacted to the wafer. The photolithographic mask design was transferred to the positive resist by casting UV light through the photomask. Subsequently, the wafer was subjected to reactive ion etching to structure the fused silica surface. Finally, the remaining photoresist was removed in a multiple step cleaning procedure. On one four inch wafer, 21 homogeneous arrays with an edge length of 2.5 x 2.5 mm, positioned in the middle of 15 x 15 mm glass slides, were generated in parallel (layout of the photolithographic chrome mask in the Appendix, Figure 7.1.1). PDMS femtoliter arrays were generated by replica molding (Figure 2.1 B). For fabrication of the master template, a negative SU-8 photoresist was spin-coated on a silicon wafer. The photolithographic mask was vacuum-contacted to the wafer and exposed to UV light. The non-crosslinked parts of the photoresist were removed and the wafer was cleaned thoroughly. For replica molding liquid PDMS was cast onto the master template and cured to complete dryness. One structured PDMS foil consisted of 21 homogeneous femtoliter arrays that were cut-out just prior to application. (A detailed protocol for the preparation of fused silica and PDMS femtoliter arrays can be found in chapter 2.3.1 "Femtoliter Array Microfabrication and Characterization").

Each femtoliter array etched into fused silica or molded in PDMS respectively, consists of 62 500 cylindrical microwells that are arranged homogeneously in a rectangular lattice with a pitch of 10 μm , resulting in an overall edge length of 2.5 x 2.5 mm². The exact feature sizes of the femtoliter arrays were confirmed using a profilometer and scanning electron microscopy (SEM) (Figure 2.2).

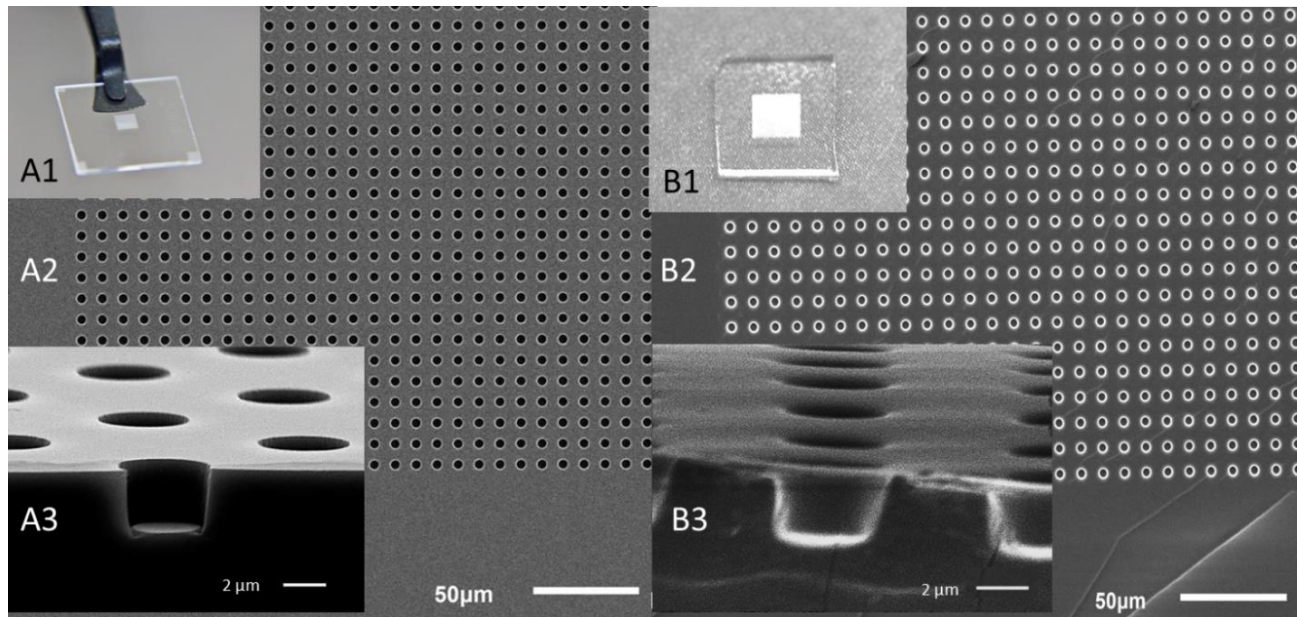


Figure 2.2 Arrays of homogeneously arranged microwells fabricated in the surface of fused silica slides by photolithography and reactive ion etching (A) or molded in PDMS (B). (A1/B1) Photograph of the femtoliter array embedded in the center of a fused silica slide (A1) or molded in PDMS (B1). (A2/B2) The Scanning electron microscopy image depicts a large section of the array demonstrating the homogenous arrangement of the 62 500 femtoliter wells. (A3) The side view of the array focuses on one of the cylindrical reaction chambers with a diameter of about $4 \mu\text{m}$ and a depth of approximately $3.5 \mu\text{m}$, defining a volume of about $40 \mu\text{m}^3$. (B3) The side view of the array shows the shape of a well that defines the identical physical dimensions as the reaction chambers of the fused silica array.

The anisotropic dry etching process of the fused silica slide yielded cylindrical wells with a steep sidewall profile ($> 88^\circ$). Each reaction chamber had a mean diameter of $4.0 \pm 0.2 \mu\text{m}$ and a well-defined depth of $3.5 \pm 0.1 \mu\text{m}$ (mean and standard deviation) across the entire wafer area, whereas the standard deviation was slightly higher ($\pm 0.3 \mu\text{m}$) on the wafer edges.

The strength of the SU-8 layer on the master template was determined by profilometry, prior to PDMS-array casting. The average height of the cylindrical posts

was $3.65 \pm 0.1 \mu\text{m}$ over the entire wafer surface. After fabrication of the master template identical wafers of 21 femtoliter arrays were generated by replica molding. Finally, the dimensions of the PDMS arrays were confirmed by SEM. With a diameter of about $4 \mu\text{m}$ and a depth of approximately $3.5 \mu\text{m}$ both types of femtoliter arrays define a well volume of approximately 40 fL.

2.2.2 Optimization of the Single Molecule Detection Platform

For single β -galactosidase measurements the femtoliter array was mounted on a custom-built array holder that ensured a thorough sealing of the individual wells (Figure 2.3). A tight array sealing is essential to prevent leakage or fluorescent product out of the wells and enable an accurate calculation of the single enzyme molecule substrate turnover rates.

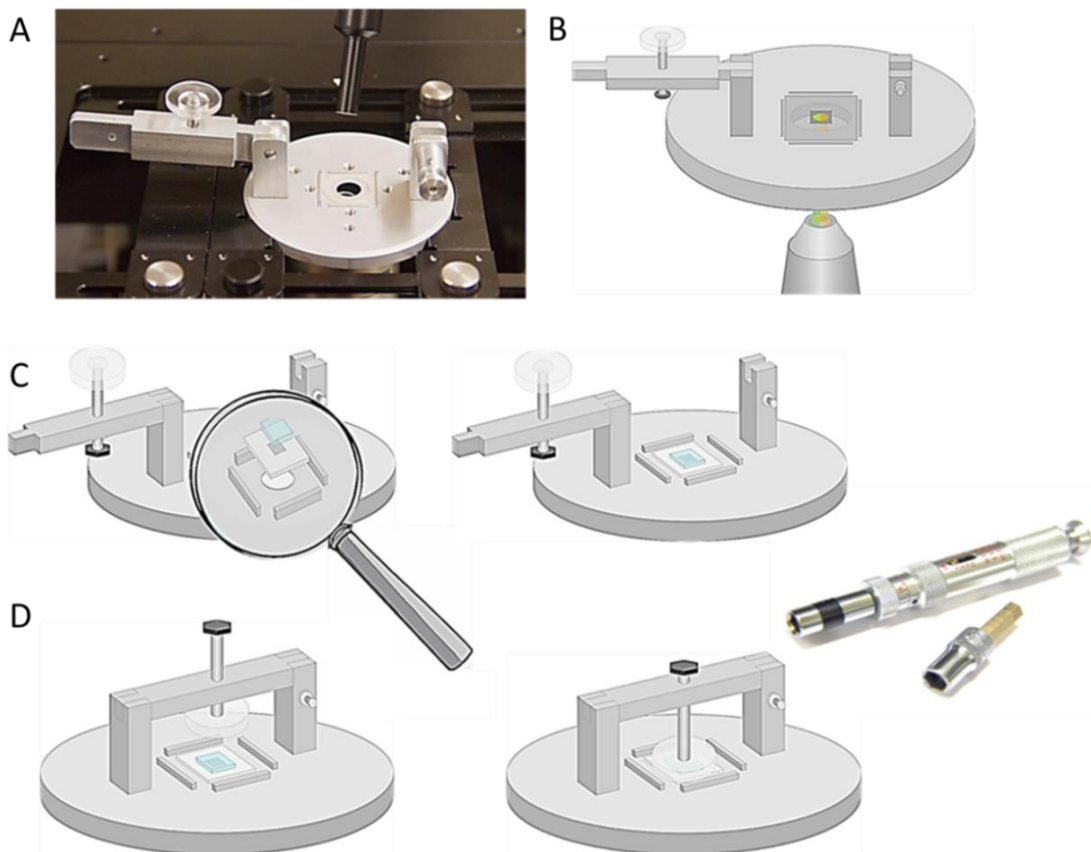


Figure 2.3 Femtoliter array positioning and sealing using the example of the fused silica array. (A) Photograph of the custom-built microscope mount (B) The array-holder foundation is a circular plate with centric frames that position the array centrally over the objective. (C) After loading, the array is covered with a thin PDMS gasket. (D) The reaction chambers are tightly sealed by pressure application. To ensure good reproducibility of array sealing a defined torque is transmitted on the PDMS seal using a torque screw driver.

The foundation of the array holder is a circular aluminum plate with a frame (15 x 15 mm) in the center to position the glass slide with the femtoliter array centrally over the objective of an inverted fluorescence microscope (Figure 2.3 B). A stamp, held by a screw which is inserted in a cantilever, is locked centrally over the femtoliter array (Figure 2.3 D). The cylindrical stamp consists of two parts. The larger upper part serves as a spacer, while the smaller part transmits mechanical pressure. A diameter of 5 mm proved to be the optimal sized for pressure transfer, ensuring tight array sealing at a minimum chip breaking rate.

Once the cantilever was locked, a defined pressure was applied to the sealed array using a torque screw driver. The crucial point in pressure application was to adjust the applied torque to a degree, where a thorough array sealing could be guaranteed without the threat of crushing the delicate glass slide. For tight sealing of fused silica femtoliter arrays a torque of 2.8 ± 0.1 cNm was applied.

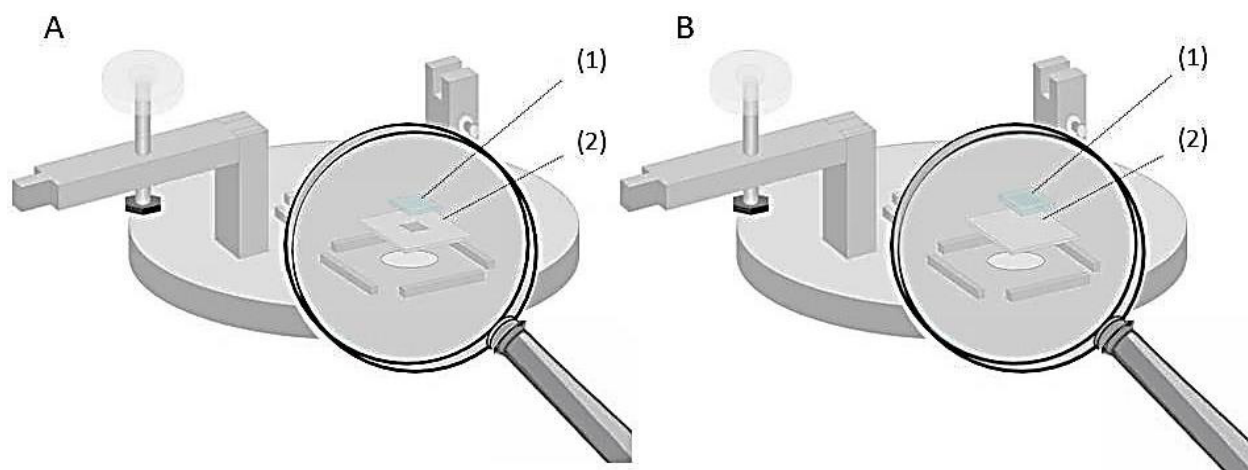


Figure 2.4 Schematic representation of the complementary experimental setups. (A) Measurement in fused silica arrays: The enzyme/substrate mixture is pipetted on the array (1). Suspending liquid is removed and the array is sealed with a PDMS gasket (2). (B) Measurement in PDMS arrays: The enzyme/substrate mixture is pipetted on the array which is located on the stamp (1). When the stamp is closed, the PDMS array is positioned centrally over the objective on top of a glass coverslip (2).

For single enzyme molecule measurements in PDMS femtoliter arrays the experimental settings had to be adjusted accordingly (Figure 2.4 B). Prior to the experiment a thin glass coverslip was positioned in the frames of the circular foundation plate. Subsequently, the reactive enzyme solution was pipetted onto the PDMS array, which was located - array-side up - on the stamp of the microscope mount. When the cantilever was closed, the stamp positioned the array centrally over the objective of the fluorescence microscope, on top the glass coverslip. The system was again sealed tightly by pressure application with a torque screw driver. The torque applied for experiments in PDMS femtoliter arrays was 3.5 ± 0.2 cNm.

The basic features of the array holder were developed by Franziska Vogl in the scope of her master's thesis. [26] The design was further optimized and refined in the course of this PhD thesis. The final settings of the microscope mount allow for tightly sealed, reproducible single enzyme molecule measurements at low chip-breaking rates.

Single enzyme molecule analysis in femtoliter arrays requires the consideration of several technical demands. [24] Some of the most important issues are an efficient suppression of background fluorescence and photobleaching, the avoidance of substrate depletion, the combination of a highly parallel readout scheme with a high resolution, the verification of a tight array sealing and the prevention of non-specific biomolecule adsorption to array or gasket. After addressing each of the named challenges an optimized experimental setup should be attained.

Background Fluorescence. An effective single molecule readout scheme requires the spectral separation of fluorescence signal from background noise. A consistent low background signal can only be obtained by using an adequate fluorogenic substrate with a low fluorescence signal and a slow auto-hydrolysis rate. For single β -galactosidase analysis the fluorogenic substrate resorufin- β -D-galactopyranoside (RGP) was applied.

Due to autohydrolysis of RGP [27] about 10 000 resorufin molecules (0.5 % of the total RGP concentration) are present in each chamber prior to analysis. Apart from the intrinsic fluorescence intensity, RGP shows a low substrate auto-hydrolysis rate. Thus the background signal was constant in chambers containing no enzyme and could be well separated from the product formation of individual enzyme molecules (Figure 2.9).

Photobleaching. Photobleaching was minimized by reducing the intensity of the excitation light (ND filter 8) and adapting the exposure time (200 ms) accordingly. To monitor the photobleaching rate, a solution of 5 μM resorufin (fluorescent product of the enzyme reaction) was enclosed in the wells of the femtoliter array and its fluorescence intensity recorded over time.

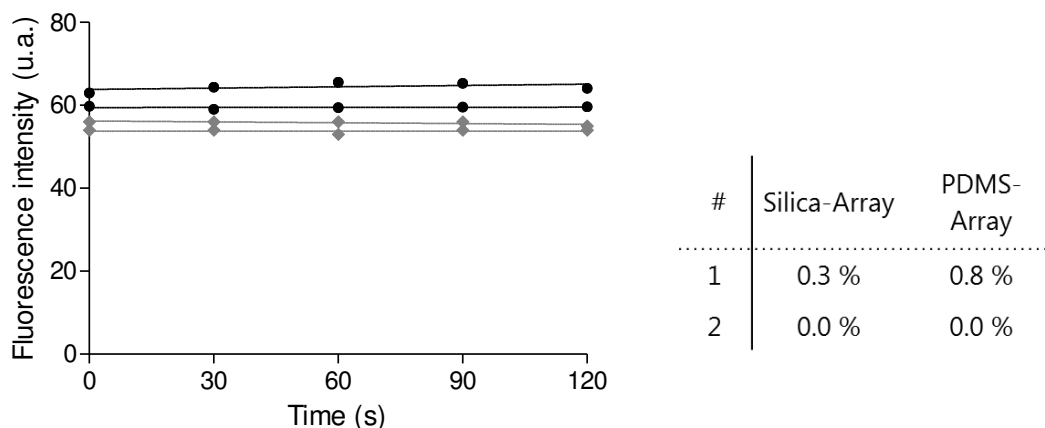


Figure 2.5 Photobleaching recorded over a time course of 120 seconds in the wells of a fused silica (black) and PDMS (grey) femtoliter array. The experiment was performed twice in both array types. For this purpose, a solution of 5 μM resorufin in PBS was enclosed in the wells of the respective array. Images were taken every 30 seconds. Subsequently, the average fluorescence intensity of 20 randomly picked wells was plotted against time.

During the first 120 seconds the recorded fluorescence signal decreased by less than 1.0 % for experiments in fused silica as well as PDMS femtoliter arrays, thus superseding the correction of the single molecules time traces for photobleaching (Figure 2.5).

Substrate Depletion. In femtoliter arrays, each well defines the same volume, thus confines the same amount of substrate. The lowest substrate concentration employed in single β -galactosidase measurements was 25 μM which is about 10^7 -fold higher than the applied enzyme concentration of 1.8 pM. A concentration of 25 μM is equivalent to a number of approximately 600 000 substrate molecules in a volume of 40 fL. The average turnover rate of a single β -galactosidase molecule, determined in fused silica arrays at a substrate concentration of 25 μM , was 165 s^{-1} (Figure 2.11). Consequently, less than 4 % of RGP is consumed over a time course of 120 s. For this reason, a constant substrate concentration can be assumed over the course of a single β -galactosidase experiment, lasting 120 seconds or less.

Highly Parallel Readout Scheme at High Resolution. The application of a 20x objective with a numerical aperture of 0.75 enabled the monitoring of a high number of reaction chambers in parallel, in combination with a relatively high resolution. Within the small dimensions of a fL-sized reaction chamber a single enzyme molecule can generate a high local concentration of fluorescent product, sufficient to pass the detection limit of a sensitive camera. For the simultaneous observation of many individual enzyme molecules, a camera is required that combines a high resolution with a high dynamic range. Modern sCMOS (scientific complementary metal oxide semiconductor) cameras offer high sensitivity, dynamic range and resolution at a comparatively low price [21, 28, 29] and thus were the ideal choice for our system.

Tight Array Sealing. Tight array sealing is essential to enable the accurate calculation of single enzyme molecule turnover rates. To guarantee a complete and secure enclosure of enzyme, substrate and fluorescent product in individual wells, a high pressure had to be applied on the fragile glass array (Figure 2.3). An alternative sealing method was investigated that should enable tight array sealing at reduced pressure: Shon *et al.* [24] proposed the application of a PDMS lid with post topography to improve

array sealing. Immediately after sealing, a thin aqueous film can develop between the fused silica surface and the smooth PDMS gasket. This film enables molecule-escape from the femtoliter wells. By introducing a topographic structure on the PDMS gasket, this film can be drained, facilitating tight array sealing. PDMS-gaskets with integrated topography (Topography structure in the Appendix, Figure 7.1.3) were applied to seal fused silica arrays. The quality of the single molecule experiment with respect to product leakage, in dependency of the applied pressure, was estimated and compared to experiments performed with smooth PMDS gaskets (Figure 2.6).

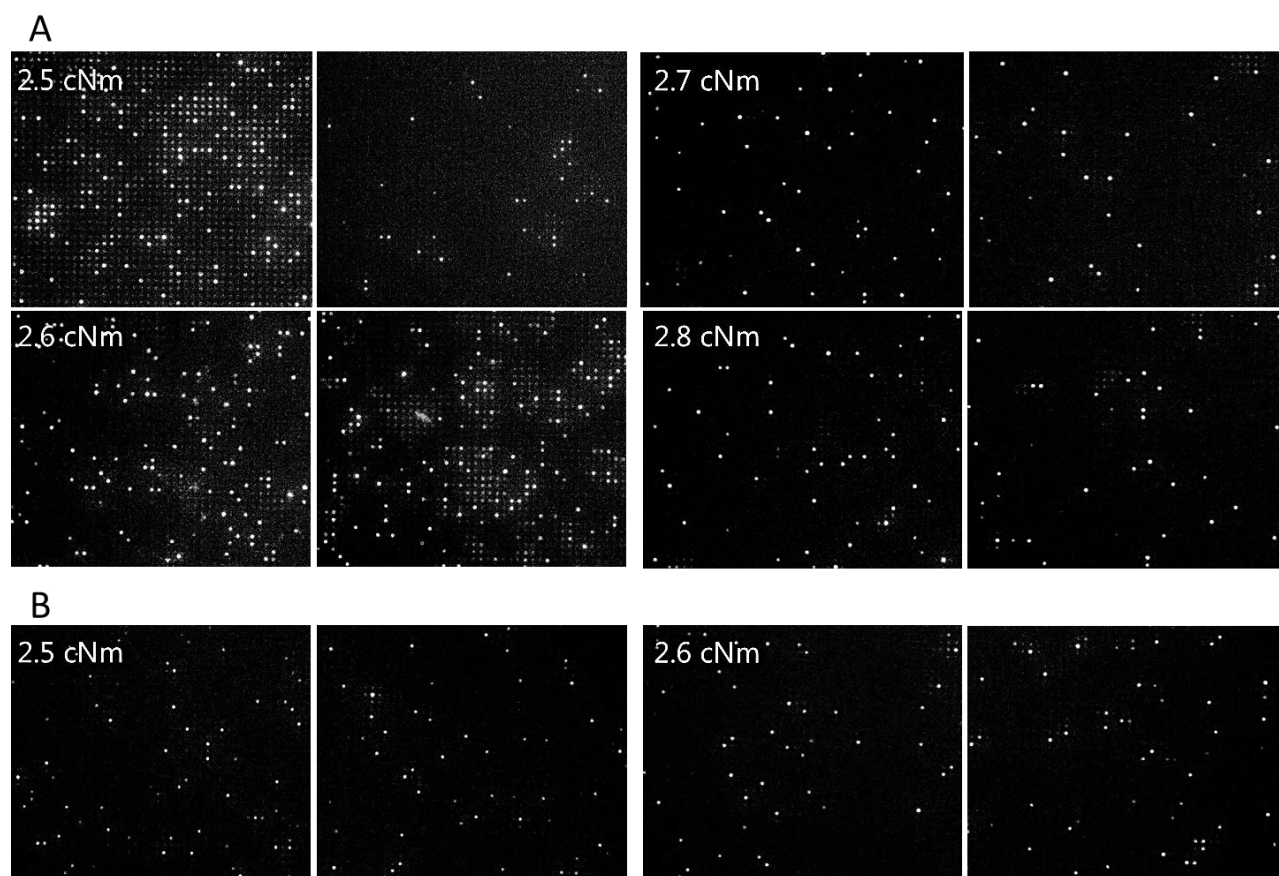


Figure 2.6 Quality of single molecule experiments with respect to fluorescent product leakage, in dependency of the applied pressure for measurements with smooth PDMS gaskets (A) and PDMS gaskets with integrated topography (B).

The application of structured PDMS-lids, allowed for tight array sealing at slightly lower pressure (2.5 - 2.6 cNm) in comparison to smooth PDMS lids (2.7 - 2.8 cNm). Fused silica femtoliter arrays, however, in general did withstand applied pressures of up to 2.9 or even 3.0 cNm. Consequently, as the reproducible fabrication of the structured PDMS gaskets was rather elaborate, whereas the difference in required torque was quite small, smooth PDMS gaskets were further applied for array sealing.

Non-specific Adsorption. Biomolecules in general and proteins in particular easily adsorb to hydrophobic surfaces such as PDMS. [30] Rissin and coworkers demonstrated that non-specific adsorption is an issue in single molecule analysis, when applying unblocked arrays. [31] In order to prevent non-specific protein adsorption to the surface of the femtoliter wells or the gasket, both 0.05 mg/mL of BSA and 0.005 % of Tween 20 were added to the buffer solution as described earlier. [31, 32] Additionally, either polyvinylpyrrolidone (PVP) [24] or 2-[methoxy(polyethyleneoxy)propyl]-trimethoxysilane (PEG) [33] were applied for surface passivation of PDMS before the single enzyme molecule experiment was performed in blocking buffer.

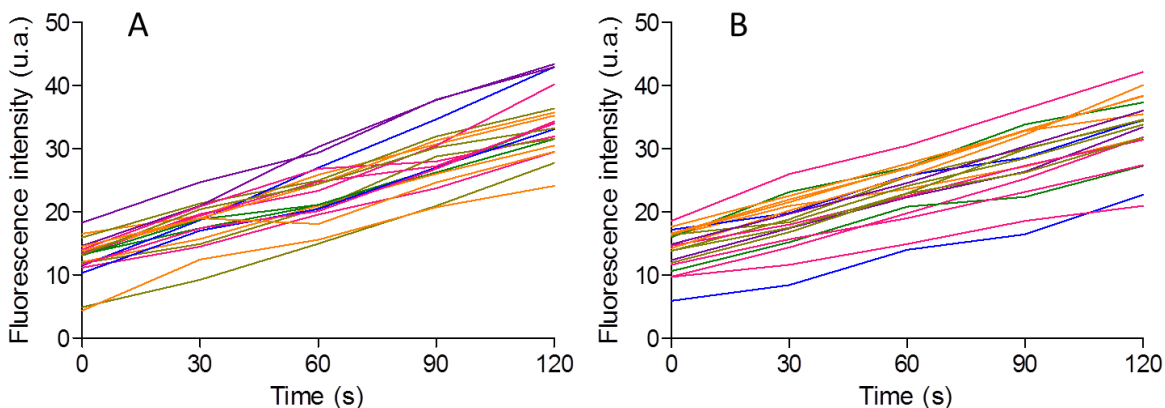


Figure 2.7 Time traces of 20 individual β -galactosidase molecules monitored in PDMS femtoliter arrays. (A) Single molecule experiment without further PDMS-array blocking besides addition of the blocking agents BSA (0.05 mg/mL) and Tween 20 (0.005 %). (B) Single molecule experiment with additional surface passivation: prior to measurement the PDMS-array was treated with PVP.

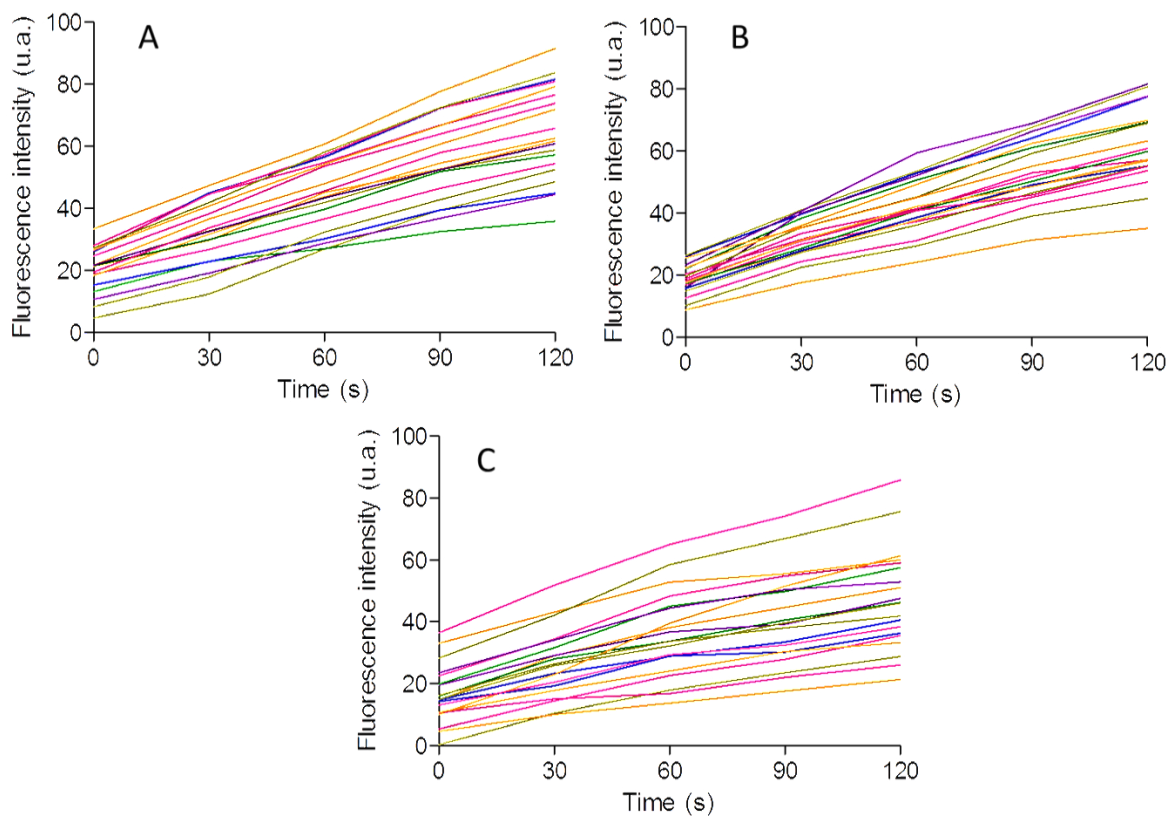


Figure 2.8 Time traces of 20 individual β -galactosidase molecules monitored in fused silica femtoliter arrays. (A) Experiment without further surface passivation besides the buffer additions BSA (0.05 mg/mL) and Tween 20 (0.005%). (B/C) Additional surface passivation: Array sealing with PVP treated (B) and PEGylated (C) PDMS gasket. A signal increase due to the additional surface passivation was detected neither for PVP-treated nor for PEGylated gaskets.

Pre-treatment of the PDMS array (Figure 2.8) or gasket (Figure 2.7) with PVP had no effect on the detected substrate turnover rates of individual enzyme molecules. A reduction of the fluorescence signal due to non-specific enzyme adsorption, as reported by Rissin *et al.* [31] for unblocked arrays (Appendix, Figure 7.1.4), was not observed. Pre-treatment of the PDMS gasket with PEG even led to an average signal decrease of 29 %, which may result from interference with the well sealing and product diffusion rather than non-specific binding. Consequently, a blocking buffer containing BSA and Tween 20 ensures both an optimal surface passivation and a tight mechanical sealing of the femtoliter chambers.

2.2.3 β -Galactosidase Single Molecule Measurements

β -Galactosidase from *Escherichia coli* is a tetrameric enzyme of four identical polypeptide chains. [34] Each monomer unites five well-defined structural domains. The enzyme's active site is formed primarily by the third, central domain, but also includes critical catalytic residues from other domains. (A schematic representation of the β -galactosidase structure can be found in the Appendix, Figure 7.1.5).

Deletion of residues near the amino-terminus causes the dissociation of the homo-tetrameric enzyme into inactive dimers. β -Galactosidase is both stable and shows a high substrate turnover rate of up to 1000 molecules per second. For those reasons it has repeatedly been used as a model enzyme for single molecule analysis. [9, 20, 31, 35-38]

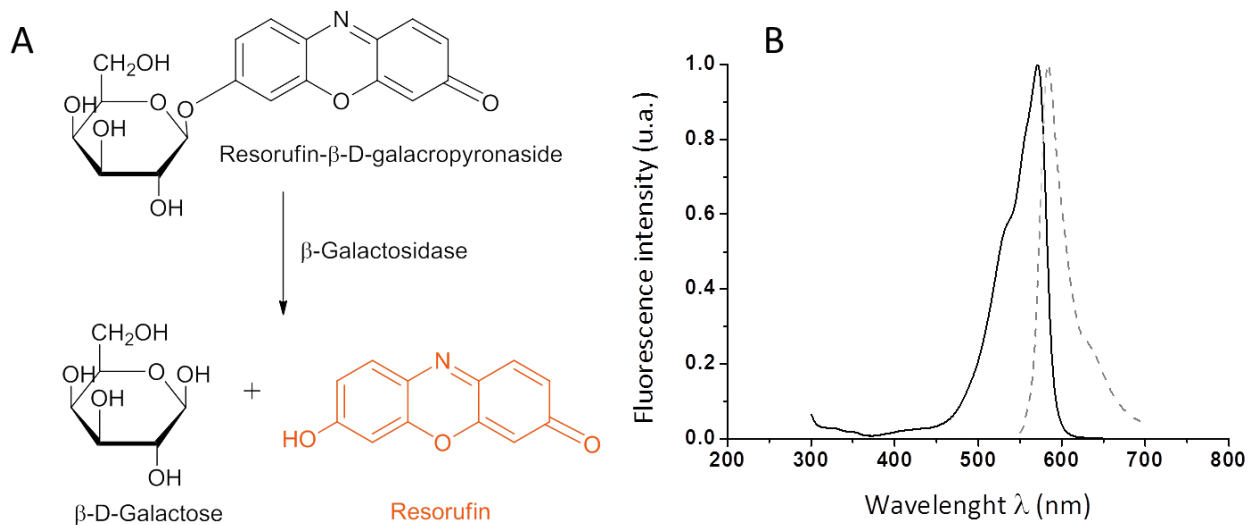


Figure 2.9 β -Galactosidase-catalyzed conversion of the fluorogenic substrate resorufin- β -D-galactopyranoside to β -D-galactose and fluorescent resorufin; (B) Normalized absorption ($\lambda_{\text{ex}} = 572$ nm, black line) and emission ($\lambda_{\text{em}} = 583$ nm grey dots) spectra of resorufin in 10 mM TRIS buffer at pH 9. [39]

β -Galactosidase catalyzes the hydrolysis of glycosidic bonds in β -galactopyranosides. The enzymatic conversion of the fluorogenic substrate resorufin- β -D-galactopyranoside (RGP) to β -D-galactose and fluorescent resorufin (Figure 2.9) was monitored with an inverted epi-fluorescence microscope. [40] Several hundred β -galactosidase molecules were isolated in the two complementary femtoliter array setups, respectively and their individual substrate turnover rates were observed over time by wide-field fluorescence microscopy. For β -galactosidase investigation, an enzyme concentration of 1.8 pM and varying concentrations of RGP were applied. The β -galactosidase molecules cannot be loaded individually into the wells of the femtoliter array. Consequently, individualization depends on the random distribution of the enzyme molecules in the reaction chambers. The Poisson distribution enables the calculation of an appropriate enzyme concentration to maximize the number of wells that contain a single enzyme molecule (chapter 1.3.4). At an enzyme concentration of 1.8 pM only 5 % of the wells are occupied with a single enzyme molecule ($P_{0.05}(1)=5\%$) while most of the reaction chambers stay empty ($P_{0.05}(0)=95\%$). However, the probability of a chamber containing more than a single β -galactosidase molecule is marginally low ($P_{0.05}(>1)=0.1\%$).

Figure 2.10 shows the substrate turnover of individual β -galactosidase molecules that are enclosed in the wells of a fused silica (A) or PDMS array (B). The image section demonstrates the increase in fluorescence intensity in individual reaction chambers 0, 60 and 120 seconds after the signal acquisition was started. The trajectories of eight randomly picked wells that are occupied by a single β -galactosidase molecule as well as one un-occupied chamber [x] that contains only RGP are shown below. The fluorescence signal in the vacant reaction chamber is constant over time and served for background correction. The resorufin concentration and thus also the fluorescence intensity of occupied wells increases linearly and enables the calculation of accurate β -galactosidase RGP turnover rates.

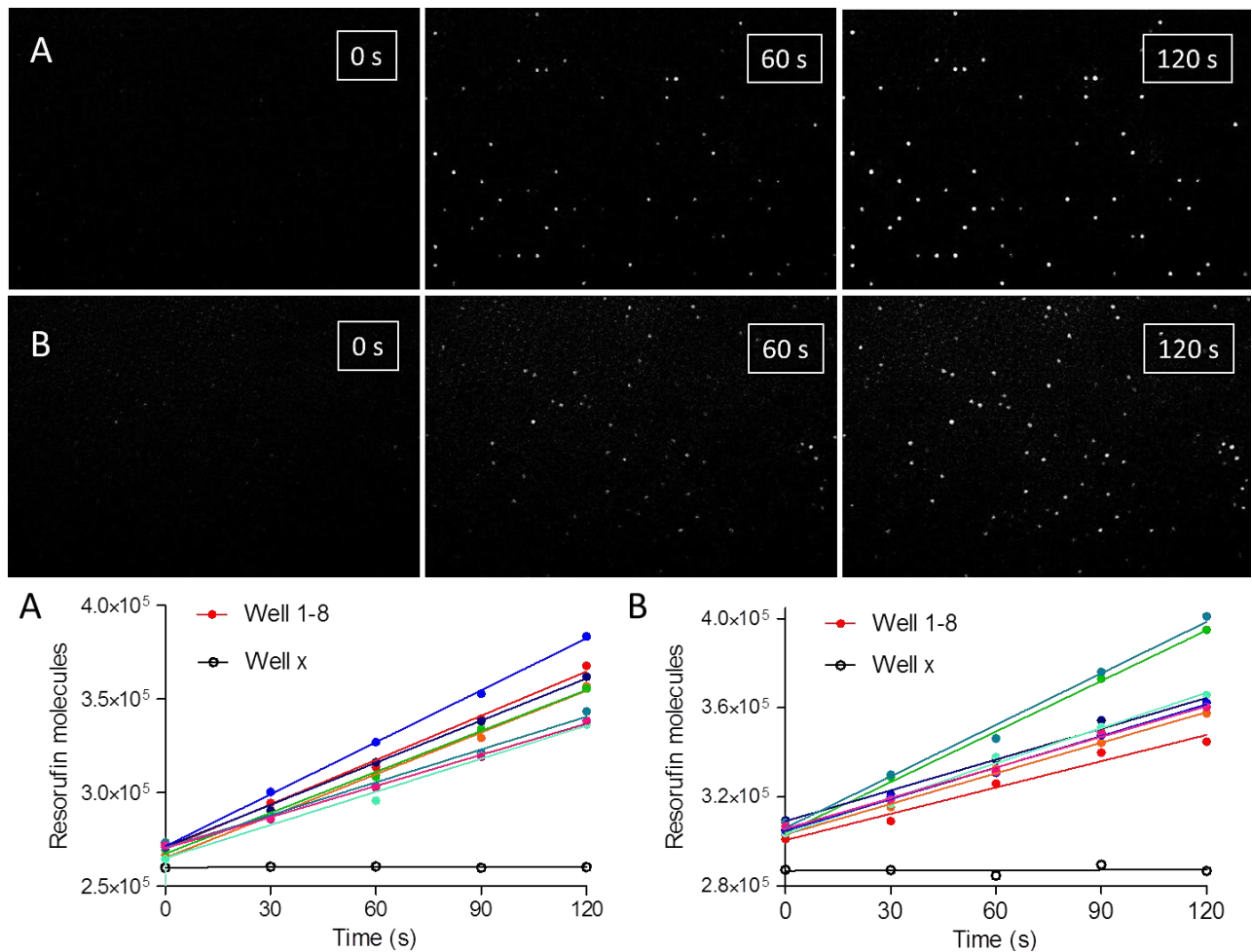


Figure 2.10 Substrate turnover of single enzyme molecules. A solution of 1.8 pM β -galactosidase and 100 μ M RGP is enclosed in femtoliter arrays that are either etched into the surface of fused silica slides (A) or molded into PDMS (B) to yield a single enzyme molecule in every twentieth chamber. Images are taken every 30 s by wide-field fluorescence microscopy. The fluorescence signal development in eight chambers containing a single enzyme molecule and one empty chamber is highlighted in the array sections and plotted against time.

The activity distribution of an enzyme population, which is hidden in the bulk experiment, can be revealed by single molecule experiments. The substrate turnover rates of single β -galactosidase molecules are broadly distributed (Figure 2.10) and can be plotted as a histogram (Figure 2.11). The activity distribution is widely independent of the substrate concentration.

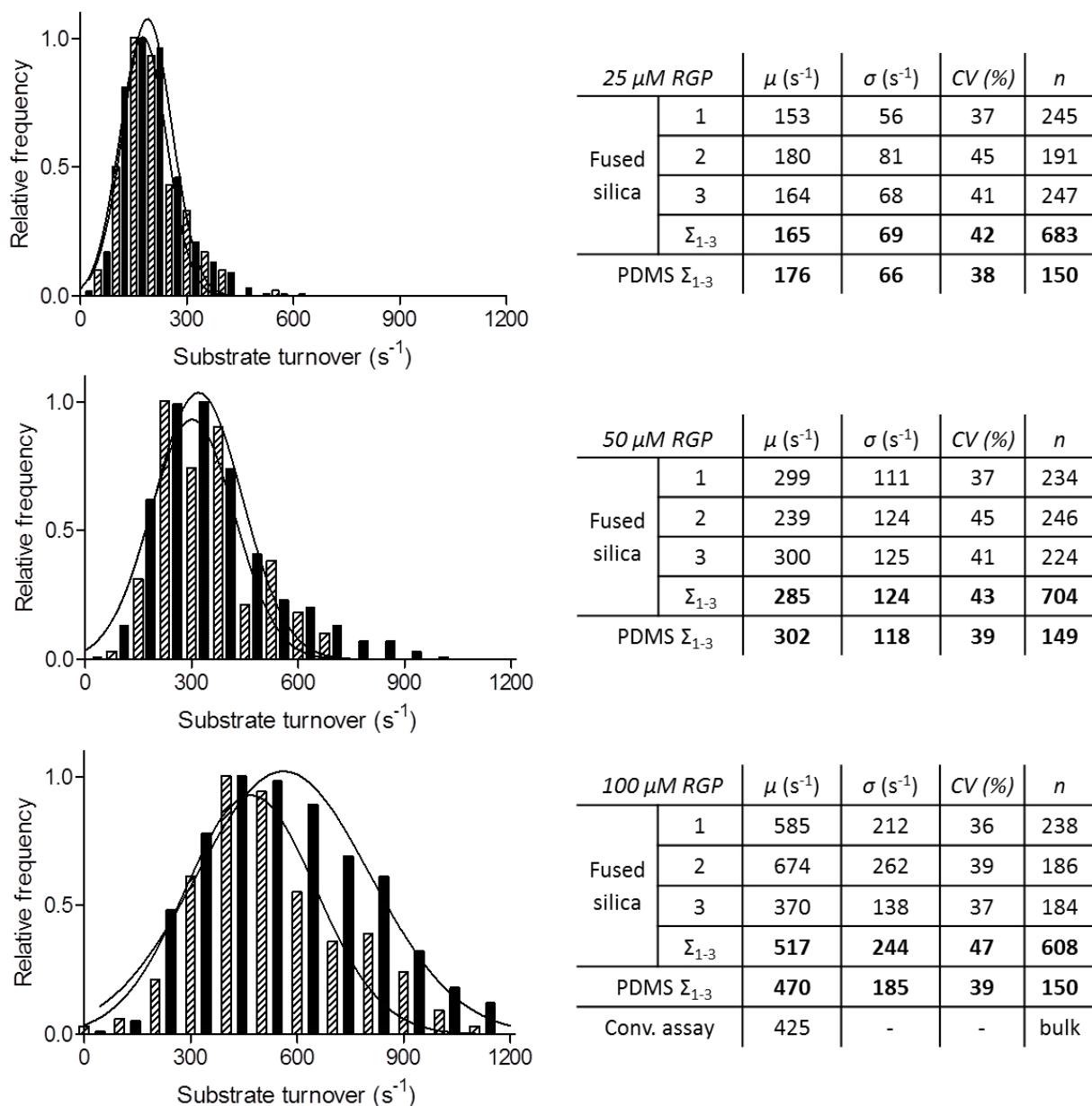


Figure 2.11 Single molecule substrate turnover distribution of β -galactosidase in fused silica (black) or PDMS (hatched) femtoliter arrays at different RGP concentrations (25 μM , 50 μM and 100 μM). The single molecule turnover rates calculated from three independent experiments were binned (binning time: 50 s^{-1} (25 μM), 75 s^{-1} (50 μM) and 100 s^{-1} (100 μM)) and used for a Gaussian analysis to determine the coefficient of variation (CV).

The Gaussian regression reveals that the mean substrate turnover in both types of femtoliter arrays (517 s^{-1} / 470 s^{-1} , at 100 μM RGP) is only slightly higher than the

respective bulk experiment (425 s^{-1}). Thus, the ensemble substrate turnover of an enzyme population can be gained from analyzing a large number of individual enzyme molecules in femtoliter arrays. It is important to note, however, that only the ensemble substrate turnover of *active* enzyme molecules is measured in the single molecule experiment, even if the bulk solution should contain a large fraction of inactive enzyme. This explains why the activity determined from a bulk reaction is typically lower compared to a single molecule experiment. [22]

The coefficient of variation (standard deviation (σ) / mean activity (μ) determined from the Gaussian regression) is a good indicator of the activity distribution in an enzyme population. β -galactosidase exhibits a broad activity distribution (Figure 2.11), which is consistent with previous single molecules studies and has been explained by conformational heterogeneity in an enzyme population. [20, 31, 41]

A strong static heterogeneity within the β -galactosidase population ($\text{CV} \approx 40 \%$) was consistently determined for single enzyme molecule experiments in fused silica and PDMS femtoliter arrays. Likewise, the individual substrate turnover rates (Figure 2.11) determined in both types of femtoliter arrays are in good agreement, reflecting the accuracy of the reported systems.

2.2.4 Features of Fused Silica and PDMS Femtoliter Arrays

Both types of femtoliter arrays represent two complementary and at first sight similar experimental setups for single enzyme molecule analysis. But the quality of the experimental results differs in some essential points.

Femtoliter arrays fabricated in fused silica slides implicate two advantages in contrast to arrays molded in PDMS: (1) The glass chips can be reused many times by means of a cleaning process in piranha solution (chapter 2.3.1), whereas PDMS arrays are disposed of after single use. (2) Due to the plasticity of PDMS, the reaction chambers deform under mechanical pressure. PDMS array-deformation leads to flattened, widened wells and thus reduced the number of reaction chambers in the field of view of the fluorescence microscope. For this reason, the number of visible wells in PDMS array experiments was diminished to approximately 3500, in comparison to about 5600 visible wells for experiments in fused silica femtoliter arrays. Additionally it is more difficult to seal and focus the squeezed PDMS array. As a consequence, a stronger diffusion of the fluorescent product into neighboring chambers was observed. Thus fewer single molecule time traces could be analyzed per experiment. Nevertheless, single molecule measurements performed in fused silica and PDMS femtoliter arrays were in good agreement regarding overall substrate turnover rates and enzyme activity distribution (Figure 2.11).

Relating to the production effort, it is much more time consuming and expensive to generate femtoliter arrays in fused silica slides. For the fabrication of one batch of 21 fused silica arrays several different lithographic, dry etching and cleaning steps are required. The complex production process entails the occurrence of slight variations in well depth ($\pm 0.1 \mu\text{m}$) and diameter ($\pm 0.2 \mu\text{m}$) between different wafers. Furthermore, the glass slides arrays are quite delicate structures that tend to break easily under pressure application.

In contrast, PDMS arrays are more robust and therefore are well suited for application in screening experiments and survey studies, where many subsequent experiments are performed in a short time. They are also the method of choice for the organization of lab courses, where experiments are performed by untrained personal. (The description of a lab course for single enzyme analysis in PDMS femtoliter arrays - at present successfully operated with chemistry graduate students in context of the lab course "Sensors, Arrays, Screening" - can be found in the Appendix, chapter 9.5).

The generation of femtoliter arrays molded in PDMS requires a one-time micro-technological production effort to manufacture the master template. Afterwards, the fabrication of PDMS-arrays only demands a simple and well-reproducible molding process. Consequently, a high number of identical arrays can be produced time-efficiently at comparatively low costs. The advantage of uniform reaction chambers with exactly the same dimensions as defined by the master mold however is lost as a consequence of the mechanical sealing procedure.

2.3 Materials and Methods

2.3.1 Femtoliter Array Microfabrication and Characterization

Preparation of fused silica femtoliter arrays. A fused silica wafer (100 ± 0.2 mm diameter, 500 ± 25 μm thickness, Siegert Wafer, www.siegertwafer.de) was cleaned in piranha acid (75 ml H_2SO_4 : 25 ml H_2O_2) for 10 min at 140 °C. After rinsing with distilled water, followed by dehydration, the hot wafer was incubated with 200 hPa of hexamethyl-disilazane (HMDS, MicroChemicals, www.microchemicals.com) to promote photoresist-adhesion.

Subsequently, one face of the wafer was covered with a layer (3.0 ± 0.1 μm) of the positive photoresist (4 mL, AZ 6632, MicroChemicals) by spin coating at 6000 rpm for 30 s. A strip of photoresist (1 cm) was removed from the periphery of the wafer to ensure good contact of photoresist and photomask. After rehydration, the chrome mask was vacuum-contacted on the wafer using the exposure system MA6 (Süss MicroTec, www.suess-microtec.de). Subsequently, 70 mJ/cm^2 of UV light was cast through the photomask and the mask design was transferred to the positive resist. To dissolve the UV-exposed areas of the photoresist, the wafer was placed face-down in 100 ml of AZ 726MIF (MicroChemicals) under stirring. Afterwards, it was rinsed for 5 min with distilled water and dried under nitrogen flow. The fused silica wafer, covered with the patterned photoresist, was then loaded into a reactive ion etching system (Oxford RIE Plasmalab 80, www.oxford-instruments.com). A mixed gas flow of 40 sccm fluorocarbon and 15 sccm argon was applied for 2 h at a chamber pressure of 4 Pa and a power of 210 W, resulting in an etching rate of 33 nm/min. Finally, the photoresist was removed using piranha acid (10 min, 140 °C), followed by rinsing with distilled water.

Array Slicing. To protect the microstructured surface a positive resist (AZ 111, MicroChemicals) was spin coated on the array prior to dicing. Subsequently, a dicing foil was attached to the wafer and it was loaded into the dicing saw (DAD 320, Giorgio Technology, www.gtsaz.com). 21 slides of 15 x 15 mm were separated at moderate dicing speed (0.4 mm/s), such that the femtoliter array was located in the center of the slide. In a last step, the dicing foil was removed and the array was cleaned thoroughly in a multistep procedure using acetone, isopropyl alcohol, piranha acid and distilled water, before it was finally dried under nitrogen.

PDMS Array Generation. For generation of the master template a silicon wafer (100 ± 0.3 mm diameter, 525 ± 20 μm thickness, Siegert Wafer) was cleaned using piranha acid (10 min, 140 °C) and distilled water. After dehydration, 4 mL of the negative photoresist (SU-8, type 5, MicoChemicals) were spin coated on the wafer (3500 rpm) resulting in a 4 μm layer. The edge bead on the periphery of the wafer was removed using propylene glycol monomethyl ether acetate (PGMEA, MicroChemicals). The wafer was heated on a hotplate (1 min/65 °C; 2 min/ 90 °C). The SU-8 layer was rehydrated and the chrome mask was vacuum contacted on the wafer using the exposure system MA6 (Süss MicroTec). Afterwards, the mask design was transferred to the negative photoresist using UV light (70 mJ/cm^2). The patterned SU-8 was baked (65 °C/1 min; 95 °C/1 min) to selectively cross-link the light-exposed regions. The non-crosslinked parts of SU-8 were removed with PGMEA. The SU-8 pattern on the silicon wafer was rinsed with isopropyl alcohol and water and finally dried under nitrogen flow. It was then used as a master template for PDMS array molding.

PDMS Array Molding. For array molding, the template was fastened in a custom-built casting form (Appendix, Figure 7.1.2). The PDMS base was mixed with the curing agent

(SYLGARD 184, Dow Corning, www.dowcorning.com) in a ratio of 10:1 and placed in a desiccator under vacuum to remove air bubbles. To obtain a homogenous 2 mm layer over the whole wafer area, 8 g of PDMS was cast onto the master template and cured for 24 h at room temperature.

Gaskets for Array Sealing. Non-structured PDMS (Sylgard 184 silicone elastomer kit, Dow Corning, www.dowcorning.com) sheets of approximately 500 μm thickness (base/curing agent: 15:1) were cast on a clean and smooth surface. After degassing under vacuum, the sheets were cured for 48 h at room temperature. The PDMS sheets were cut to pieces of 5 x 5 mm and used as a gasket for single molecule experiments in fused silica arrays.

Microscope coverslips, square 15 x 15 mm (Menzel-Gläser, www.menzel.de), made of transparent hydrolytic glass with a thickness of 0.5-0.6 mm were applied as gaskets for sealing PDMS arrays.

Femtoliter Array Characterization. The feature sizes of the femtoliter arrays were confirmed online by profilometry (KLA Tencor P60 Stylus-profilometer, equipped with a 2 μM , 60° diamond include-cone, www.kla-tencor.com). With an include cone of 60°, the tip of the applied profilometer was too large to reach the bottom of the femtoliter wells. A non-destructive, online characterization of the glass chips could be enabled by implanting a reference structure with a width of 10 microns into the chrome mask. This reference structure could be used as an indicator for the actual well depth. Likewise, the final height of the SU-8 master mold for PDMS-array generation was determined by profilometry, prior to array casting.

After completion, the arrays were characterized by scanning electron microscopy (SEM, JEOL JSM-6510 scanning electron microscope (acceleration voltage: 10 kV;

amplification: x5-x300000), www.jeol.com) using the standard Smile Shot™ software. SEM image acquisition was improved by coating the cleaned array surface with a thin gold layer (tabletop sputter coated S150B, Edwards, www.edwardsvacuum.com) prior to measurements.

The fabrication process for fused silica femtoliter arrays was evolved by Florian Götz, in the scope of his master's thesis "Integration von Femtoliter Arrays auf Quarzobjektträgern für Fluoreszenzanalysen" [42] in the group of Professor Hummel at the Faculty of Microsystems Engineering (University of Applied Sciences, Regensburg). Later on, femtoliter array generation in fused silica and PDMS was performed and characterized by Albert Hutterer (Faculty of Microsystems Engineering, University of Applied Sciences).

2.3.2 Optimizing Single Molecule Detection in Femtoliter Arrays

Chemicals and Materials. Torque screw driver 659949-15 (Buerklin, www.boerklin.com), adjustable from 1.0 to 15.0 cNm (centiNewtonmeter) in steps of 0.1 cNm; Phosphate buffered saline (PBS) (136 mM NaCl, 8.1 mM Na₂HPO₄, 2.7 mM KCl and 1.5 mM KH₂PO₄, pH 7.4), bovine serum albumin (BSA, Sigma-Aldrich, www.sigmaaldrich.com), Tween 20 (Sigma Aldrich), Polyvinylpyrrolidone (PVP, mol wt 10 000, Sigma), 2-[Methoxy (polyethyleneoxy)propyl]-trimethoxysilane (90%, 6-9 PE units, ABCR, www.abcr.de); Unless otherwise stated, all other chemicals and solvents were purchased from Sigma-Aldrich, Merck and ABCR. They were of analytical grade and used without further purification.

Monitoring of Photobleaching. To estimate the photobleaching rate of the fluorescent product resorufin during single molecule experiments, a solution of 5 μ M resorufin in PBS was enclosed in the wells of both PDMS and fused silica femtoliter arrays. Fluorescence microscope images were taken every 30 seconds over a time course of several minutes. Subsequently, the average fluorescence intensity of 20 randomly picked wells, monitored every 30 s was plotted against time (Figure 2.5). The photobleaching experiment was performed twice in both types of femtoliter arrays. Fluorescence depletion rates are given as an average of both measurements.

PDMS-gasket with Topographic Structure. PDMS-gaskets with topographic structure were cut from a PDMS-sheet that was cast on an unpolished silicon wafer. The roughness of the topographic structure ($R_a = 225$ nm, $P_p = 572$ nm and $P_v = 942$ nm) was determined by profilometry (Appendix, Figure 7.1.3), using a P-16+ profilometer from LOT-Oriel (www.lot-oriel.com) equipped with a diamond-tip (2 μ M radius, opening cone: 60°) at an

acquisition speed of 20 $\mu\text{m/s}$. The PDMS-foil was fabricated and characterized by Albert Hutterer at the Faculty of Microsystem Engineering, University of Applied Sciences, Regensburg.

PDMS-Surface Passivation with Polyvinylpyrrolidone (PVP). The water-soluble polymer PVP has good wetting properties and readily forms thin films on surfaces. Therefore it is a popular blocking agent. [24] For surface passivation with PVP the PDMS gaskets and arrays were cut into pieces of 5 x 5 mm and deposited on a clean silica slide. They were then incubated in a solution of 1 % PVP in bidistilled water for 90 min at r.t.. Afterwards, the gaskets or arrays were washed with bidistilled water and air dried.



Figure 2.12 PDMS-gaskets and arrays (5x5 mm) were deposited on a clean glass slide and incubated in a solution of 1% Polyvinylpyrrolidone (PVP) in PBS for 90 min at room temperature.

Surface-PEGylation of PDMS-gaskets. Poly(ethylene glycol) (PEG)-functionalization yields wettable PDMS-surfaces that exhibit protein-repelling characteristics. [43] The PDMS-gaskets for silica array sealing were treated with 2-[Methoxy(polyethyleneoxy)-propyl]trimethoxysilane according to an optimized protocol applied by G. Sui *et al.* for surface passivation of PDMS microfluidic channels. [33] Prior to PEGylation the PDMS gaskets were cut into pieces of 5 x 5 mm, deposited on a clean silica slide and oxidized

in a mixture of water, hydrogen peroxide and 1M hydrochloric acid (5:1:1) for 15 minutes at r.t. The PDMS gaskets were then washed with bidistilled water and dried under nitrogen.



Figure 2.13 For PEGylation the PDMS-gaskets (5x5 mm) were oxidized (not shown) and subsequently incubated with a 90 % solution of 2-[Methoxy(polyethylenxy)propyl]-trimethoxysilane under nitrogen at r.t. for 30 min. After PEGylation the gaskets were washed with bidistilled water. The surface-modified gaskets were dried and stored under nitrogen.

Afterwards the gaskets were incubated for 30 min in a solution of 2-[Methoxy-(polyethylenxy)propyl]-trimethoxysilane (90%) under nitrogen at r.t.. After PEGylation they were again washed with bidistilled water. The surface-modified PDMS-gaskets were dried and stored under nitrogen. Functionalization took place at least 24 hours before application.

2.3.3 Experiments on Enzyme Kinetics

Buffers and Reagents. Dilutions and single molecule experiments were performed at room temperature (22 °C, air conditioning) in phosphate buffered saline (PBS: 2.7 mM KCl, 2 mM KH₂PO₄, 137 mM NaCl, 10 mM Na₂HPO₄, pH 7.4) containing: (a) 1 mM MgCl₂, 0.05 mg/mL BSA and 0.005 % Tween 20 (β -D-galactosidase measurements), (b) 0.05 mg/mL BSA (β -glucuronidase experiments).

Lyophilized β -D-galactosidase from *E. coli* (≥ 500 units/mg) was purchased from Sigma-Aldrich and reconstituted to 2 μ M in PBS/MgCl₂, divided into 20 μ L aliquots, quick-frozen in liquid nitrogen and stored at -20°C. Stock solutions of the fluorogenic substrates resorufin- β -D-galactopyranoside (10 mM) (RGP, Iris Biotech GmbH, www.iris-biotech.de), resorufin- β -D-glucuronide (5 mM) (ReG, Sigma-Aldrich) and resorufin sodium salt (200 μ M) (Invitrogen, www.invitrogen.com) in dimethyl sulfoxide (DMSO, Merck, www.merck-chemicals.de) were aliquoted (20 μ L) and stored at -20 °C.

Femtoliter Arrays. Single molecule experiments were performed with femtoliter arrays that were microstructured into the surface of a fused silica wafer by photolithography and anisotropic reactive ion etching or molded in PDMS as described in chapter 2.3.1. The arrays consisted of 250 x 250 cylindrical wells that were arranged in the middle of a 1.5 x 1.5 cm² glass slide in a rectangular lattice with a pitch of 10 μ m, resulting in an overall edge length of 2.5 x 2.5 mm². With a diameter of 4 μ m and a depth of 3 μ m the wells defined a volume of approximately 40 femtoliter as confirmed by scanning electron microscopy (Figure 2.2). Before usage in single molecule or functionalization experiments the arrays were cleaned with piranha solution (1:3 ration of 30 % H₂O₂ and conc. H₂SO₄, Merck) for 15 minutes, immersed in distilled water for about 10 minutes, sonicated in water and ethanol and finally air-dried. The femtoliter arrays were sealed with a polydimethylsiloxane (PDMS) gasket (fused silica arrays) or a microscope coverslip

(PDMS arrays). Fused silica femtoliter arrays and microscope coverslips were used repeatedly. Before each experiment they were cleaned with piranha solution (1:3 ratio of 30 % H₂O₂ and conc. H₂SO₄) for 10 min then washed with bidistilled water under ultrasonication and finally air dried.

Single Enzyme Molecule Experiments. For single enzyme molecule measurements, the femtoliter array was fastened in the custom-built array holder (chapter 2.2.2, Figure 2.3 and Figure 2.4) and mounted on the xy-stage of an inverted epi-fluorescence microscope (Eclipse Ti-E, Nikon, www.nikoninstruments.com). Enzyme and fluorogenic substrate were diluted in PBS and mixed just prior to measurement. The wells of the femtoliter array were filled by dispensing 5 μ L of the dilute enzyme solution (1.8 pM) on top of the array, followed by up- and down-pipetting. The array was covered with a PDMS gasket (measurements in fused silica arrays) or lowered onto the microscope coverslip (PDMS array) and sealed by applying a mechanical pressure (torque screwdriver, Bürklin, www.buerklin.com).

Image acquisition was started within 2 minutes after mixing enzyme and substrate. The fluorescence intensity in individual chambers of the femtoliter array was recorded over time through the opposite side of the fused silica slide/ microscope coverslip by wide-field fluorescence microscopy. Images were acquired every 30 s with an exposure time of 200 ms (neutral density filter: (a) ND 8 (β -D-galactosidase measurements), (b) ND 4 (β -glucuronidase experiments) for several minutes.

Enzymatic substrate turnover rates were calculated from the first 120 seconds of each measurement. The fluorescence signal generated by individual enzyme molecules was background corrected by subtracting the fluorescence intensity of reaction chambers containing just substrate and no enzyme molecule. The signal was calibrated

by measuring standard solutions of resorufin in the wells of the femtoliter array (calibration curve in the Appendix, Figure 7.1.6 (for β -D-galactosidase measurements).

Some of the single β -D-galactosidase measurements in fused silica/PDMS arrays were conducted by Franziska Vogl/ Andrea Beutner in the scope of their master's/ bachelor's thesis, performed in our group in 2012. The experiments were completed, evaluated and interpreted in the scope of this PhD thesis.

Fluorescence Microscopy. The inverted epi-fluorescence microscope TiE-ECLIPSE from Nikon was employed to monitor the single enzyme molecule substrate turnover (Figure 2.14).

	Component	Specification	Manufacturer
1	Microscope	ECLIPSE Ti-E	Nikon
2	Object lens	CFI60, Plan Apo, 20x, NA 0.75	Nikon
3	Filter cube	41034-Rhodamine x/ Resorufin	Chroma Technology
4	sCMOS-camera	DC-152-Q-FI	Andor Technology
5	External Lamp	KL 1500 LED	Schott
6	Motorized XY stage	Ti-SH-U	Nikon
7	Light Source	Intensilight C-HGFIE	Nikon
8	Imaging Software	NIS-Elements BR	Nikon

Table 2.1 Components of the Inverted epi-fluorescence microscope TiE-Eclipse. Microscope components, their specifications and manufacturers are listed.

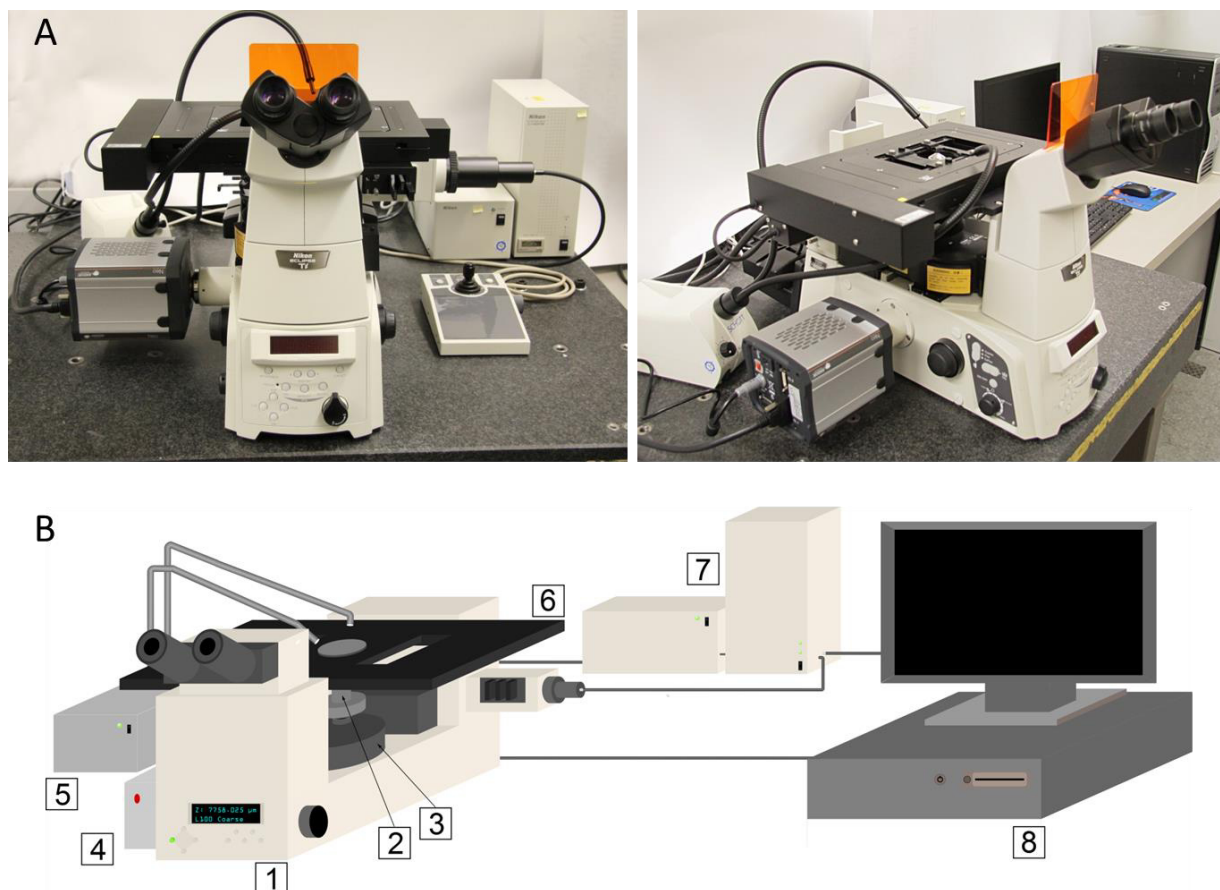


Figure 2.14 Inverted epi-fluorescence microscope TiE-Eclipse. (A) Photograph of the microscope setup. (B) Schematic presentation, indicating the individual components of the microscope, summarized in Table 2.1.

The inverted epi-fluorescence microscope TiE-ECLIPSE (1) is equipped with a 20x objective (2) (CFI60 Plan Apo, NA = 0.75, Nikon) and a filter cubes (3) for fluorescein ($\lambda_{ex}/\lambda_{em}$: 492/537 nm) and resorufin (Chroma Technology, www.chroma.com; HQ577/10x excitation filter, HQ620/60m emission filter and Q585LP dichroic mirror) (Filter spectra in the Appendix, Figure 7.1.7). The microscope equipment further includes a scientific CMOS camera (4) (DC-152-Q-FI, Andor Technology, www.andor.com). The sCMOS-camera has a resolution of 5.5 megapixels. In combination with the 20x objective it covers an area of approximately 700 x 800 μm which equals a field of view of about 5600

(fused silica array) respectively 3500 (PDMS array under pressure) femtoliter wells. The camera was cooled to -31 °C to reduce temperature noise. Prior to measurements, the femtoliter array was fastened on the motorized xy-stage (6) and the wells were brought into focus with help of an external fiber optic cold light source (5) (KL 1500 LED, Schott, www.schott.com). The light source of the fluorescence microscope was a pre-centered fiber-optical mercury lamp (7) (Intensilight C-HGFIE, Nikon). In comparison to conventional mercury lamps, the Intensilight offers a more homogeneous spectrum and a higher intensity in the range of 450 to 600 nm. The incorporation of six neutral density filters (ND 1 - 32) allows for a gradual reduction of the excitation light. Standard imaging software (NIS-Elements, Nikon, www.nikon-instruments.com) was applied to control image acquisition and retrieve the fluorescence signals from defined regions of interest (ROI). The NIS-imaging software enables the acquisition of four independent array positions, hence 22 400 (fused silica)/ 14 000 (PDMS) individual wells in parallel.

Bulk Experiment. The bulk experiment was performed at 25 °C in a Fluostar Optima MTP-reader ($\lambda_{\text{ex}}=544$ nm, $\lambda_{\text{em}}=590$ nm, bmg-Labtech, www.bmg-labtech.com). The substrate turnover of 36 pM β -D-galactosidase at 100 μ M RGP was determined in a volume of 200 μ L (flat bottomed, polystyrene 96-well MTP, Nunc, www.nunc-brand.com). The substrate turnover was calibrated with resorufin standard concentrations.

Data Analysis and Plotting. Data analysis and plotting was performed with Microsoft Excel 2010 (office.microsoft.com), Origin 6.1 from Origin lab Corporation (www.originlab.de) or GraphPad Prism 5 (www.graphpad.com). Chemical structures and schemes were drawn using ChemBioDraw Ultra 12.0 (www.cambridgesoft.com) in combination with the vector graphics software Inkscape (www.inkscape.org/de) or Microsoft Office PowerPoint (office.microsoft.com).

2.4 Conclusion

The fabrication, characterization and technical features of two different types of femtoliter arrays for single enzyme molecule analysis were discussed in detail. The arrays consist of 62 500 homogeneous, reaction chambers with a diameter of 4 μm and a depth of approximately 3.5 μm . The wells were etched into the surface of fused silica slides by photolithography and reactive ion etching or molded in PDMS. Both types of complementary femtoliter arrays are perfectly suited for the enclosure of a high number of single enzyme molecules and the investigation of their individual substrate turnover rates.

An experimental setup for single molecule enzymology was presented. It was further described, how the setup was improved in several steps, considering aspects such as tight array sealing, photobleaching, signal readout and non-specific protein adsorption. The effectiveness of the optimized setup was evaluated by single β -galactosidase experiments in fused silica and PDMS femtoliter arrays. Therefore several hundred enzyme molecules were isolated in separate wells and their individual substrate turnover recorded over time by wide-field fluorescence microscopy. β -galactosidase exhibited a broad activity distribution, which was in good agreement with previous reports on the *static* heterogeneity of β -galactosidase. [20, 31, 41, 44]

Finally, the two complementary array systems in fused silica and PDMS, were contrasted regarding their applicability for single molecule enzymology. Varying aspects, such as production effort, array stability and experiment quality were discussed. While fused silica femtoliter arrays are superior regarding the quality of the experimental results, substrate turnover rates of individual β -galactosidase and their activity distribution determined in both types of femtoliter arrays were in good agreement.

2.5 References

1. Goodsell, D.S., *Inside a living cell*. Trends Biochem. Sci., **1991** (16): 203.
2. Piwonski, H.M., M. Goomanovsky, D. Bensimon, A. Horovitz, and G. Haran, *Allosteric inhibition of individual enzyme molecules trapped in lipid vesicles*. Proc. Natl. Acad. Sci. U. S. A., **2012** (109): E1437.
3. Hsin, T.M. and E.S. Yeung, *Single-molecule reactions in liposomes*. Angew. Chem. Int. Ed., **2007** (46): 8032.
4. Rhoades, E., E. Gussakovsky, and G. Haran, *Watching proteins fold one molecule at a time*. Proc. Natl. Acad. Sci. U. S. A., **2003** (100): 3197.
5. Boukobza, E., A. Sonnenfeld, and G. Haran, *Immobilization in surface-tethered lipid vesicles as a new tool for single biomolecule spectroscopy*. J. Phys. Chem. B, **2001** (105): 12165.
6. de la Escosura, A., R.J.M. Nolte, and J.J.L.M. Cornelissen, *Viruses and protein cages as nanocontainers and nanoreactors*. J. Mater. Chem., **2009** (19): 2274.
7. Comellas-Aragones, M., H. Engelkamp, V.I. Claessen, N.A. Sommerdijk, A.E. Rowan, *et al.*, *A virus-based single-enzyme nanoreactor*. Nat. Nanotechnol., **2007** (2): 635.
8. Comellas-Aragones, M., A. de la Escosura, A.J. Dirks, A. van der Ham, A. Fuste-Cune, J.J.L.M. Cornelissen, and R.J.M. Nolte, *Controlled Integration of Polymers into Viral Capsids*. Biomacromolecules, **2009** (10): 3141.
9. Rotman, B., *Measurement of activity of single molecules of beta-D-galactosidase*. Proc. Natl. Acad. Sci. U. S. A., **1961** (47): 1981.
10. Lee, A.I. and J.P. Brody, *Single-molecule enzymology of chymotrypsin using water-in-oil emulsion*. Biophys. J., **2005** (88): 4303.
11. Mazutis, L., A.F. Araghi, O.J. Miller, J.C. Baret, L. Frenz, *et al.*, *Droplet-Based Microfluidic Systems for High-Throughput Single DNA Molecule Isothermal Amplification and Analysis*. Anal. Chem., **2009** (81): 4813.
12. Mazutis, L., J.C. Baret, P. Treacy, Y. Skhiri, A.F. Araghi, *et al.*, *Multi-step microfluidic droplet processing: kinetic analysis of an in vitro translated enzyme*. Lab. Chip, **2009** (9): 2902.
13. Margulies, M., M. Egholm, W.E. Altman, S. Attiya, J.S. Bader, *et al.*, *Genome sequencing in microfabricated high-density picolitre reactors*. Nature, **2005** (437): 376.

14. Nakano, M., J. Komatsu, S. Matsuura, K. Takashima, S. Katsura, and A. Mizuno, *Single-molecule PCR using water-in-oil emulsion*. *J. Biotechnol.*, **2003** (102): 117.
15. Kiss, M.M., L. Ortoleva-Donnelly, N.R. Beer, J. Warner, C.G. Bailey, *et al.*, *High-Throughput Quantitative Polymerase Chain Reaction in Picoliter Droplets*. *Anal. Chem.*, **2008** (80): 8975.
16. Xie, X.S., J. Yu, and W.Y. Yang, *Perspective - Living cells as test tubes*. *Science*, **2006** (312): 228.
17. Xie, X.S., P.J. Choi, G.W. Li, N.K. Lee, and G. Lia, *Single-molecule approach to molecular biology in living bacterial cells*. *Annu. Rev. Biophys.*, **2008** (37): 417.
18. Golding, I., J. Paulsson, S.M. Zawilski, and E.C. Cox, *Real-time kinetics of gene activity in individual bacteria*. *Cell*, **2005** (123): 1025.
19. Tan, W.H. and E.S. Yeung, *Monitoring the reactions of single enzyme molecules and single metal ions*. *Anal. Chem.*, **1997** (69): 4242.
20. Rondelez, Y., G. Tresset, K.V. Tabata, H. Arata, H. Fujita, S. Takeuchi, and H. Noji, *Microfabricated arrays of femtoliter chambers allow single molecule enzymology*. *Nat. Biotechnol.*, **2005** (23): 361.
21. Ehrl, B.N., R.B. Liebherr, and H.H. Gorris, *Single molecule kinetics of horseradish peroxidase exposed in large arrays of femtoliter-sized fused silica chambers*. *Analyst*, **2013** (138): 4260.
22. Liebherr, R.B., M. Renner, and H.H. Gorris, *A Single Molecule Perspective on the Functional Diversity of in Vitro Evolved beta-Glucuronidase*. *J. Am. Chem. Soc.*, **2014** (136): 5949.
23. Zhang, H., S. Nie, C.M. Etson, R.M. Wang, and D.R. Walt, *Oil-sealed femtoliter fiber-optic arrays for single molecule analysis*. *Lab. Chip*, **2012** (12): 2229.
24. Shon, M.J. and A.E. Cohen, *Mass action at the single-molecule level*. *J. Am. Chem. Soc.*, **2012** (134): 14618.
25. Fowlkes, J.D. and C.P. Collier, *Single-molecule mobility in confined and crowded femtolitre chambers*. *Lab. Chip*, **2013** (13): 877.
26. Vogl, F.C., *Master Thesis: Optimization of an experimental setup to analyze single enzyme molecules in femtoliter arrays*. Institute of Analytical Chemistry, Chemo- and Biosensors, **2012**. University of Regensburg.

27. English, B.P., W. Min, A.M. van Oijen, K.T. Lee, G. Luo, *et al.*, *Ever-fluctuating single enzyme molecules: Michaelis-Menten equation revisited*. *Nat. Chem. Biol.*, **2006** (2): 87.
28. Huang, Z.L., H. Zhu, F. Long, H. Ma, L. Qin, *et al.*, *Localization-based super-resolution microscopy with an sCMOS camera*. *Opt. Express.*, **2011** (19): 19156.
29. Saurabh, S., S. Maji, and M.P. Bruchez, *Evaluation of sCMOS cameras for detection and localization of single Cy5 molecules*. *Opt. Express.*, **2012** (20): 7338.
30. Walt, D.R., *Protein measurements in microwells*. *Lab. Chip*, **2014**.
31. Rissin, D.M., H.H. Gorris, and D.R. Walt, *Distinct and long-lived activity states of single enzyme molecules*. *J. Am. Chem. Soc.*, **2008** (130): 5349.
32. Sapsford, K.E. and F.S. Ligler, *Real-time analysis of protein adsorption to a variety of thin films*. *Biosens. Bioelectron.*, **2004** (19): 1045.
33. Sui, G., J. Wang, C.C. Lee, W. Lu, S.P. Lee, *et al.*, *Solution-phase surface modification in intact poly(dimethylsiloxane) microfluidic channels*. *Anal. Chem.*, **2006** (78): 5543.
34. Juers, D.H., B.W. Matthews, and R.E. Huber, *LacZ beta-galactosidase: structure and function of an enzyme of historical and molecular biological importance*. *Protein Sci.*, **2012** (21): 1792.
35. Craig, D.B., A.M. Haslam, J.M.L. Coombs, and E.R. Nichols, *Kinetic studies of unmodified individual Escherichia coli beta-galactosidase molecules in free solution*. *Biochem. Cell Biol.*, **2010** (88): 451.
36. Craig, D.B., *Single enzyme molecule assay with time resolution using capillary electrophoresis*. *Rev. Anal. Chem.*, **2013** (32): 103.
37. Min, W., B.P. English, G. Luo, B.J. Cherayil, S.C. Kou, and X.S. Xie, *Fluctuating enzymes: lessons from single-molecule studies*. *Acc. Chem. Res.*, **2005** (38): 923.
38. Rissin, D.M. and D.R. Walt, *Digital concentration readout of single enzyme molecules using femtoliter arrays and Poisson statistics*. *Nano Lett.*, **2006** (6): 520.
39. TUGraz. *Database of Fluorescent Dyes, Properties and Applications*. 2015 [cited 2015 April 07]; Available from: www.fluorophores.tugraz.at.
40. Lichtman, J.W. and J.A. Conchello, *Fluorescence microscopy*. *Nat. Methods*, **2005** (2): 910.
41. Craig, D.B. and N.J. Dovichi, *Escherichia coli beta-galactosidase is heterogeneous with respect to the activity of individual molecules*. *Can. J. Chem.*, **1998** (76): 623.

42. Götz, F., *Master Thesis: Integration von Femtoliter-Arrays auf Quarzobjektträgern für Fluoreszenzanalysen*. Faculty of Microsystems Engineering, **2010**. University of Applied Sciences, Regensburg.
43. Papra, A., A. Bernard, D. Juncker, N.B. Larsen, B. Michel, and E. Delamarche, *Microfluidic networks made of poly(dimethylsiloxane), Si, and Au coated with polyethylene glycol for patterning proteins onto surfaces*. *Langmuir*, **2001** (17): 4090.
44. Ota, S., H. Kitagawa, and S. Takeuchi, *Generation of femtoliter reactor arrays within a microfluidic channel for biochemical analysis*. *Anal. Chem.*, **2012** (84): 6346.

3. A Single Molecular Perspective on the Functional Diversity of Wild-Type and *in Vitro* Evolved β -Glucuronidase

This chapter is based upon the Journal Article "*A Single Molecule Perspective on the Functional Diversity of in Vitro Evolved β -Glucuronidase*", Liebherr R.B., M. Renner and H.H. Gorris, J. Am. Chem. Soc., **2014** (136): 5949. [1]

3.1. Introduction

Enzymatic catalysis plays a crucial role in most biochemical processes. Thus, the analysis of the catalytic mechanisms of enzymes and their evolution is of immediate interest in life sciences. Already in 1913, the landmark work of Michaelis and Menten provided a first comprehensive concept for the analysis of enzyme kinetics in bulk experiments. [2] The functional diversity between the individual molecules of an enzyme population, however, cannot be investigated from this macroscopic point of view. The emerging field of single molecule analysis provided a more explicit insight into complex enzyme dynamics. Single molecule experiments unraveled kinetic details of enzyme reactions such as dynamic disorder in subsequent catalytic cycles of β -galactosidase, [3-5] horseradish peroxidase, [6, 7] lipase B, [8, 9] cholesterol oxidase, [10] bovine α -chymotrypsin [11, 12] and lactate dehydrogenase. [13]

In arrays of femtoliter-sized reaction chambers, etched into the surface of fused silica slides, individual enzyme molecules can be separated and monitored free in solution without surface-immobilization. The large array format of 62 500 homogeneously arranged reaction chambers enables the simultaneous investigation of several

hundred individual enzyme molecules. This high degree of parallelization provides excellent statistics on the functional diversity in an enzyme population.

If single enzyme molecules are isolated in the individual reaction chambers of the fL-array together with an excess of fluorogenic substrate, the signal of the cumulated product of many subsequent catalytic cycles is recorded over time by fluorescence microscopy. In this way, it could be demonstrated that individual molecules of β -galactosidase [3, 5, 14] – as well as other enzymes [6, 7, 13] – possess distinct and long-lived activity states. Single enzyme molecule experiments on β -galactosidase further revealed a broad activity distribution within the enzyme population (chapter 2.2.3) with a coefficient of variation of about 30 to 40% for all substrate concentrations investigated up to 150 μ M. [3]

β -Galactosidase and β -glucuronidase (GUS) from *E. coli* catalyze the hydrolysis of very similar glycosidic substrates. Both enzymes are only active in their homotetrameric state as their active sites are composed of the elements of two or more monomers (Appendix, Figure 7.1.5 and Figure 3.1 A). [15-17] The genes of β -galactosidase and GUS diverged from an ancient common ancestor. [18] During evolution the amino acid sequence of GUS was altered, resulting in the modern 273 kDa [19] enzyme, approximately half the size of β -galactosidase.

Matsumura and Ellington were able to convert the native substrate specificity of wild-type GUS to β -galactosidase activity by *in vitro* evolution within a few steps of mutation and screening. [20, 21] In the process, the inversion of the GUS activity proceeds through nonspecific intermediates (so-called generalists) that still possess their native wild-type activity but also convert a variety of alternative glycosidic substrates. In the end of the evolutionary process a specialized evolved GUS is generated that exclusively accepts galactopyranoside substrates. (For an overview of the substrate specificities of the evolved variants see Appendix, Figure 7.2.1)

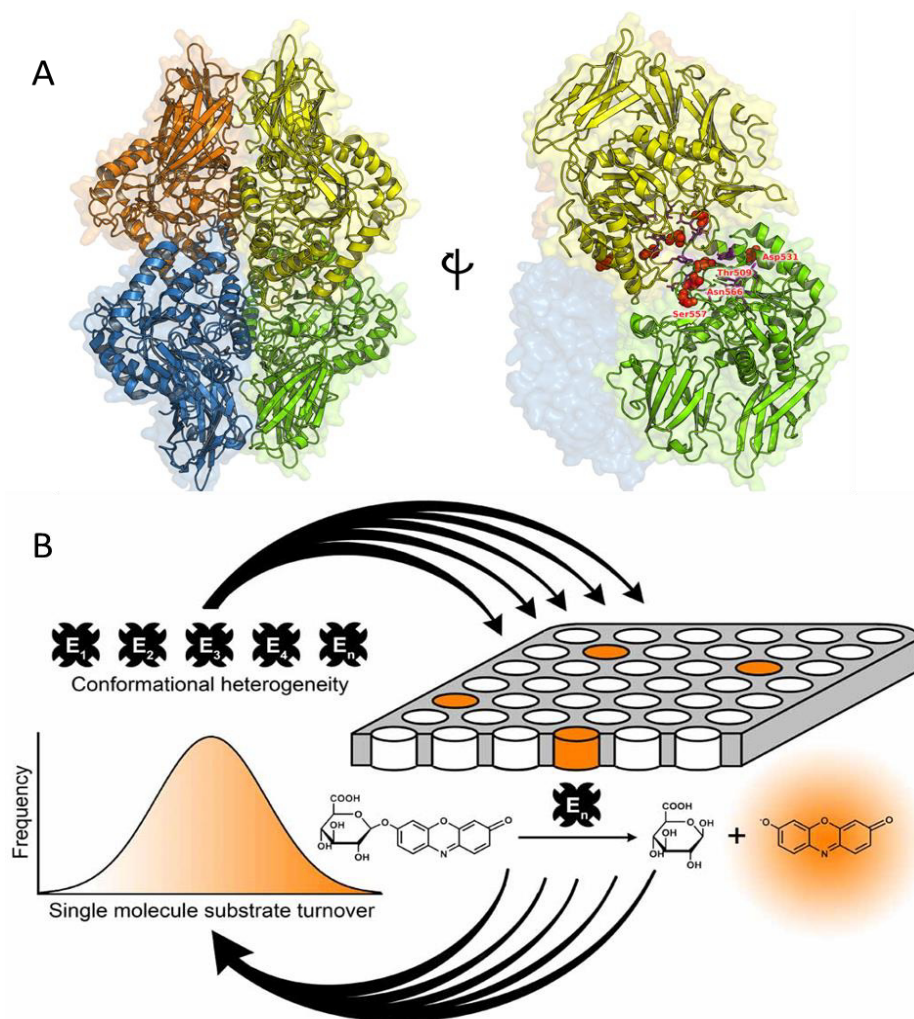


Figure 3.1 Investigation of single GUS molecules in the wells of a fused silica femtoliter array: (A) Crystal structure of the *E. coli* GUS tetramer (left) and the interface of two monomers (right) with the four amino acid positions that are mutated in the partially evolved GUS highlighted in red. (B) Individual molecules of a conformationally heterogeneous enzyme population ($E_1 - E_n$) are separated in the wells of the femtoliter array where they hydrolyze the non-fluorescent substrate ReG to fluorescent resorufin (indicated in orange). Product generation of hundreds of individual GUS molecules in separate reaction chambers is monitored over time by wide-field fluorescence microscopy. The substrate turnover rates of individual GUS are assembled in a histogram to demonstrate the activity distribution within the enzyme population.

Tawfik *et al.* demonstrated that the evolutionary process observed by Matsumura and Ellington, can be transferred to many other types of enzymes and represents a basic

principle of adaptive evolution. [22-25] The broad substrate specificity of the intermediate generalists – described as promiscuous enzyme activity – has been assigned to a higher diversity of conformational states between individual enzymes of the evolved variant. [25] The high conformational flexibility of the generalists potentially represents the origin for the evolutionary development of new enzyme functions. [23, 26-28]

To date, studies on the promiscuous activity of evolved enzymes have only been performed in bulk experiments, such as X-ray crystallography, NMR and pre-steady-state kinetics [29, 30] that conceal the effects of higher conformational diversity on the substrate turnover of individual enzyme molecules. The single molecule measurements conducted in this work provide a new perspective on the subject: Hundreds of individual wild-type β -glucuronidase and *in vitro* partially evolved β -glucuronidase molecules were isolated in the wells of a fused silica femtoliter array to monitor and compare their respective substrate turnover rates at the single molecule level (Figure 3.1 B). [1] With the introduction of modern single molecule technologies, we thus hope to make a significant contribution to a complete elucidation of the fundamental mechanisms of enzyme evolution.

3.2. Results and Discussion

3.2.1. Single Molecule Analysis of Wild-Type β -Glucuronidase

The expression plasmids (wild-type GUS and partially evolved variant T509A/D531E/S557P/N566S) were provided by Ichiro Matsumura. The his-tagged GUS was expressed in *E. coli* and highly purified by nickel chelate chromatography and subsequent size exclusion chromatography (Appendix, Figure 7.2.2).

The static heterogeneity of the β -glucuronidase wild-type population was investigated by confining hundreds of individual enzyme molecules in the wells of a fused silica femtoliter array. A 1.8 pM solution of GUS was enclosed in the array, yielding a distribution of one enzyme molecule in every twentieth reaction chamber according to Poisson statistics (chapter 1.1.3). In order to block non-specific binding of GUS molecules to the surface of the fused silica chambers, BSA was added to the PBS buffer according to protocols described earlier. [3]

Enzymatic substrate turnover was monitored using the non-fluorescent substrate ReG. The catalytic hydrolysis of ReG to highly fluorescent resorufin by individual GUS molecules was recorded at various substrate concentrations. The lowest concentration applied was 12.5 μ M. At a 12.5 μ M substrate concentration, equaling approximately 3 million molecules in a volume of about 40 femtoliter, wild-type GUS hydrolyses ReG with an average turnover rate of 50 molecules per second. Consequently, after a reaction time of 300 s, there is less than 1 % substrate depletion. Accordingly, substrate depletion effects could be ignored, assuming a constant ReG concentration. A constant substrate concentration over time is mandatory to accurately calculate the enzymatic substrate turnover rate.

The catalytic hydrolysis of ReG to highly fluorescent resorufin was monitored simultaneously in more than 100 wells that contained a single GUS molecule by wide-

field fluorescence microscopy (Video in the Appendix). Figure 3.2 (A) depicts a small section of the femtoliter array 60, 150 and 300 seconds after image acquisition was started. Four “active” wells [1-4] occupied with an individual wild-type GUS molecule and one “inactive” well [x] that contains only substrate without enzyme, are highlighted.

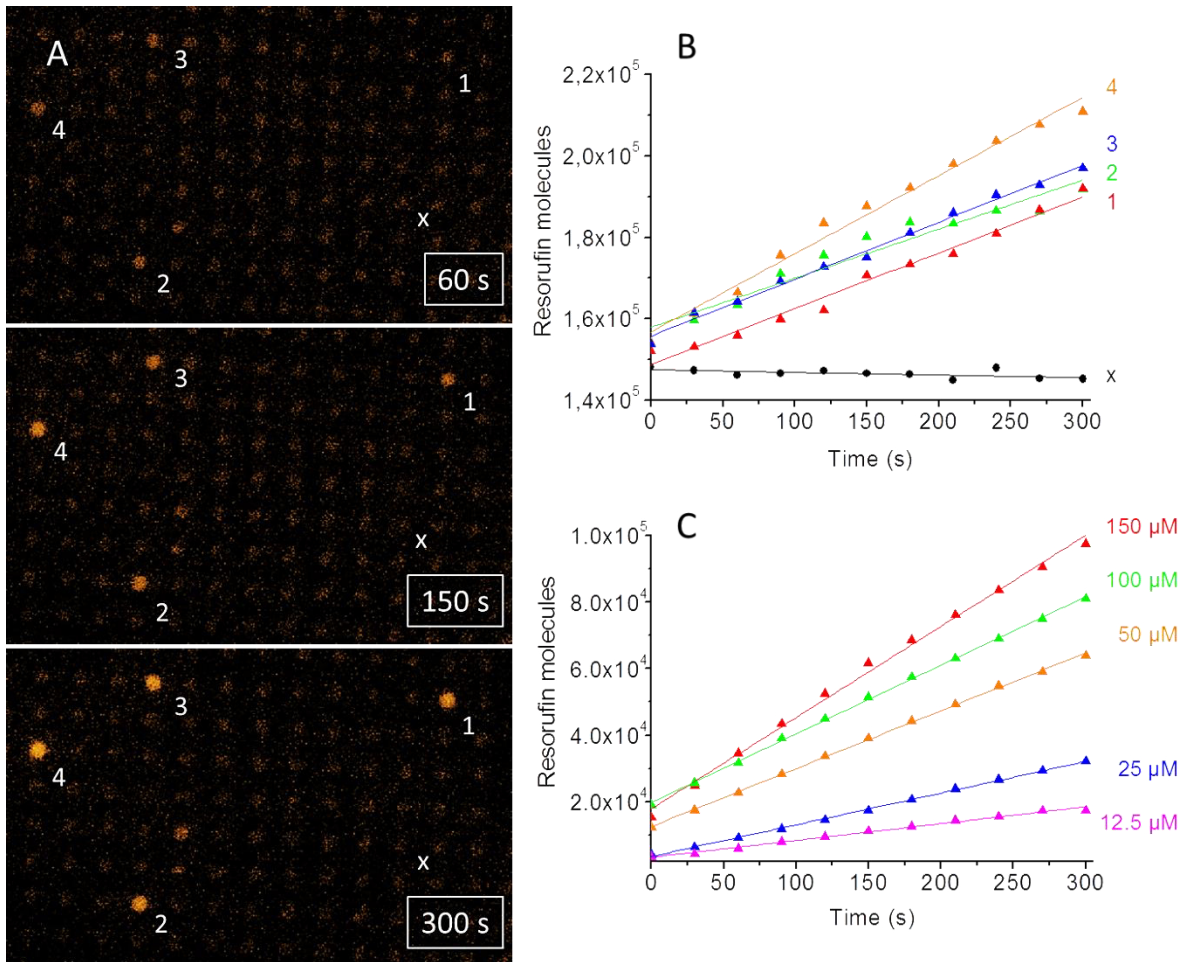


Figure 3.2 Substrate turnover of individual wild-type GUS enclosed in the wells of a femtoliter array. (A) Three images of a movie demonstrate the accumulation of fluorescent resorufin generated by individual GUS molecules in the presence of 100 μM ReG. A constant product formation can be observed in each occupied chamber with individually different substrate turnover rates (B). The background fluorescence is constant over time. (C) Ensemble trajectories of several hundred background corrected trajectories of single GUS molecules are displayed. They show a strong dependency on the ReG concentration as expected from classical Michaelis-Menten kinetics.

In Figure 3.2 (B) the trajectories of the five selected reaction chambers are shown. The overall fluorescence intensity in the unoccupied reaction chamber is constant over the course of the experiment (Table 3.1) and was applied for background correction. On the contrary, wells that contain a single wild-type GUS molecule generate a constant amount of fluorescent resorufin over time.

<i>Fluctuations without enzyme</i>	<i>SD</i>	<i>Trajectories of individual GUS</i>	<i>SD</i>
100 μM ReG (substrate only)	0.006	WT GUS (150 μM ReG)	46.4
15 μM Resorufin (high signal)	0.038	WT GUS (100 μM ReG)	27.5
1 μM Resorufin (low signal)	0.008	WT GUS (50 μM ReG)	19.7
		WT GUS (25 μM ReG)	17.6
		WT GUS (12.5 μM ReG)	11.9

Table 3.1 Background fluctuations of single molecule measurements. Fluctuations in the background signal were estimated from the time traces of wells without enzyme molecule (left column). All time traces in wells without GUS were constant over the course of the experiment as demonstrated by a very low standard deviation (SD). In contrast, the standard deviation of occupied wells, containing a single GUS molecule, was considerably higher at all tested ReG concentrations (right column). (Estimations are based on the average results from 50 independent reaction chambers.)

Measurements in fused silica femtoliter arrays further revealed individually different substrate turnover rates for single GUS molecules, which is in accordance with the static heterogeneity observed previously for individual β -galactosidase molecules. [3-5] The averaged ensemble trajectories of several hundred individual wild-type GUS, assembled from three independent measurements, are depicted in Figure 3.2 (C). The average enzyme activity strongly depends on the applied ReG concentration in the range of 12.5 to 150 μM and is consistent with Michaelis-Menten kinetics in the bulk reaction (Figure 3.3).

The substrate saturation curve of wild-type GUS in bulk solution was obtained under the same reaction conditions as the single molecule experiment. The applied bulk enzyme concentration of 36 pM equals a single enzyme molecule in a volume of 40 femtoliter. The enzyme activity of wild-type GUS showed a typical hyperbolic dependency for ReG concentrations in the range of 12.5 μM to 150 μM . Due to the limited solubility of ReG in aqueous buffer solutions, concentrations higher than 150 μM could not be investigated. (Equally, it was not possible to perform a Michaelis-Menten analysis of the partially evolved GUS variant ($K_M = 1260 \mu\text{M}$ in the reaction with *para*-nitrophenyl (*p*NP)-glucuronide (Appendix, Table 7.2.1). [1])

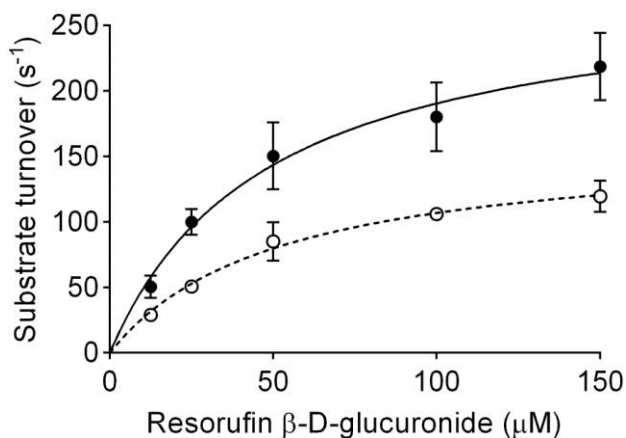


Figure 3.3 Substrate saturation curves of wild-type GUS. Full circles depict the average activity and standard deviation of six independent measurements in fused silica femtoliter arrays ($K_M = 49 \pm 8 \mu\text{M}$; $k_{cat} = 283 \pm 19 \text{ s}^{-1}$). Empty circles indicate the average enzyme activity and standard deviation of three bulk experiments ($K_M = 52 \pm 8 \mu\text{M}$; $k_{cat} = 162 \pm 10 \text{ s}^{-1}$).

The mean enzyme activity deviated from single molecule trajectories was higher than the respective turnover rate in bulk solution as it is impossible to completely exclude the presence of an inactive fraction of GUS (e.g. resulting from tetramer dissociation) during enzyme expression and purification. A percentage of inactive GUS inevitable leads to an

apparent decrease in the overall substrate turnover rates determined from bulk phase experiments. In contrast, single molecule experiments in femtoliter arrays only consider active GUS molecules which are included in the activity calculation. [31, 32] Consequently, k_{cat} ($v_{max}/[E]_0 = 162 \text{ s}^{-1}$) determined from the bulk experiment is lower than k_{cat} calculated directly from single wild-type GUS substrate turnover trajectories (283 s^{-1}). In opposition to the overall enzyme velocity, K_M is independent of the enzyme concentration. Consequently, the averaged single molecule and bulk K_M values were in excellent agreement ($K_M \approx 50 \text{ }\mu\text{M}$).

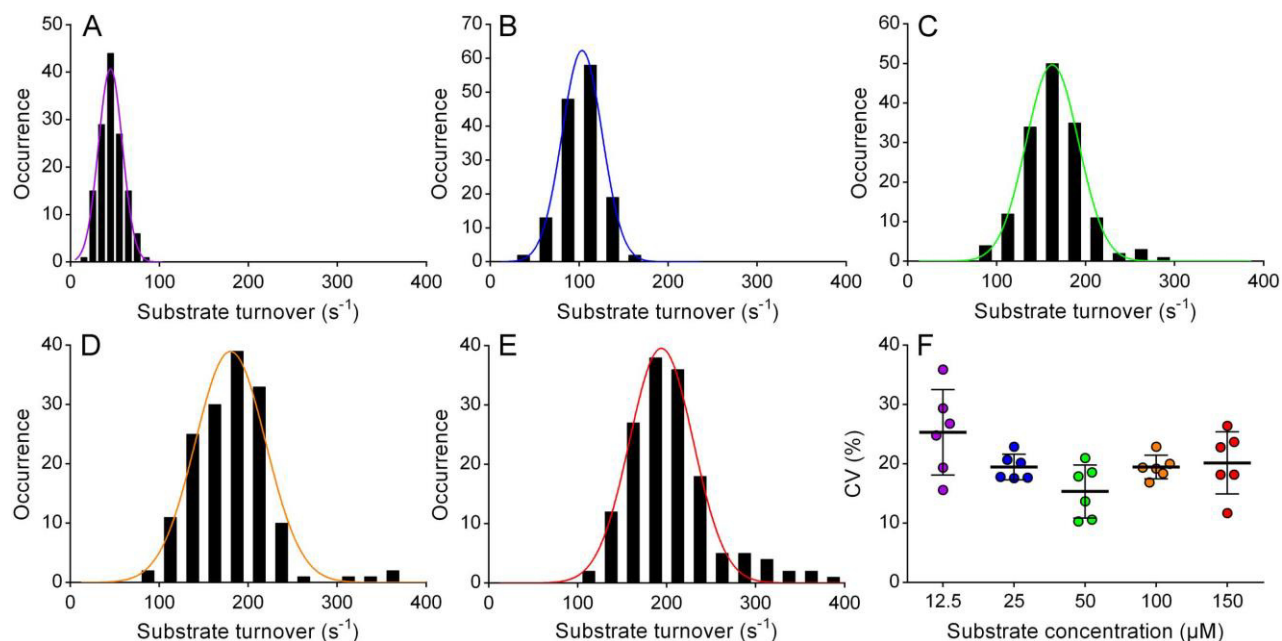


Figure 3.4 Substrate turnover distribution of several hundred individual wild-type GUS molecules. Each histogram depicts a representative single molecule experiment monitored for 5 minutes in the separate wells of a femtoliter array. Single GUS substrate turnover rates were recorded at ReG concentrations of (A) 12.5 μM , (B) 25 μM , (C) 50 μM , (D) 100 μM , and (E) 150 μM . A bin time of 10 s^{-1} was applied for (A) and 25 s^{-1} for (B - E). The activity distribution in each histogram follows a Gaussian distribution. (F) The plot demonstrates the coefficients of variation (CV) calculated from the Gaussian distribution of six independent single molecule experiments per ReG concentration.

The substrate turnover rates of several hundred single GUS molecules, monitored at different ReG concentrations, are assembled as histograms in Figure 3.4 (A-E). Each histogram displays one representative femtoliter array experiment – out of six independent measurements per substrate concentration – recorded over a time course of 5 minutes. (Histograms of all six measurements per enzyme concentration as well as an overview table can be found in the Appendix, Figure 7.2.3 and Table 7.2.2.)

Some histograms show a very small subpopulation, which is on average twice as active as the main population and can thus be attributed to a small number of femtoliter wells occupied with two enzyme molecules. This subpopulation, however, can be readily separated from the majority of single GUS trajectories that follow a Gaussian distribution. The activity distribution within the wild-type GUS population was determined from the coefficient of variation (CV) at each substrate concentration, calculated from the Gaussian distribution ($CV = \text{standard deviation} / \text{mean}$). For ReG concentrations between 25 μM and 150 μM the activity distribution was largely constant ($CV \approx 20\%$) (Figure 3.4). A slightly broader activity distribution ($CV = 25\%$) was determined for measurements at low substrate concentrations (12.5 μM). This observation can be attributed to the low intensity of the single molecule trajectories entailing an elevated background noise.

The activity distribution between individual molecules of wild-type GUS was compared with β -galactosidase, which is more than twice as active as GUS. β -Galactosidase and GUS both display an activity distribution that is largely independent of the applied substrate concentration (chapter 2.2.3). Consequently, the fluctuations in enzyme activity can be attributed to differences in k_{cat} rather than K_M , as discussed previously by Rissin and colleagues. [3] Single molecule femtoliter measurements of β -galactosidase, however, on average yield a broader activity distribution than GUS ($CV \approx 40\%$) (chapter 2.2.3). This finding may be explained by several facts: (1) β -Galactosidase

binds two magnesium(II) ions per monomer, which can lead to metal heterogeneity. [33] In contrast, GUS binds no metal ions. [34] (2) With 465 kDa [35] β -Galactosidase from *E. coli* is about twice as large as GUS (273 kDa). Consequently, due to its larger size, it can adopt more conformational alterations. (3) The hydrolysis of β -glucuronides is the only known natural function of GUS. On the contrary, β -galactosidase unites three catalytic functions: [36] primarily, the enzyme hydrolyzes its natural substrate lactose to galactose and glucose. In addition, β -galactosidase in part ($\approx 50\%$) performs a transgalactosylation reaction on lactose to generate allolactose. Allolactose binds to the *lac* repressor of the *lacZ* gene and thus induces the *lac* operon, resulting in the expression of β -galactosidase. As a third function, β -galactosidase hydrolyzes allolactose, yielding the monosaccharides. [37] The combination of three catalytic functions in one enzyme potentially requires a higher conformational plasticity from β -galactosidase than GUS, reflected in a broader distribution of substrate turnover rates.

3.2.2. Molecular Evolution from a Single Molecule Perspective

According to a concept on the general principle of adaptive evolution, elaborated by Tawfik and colleagues, [22-25] the evolution of new enzyme functionalities proceeds via non-specific intermediates (so-called generalists) that possess a promiscuous enzyme activity. These generalists maintain their native wild-type activity through several rounds of mutation and screening, but simultaneously adopt new properties that allow them to convert a variety of alternative substrates. After passing through the non-specific generalists, the enzyme finally specializes for a new substrate that is converted with a high enzymatic activity.

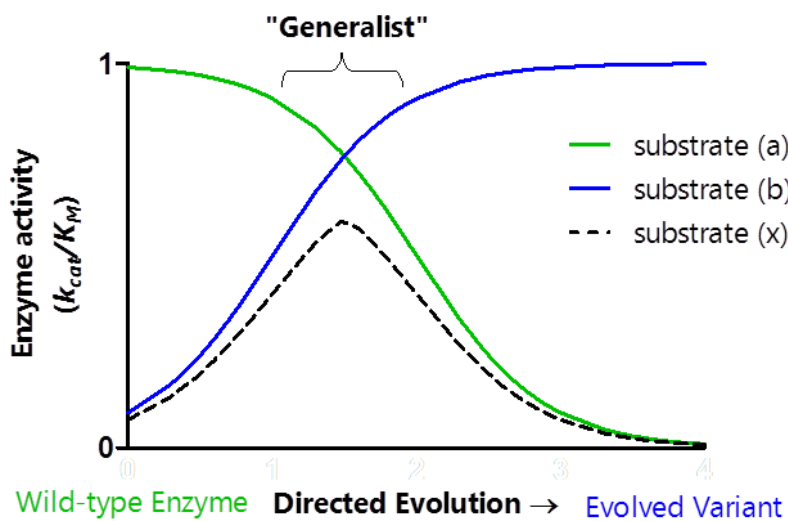


Figure 3.5 Schematic presentation of the *in vitro* evolution of enzymes. The adaptive evolution of new enzyme functionalities proceeds via non-specific generalists that keep their native wild-type activity but also convert a variety of alternative substrates, thus show a broad substrate specificity.

The broad substrate specificity of the generalists can be attributed to a higher conformational plasticity of the intermediates. Thus, one conformation is concerned with the native enzyme function while alternative conformations accept other substrates and

catalyze novel reactions. To date, all studies concerned with the identification of a higher conformational plasticity in evolutionary intermediates were conducted in bulk solution, where an averaged signal of millions of individual enzyme molecules is recorded. The recent development of sensitive single molecule technologies, however, enables us to investigate the contribution of individual molecules to the conformational diversity of a population of partially evolved enzymes.

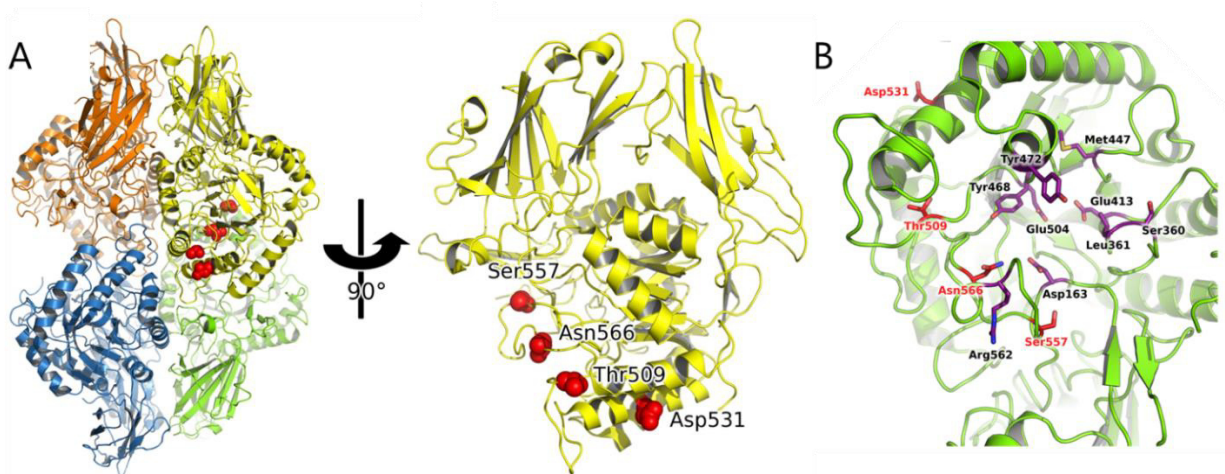


Figure 3.6 Structure of the partially evolved GUS variant. (A) Crystal structures of the *E. coli* GUS tetramer and monomer. The four amino acid substitutions in the partially evolved GUS variant (T509A/D531E/S557P/N566S) are indicated in red. (B) The enlarged cutout of the enzyme structure demonstrates the positions of the substituted amino acids relative to the active center.

For the single molecule investigation of adaptive enzyme evolution we isolated several hundred individual molecules of a partially evolved GUS variant (T509A/D531E/S557P/N566S) in the wells of a fused silica femtoliter array and analyzed them under the same reaction conditions as wild-type GUS. Matsumura *et al.* isolated the applied GUS variant during the *in vitro* evolution of wild-type GUS toward a higher activity for β -galactoside substrates in the second round of screening. [20] The wild-type GUS was altered by four amino acid substitutions (Figure 3.6): the D531E point mutation is located in a solvent

exposed α -helix and was reported to have no functional effect. [20] The other three substitutions, T509A, S557P and N566S, however, are located in the active-site loops of the GUS tetramer. The isolated, partially evolved GUS unites the characteristic properties of a generalist according to the definition by Tawfik and colleagues: it still shows a high catalytic activity towards glucuronides but also accepts several new glycosidic substrates (Appendix, Figure 7.2.1).

Other partially evolved GUS variants, identified during the *in vitro* evolution process, could not be investigated by single molecule enzymology as their relatively low substrate turnover rates did not suffice for a reliable detection in femtoliter arrays. Equally, it would also have been interesting to investigate the new enzyme function of partially evolved GUS by using galactoside substrates. However, even the substrate turnover of the most active evolved GUS variant (T509A/S557P/N566S/K567Q) towards galactoside substrates, was still far too low ($k_{cat}/K_M = 200 \text{ s}^{-1}\text{M}^{-1}$ in the reaction with *p*NP galactoside) [20] to enable a detection at the single molecule level. (A summary of the respective activities of the partially evolved variants, identified by Matsumura and Ellington during the *in vitro* evolution, can be found in the Appendix, Figure 7.2.1).

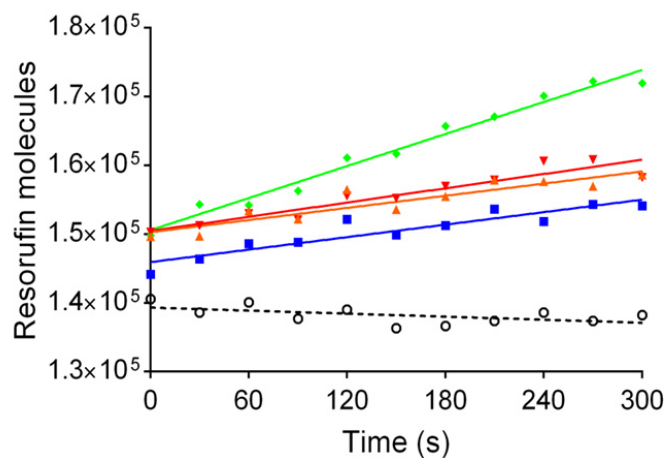


Figure 3.7 Single molecule substrate turnover of partially evolved GUS: Single molecule trajectories of partially evolved GUS display long-lived substrate turnover rates.

The original β -glucuronidase activity of the partially evolved variant T509A/D531E/S557P/N566S could readily be investigated in fused silica femtoliter arrays at a concentration of 100 μ M ReG. Similar to the results obtained for wild-type GUS, individual molecules of the generalist displayed long-lived substrate turnover rates (Figure 3.7) that followed a Gaussian distribution.

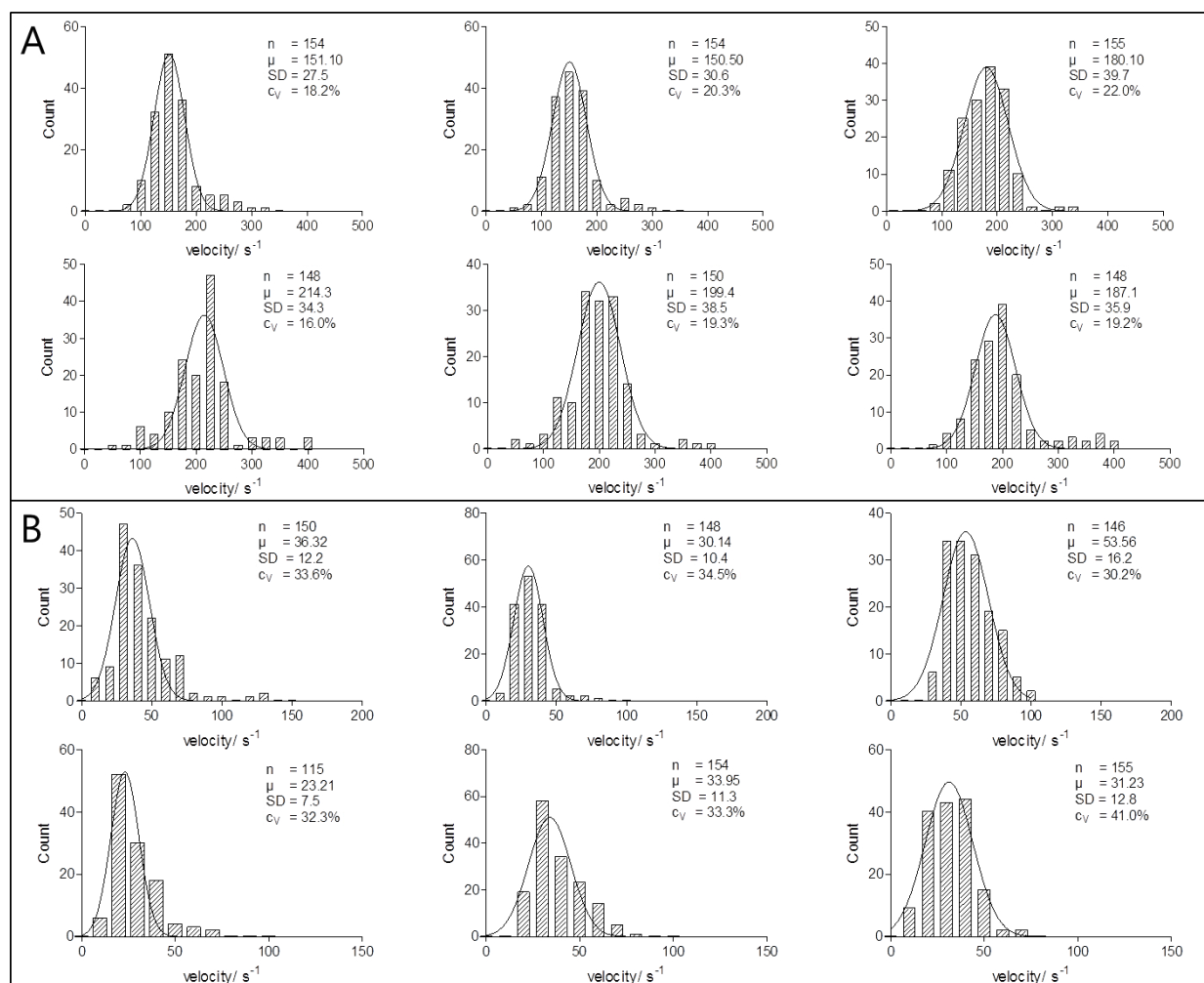


Figure 3.8 Histograms of the assembled substrate turnover rates of several hundred individual molecules of (A) wild-type GUS and (B) partially evolved GUS from six independent measurements. Each histogram shows a single molecule experiment recorded for 5 min at 100 μ M ReG.

Figure 3.8 (A) and (B) display the histograms of the assembled substrate turnover rates of several hundred wild-type (A) and partially evolved (B) GUS from six independent measurements in fused silica femtoliter arrays.

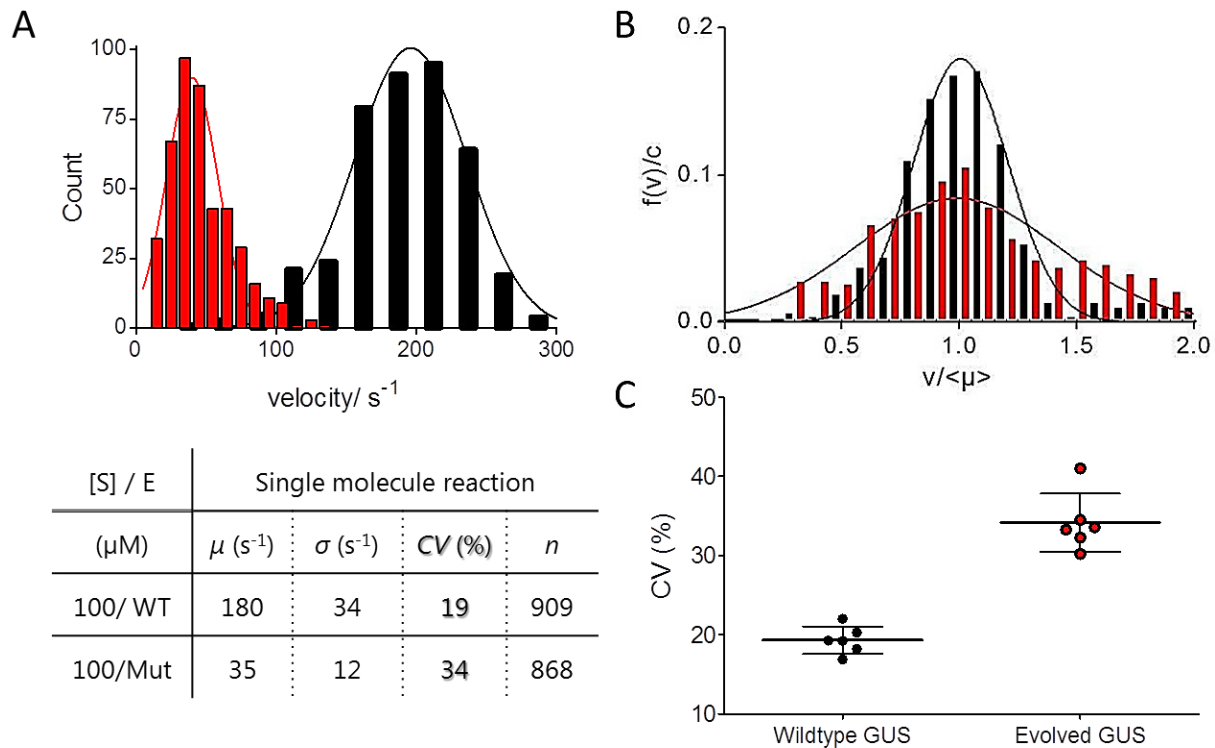


Figure 3.9 Differences in the single molecule substrate turnover distribution between wild-type GUS and partially evolved variant at 100 μM ReG. (A) The substrate turnover rates of the generalist (red, bin time 10 s) and wild-type GUS (black, bin time 25 s) both follow a Gaussian distribution. The histograms of the normalized substrate turnover rates (B) as well as the comparison of the CVs in an unpaired t-test (C) confirm a significantly broader activity distribution for partially evolved GUS than wild-type GUS.

The enzymatic activity in a population of partially evolved GUS variants is significantly more broadly distributed (CV = 34 %) compared to the wild-type GUS activity at 100 μM ReG (CV = 19 %) (Figure 3.9 A) or any other substrate concentration (Appendix, Figure 7.2.4). For better lucidity, the individual substrate turnover rates calculated from single

molecule experiments were normalized to their respective mean activity (μ). The normalized substrate turnover rates were then assembled to histograms (Figure 3.9 B). The histograms of the normalized substrate turnover rates further confirmed a significantly broader activity distribution in a population of partially evolved GUS than in wild-type GUS.

Additionally, the coefficients of variation ($CV = \mu/\sigma$), calculated from six independent single molecule experiments, of both wild-type and partially evolved GUS, were compared using a t-test to determine the significance (Figure 3.9 C): The difference in the activity distribution between wild-type GUS and generalist was significant ($p \leq 0.0001$) and thus again confirmed that the activity of partially evolved GUS is more broadly distributed among individual molecules than the respective activity of wild-type GUS.

The broader distribution of substrate turnover rates among individual enzyme molecules illustrates that partially evolved GUS is able to adopt a larger number of stable conformational states than the wild-type enzyme. Previous studies revealed that enzymes exhibit both fast interconversion between different activities ("*dynamic heterogeneity*") as well as distinct, long-lived activity states resulting in a distribution of substrate turnover rates ("*static heterogeneity*"). [3, 10, 38-42] The fast, dynamic changes result from low energy barriers between adjacent energy states, compared to the Boltzman energy (k_bT), that enable rapid transition between different enzymatic conformations, arising from minor intermolecular fluctuations. [23, 43]

The *static* heterogeneity observed in enzyme populations, however, can originate from two different sources or a combination of both: One possibility is that the enzyme molecules differ in their primary structure due to errors in transcription or translation. [23, 44-46] Both, transcription and translation processes, are rarely free of errors. For

example, the probability of a β -galactosidase tetramer molecule from *E. coli* being expressed without any errors is only 25%. [47] Otherwise, the *static* heterogeneity may also arise from different stable protein conformations and thus different activities between individual enzyme molecules, even when they possess the same amino acid sequence. [41]

According to Frauenfelder *et al.*, protein folding is based upon a rugged energy landscape, in which exist many local energy minima that represent conformational substates with varying structural and dynamic properties. [48] During protein folding, individual enzyme molecules can become trapped in different local minima. Consequently, a higher degree of conformational heterogeneity can be explained by the accommodation of more conformational states in each local minimum of partially evolved GUS compared to wild-type GUS.

Corresponding to the concept of *dynamic* and *static* heterogeneity, there not only occur slow transitions between stable conformational states with high energy barriers but also fast transitions between energy levels that are separated by a low energy barrier. The fast dynamic transitions between different energy states cannot be resolved with the time resolution of the single molecule readout in femtoliter arrays. With the available experimental setup we can only observe long-lived activity states. For a more comprehensive picture of the degree of heterogeneity within a population of partially evolved enzymes, thus, other types of single molecule experiments that also enable the resolution of faster transitions will be necessary.

The long-lived and broadly distributed activity states, observed in the single molecule femtoliter array experiments of partially evolved GUS, indicate a functional specialization among the individual members of the enzyme population, which accounts for the promiscuous enzyme activity of the generalist. In this way, one conformation can execute the native enzyme function while alternative conformations react with other

substrates and catalyze novel reactions. The formation of individually specialized enzyme molecules as a motor for protein dynamism and evolvability [24, 49] challenges the traditional view of proteins as single fixed structures that possess absolute functional specificity. [23]

Additionally, the single molecule investigation of directed enzyme evolution can make an interesting contribution to the disclosure of the fundamental principles of primordial enzyme evolution (Figure 3.10). In the mid-seventies, Ycas [26] and Jensen [28] established the “patchwork” hypothesis, which states that primordial enzymes possessed a very broad substrate specificity. In this way, ancient cells with minimal gene content could command a highly flexible metabolism. During evolution, gene duplication events provided the basis for an increasing diversification and specialization of enzyme activities. In combination with the development of regulatory unites, the step-wise specialization gradually led to the establishment of the highly efficient metabolism of modern cells.

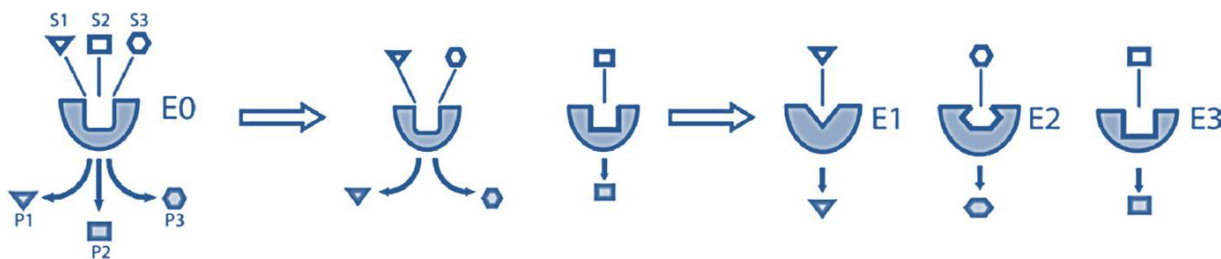


Figure 3.10 The evolution of primordial enzymes: Primordial enzymes possessed a very broad substrate specificity that allowed for the compensation of the low gene content in ancient cells. Later, gene duplication led to the step-wise diversification and specialization of enzyme activities. Modified, schematic presentation of enzyme evolution reprinted with permission from [50], ©2009 Elsevier Masson SAS. All rights reserved.

The “division of work”, here observed among individual molecules of a partially evolved enzyme population, may have enabled ancient cells to compensate for their low gene content. By adopting distinct and long-lived conformational states that accept various substrates, individual enzymes with a single amino acid sequence could conveniently overcome the limited cellular resources of primordial cells. Later, with incipient diversification and specialization, the catalytic information, stored in the conformational composition of individual enzyme molecules, was delegated to the RNA and DNA level to avoid adverse side reactions in the more complex cellular environment. With this task handover, the promiscuous activity of enzymes became obsolete, resulting in modern enzymes with a more homogeneous activity. [51]

3.2.3. Circular Dichroism Analysis

According to Mauno Vihinen, the conformational flexibility of a protein is reflected in its thermostability: [52] There is a fine balance between the flexibility required to perform a catalytic function and the structural stability of an enzyme. [53] Consequently, the achievement of information on the structural stability of wild-type and partially evolved GUS can make an important contribution to the discussion on the enzyme's conformational diversity.

We analyzed the changes in secondary structure of wild-type and partially evolved GUS at elevated temperatures by circular dichroism (CD). The primary structure of both enzymes differs only in four (T509A/S557P/N566S/K567Q) out of 603 amino acids. Consequently, they adopt a very similar secondary structure at room temperature (Figure 3.11 A).

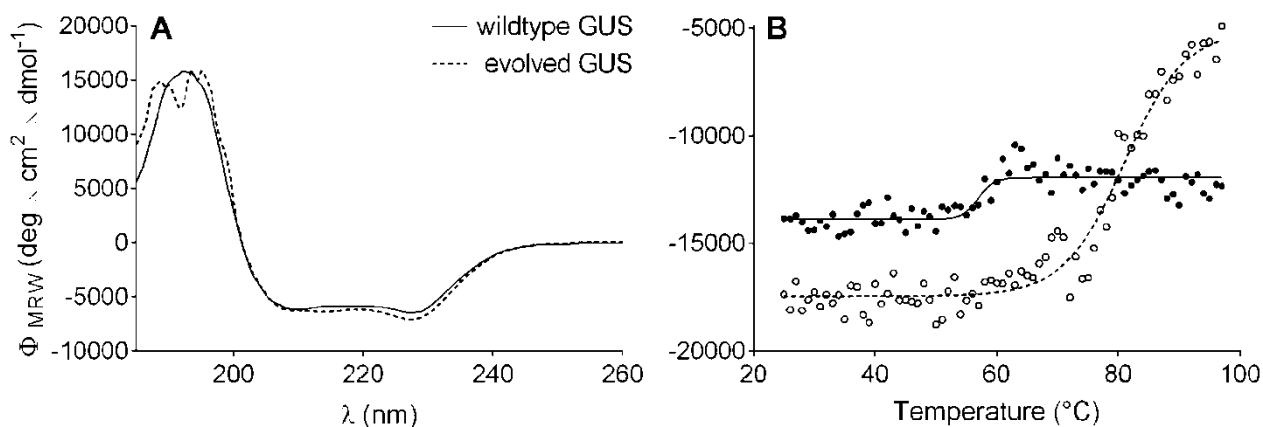


Figure 3.11 Circular dichroism analysis of wild-type and partially evolved GUS. (A) The CD spectra show a similar secondary structure for both wild-type (solid line) and partially evolved (hatched line) GUS at room temperature. (B) The conformational stability of wild-type (full dots) and partially evolved (empty dots) GUS was investigated by circular dichroism at increasing temperature. Wild-type GUS showed to be stable up to 100 $^{\circ}\text{C}$ with only a minor change in secondary structure at around 60 $^{\circ}\text{C}$, attributed to tetramer dissociation. In contrast, the evolved variant shows a typical thermal denaturation profile at temperatures higher than 60 $^{\circ}\text{C}$, resulting from monomer unfolding.

However, it has already been demonstrated in previous studies [54, 55], that the substitution of only a few amino acids can have a strong impact on the thermostability of GUS. Figure 3.11 (B) displays the CD spectra of wild-type and partially evolved GUS at increasing temperature, revealing significant differences in thermostability between the wild-type and partially evolved GUS. The overall secondary structure of wild-type GUS remains largely constant up to 100 °C, indicating highly thermostable monomer subunits. At temperatures higher than 60 °C, a minor change in secondary structure is observed that can be attributed to tetramer dissociation and is accompanied by a loss of enzymatic activity. [54] In opposition to the wild-type enzyme, CD analysis of partially evolved GUS yields a typical thermal denaturation profile at temperatures higher than 60 °C that suggests monomer unfolding.

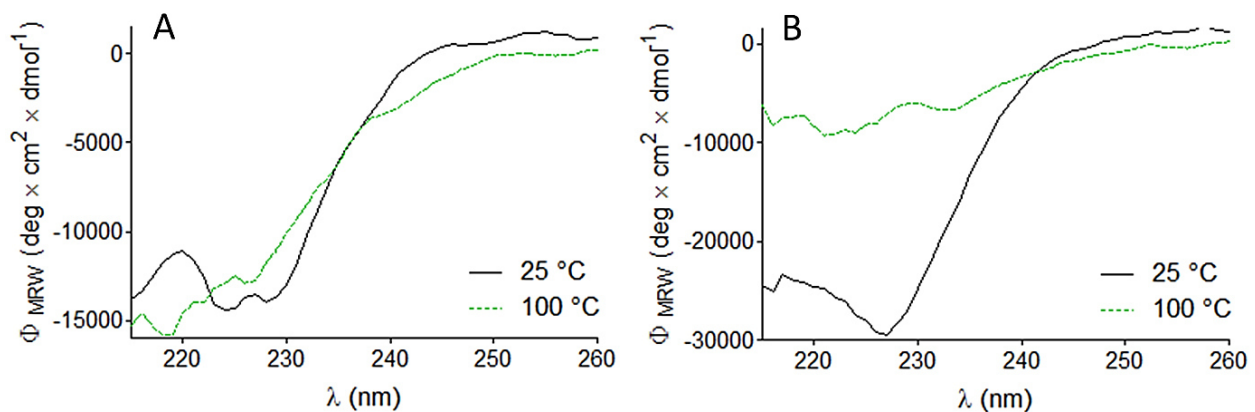


Figure 3.12 CD spectra of wild-type and partially evolved GUS recorded at 25 °C (solid black line) and 100 °C (hatched green line). (A) The CD spectrum of wild-type GUS displays only minor changes in secondary structure at elevated temperature. Otherwise, the enzyme remains intact even at high temperature. (B) The significant changes in the CD spectrum of partially evolved GUS recorded at 100 °C reflects the protein denaturation at high temperature.

Figure 3.12 displays the CD spectra of wild-type (A) and partially evolved (B) GUS recorded at room temperature (solid black line) and 100 °C (hatched green line). While

the CD spectrum of the wild-type enzyme shows only minor changes in secondary structure after heat treatment, the spectrum of partially evolved GUS reflects the thermal denaturation of the protein structure at elevated temperatures.

The observed lower thermostability of the generalist compared to the wild-type, is an evidence of its higher conformational flexibility and thus supports the results obtained from single molecule measurements. The more flexible conformation of the partially evolved GUS variant is reflected in the broader activity distribution. Hence, the combined results of the single molecule measurements in femtoliter arrays and CD analysis confirmed the thesis proclaimed formerly by Tawfik and colleagues on the basis of bulk phase experiments.

3.3. Materials and Methods

3.3.1. General Preparatory and Analytical Methods

Centrifugation. Centrifugation steps were either performed with a Sorvall™ RC2-B plus high-speed refrigerated centrifuge equipped with SS34- and GS3-rotors (DU PONT Instruments, www.labx.com) or a 5415 D/R Eppendorf micro-centrifuge (www.eppendorf.com).

UV and Emission Spectra. UV-VIS spectra were acquired with a Cary 50 Bio UV-visible spectrophotometer from Varian (Agilent Technologies Inc.). Measurements were performed in standard quartz cuvettes. Emission spectra were recorded on a Jasco FP6300 luminescence spectrometer equipped with a 150-W continuous wave Xenon lamp as the excitation source. Spectra were recorded in standard or semi-micro fluorescence cuvettes.

Microplate measurements were acquired on a Fluostar Optima microtiter plate reader (BMG labtech, www.bmg-labtech.com) equipped with a high energy Xenon flash lamp.

Crystal Structures. The crystal structures of the *E. coli* GUS tetramer and the interface of two monomers (chapter 3.1, Figure 3.1 and chapter 3.2.2, Figure 3.6) were rendered with PyMOL (DeLano Scientific LLC) (PDB ID: 3k46) by Max Renner in the context of a research project at the group of Prof. Reinhard Sterner, institute for biophysics and physical biochemistry, University of Regensburg.

Analysis and Plotting. Data analysis and plotting was performed with Microsoft Excel 2010 (office.microsoft.com), Origin 6.1 from Origin lab Corporation (www.originlab.de) or GraphPad Prism 5 (www.graphpad.com). Chemical structures and schemes were drawn using ChemBioDraw Ultra 12.0 (www.cambridgesoft.com) in combination with Microsoft Office PowerPoint (office.microsoft.com).

3.3.2. Protein Expression and Purification

Expression plasmids. The expression plasmids pET-28a(+), containing sequences for N-terminally his-tagged wild-type β -glucuronidase (GUS) or the partially evolved variant T509A/D531E/S557P/N566S, were kind gifts of Ichiro Matsumura. A detailed description of the plasmid can be found in the work of Matsumura and Ellington. [20]

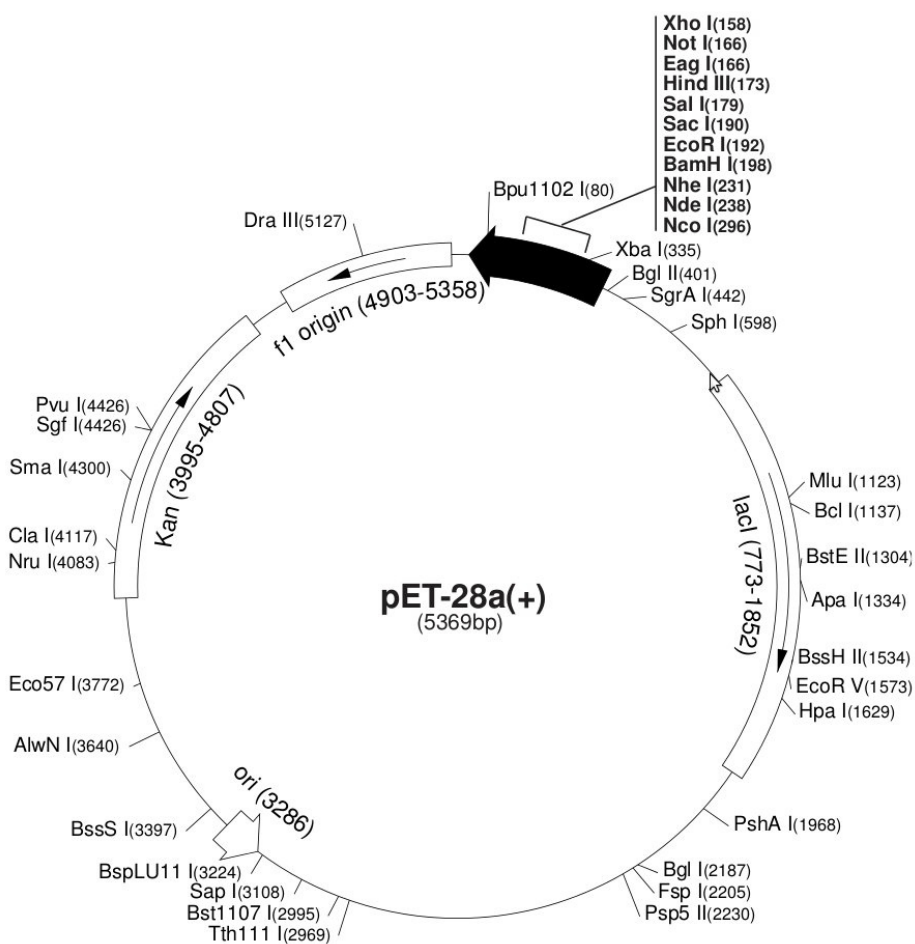


Figure 3.13 Schematic presentation of a pET-28a(+) vector (Novagen, www.novagen.com.br). The vector bears a (His)₆-tag/thrombin unity upstream of the MCS (multiple cloning site). Additionally, the vector possesses an optional C-terminal (His)₆-tag. Besides, the vector includes a kanamycin-resistance gene. The genes of the MCS are transcribed by RNA-polymerases of the phage T7. [56]

Expression of wild-type and partially evolved GUS. Enzyme expression and purification was performed by Max Renner in the context of a research project at the group of Prof. Reinhard Sterner, institute for biophysics and physical biochemistry, University of Regensburg.

The pET-28a(+) plasmids were applied for the transformation of *Escherichia coli* T7 Express cells (New England Biolabs, www.neb.com). For protein expression, the transformed cells were cultivated in one liter batches of Luria-Bertani (LB) medium (0.5 % (w/v) yeast extract, 1 % (w/v) tryptone, 1 % (w/v) NaCl) at 37 °C in the presence of kanamycin (25 µg/mL). The cell culture was grown to an OD₆₀₀ (optical density at 600 nm) of 0.4-0.6 at 37 °C under shaking. Protein expression was then induced by the addition of 0.5 mM isopropyl-β-D-thiogalactopyranosid (IPTG) in water. After further cultivation at 37 °C (16 h), the cells were harvested by centrifugation at 3000 x g and 4 °C for 20 min.

The cell pellets were resuspended in 20 mL of nickel chelate chromatography running buffer (50 mM sodium phosphate, pH 7.0, 300 mM NaCl, 10 mM imidazole, 5 mM β-mercaptoethanol, 1 mM EDTA) per liter medium. The cells were lysed by sonication on ice (Branson Sonifier 250 D, Heinemann Ultraschall- und Labortechnik, www.gheinemann.de), followed by pelleting via centrifugation at 23 000 x g and 4 °C for 30 min. The supernatant was filtered through a pre-equilibrated HisTrap FF crude affinity column (GE Healthcare, www.gehealthcare.com, column volume 5 mL; elution rate: 4 mL/min). For elution, the imidazole concentration of the running buffer was linearly increased. The recombinant proteins were further purified by size exclusion chromatography (SEC) using a S200 2/0 column (GE Healthcare), pre-equilibrated in SEC running buffer (50 mM sodium phosphate, pH 7.0, 300 mM NaCl).

The purity of the obtained enzyme preparations was confirmed by SDS-PAGE (Appendix, Figure 7.2.2). Protein concentrations were determined by a Bradford assay

(Sigma Aldrich) [57] or UV-absorption spectroscopy. [58] The purified enzymes were concentrated using Amicon Ultra 4 centrifugal units (Millipore, www.millipore.com). Droplets of the protein solution were snap-frozen in liquid nitrogen and stored at -80 °C.

3.3.3. Experiments on Enzyme Kinetics

Single Enzyme Molecule Experiments. The procedure of the standard single molecule experiment as well as information on the applied buffers, reagents and femtoliter arrays can be found in the chapter 2.3.3 "Single Molecule Enzyme Experiment". Additionally, the chapter 2.3.3 covers a detailed description of the applied wide-field fluorescence microscope, the explicit experimental microscope settings for all single enzyme experiments as well as details on image processing and data analysis. (calibration curve in the Appendix, Figure 7.2.5 A)

Bulk Experiment. The activity of wild-type GUS in bulk solution was determined in transparent 96-well microtiter plates (Nunc, www.nuncbrand.com) under the same reaction conditions as the single molecule experiment. The substrate turnover of various ReG concentrations was monitored on a microtiter plate reader ($\lambda_{\text{ex}} = 544 \text{ nm}$, $\lambda_{\text{em}} = 575 \text{ nm}$) and calibrated with help of a resorufin standard curve recorded under identical conditions (calibration curve in the Appendix, Figure 7.2.5 B).

3.3.4. Circular Dichroism Experiments

Circular Dichroism (CD)-Spectra Acquisition. All CD-spectra were recorded in GUS-buffer (50 mM sodium phosphate, 5 mM β -mercaptoethanol, 1 mM EDTA) on a Jasco-J-815 CD-spectrometer (www.jasco.de), flooded with nitrogen.

CD-Spectra of Secondary Enzyme Structure. The CD-spectra of wild-type and partially evolved GUS representing the secondary enzyme structure at room temperature (chapter 3.2.3, Figure 3.11) were recorded using a round cuvette with a glass thickness of 0.2 mm (Thomas Scientific, www.thomassci.com). Data were collected from 185 to 260 nm with a recording velocity of 20 nm per min. The final spectra were assembled from three independent measurements. After baseline correction the spectra were fitted with a digital Savitzky-Golay filter. [59]

Temperature-Dependent CD-Spectra. For CD-Spectra recorded at increasing temperature (chapter 3.2.3, Figure 3.12), a round cuvette with a glass thickness of 1.0 mm (Thomas Scientific) was applied. The conformational stability of the proteins was analyzed by increasing the temperature from 25 °C to 100 °C in increments of 1 °C per min and recording the molar ellipticity (Φ) at $\lambda = 228$ nm.

Survey-Measurements at 100 °C. The survey CD-spectra recorded at 100 °C were performed in a round cuvette with a glass thickness of 1.0 mm (Thomas Scientific). Data was collected from 210 to 260 nm with a recording velocity of 20 nm per min. The final survey spectra were constructed from a single measurement.

3.4. Conclusion

Most biochemical processes rely on enzymatic catalysis. Consequently, for a deeper understanding of the fundamental principles of life, the analysis of the catalytic mechanisms of enzymes and their evolution is essential and of immediate interest in biological sciences. In this work, it was demonstrated that single molecule experiments in femtoliter arrays provide new insights, not only into the catalysis of enzymes, but also how new catalytic activities evolve.

β -Glucuronidase (GUS) catalyzes a simple hydrolytic reaction with high activity that can be readily observed at the single molecule level. Several hundred single GUS molecules were separated in large arrays of 62 500 ultrasmall reaction chambers etched into the surface of fused silica slides. Their individual substrate turnover rates were observed in parallel by fluorescence microscopy and compared to the closely related enzyme β -galactosidase. Both enzymes display distinct, long-lived substrate turnover rates. Their mean activities are consistent with traditional Michaelis-Menten kinetics in bulk solution. In comparison to β -glucuronidase, the activity of individual β -galactosidase molecules is more broadly distributed, which may be attributed to the broader range of catalytic functions united by β -galactosidase.

Without doubt, analyzing the mechanisms that drive the evolution of new enzyme activities is crucial to understanding the biochemical principles of life. Consequently, how enzymes adapt to new functions, is a fundamental question of evolutionary biology. In recent years, it was shown by *in vitro* evolution that new enzyme functions evolve from non-specific generalists that accept a broad range of substrates. From these non-specific intermediates emerge perfected enzyme variants, which are highly specific for a new catalytic function. The broad substrate specificity – so-called promiscuous activity - of the generalists was attributed to a higher conformational plasticity, such that different enzyme conformations attend to varying enzymatic functions.

In this work, the substrate turnover of wild-type GUS and an *in vitro* evolved generalist were analyzed at the single molecule level in the wells of a fused silica femtoliter array. The partially evolved GUS variant T509A/D531E/S557P/N566S, which was isolated during the *in vitro* evolution of GUS into β -galactosidase, displayed a much broader activity distribution than the wild-type enzyme. The broader distribution indicates a higher conformational plasticity of partially evolved enzymes. This finding was confirmed by a circular dichroism analysis of both wild-type and partially evolved GUS that revealed a significantly lower thermostability of the generalist, reflecting its higher structural flexibility.

The broad static heterogeneity found among individual substrate turnover rates of the non-specific generalists can be transferred to the mechanisms of ancient enzyme evolution. It was proposed that the higher structural flexibility of primordial enzymes enabled them to adapt new functions and thus helped ancient cells to survive, in spite of their limited gene content.

3.5. References

1. Liebherr, R.B., M. Renner, and H.H. Gorris, *A Single Molecule Perspective on the Functional Diversity of in Vitro Evolved beta-Glucuronidase*. *J. Am. Chem. Soc.*, **2014** (136): 5949.
2. Michaelis, L. and M.L. Menten, *Die Kinetik der Invertinwirkung*. *Biochem. Z.*, **1913** (49): 333.
3. Rissin, D.M., H.H. Gorris, and D.R. Walt, *Distinct and long-lived activity states of single enzyme molecules*. *J. Am. Chem. Soc.*, **2008** (130): 5349.
4. Craig, D.B. and N.J. Dovichi, *Escherichia coli beta-galactosidase is heterogeneous with respect to the activity of individual molecules*. *Can. J. Chem.*, **1998** (76): 623.
5. Rondelez, Y., G. Tresset, K.V. Tabata, H. Arata, H. Fujita, S. Takeuchi, and H. Noji, *Microfabricated arrays of femtoliter chambers allow single molecule enzymology*. *Nat. Biotechnol.*, **2005** (23): 361.
6. Gorris, H.H. and D.R. Walt, *Mechanistic aspects of horseradish peroxidase elucidated through single-molecule studies*. *J. Am. Chem. Soc.*, **2009** (131): 6277.
7. Ehrl, B.N., R.B. Liebherr, and H.H. Gorris, *Single molecule kinetics of horseradish peroxidase exposed in large arrays of femtoliter-sized fused silica chambers*. *Analyst*, **2013** (138): 4260.
8. Velonia, K., O. Flomenbom, D. Loos, S. Masuo, M. Cotlet, *et al.*, *Single-enzyme kinetics of CALB-catalyzed hydrolysis*. *Angew. Chem. Int. Ed.*, **2005** (44): 560.
9. Flomenbom, O., K. Velonia, D. Loos, S. Masuo, M. Cotlet, *et al.*, *Stretched exponential decay and correlations in the catalytic activity of fluctuating single lipase molecules*. *Proc. Natl. Acad. Sci. U. S. A.*, **2005** (102): 2368.
10. Lu, H.P., L. Xun, and X.S. Xie, *Single-molecule enzymatic dynamics*. *Science*, **1998** (282): 1877.
11. Terentyeva, T.G., H. Engelkamp, A.E. Rowan, T. Komatsuzaki, J. Hofkens, C.B. Li, and K. Blank, *Dynamic disorder in single-enzyme experiments: facts and artifacts*. *ACS Nano*, **2012** (6): 346.
12. De Cremer, G., M.B. Roeffaers, M. Baruah, M. Sliwa, B.F. Sels, J. Hofkens, and D.E. De Vos, *Dynamic disorder and stepwise deactivation in a chymotrypsin catalyzed hydrolysis reaction*. *J. Am. Chem. Soc.*, **2007** (129): 15458.
13. Tan, W.H. and E.S. Yeung, *Monitoring the reactions of single enzyme molecules and single metal ions*. *Anal. Chem.*, **1997** (69): 4242.

14. Gorris, H.H., D.M. Rissin, and D.R. Walt, *Stochastic inhibitor release and binding from single-enzyme molecules*. Proc. Natl. Acad. Sci. U. S. A., **2007** (104): 17680.
15. Wallace, B.D., H.W. Wang, K.T. Lane, J.E. Scott, J. Orans, *et al.*, *Alleviating Cancer Drug Toxicity by Inhibiting a Bacterial Enzyme*. Science, **2010** (330): 831.
16. Jacobson, R.H., X.J. Zhang, R.F. Dubose, and B.W. Matthews, *3-Dimensional Structure of Beta-Galactosidase from Escherichia-Coli*. Nature, **1994** (369): 761.
17. Jain, S., W.B. Drendel, Z.W. Chen, F.S. Mathews, W.S. Sly, and J.H. Grubb, *Structure of human beta-glucuronidase reveals candidate lysosomal targeting and active-site motifs*. Nat Struct Biol, **1996** (3): 375.
18. Henrissat, B., *Sequence homology between a beta-galactosidase and some beta-glucosidases*. Protein Seq Data Anal, **1991** (4): 61.
19. Jefferson, R.A., T.A. Kavanagh, and M.W. Bevan, *GUS fusions: beta-glucuronidase as a sensitive and versatile gene fusion marker in higher plants*. EMBO J., **1987** (6): 3901.
20. Matsumura, I. and A.D. Ellington, *In vitro evolution of beta-glucuronidase into a beta-galactosidase proceeds through non-specific intermediates*. J. Mol. Biol., **2001** (305): 331.
21. Matsumura, I., J.B. Wallingford, N.K. Surana, P.D. Vize, and A.D. Ellington, *Directed evolution of the surface chemistry of the reporter enzyme beta-glucuronidase*. Nat. Biotechnol., **1999** (17): 696.
22. Aharoni, A., L. Gaidukov, O. Khersonsky, Q.G.S. Mc, C. Roodveldt, and D.S. Tawfik, *The 'evolvability' of promiscuous protein functions*. Nat. Genet., **2005** (37): 73.
23. James, L.C. and D.S. Tawfik, *Conformational diversity and protein evolution--a 60-year-old hypothesis revisited*. Trends Biochem. Sci., **2003** (28): 361.
24. Tokuriki, N. and D.S. Tawfik, *Protein dynamism and evolvability*. Science, **2009** (324): 203.
25. Khersonsky, O., C. Roodveldt, and D.S. Tawfik, *Enzyme promiscuity: evolutionary and mechanistic aspects*. Curr. Opin. Chem. Biol., **2006** (10): 498.
26. Ycas, M., *On earlier states of the biochemical system*. J. Theor. Biol., **1974** (44): 145.
27. Meier, S. and S. Ozbek, *A biological cosmos of parallel universes: does protein structural plasticity facilitate evolution?* BioEssays, **2007** (29): 1095.
28. Jensen, R.A., *Enzyme recruitment in evolution of new function*. Annu. Rev. Microbiol., **1976** (30): 409.

29. Claren, J., C. Malisi, B. Hocker, and R. Sterner, *Establishing wild-type levels of catalytic activity on natural and artificial (beta alpha)(8)-barrel protein scaffolds*. Proc. Natl. Acad. Sci. U. S. A., **2009** (106): 3704.
30. Pervushin, K., K. Vamvaca, B. Vogeli, and D. Hilvert, *Structure and dynamics of a molten globular enzyme*. Nat. Struct. Mol. Biol., **2007** (14): 1202.
31. Rissin, D.M. and D.R. Walt, *Digital concentration readout of single enzyme molecules using femtoliter arrays and Poisson statistics*. Nano Lett., **2006** (6): 520.
32. Gorris, H.H. and D.R. Walt, *Analytical chemistry on the femtoliter scale*. Angew. Chem. Int. Ed., **2010** (49): 3880.
33. Uda, N.R., G. Upert, G. Angelici, S. Nicolet, T. Schmidt, T. Schwede, and M. Creus, *Zinc-selective inhibition of the promiscuous bacterial amide-hydrolase DapE: implications of metal heterogeneity for evolution and antibiotic drug design*. Metallomics, **2014** (6): 88.
34. Edman, L., Z. Foldes-Papp, S. Wennmalm, and R. Rigler, *The fluctuating enzyme: a single molecule approach*. Chem. Phys., **1999** (247): 11.
35. Marchesi, S.L., E. Steers, and S. Shifrin, *Purification and Characterization of Multiple Forms of Beta-Galactosidase of Escherichia Coli*. Biochim. Biophys. Acta, **1969** (181): 20.
36. Juers, D.H., B.W. Matthews, and R.E. Huber, *LacZ beta-galactosidase: structure and function of an enzyme of historical and molecular biological importance*. Protein Sci., **2012** (21): 1792.
37. Huber, R.E., K. Wallenfels, and G. Kurz, *The action of beta-galactosidase (Escherichia coli) on allolactose*. Can J Biochem, **1975** (53): 1035.
38. English, B.P., W. Min, A.M. van Oijen, K.T. Lee, G. Luo, *et al.*, *Ever-fluctuating single enzyme molecules: Michaelis-Menten equation revisited*. Nat. Chem. Biol., **2006** (2): 87.
39. Min, W., B.P. English, G. Luo, B.J. Cherayil, S.C. Kou, and X.S. Xie, *Fluctuating enzymes: lessons from single-molecule studies*. Acc. Chem. Res., **2005** (38): 923.
40. Xue, Q. and E.S. Yeung, *Differences in the chemical reactivity of individual molecules of an enzyme*. Nature, **1995** (373): 681.
41. Rojek, M.J. and D.R. Walt, *Observing single enzyme molecules interconvert between activity states upon heating*. PLoS One, **2014** (9): e86224.
42. Dyck, A.C. and D.B. Craig, *Individual molecules of thermostable alkaline phosphatase support different catalytic rates at room temperature*. Luminescence, **2002** (17): 15.

43. Henzler-Wildman, K. and D. Kern, *Dynamic personalities of proteins*. Nature, **2007** (450): 964.
44. van Oijen, A.M., P.C. Blainey, D.J. Crampton, C.C. Richardson, T. Ellenberger, and X.S. Xie, *Single-molecule kinetics of lambda exonuclease reveal base dependence and dynamic disorder*. Science, **2003** (301): 1235.
45. Craig, D.B. and E.R. Nichols, *Continuous flow assay for the simultaneous measurement of the electrophoretic mobility, catalytic activity and its variation over time of individual molecules of Escherichia coli beta-galactosidase*. Electrophoresis, **2008** (29): 4298.
46. Drummond, D.A. and C.O. Wilke, *The evolutionary consequences of erroneous protein synthesis*. Nat. Rev. Genet., **2009** (10): 715.
47. Craig, D.B., T. Schwab, and R. Sterner, *Random mutagenesis suggests that sequence errors are not a major cause of variation in the activity of individual molecules of beta-galactosidase*. Biochem. Cell Biol., **2012** (90): 540.
48. Frauenfelder, H., S.G. Sligar, and P.G. Wolynes, *The energy landscapes and motions of proteins*. Science, **1991** (254): 1598.
49. Peisajovich, S.G. and D.S. Tawfik, *Protein engineers turned evolutionists*. Nat. Methods, **2007** (4): 991.
50. Fondi, M., G. Emiliani, and R. Fani, *Origin and evolution of operons and metabolic pathways*. Res. Microbiol., **2009** (160): 502.
51. O'Brien, P.J. and D. Herschlag, *Catalytic promiscuity and the evolution of new enzymatic activities*. Chem. Biol., **1999** (6): R91.
52. Vihinen, M., *Relationship of protein flexibility to thermostability*. Protein Eng., **1987** (1): 477.
53. Zavodszky, P., J. Kardos, Svingor, and G.A. Petsko, *Adjustment of conformational flexibility is a key event in the thermal adaptation of proteins*. Proc. Natl. Acad. Sci. U. S. A., **1998** (95): 7406.
54. Flores, H. and A.D. Ellington, *Increasing the thermal stability of an oligomeric protein, beta-glucuronidase*. J. Mol. Biol., **2002** (315): 325.
55. Xiong, A.S., R.H. Peng, Z.M. Cheng, Y. Li, J.G. Liu, et al., *Concurrent mutations in six amino acids in beta-glucuronidase improve its thermostability*. Protein Eng Des Sel, **2007** (20): 319.

56. Studier, F.W., A.H. Rosenberg, J.J. Dunn, and J.W. Dubendorff, *Use of T7 RNA polymerase to direct expression of cloned genes*. *Methods Enzymol.*, **1990** (185): 60.
57. Bradford, M.M., *A rapid and sensitive method for the quantitation of microgram quantities of protein utilizing the principle of protein-dye binding*. *Anal. Biochem.*, **1976** (72): 248.
58. Pace, C.N., F. Vajdos, L. Fee, G. Grimsley, and T. Gray, *How to measure and predict the molar absorption coefficient of a protein*. *Protein Sci.*, **1995** (4): 2411.
59. Savitzky, A. and M.J. Golay, *Smoothing and Differentiation of Data by Simplified Least Squares Procedures*. *Anal. Chem.*, **1964** (36): 1627.

4. Femtoliter Arrays for Concentration Analysis

This chapter is based upon the Journal Article "*Three-in-one enzyme assay based on single molecule detection in femtoliter arrays*", Liebherr R.B., A. Hutterer, M.J. Mickert, F.C. Vogl, A. Beutner, A. Lechner, H. Hummel and H.H. Gorris, **2015**, submitted.

4.1. Introduction

In addition to manifold applications in the field of basic research, the detection of single enzyme molecules in arrays of femtoliter-sized reaction chambers can also be employed for highly sensitive concentration analysis. [1-5]

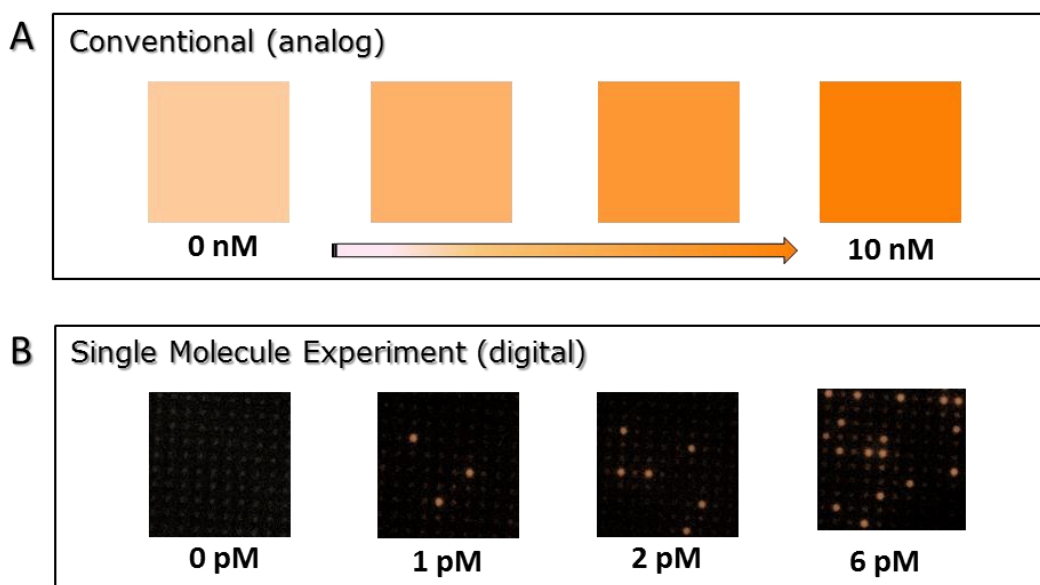


Figure 4.1 Comparison of analog and digital concentration readout: (A) Traditional bulk phase experiment on a μL scale that requires millions of analyte molecules to attain the limit of detection. (B) Experiment in an array of fL-sized reaction vessels: The binary readout system ("yes/no"-response) allows for the digital readout of analyte concentrations and clears the path for the development of ultrasensitive bioassays.

When an enzyme solution is highly diluted and spread over a femtoliter array, individual enzyme molecules are distributed randomly among the reaction chambers. At a specific concentration limit, which depends on the well size, there is statistically one molecule present per chamber. For femtoliter arrays with a chamber size of about 40 fL, a concentration of 36 pM yields on average one enzyme molecule per reaction chamber ($\mu = 1$). Increased dilution of the sample further reduces the ratio of occupied wells, as summarized in Table 4.1.

enzyme concentration (pM)	36	18	3.6	1.8	0.72	0.36
ratio of occupied wells	1.00	0.50	0.10	0.05	0.02	0.01

Table 4.1 Ratio of occupied wells at different enzyme concentrations for fL-arrays with a well-size of 40 femtoliters: For high dilutions (number of enzyme molecules \ll number of reaction chambers) the number of occupied wells depends linearly on the enzyme concentration according to the Poisson distribution.

For highly diluted samples, the percentage of occupied wells directly correlates with the inserted bulk phase concentration and follows a Poisson distribution (chapter 1.3.4):

$$P_{\mu}(x) = \frac{e^{-\mu} \mu^x}{x!} \quad (4.1)$$

In general, the Poisson distribution describes the probability of a small number of events in a large number of trials. For highly diluted enzyme concentrations, the probability $P_{\mu}(x)$ of finding x enzyme molecules in a distinct fL-chamber is given by equation 4.1, whereas μ represents the mean number of enzyme molecules per reaction chamber.

In concentration analysis of highly diluted samples in femtoliter arrays, the analyte concentration is determined by simply observing the presence or absence (“yes/no”-response) of a fluorescent product, resulting from single enzyme molecule substrate turnover. From the number of “active”, thus fluorescent chambers the ensemble concentration can be calculated. This binary readout scheme can be applied to determine analyte concentrations way below the detection limit of traditional methods. [6-11] In contrast to conventional (analog) bioassays, the signal will never fall below the detection limit. Instead the number of active chambers decreases when the analyte is diluted.

The principle of digital concentration readout by means of single enzyme molecule detection can be used for the development of a variety of ultra-sensitive bioassays, such as immunoassays. In this case, the enzyme is applied as a reporter for the detection of biological analytes. Enzymatic signal amplification enables the detection of analytes with very high sensitivity. As the reporter enzyme can be detected at the single molecule level, also individual molecules of the analyte can be detected, representing ultimate sensitivity. Thus, the establishment of ultra-sensitive bioassays, conducted in the wells of large femtoliter arrays, has the potential to revolutionize conventional analytical chemistry.

4.2. Results and Discussion

To test the principle of digital concentration readout in the wells of a fused silica femtoliter array, varying concentrations of the model-enzyme β -galactosidase were applied. The diluted enzyme solution in combination with the fluorogenic substrate resorufin- β -D-galactopyranoside (RGP) was enclosed in the homogeneous wells of the glass femtoliter arrays. The fluorescence signal generated in individual wells due to the accumulation of fluorescent resorufin from single β -galactosidase substrate turnover was read out by wide-field fluorescence microscopy.

The volume of the employed reaction vessels defines the dynamic range of concentrations that can be determined by digital concentration readout in femtoliter arrays. The wells employed in this experiment were about 3.5 μm in depth and 4 μm in diameter thus defined a volume of approximately 40 femtoliter. Consequently, an applied solution of 36 pM β -galactosidase would yield, on average, one enzyme molecule per reaction chamber (chapter 4.1).

However, due to the random distribution of enzymes, the entrapment of a 36 pM enzyme solution in the wells of the fL-array does not result in the assignment of exactly one β -galactosidase molecule per vessel. Instead, statistically, some wells are occupied by several enzyme molecules while others would contain none. At a 36 pM enzyme concentration, Poisson statistics calculate an assignment of zero to five molecules per reaction chamber, whereat zero or one molecule per well are the most probable events ($P_{\mu}(5) = 0.3\%$, $P_{\mu}(4) = 1.3\%$, $P_{\mu}(3) = 5.6\%$, $P_{\mu}(2) = 17.5\%$, $P_{\mu}(1) = 36.7\%$, $P_{\mu}(0) = 38.5\%$). Accordingly, although zero or one molecule per well are the most probable events, some vessels will contain two, three or even more β -galactosidase molecules.

For concentrations considerably lower than 36 pM, the probability of gathering more than one β -galactosidase molecule per chamber is very low. For an enzyme concentration of 3.6 pM the probability of enclosing two enzyme molecules in one well

$(P_{\mu}(2))$ is smaller than 0.5 % and the probability of gathering three or more molecules in one reaction chamber ($P_{\mu}(\geq 3)$) equals 0.0 %. At such low concentrations, an approximately linear correlation between the ratio of occupied, thus active wells and the bulk enzyme concentration is observed. This linear relation allows for a simple, digital readout of enzyme concentrations (chapter 4.1).

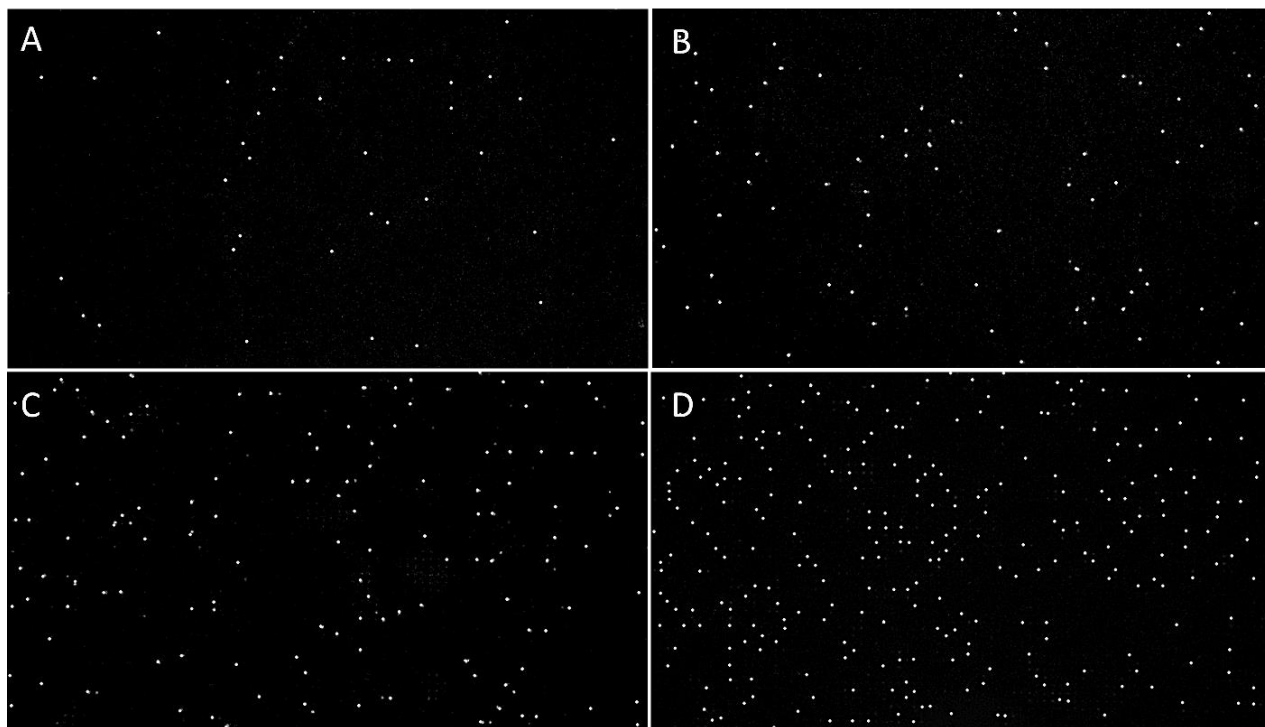


Figure 4.2 Substrate turnover of individual β -galactosidase molecules enclosed in the wells of a fL-array. The images (A) to (D) show one representative measurement out of three repeats at four different enzyme concentrations: (A) 0.36 pM, (B) 0.9 pM, (C) 1.8 pM and (D) 3.6 pM. The solutions with varying β -galactosidase concentration each were enclosed separately in the wells of a fL-array together with a constant RGP concentration of 100 μ M. The number of “active” wells that light up due to fluorescent product formation clearly decreases with lower enzyme concentration.

In the proof of principle experiment four different β -galactosidase concentrations were investigated at 100 μ M ReG in three repetitive measurements. For concentration

analysis, the number of “active”, thus bright wells was counted. Figure 4.2 depicts a section of 5600 reaction chambers of a fused silica array 300 seconds after the signal acquisition started. Figure 4.2 shows one representative measurement for each of the four tested RGP concentrations. As expected, the number of occupied wells that light up due to formation of fluorescent resorufin clearly decreases with lower enzyme concentration.

Figure 4.3 graphically displays the correlation between the amount of β -galactosidase present in the sample and the percentage of wells that were occupied by an enzyme. The linear relationship ($R^2 = 0.9959$) between enzyme concentration and ratio of active reaction chambers confirms the applicability of the binary readout detection scheme in fused silica femtoliter arrays.

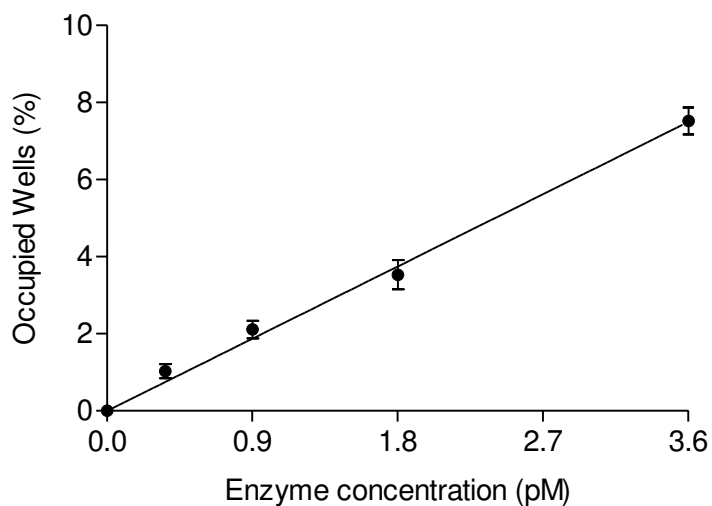


Figure 4.3 Plot displaying the percentage of “active” reaction chambers at the respective deployed β -galactosidase concentrations. All experiments were performed thrice, with the standard deviation being represented by error bars.

Digital concentration readout was performed, by applying a Poisson statistical analysis: The ratio of fluorescent reaction chambers was calculated for each deployed enzyme

concentration and compared to the expected percentage of active wells according to the Poisson distribution (Table 4.2).

Enzyme-to- well ratio	Concentration [pM]	Poisson active [%]	E1 [%]	E2 [%]	E3 [%]	Average [%]	SD [%]
1/10	3.6	9.1	7.68	7.12	7.77	7.5	0.4 %
1/20	1.8	4.6	3.82	3.67	3.10	3.5	0.4 %
1/40	0.9	2.3	2.02	1.95	2.38	2.1	0.2 %
1/80	0.36	0.9	1.23	0.95	0.91	1.0	0.2 %

Table 4.2 Digital Concentration Readout of different β -galactosidase concentrations from fL-arrays etched into fused silica slides. The expected ratio of occupied to empty wells according to Poisson statistics, the actual percentages of “active” wells exhibiting enzyme activity from three independent measurements (E1 to E3), the average ratio of actually “active” wells and the standard deviation are listed.

The slight variations between the calculated and the experimental results, as shown in Table 4.2, can be attributed to several different reasons. First, the Poisson distribution, like any distribution, shows an intrinsic variability that will be reflected in the results.

Negative deviations between the actual and expected number of “active” wells, in particular stated for more concentrated samples, may arise from an elevated number of reaction chambers that are occupied by more than one enzyme molecule. Additionally, a negative deviation may also be the result of experimental errors in the preparation of the enzyme solution or an insufficient sealing of the femtoliter wells responsible for the occurrence of small air bubbles in some of the wells that prevent the placement of a β -galactosidase molecule. Another possible reason may be some extent of enzyme adhesion to the spacing between the femtoliter wells prior to array sealing, especially in

more concentrated samples. Positive deviations, as observed to some minor extent in highly diluted samples, may also arise from an insufficient array sealing resulting in fluorescent product leakage into neighboring wells.

4.3. Materials and Methods

Single Enzyme Molecule Experiments. The procedure of the standard single molecule experiment as well as information on the applied buffers, reagents and femtoliter arrays can be found in the chapter 2.3.3 "Single Molecule Enzyme Experiment". Additionally, the chapter 2.3.3 covers a detailed description of the applied wide-field fluorescence microscope, the explicit experimental microscope settings for all single enzyme experiments as well as details on image processing and data analysis.

Some initial measurements at varying β -D-galactosidase concentrations were conducted by Franziska Vogl during her Master thesis. The test series was completed, evaluated and interpreted in the scope of this PhD thesis.

4.4. Conclusion

The confinement of bioanalytical reactions in arrays of uniform, fL-sized reaction chambers discloses new insights into the mechanistic relations in biochemical processes. Femtoliter arrays are mainly employed for fundamental research on single molecule kinetics, but they can also be applied for analytical measurements. The application of a large array of homogeneously arranged ultra-small reaction chambers in combination with enzymatic signal amplification enables the digital readout of low target concentrations in complex biological or environmental samples. [7-10] While traditional bulk phase experiments indicate the analyte concentration by an analog response, single molecule measurements enable the digital readout of an analyte content by simply counting the number of occupied, thus "active" and empty, thus "non-active" wells. Due to this digital readout scheme, concentration analysis in femtoliter arrays has the potential to distinctly increase the sensitivity of common bioanalytical assays to the point of an "ultimate" sensitivity, the single molecule detection. [5, 12, 13]

In a proof of principle experiment, the applicability of fused silica femtoliter arrays for digital concentration readout was demonstrated. The obtained results were in good correlation with the theoretical calculated values and perfectly agreed with the results from previous studies. [2, 14]

Thus it was demonstrated, that enzyme analysis in femtoliter arrays can indeed give answers to three different analytical problems. First, the analysis of a large number of individual enzyme molecules in femtoliter arrays can give information on the ensemble substrate turnover of the population (chapter 2.2.3). Second, the same single molecule experiment can disclose the activity distribution in the enzyme population, which is hidden in a bulk experiment (chapter 2.2.3 and 3.3.2). Finally, the random distribution of single enzyme molecules in a femtoliter array enables the digital determination of the enzyme concentration.

4.5. References

1. Rissin, D.M. and D.R. Walt, *Duplexed sandwich immunoassays on a fiber-optic microarray*. Anal. Chim. Acta, **2006** (564): 34.
2. Rissin, D.M. and D.R. Walt, *Digital concentration readout of single enzyme molecules using femtoliter arrays and Poisson statistics*. Nano Lett., **2006** (6): 520.
3. Li, Z., R.B. Hayman, and D.R. Walt, *Detection of single-molecule DNA hybridization using enzymatic amplification in an array of femtoliter-sized reaction vessels*. J. Am. Chem. Soc., **2008** (130): 12622.
4. Rissin, D.M., D.R. Walt, and H.H. Gorris, *Methods and arrays for target analyte detection and determination of target analyte concentration in solution*. Tufts College USA (**2007**), Patent WO 2007/098148-A3.
5. Walt, D.R., *Protein measurements in microwells*. Lab Chip, **2014** (14): 3195.
6. Rissin, D.M., C.W. Kan, T.G. Campbell, S.C. Howes, D.R. Fournier, *et al.*, *Single-molecule enzyme-linked immunosorbent assay detects serum proteins at subfemtomolar concentrations*. Nat. Biotechnol., **2010** (28): 595.
7. Wilson, D.H., D.W. Hanlon, G.K. Provuncher, L. Chang, L. Song, *et al.*, *Fifth-generation digital immunoassay for prostate-specific antigen by single molecule array technology*. Clin. Chem., **2011** (57): 1712.
8. Song, L., D.W. Hanlon, L. Chang, G.K. Provuncher, C.W. Kan, *et al.*, *Single molecule measurements of tumor necrosis factor alpha and interleukin-6 in the plasma of patients with Crohn's disease*. J. Immunol. Methods, **2011** (372): 177.
9. Rissin, D.M., D.R. Fournier, T. Piech, C.W. Kan, T.G. Campbell, *et al.*, *Simultaneous Detection of Single Molecules and Singulated Ensembles of Molecules Enables Immunoassays with Broad Dynamic Range*. Anal. Chem., **2011** (83): 2279.
10. Rissin, D.M., C.W. Kan, L. Song, A.J. Rivnak, M.W. Fishburn, *et al.*, *Multiplexed single molecule immunoassays*. Lab Chip, **2013** (13): 2902.
11. Kan, C.W., A.J. Rivnak, T.G. Campbell, T. Piech, D.M. Rissin, *et al.*, *Isolation and detection of single molecules on paramagnetic beads using sequential fluid flows in microfabricated polymer array assemblies*. Lab Chip, **2012** (12): 977.
12. Gorris, H.H. and D.R. Walt, *Analytical chemistry on the femtoliter scale*. Angew. Chem. Int. Ed., **2010** (49): 3880.

13. Gorris, H.H. and D.R. Walt, *Analytische Chemie im Femtoliter*. *Angew. Chem.*, **2010** (122): 3970.
14. Rissin, D.M. and D.R. Walt, *Digital readout of target binding with attomole detection limits via enzyme amplification in femtoliter arrays*. *J. Am. Chem. Soc.*, **2006** (128): 6286.

5. Array Functionalization for Application in Concentration Analysis

5.1. Introduction

For the implementation of ultra-sensitive bioanalytical assays such as single molecule ELISAs in fused silica femtoliter arrays, the introduction of suitable functional groups and the immobilization of specific biomolecules on the well surface are obligatory. In the framework of this thesis two different methods were employed in order to bind certain biomolecules, such as peptides, antibodies or even whole enzymes to the surface of the wells of a fused silica femtoliter array.

On the one hand, an organic reaction generally known under the term “click chemistry” was applied for the introduction of peptides to the array surface. To be named “click reaction” a chemical process must meet specific criteria determined by Sharpless *et al.* in 2001: [1] It must be of a modular reaction type, be of wide scope and provide high yields. Additionally, the reaction has to be carried out with readily available starting material, under simple reaction conditions and without the use of any hazardous solvents. The term “click reaction” also requires a process, which is insensitive towards water or oxygen with simple reaction work-up and purification, excluding offensive byproducts. Finally, physiological stable products and stereospecificity are mandatory characteristics. [1, 2] Multiple processes such as cycloadditions, hetero-Diels-Alder reactions, nucleophilic substitution reactions, epoxidations and several more meet the “click chemistry” criteria. [1] The most established and popular example of a click reaction, however, is the copper(I)-catalyzed 1,3-dipolar cycloaddition of azides and alkynes (CuAAC) resulting in 1,2,3-triazoles, extensively investigated by R. Huisgen in the 1960s (see Figure 4.1). [3-5]

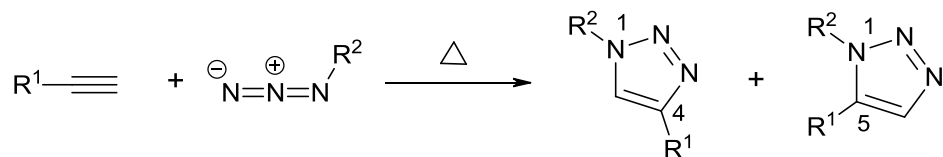


Figure 4.1 The principal reaction scheme of the Huisgen 1,3-dipolar cycloaddition of azides and alkynes.

Principally, the cycloaddition is not regioselective but results in the equimolar generation of the 1,4- and 1,5-disubstituted 1,2,3-triazoles. The reaction further requires long reaction times at elevated temperatures and thus does not meet the criteria of a “click reaction”. Meldal *et al.* [6] as well as Sharpless *et al.* [7, 8], however, simultaneously, yet independently, discovered the reaction conditions required for the Huisgen 1,3-dipolar cycloaddition to become a “click reaction” according to definition: When the cycloaddition is catalyzed by copper(I) ions the reaction proceeds at room temperature within short time in aqueous solutions and selectively delivers the 1,4-regioisomer. Copper(I) ions can be added directly in the form of salts such as CuI or generated *in situ* by adding copper(II) salts like CuSO₄ together with a reducing agent such as sodium ascorbate. A 0.01 molar equivalent of the copper(I) catalyst proved to be sufficient to promote the reaction as displayed in Figure 4.2.

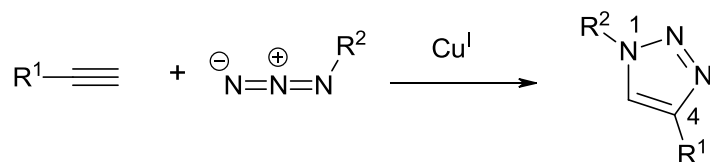


Figure 4.2 Reaction scheme of the Cu(I)-catalyzed 1,3-dipolar cycloaddition of azides and alkynes (CuAAC) resulting in the regioselective formation of the 1,4-disubstituted 1,2,3-triazole. Due to the regioselectivity, the mild reaction conditions and the short reaction time this altered 1,3-dipolar cycloaddition belongs to the group of “click reactions”.

The CuAAC (Figure 4.2) is bioorthogonal: [9-12] The low reactivity of azido and alkyne functional groups implicates inertness towards biological molecules. Additionally, the CuAAC can be performed in aqueous solutions, at room temperature and over a wide pH range. The introduction of the clickable reactive groups to biomolecules is comparatively easy and the starting materials as well as products are insensitive to oxygen. Finally, the reaction is chemoselective with almost no side reactions. Consequently, this click reaction excellently qualifies for biological applications. In addition, azido groups as well as terminal alkyne groups are especially suited as binding sites in proteins as they are not present in any side chain of natural amino acids. For all those reasons, the copper(I)-catalyzed cycloaddition of azides and terminal alkynes is perfectly suited for the introduction of peptides to the surface of fused silica femtoliter wells to allow for their application in biological assays.

The stable, covalent attachment of antibodies to the femtoliter array surface enables the development of a broad variety of bioanalytical assays, notably immunoassays. Immunological assays are well established in bioanalytical sciences, but are also important tools in food analysis and environmental investigation. Due to their high specificity, their broad practicability and applicability, they are of great use for the analysis of complex biological samples. Conventional immunological assays, based on bulk phase experiments, already cover a broad range of analyte concentrations. However, with the introduction of digital signal readout, the limit of detection can be reduced to unprecedented limits. [13-16]

Antibodies were attached to the surface of fused silica femtoliter arrays using common peptide chemistry. This well-established and simple method enables the covalent immobilization of any biomolecule that possesses primary amino groups. Primary amines are present at the N-terminus of each polypeptide chain as well as in

some amino acid side chains and are generally found on the outside of the protein tertiary structure, where they are easily accessible to conjugation reagents.

A broad variety of functional groups exist that will form a chemical bond with primary amines. The most common ones are carboxyl functionalities, which can be readily introduced to the surface of fused silica femtoliter arrays. Prior to peptide-bond formation, the carboxylic group is activated. A multitude of different techniques for carboxyl activation are applied in modern peptide chemistry. [17, 18] In peptide-chemistry, the carboxylic group is typically activated *in situ* by DCC (dicyclohexylcarbodiimide) and subsequent formation of an active ester using NHS (*N*-hydroxysuccinimide) (Figure 4.3). [19-21] NHS-ester activated compounds readily react with primary amines at physiological pH, yielding stable peptide bonds. [22]

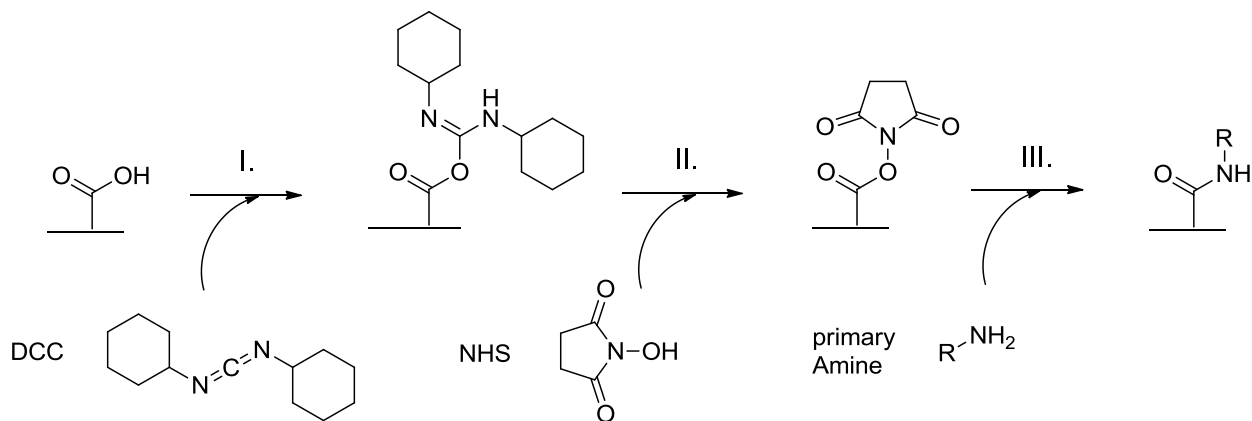


Figure 4.3 Reaction scheme of the carboxylic acid activation, using DCC (dicyclohexylcarbodiimide) (I) with subsequent formation of a NHS active-ester (II). The NHS-activated carboxylic group readily reacts with primary amines (III) that exist at the N-terminus of each polypeptide chain in protein-based biomolecules, such as antibodies, at physiologic conditions.

5.2. Results and Discussion

5.2.1. Array Functionalization Using Click Chemistry

In a first step, the surface of the fused silica femtoliter array was made applicable for click chemistry by the introduction of either azido or terminal alkyne functional groups with help of the clickable silanes (1) and (2) shown in Figure 4.4. The dimethoxy- and trimethoxysilanes are capable of reacting with the surface hydroxyl groups of the fused silica surface [23, 24] yielding a covalent, stable connection.

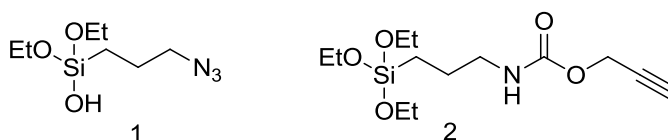


Figure 4.4 Chemical structure of the clickable silanes 1 ((3-Azidopropyl)diethoxy(hydroxyl)silane) and 2 (O-(Propargyloxy)-N-(triethoxysilylpropyl)urethane) applied for the functionalization of the fused silica surface of the fL-wells to make them applicable for click chemistry.

In the style of two different, but likewise successful silanization protocols described in literature, two alternative types of silanization reactions were evolved (Figure 4.5): (A) In 1993, Kallury *et al.* published the silanization of silica particles in toluene under varying conditions. [25] Eventually, they found surface silanization performed in dry toluene for several hours at high temperatures to be most efficient. In the meantime, this method has already been applied successfully in several studies. [26-29] (B) Rissin *et al.* applied a different method, when preparing the femtoliter wells of optical-fiber bundles for bioanalytical assays: [30] The fiber-optic bundle was silanized at room temperature in 2-propanol for one hour. A similar approach was published by Karrasch *et al.* [31], who conducted silanization reactions in aqueous acetone under standard aerobic conditions for several minutes at room temperature.

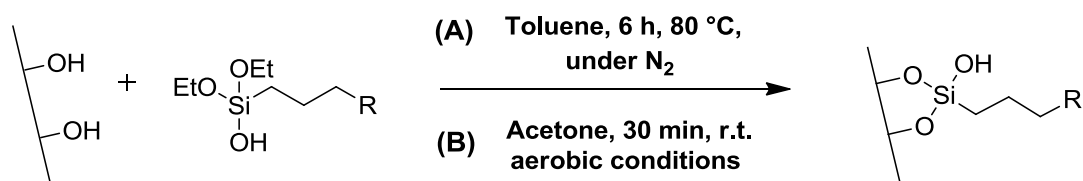


Figure 4.5 Two types of silanization procedures applied for the functionalization of fused silica fl-wells with clickable silanes. (A) Silanization in toluene under reflux and anaerobic conditions for several hours. (B) Open-vial silanization in acetone at room temperature for several minutes.

The successful realization of the respective silanization protocols was verified by ATR (attenuated total reflection)-IR-spectroscopy and/ or goniometric measurement of the resulting surface contact angles. The generation of a strong ATR-IR-signal requires a close approximation of ATR-crystal and sample. Due to the difficulty of achieving a sufficient approximation of ATR-crystal and silanized surface, the signal obtained for functionalized glass slides was rather weak. In consequence, surface-silanization performed in toluene under nitrogen (protocol A), could not be characterized by ATR-IR-spectroscopy, because the silane film was too thin to detect its functional groups. In contrast, the open-vial silanization in acetone (protocol B), yielded a thicker silane film that allowed for ATR-IR-characterization.

The ATR-IR-spectra of the unbound clickable silanes and the unmodified silica surface were used as a reference (for detailed IR-spectra see Appendix, Figure 7.3.1). The clickable silane (1) could easily be identified by ATR-IR-spectroscopy, due to the anti-symmetric stretching vibration of the azido group, [32] yielding a distinct peak at $\approx 2096 \text{ cm}^{-1}$. In contrast the alkyne functionality of compound (2) did not show an equally intense IR-signal. Instead, the peak at $1700\text{-}1712 \text{ cm}^{-1}$, assigned to the stretching vibrations of the carbonyl functional group, confirmed the successful introduction of the alkyne functional group on the fused silica surface.

Contact angle measurements of the azido- and alkyne-functionalized fused silica slides finally ensured the successful application of both silanization protocols (A) and (B) (Table 4.1). Untreated, dry fused silica slides that had previously been cleaned in piranha solution, with subsequent incubation in distilled water, were used as a reference. Goniometric analysis provided an average contact angle of $39.8^\circ \pm 2.1$ on the unmodified, clean glass slides. For slides functionalized with compound (1) an elevated mean contact angle of $59.7^\circ \pm 0.9$ (procedure A) or $60.4^\circ \pm 5.1$ (procedure B) was measured. For fused silica surfaces treated with the clickable silane (2), similarly increased average contact angles of $79.3^\circ \pm 0.8$ (procedure A) and $62.7^\circ \pm 1.5$ (procedure B) were obtained.

Contact angle	Silane (1)		Silane (2)		untreated
	Acetone	Toluene	Acetone	Toluene	
# 1	59.4	60.4	64.4	78.9	41.8
# 2	55.8	58.7	61.5	78.8	37.7
# 3	66.0	60.1	62.3	80.2	40.0
mean	60.4 ± 5.2	59.7 ± 0.9	62.7 ± 1.5	79.3 ± 0.8	39.8 ± 2.1

Table 4.1 Contact angles measured with DI-water in three independent measurements for fused silica slides treated with the clickable silanes (1) and (2) under different reaction conditions, as well as for untreated fused silica slides are listed. Additionally, the mean contact angle of all three measurements is stated.

Estimation of alterations in surface contact angles represents a well-established and rapid qualitative test for the presence of silanes on glass surfaces. [29] Goniometric analysis is widely used for assessing the hydrophobic nature of surfaces. [33-36] Before silanization, fused silica slides are typically cleaned in piranha solution, followed by a washing step with distilled water. The acidic cleaning process yields a hydrophilic glass surface with low water contact angles. [33] Upon silane deposition, the hydrophobicity

increases, depending on the type of silane, the surface roughness and packing of the chains. [37, 38] When the cleaned glass slides are stored before measurements, the contact angles of the unmodified slides increase to some extent, yielding a mediocre value ("silane-aging" [39, 40]). Nevertheless, a distinct increase in average contact angle could be observed after surface silanization. The mean contact angles for all silanized slides were between 60° and 80°. This result is in good agreement with literature reports. [29, 33]

In the next step, two clickable fluorescent dyes (3) and (4) (Figure 4.6) were applied, to ensure the feasibility of a CuAAC on the surface of the silanized femtoliter wells.

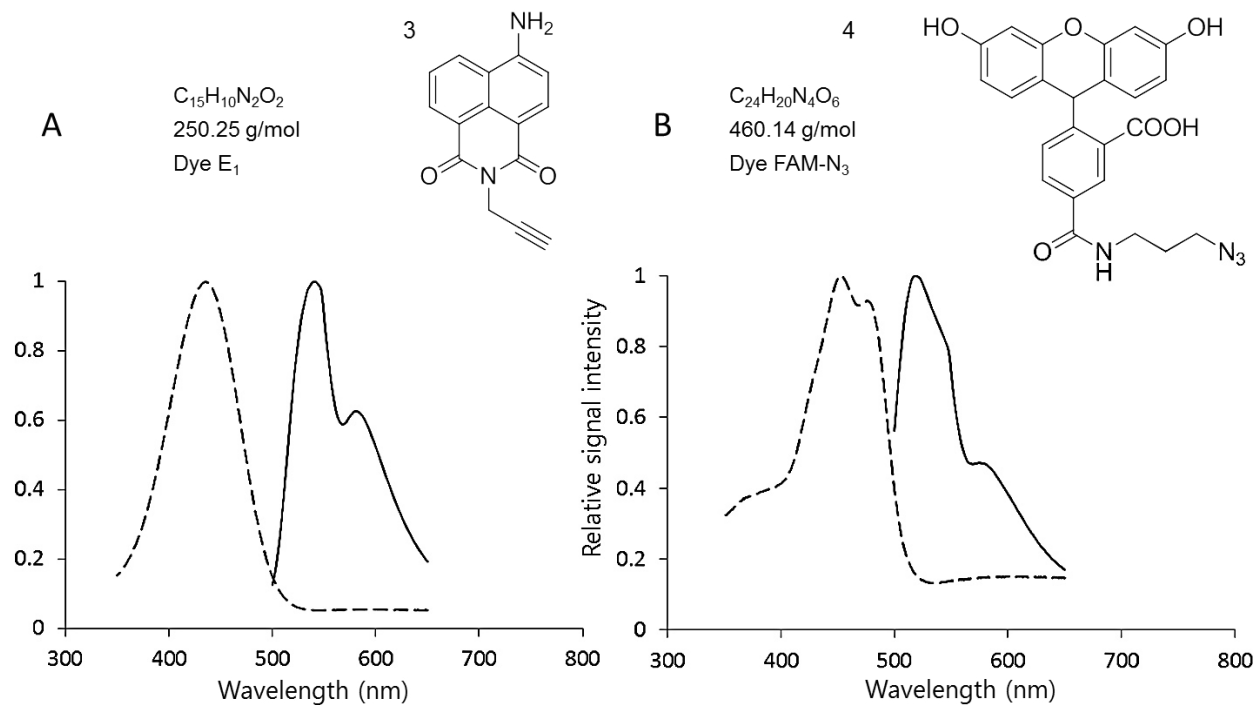


Figure 4.6 Two fluorescent dyes with a terminal alkyne group (3) and a clickable azido moiety (4) were applied for the characterization of the silanized fused silica femtoliter wells. The chemical structure and the absorption and emission spectra of (A) the alkyne modified naphthalimide E_1 ($\lambda_{exc} / \lambda_{em} : 436 \text{ nm} / 541 \text{ nm}$) and (B) the azide dye FAM- N_3 ($\lambda_{exc} / \lambda_{em} : 453 \text{ nm} / 519 \text{ nm}$) are presented. Both dyes can be imaged by using a commercial fluorescein filter cube.

The click coupling reaction was performed in a sealable incubation chamber, designed to guarantee a reproducible functionalization procedure, while simultaneously reducing the reaction volume to several microliters (Figure 4.7). The custom-built device consists of a foundation plate and a T-piece with a solution reservoir that is positioned centrally above the array. A rubber ring, integrated in the T-piece, enables a tight sealing of the system. To avoid solvent evaporation, the loading device can be sealed by a Teflon buckler after loading.



Figure 4.7 Incubation chamber for the functionalization of fused silica femtoliter arrays. The foundation of the holder is a plate with frames that position the array precisely under the opening of the T-piece. The array is securely fastened onto the plate with help of two screws. A rubber ring (not pictured) on the bottom of the T-piece allows for a tight closure of the system.

According to standard click protocols [41] the coupling of the fluorescent dyes (3) and (4) to the functionalized surface was performed in an alkaline, aqueous solution in the presence of CuSO_4 and sodium ascorbate over several hours at room temperature. Thus, the Cu(I) -catalyst was generated *in situ*. The reference experiment was equally conducted with silanized slides under identical reaction conditions but without addition of CuSO_4 (Figure 4.8). In absence of the catalyst no CuAAC took place and no specific binding of the respective fluorescent dye to the silanized surface should be possible. After incubation with the fluorescent dyes, the slides were subjected to several washing steps and examined under a wide-field fluorescence microscope.

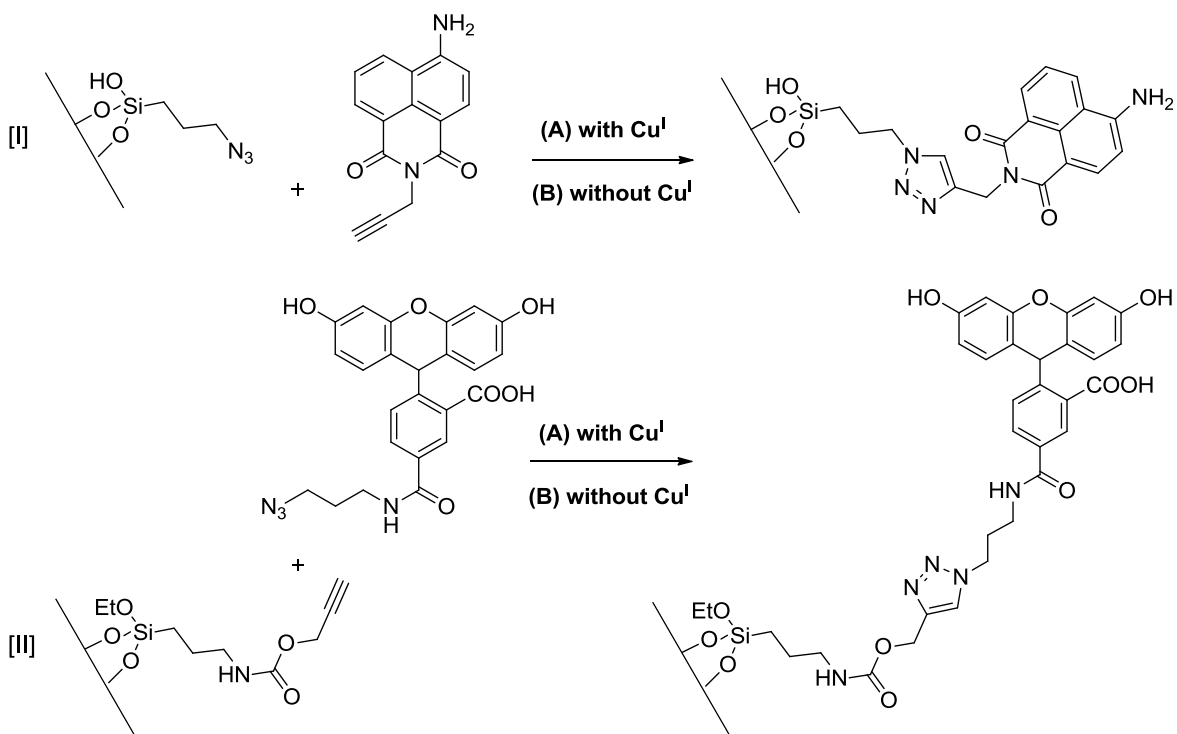


Figure 4.8 The feasibility of a CuAAC reaction on the surface of the femtoliter wells was tested by using the fluorescent dyes E₁ [I] and FAM-N₃ [II]. (A) The click coupling of the fluorescent dyes to the silanized well surface was performed in an alkaline, aqueous solution in the presence of an *in situ* generated Cu(I) catalyst. (B) The reference experiment was conducted under identical reaction conditions, but without addition of Cu(I).

Figure 4.9 depicts the relative fluorescence intensity of the fused silica test slides and negative control slides. Additionally, the relative fluorescence intensity of an untreated slide loaded with PBS only, is indicated. Contrary to expectations, fluorescence measurements disclosed a high signal for both test slide and negative control (Figure 4.9). Since no Cu(I) was present in the reference sample during incubation with either dye, a specific click-coupling can be excluded. Instead, the fluorescence signal has to be attributed to non-specific binding. A high potential for non-specific binding, especially to silanized surfaces, has already been reported in previous works. [42-44]

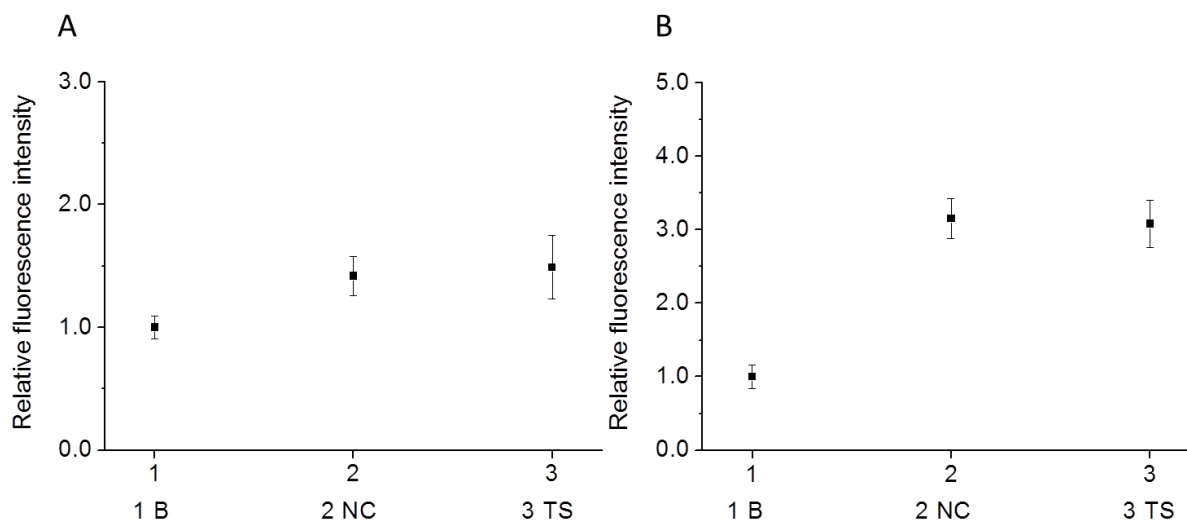


Figure 4.9 Coupling of the fluorescent dyes (A) E₁ and (B) FAM-N₃ to the surface of silanized fused silica femtoliter-wells (silanization in toluene according to protocol (A)): The relative mean fluorescence intensity of the blind (B), the negative control (NC) without copper(I) catalysis and the test slide (TS) are depicted. For illustration, 30 randomly selected regions of interest (ROI) were picked and their fluorescence signal recorded and averaged (mean and standard deviation (error bars) are displayed). For referencing, the mean signal intensity of B was defined as 1.0 and the intensities of TS and NC adjusted accordingly.

The phenomenon of non-specific dye-binding to the silanized slides was observed for both azido- and alkyne-modified surfaces (Figure 4.9) as well as for arrays silanized in toluene under reflux (method A) or treated in acetone at r.t. (method B). However, while slides silanized according to protocol (A) generally showed high fluorescent signals, repeated experiments with slides functionalized according to protocol (B) yielded greatly differing results (Appendix, Figure 7.3.2): Next to high fluorescent signals for both test slide and negative control, some measurements randomly yielded low signals. This inconsistency in experimental results can be attributed to a phenomenon described by Vandenberg *et al.* in 1991: [45] the researchers investigated the deposition of APTES ((3-Aminopropyl)triethoxysilane) onto silica surfaces under various conditions. They suggested that the microscopic binding structure of a silane film varies for different

deposition conditions: While silanization under reflux and anaerobic conditions most likely yields a condensation reaction between the hydroxyl groups of the silica surface and the silane, non-covalent connections such as hydrogen bonds predominate for silanization reactions conducted in aqueous solutions at room temperature under aerobic conditions (Figure 4.10).

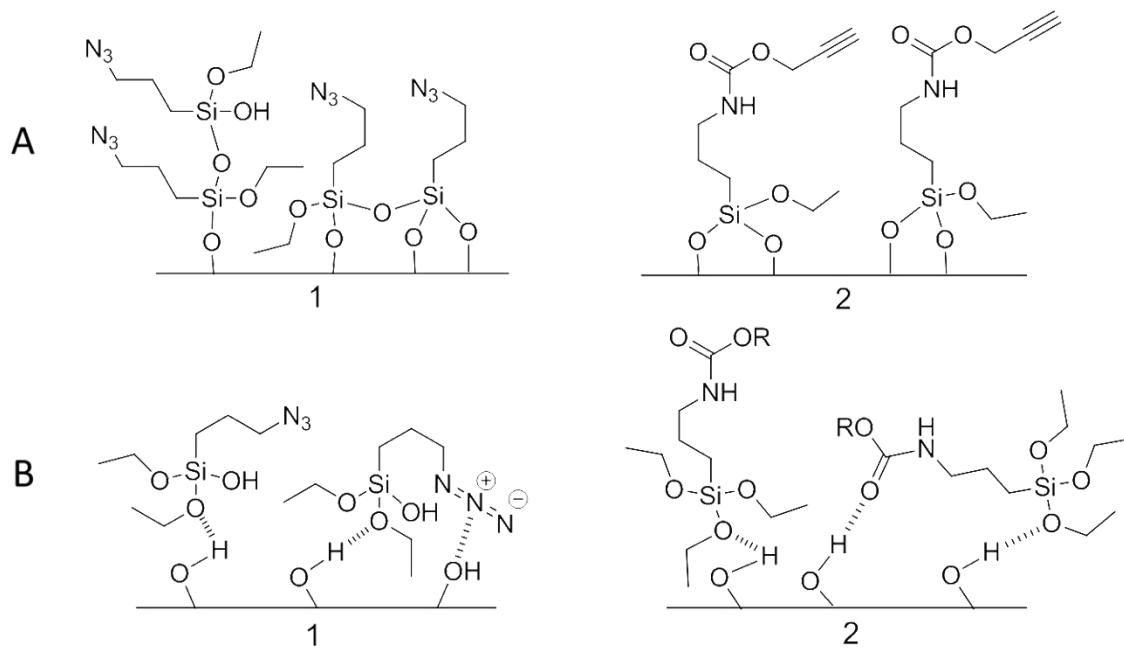


Figure 4.10 Silane deposition on fused silica surfaces. (A) Silanization under reflux at anaerobic conditions most likely yields a covalent silane-attachment of the silane. (B) In contrast, non-covalent bonds prevail for silanization under aerobic conditions at r.t.

In consequence, the surface silanization is less stable when generated according to protocol (B) and with high probability the silane will be partially stripped from the surface during the extensive washing steps after dye-binding. Thus surface silanization corresponding to protocol (B) is less suited in this assay and was therefore no longer employed in further experiments.

Next, the non-specific binding should be suppressed. A series of different techniques was tested in order to reduce the amount of non-specific binding. The femtoliter array surfaces were blocked using PVP. Additionally, surface active buffer additives such as BSA and Tween 20 were applied. The incubation time of the fluorescent dyes was reduced and supplementary washing steps were introduced. Yet, none of the applied measures yielded satisfactory results. However, it was noticed, that slides treated with the azido-silane (1) did generally show a lower fluorescence intensity and stronger experimental variability. For this reason further experiments were conducted with slides functionalized with the alkyne-silane (2), according to protocol (A).

In an attempt to replace the fluorescent dyes, an alternative test protocol was developed (Figure 4.11):

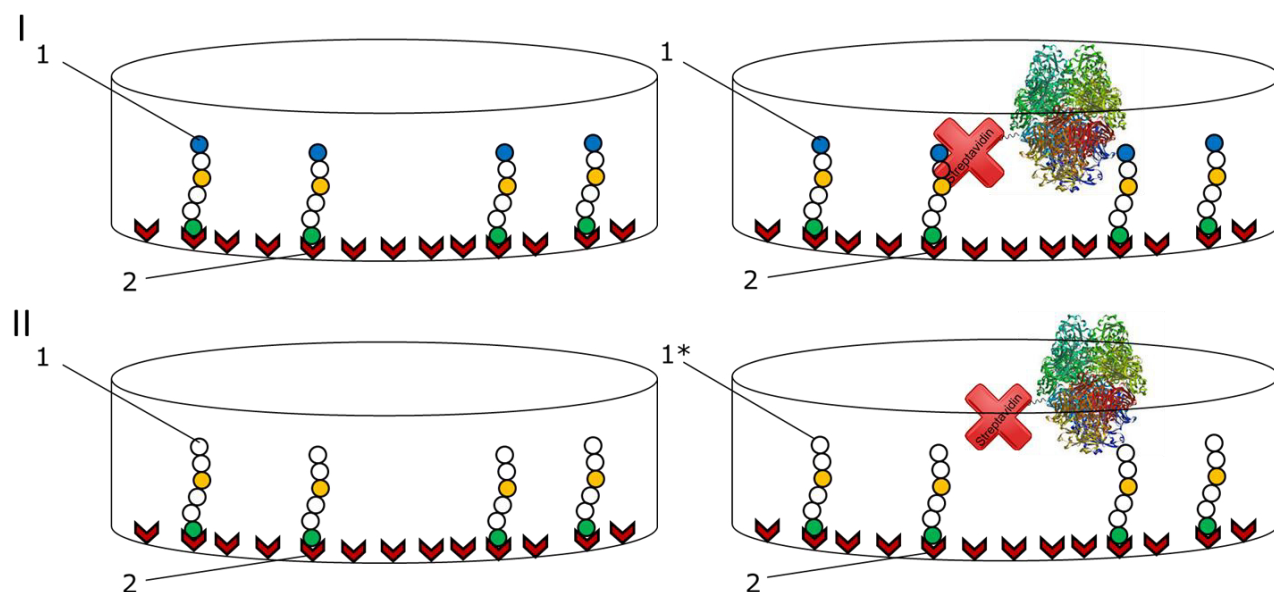


Figure 4.11 Schematic presentation of the advanced CuAAC test protocol. [I] A biotinylated-peptide (1) was clicked to the silanized well surface (2). After incubation with a streptavidin- β -galactosidase conjugate and subsequent bound-free separation, a high fluorescence signal was expected. [II] In the negative control a peptide without biotin label was applied, thus Strep-Gal binding should not be possible.

A specifically designed, clickable peptide (chemical structure: Appendix, Figure 7.3.3) was linked to the silanized array surface using CuAAC. The peptide was further equipped with a biotin-functionality that enabled specific binding to a streptavidin-labeled β -galactosidase (Strep-Gal). In the reference experiment an alternative clickable peptide without biotin-linker was applied. Upon incubation with the fluorogenic substrate RGP a strong signal increase was expected for the test slide due to the specific binding between the surface-bound biotin and streptavidin-labeled β -galactosidase [46, 47]. In contrast, the reference slide should not yield an increase in fluorescence signal after a washing step (Figure 4.11 II).

Figure 4.12 displays the result of the advanced CuAAC protocol with streptavidin- β -galactosidase application.

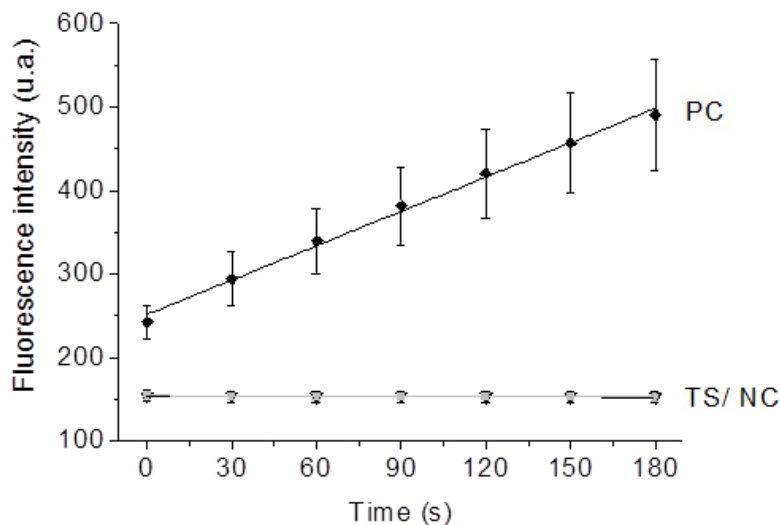


Figure 4.12 Advanced CuAAC test protocol with Strep-Gal: The relative fluorescence intensity of the positive control (PC), the negative control (NC) and the test slide (TS) is demonstrated. In the presence of active β -galactosidase (PC), RGP turnover results in a detectable increase in fluorescence signal. The lack of signal increase confirms the absence of (active) enzyme on the test slide and negative control slide. For illustration, 30 randomly selected regions of interest (ROI) were picked and their fluorescence signal recorded and averaged (mean and standard deviation (error bars) are displayed).

In the positive control, active Strep-Gal was enclosed in an unmodified fused silica array. Upon incubation with RGP, the wells exhibited a signal increase over time. In contrast, neither the test slide nor the negative control did show any increase in fluorescence intensity over the time course of three minutes. This total lack of β -galactosidase activity, observed in particular for the test slide, indicates that the CuAAC did not work as expected. At this point two possible scenarios can be discussed: On the one hand, the click reaction itself may have been unsuccessful. Consequently, the peptide bearing the biotin-functionality would not be firmly attached to the well-surface and wash off during bound-free separation. In this case no β -galactosidase molecules can bind to the well, and after washing, no enzyme molecules would be left in the femtoliter array. Thus, no signal increase could occur. On the other hand, one can assume an effective click reaction resulting in the covalent and stable attachment of the biotin-labeled peptide. However, due to some toxic byproducts of the CuSO_4 and sodium ascorbate catalyzed click reaction the enzyme-probe and/or the peptide-structure are severely damaged. Consequently, the Strep-Gal could either not be attached properly to the slide-surface or the enzyme became dysfunctional and is no longer able to convert the substrate.

In consideration of the existent conditions and relevant literature reports, the second hypothesis was considered more probable. Application of Cu(II) in combination with sodium ascorbate for the catalysis of bioconjugations has already been shown to entail negative side-effects in previous experiments: [48-50] Molecular oxygen in the reaction sample mediates the oxidation of sodium ascorbate to hydrogen peroxide. The peroxide again is source for the copper-induced generation of reactive oxygen species. [48, 51, 52] In the presence of polypeptides these side-products may lead to oxidation or cleavage of biomolecules. [53] Additionally, dehydroascorbate and other ascorbate byproducts can covalently modify amino acid side-chains resulting in adduct formation, crosslinking and protein precipitation (Appendix, Figure 7.3.4). [54, 55]

5.2.2. Biocompatible Click Chemistry

Finn *et al.* [50] recently developed a biocompatible click reaction protocol that allows for the use of sodium ascorbate and Cu(II) in the presence of atmospheric oxygen. For this purpose they introduced a water-soluble, Cu(I) stabilizing tris(triazolylmethyl)amine ligand: (tris(3-hydroxypropyltriazolylmethyl)amine (THPTA)) (5). [50, 56] In the biocompatible click reaction, CuSO₄ is pre-complexed with THPTA. The catalyst is then mixed with the alkyne- and azide-agents, followed by the addition of sodium ascorbate to initiate the reaction. The tetradentate THPTA ligand is supposed to completely insulate the Cu(I) center from any potential destabilizing interactions. [56, 57] Additionally, to prevent protein crosslinking reactions mediated by ascorbate by-products, Finn *et al.* added aminoguanidine (6) to the reaction solution.

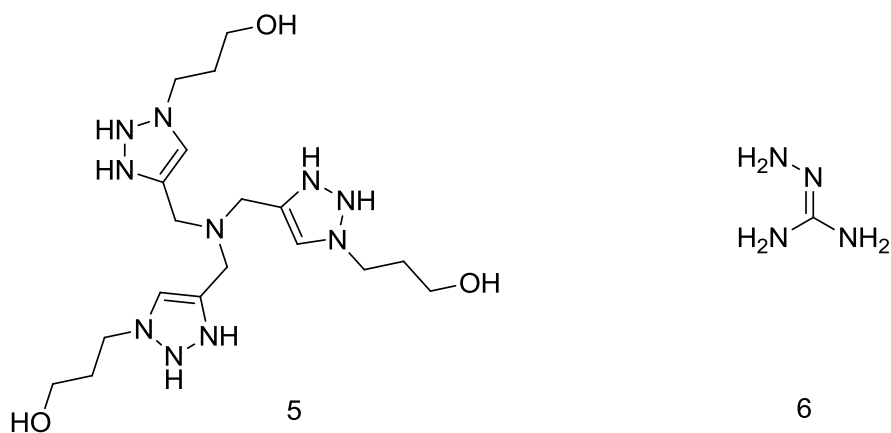


Figure 4.13 Chemical structure of the additives applied by Finn *et al.* for the development of a biocompatible copper(II)/ sodium ascorbate catalyzed click reaction. The tris(3-hydroxypropyl-triazolylmethyl)amine (THPTA) ligand (5) efficiently protects biomolecules from H₂O₂ and related side-reactions. Amino guanidine (6) prevents protein crosslinking reactions mediated by ascorbate byproducts.

In a control experiment, we tested the optimized CuAAC protocol for its biocompatibility in comparison to the traditional reaction conditions (Figure 4.14). For this purpose, the

enzymatic activity of Strep-Gal, in the presence of an excess of RGP, was tested under three different reaction conditions: (1) in PBS without the addition of supplementary reactants, (2) in a click reaction solution according to the previously applied protocol, containing CuSO_4 and sodium ascorbate, (3) in the optimized reaction mixture also including the ligand THPTA and aminoguanidine next to CuSO_4 and sodium ascorbate. The buildup of resorufin, the fluorescent product of the enzyme reaction, was monitored over time for all three experiments in parallel in the wells of a microtiter plate.

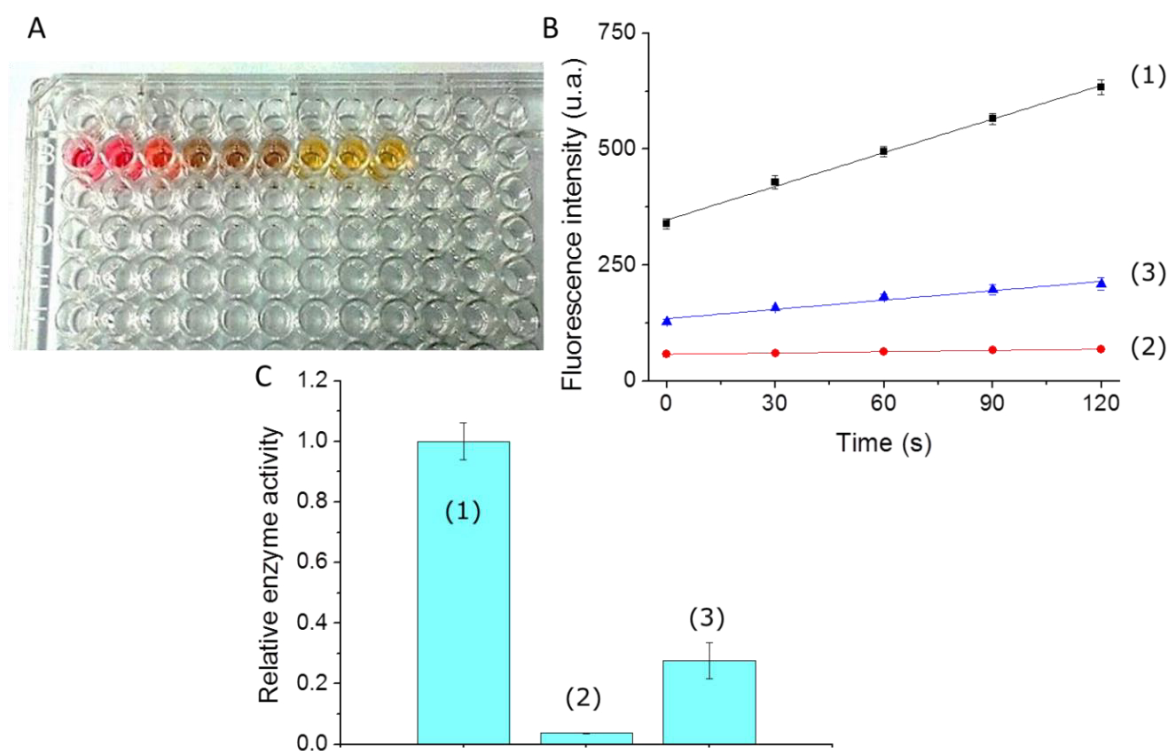


Figure 4.14 Biocompatibility of the alternative CuAAC: (A) The RGP turnover rate of a streptavidin β -galactosidase conjugate was monitored in a MTP under three reaction conditions: (1) in PBS only, (2) in PBS with addition of CuSO_4 and sodium ascorbate, (3) in a reaction mixture containing the ligand THPTA and aminoguanidine in addition to CuSO_4 and sodium ascorbate. (B) A high enzymatic activity is observed in the buffer medium (1). In contrast, the increase in fluorescence signal is greatly reduced in the presence of CuSO_4 and sodium ascorbate (2) and (3). (C) However, while virtually no enzyme activity is observed in the traditional click reaction mixture, indicating severe damage of the protein, the optimized solution composition allows for enzymatic activity, although at a lower rate.

A glance at the microtiter plate several minutes after measurement-initiation (Figure 4.14 A) already allowed for a first suggestion on the outcome of the experiment. The first three wells containing only buffer, next to RGP and β -galactosidase, displayed a pinkish color, symptomatic for the product of the enzymatic reaction, resorufin. In contrast, the adjacent three wells containing also CuSO_4 and sodium ascorbate without addition of any supplementary reactants exhibited a brownish coloring. This color-change indicates some sort of damage probably on both, the substrate RGP, which usually appears yellow, as well as the enzyme itself. In contrast, the reaction solution composed according to the optimized click reaction protocol, presented in the last three wells, still showed the characteristic yellow staining of the RGP substrate after several minutes. While no indication of any damage on neither β -galactosidase nor RGP could be stated, the enzyme activity however seemed to be significantly reduced in comparison to its usual activity in buffer solutions.

On closer examination of the respective turnover rates significant differences became evident (Figure 4.14 B and C). While a distinct increase in fluorescence intensity was recorded for the experiment in PBS only ((1) relative slope: 1.00), the activity is greatly reduced upon addition of CuSO_4 and sodium ascorbate ((2) relative slope: 0.04). The byproducts of the conventional click reaction severely inhibit the enzyme reaction, diminishing the signal increase to virtually zero. In contrast, upon addition of amino-guanidine and THPTA, according to the optimized click protocol by Finn *et al.*,^[50] enzymatic activity can be observed, resulting in a visible signal increase in fluorescence intensity ((3) relative slope: 0.28). Hence, while the enzymatic reaction is clearly restrained in the presence of CuSO_4 and ascorbic acid, the protecting additives (5) and (6) seem to prevent any severe damage to the enzyme and thus enable substrate turnover. Consequently, the advanced CuAAC test protocol was performed under the optimized reaction conditions (Figure 4.15 A) and the accumulation of fluorescent

resorufin upon incubation with RGP was monitored by fluorescence microscopy (Figure 4.15 B).

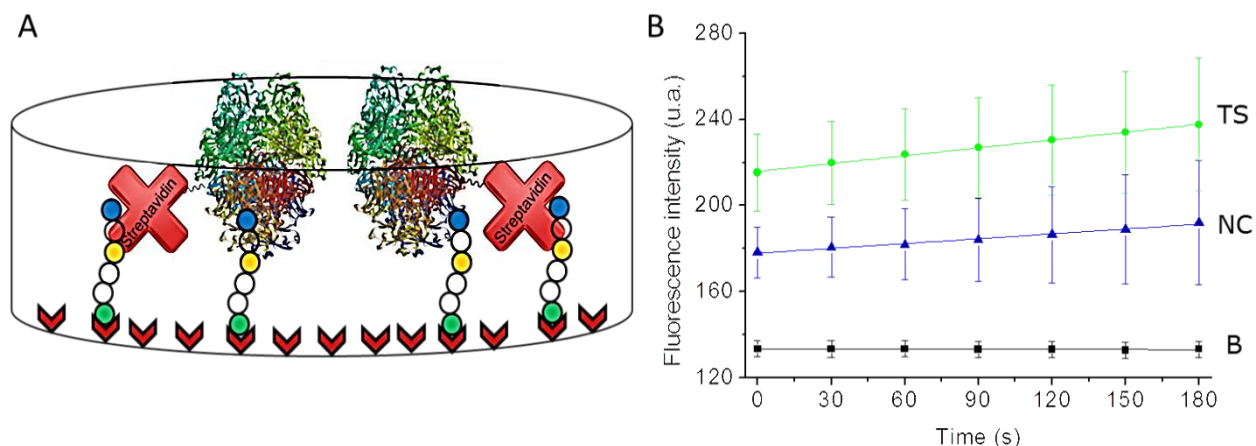


Figure 4.15 Advanced CuAAC protocol under optimized reaction conditions according to Finn *et al.* (A) Schematic presentation of the setup: A clickable, biotinylated peptide was linked to the well surface and specifically bound by a Strep-Gal conjugate (TS). In the negative control (NC) a peptide without biotin-group was applied, thus no specific Strep-Gal binding is possible. (B) Increase in fluorescence intensity due to the β -galactosidase activity, of the test slide and the negative control, respectively, in comparison to the background signal (B) obtained when no enzyme is present in solution.

A constant signal was obtained for the blind (slope: 0.00), where no enzyme is present. In contrast, both test slide and negative control show an increase in fluorescence intensity over time, indicating the presence of active β -galactosidase. However, while only a minor accumulation of fluorescent product was observed for the negative control (slope: 0.07), the average increase in fluorescence intensity was about twice as high for the test slide (slope: 0.12). This is a promising result that points to a successful outcome of the experiment.

Thus, eventually, we could verify a specific binding of the Strep-Gal conjugate to the biotinylated well surface. Thereby we could also give evidence of the successful

operation of the click reaction, and accordingly, the effective introduction of peptide molecules on the surface of the femtoliter array. As a matter of course, the positive result of this experiment has to be reproduced in further measurements to ensure a successful operation of the CuAAC. Additionally, some optimizations regarding the undesired fluorescence signal of the negative control as well as the relatively low signal intensity of the test slide have to be introduced.

The β -galactosidase activity monitored in the negative control was attributed to an insufficient bound-free separation after Strep-Gal incubation. The size of a femtoliter chamber certainly complicates the washing process. While it can be difficult to confine a biomolecule into the dimensions of such very small vessels, it is at least equally demanding to again release a biomolecule once trapped in the confinement of a femtoliter well. So far, bound-free-separation was conducted by repeated washing of the array with different solvents. In each washing step the cleaning solution was pipetted onto the array and flushed through the wells by repeated up- and down pipetting. This procedure was rerun several times for every washing solution. For future experiments additional cleaning procedures, involving array incubation in solvents under shaking or vibration, as well as the introduction of centrifugation in combination with other, alternative washing steps, should be considered. Besides, a reduction of the employed Strep-Gal concentration may also be beneficial.

Furthermore, an increase in enzyme activity of the specifically bound Strep-Gal conjugates would be eligible in order to improve the signal intensity obtained for the test slide measurements. A higher overall enzyme activity may be achieved by performing the click reaction with reduced concentrations of CuSO_4 and sodium ascorbate. In theory, all catalytic agents, together with excess peptide, are removed in the course of several washing steps after completion of the click reaction. However, it has to be assumed that, to some extent, the catalytic reagents non-specifically bind to

the walls and the racks of the array. Even these trace contaminations might influence the activity of subsequently bound streptavidin- β -galactosidase molecules. So far, relatively high concentrations of CuSO_4 and sodium ascorbate have been added to ensure the constant availability of the instable Cu(I) species. Especially in biological samples a rather high ascorbate concentration is required to remove oxygen from the aqueous solution and maintain a constant supply of catalytically active Cu(I). [50] Besides, a higher Cu(II) concentration is often applied in biological samples, as biomolecule substrates, such as proteins, potentially contain groups that strongly bind copper ions [58-60] and thus render the metal unavailable for CuAAC catalysis. However, for the stated experiment, a slight reduction of the concentration of catalytic agents should not affect the effectiveness of the click reaction but may be beneficial to the final outcome of the experiment.

An alternative that directly eliminates any discussion on required copper concentrations would be the introduction of the copper-free click chemistry. In 2004, Bertozzi *et al.* [61] published a click reaction that proceeds without addition of a copper catalyst. Hereby, a substituted cyclooctyne is applied instead of the terminal alkyne group. The ring-strain promotes the cycloaddition and renders the copper activation redundant. The copper-free azido-alkyne click reaction was found to be an ideal tool for various biological applications, such as bioorthogonal cycloadditions *in vivo*, [62, 63] as no cytotoxic side-products are generated.

5.2.3. Introduction of Enzymes by Click Chemistry – An Example

Bioanalytical assays in glass femtoliter arrays are in large part based upon the introduction of antibodies or peptide-substrates on the surface of the wells. However, occasionally, also the covalent attachment of whole enzymes may be attractive.

In this chapter the introduction of clickable azide groups into enzymes is described using horseradish peroxidase (HRP) as a model system. HRP is a monomeric, 44 kDa glycoprotein that consists of 308 amino acids, eight carbohydrate side chains, two calcium(II) ions and a heme-group. [64] The enzyme belongs to the class of oxidoreductases and catalyzes the reduction of hydrogen peroxide to water in a radical peroxidase-cycle. HRP is a popular enzyme, which is widely used in bioanalytical assays.

For the introduction of azides into the enzyme structure a diazo-transfer reaction was performed, according to protocols published by Goddard-Borger *et al.* [65] and van Dongen *et al.* [66] The applied method enables a facile introduction of azide groups into the side chains of lysine residues and the *N*-terminus of proteins. The effective introduction of azide-groups was verified by ESI-mass spectrometry (Appendix, Figure 7.3.5).

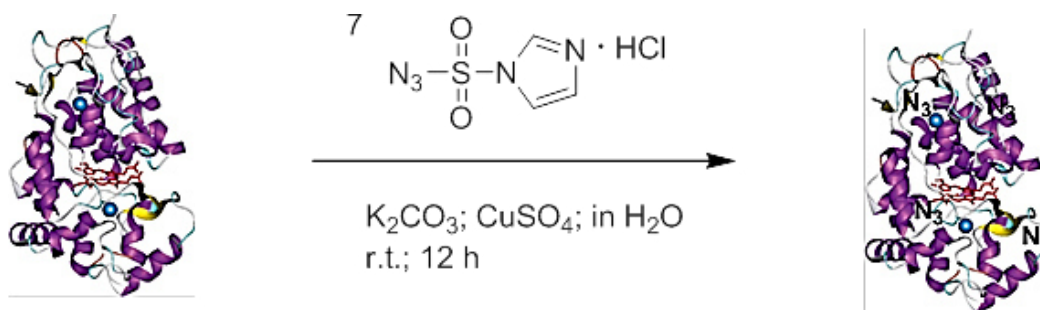


Figure 4.16 Schematic presentation of the diazo-transfer reaction. HRP (1 eq.) was dissolved in water together with K_2CO_3 and CuSO_4 . The transfer agent imidazole-1-sulfonyl azide hydrochloride (7) (1.75 eq.) was added and the reaction was left shaking overnight. After purification the effective introduction of azide groups was confirmed by mass spectrometry.

Van Dongen *et al.* [66] reported in their work an average conversion of four amino groups per HRP molecule into azide functionalities. The modification of a primary amine (NH_2) into an azide (N_3) equals an increase in molecular weight (MW) of 26 Da. The MW of native HRP was found to be 43175 Da. In contrast, the molecular ion peak of the generated azido-HRP (N_3 -HRP) corresponded to a MW of 43279 Da (Appendix, Figure 7.3.5). The shift in overall MW, recorded by ESI-TOF MS, perfectly equates to the conversion of an average of four amino groups to azide groups per HRP molecule and thus confirms the successful diazo-transfer reaction on the target enzyme.

Next, it was verified that the modified HRP was still catalytically active. For this purpose, we compared the catalytic activity of native HRP and N_3 -HRP upon incubation with the fluorogenic substrate Amplex Red at different H_2O_2 concentrations. HRP catalysis follows a complex catalytic cycle (see Figure 4.17) that has already been studied in detail in both bulk phase [67-70] and single molecule [71-73] experiments.

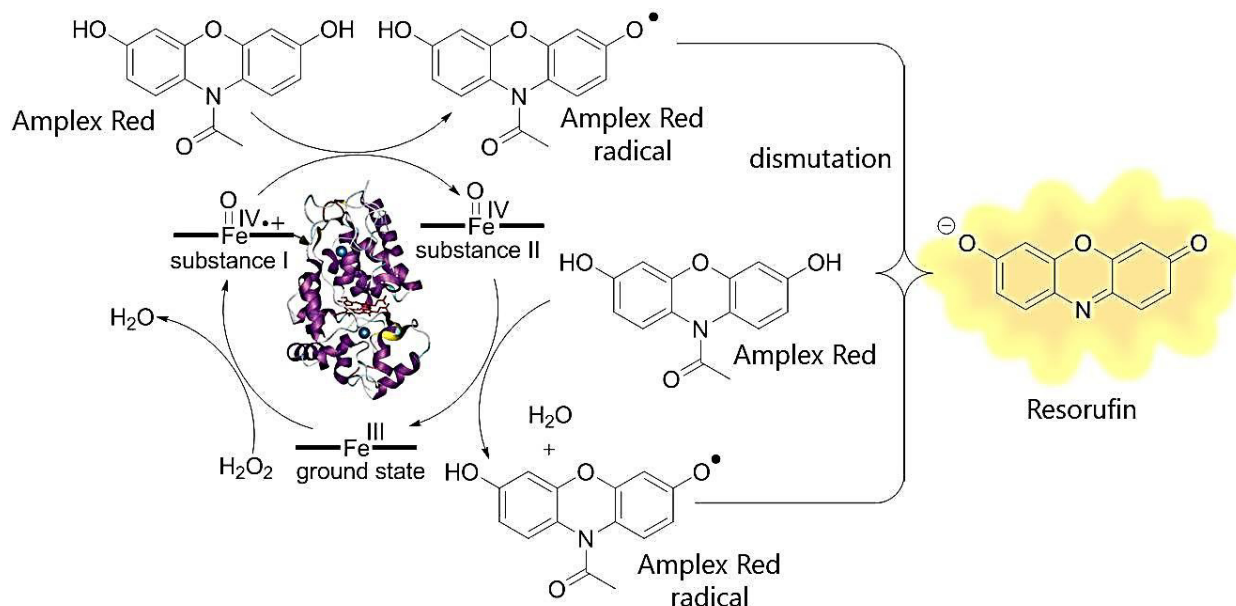


Figure 4.17 Schematic presentation of the HRP-catalysis of Amplex Red. In a two-step redox reaction the enzyme catalyzes the generation of non-fluorescent Amplex Red radicals that undergo a dismutation reaction resulting in highly fluorescent resorufin and Amplex Red.

Amplex Red is oxidized by HRP to highly fluorescent resorufin in a two-step redox reaction mechanism. In this process the heme prosthetic group of HRP undergoes a three-step redox cycle: H_2O_2 oxidizes the ground state of substance I in a two-electron transfer step. The ensuing reduction of substance I involves two successive one-electron transfer steps from two Amplex Red molecules and the generation of substance II as a reaction intermediate. Thereby, two non-fluorescent radical molecules of Amplex Red per H_2O_2 molecule emerge that subsequently turn into one molecule of resorufin and one molecule of Amplex Red in a dismutation reaction.

The turnover of 250 μM Amplex Red, at concentrations from 0.5 μM to 1 mM H_2O_2 was monitored in a microtiter plate experiment for both HRP and N_3 -HRP, respectively. Identical concentrations of native and modified enzyme were applied. The enzyme velocities were standardized, with the maximum substrate turnover rate of native HRP at 1 mM H_2O_2 defined as 100%. The standardized rates were plotted against the H_2O_2 concentrations (Figure 4.18).

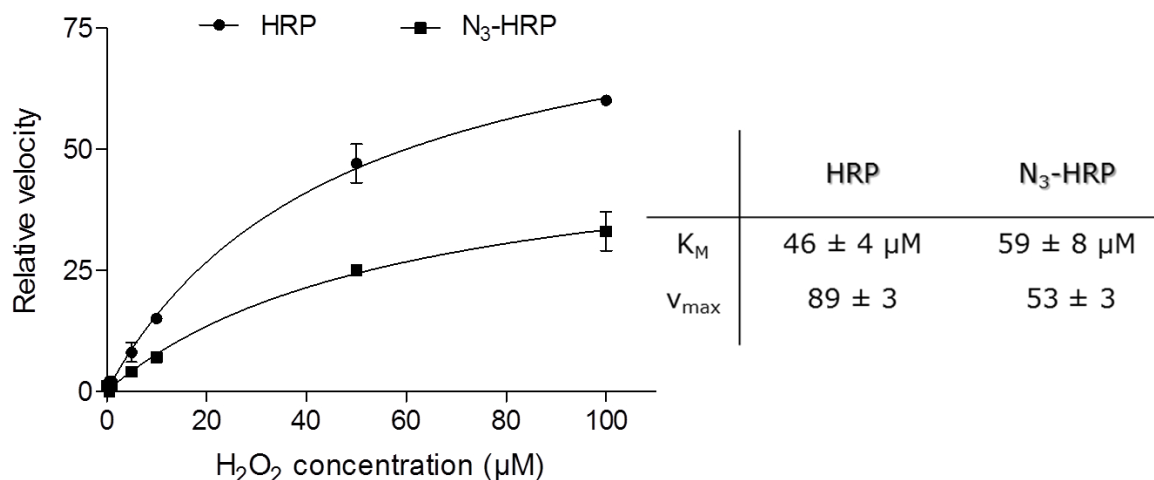


Figure 4.18 Substrate saturation curves of HRP and N_3 -HRP. Average activity and standard deviation of three bulk experiments with HRP (circles) and N_3 -HRP (squares). The average normalized N_3 -HRP activity amounts to two thirds of the normalized activity of unmodified HRP. The mean and standard deviation (error bars) of three wells on a MTP per H_2O_2 concentration are displayed.

A typical Michaelis-Menten saturation curve was yielded for both HRP and N₃-HRP (Figure 4.18). The kinetic constants were $K_M = 46 \pm 4 \mu\text{M}$ and $v_{\text{max}} = 89 \pm 3$ for native HRP and $K_M = 59 \pm 8 \mu\text{M}$ and $v_{\text{max}} = 53 \pm 3$ for N₃-HRP. The MM-curves, indicated in Figure 4.18, confirm that the azide-functionalized enzyme is still active after the diazo-transfer. The normalized activity of N₃-HRP amounts to approximately two thirds of the normalized activity of native HRP, which is in good agreement with literature reports. [66] Thus, the diazo-compound (8) proved to be an efficient transfer reagent for the introduction of azide groups into proteins. It was further demonstrated that the catalytic activity of enzymes, such as HRP, was not substantially reduced after the diazo transfer reaction. The controlled introduction of azide functionalities in proteins enables the application of the bioorthogonal, fast and quantitative CuAAC click reaction for the attachment of biomolecules on the surface of fused silica femtoliter arrays.

5.2.4. Immobilization of Antibodies via Peptide Chemistry

In order to bind antibodies to the femtoliter array surface by peptide chemistry, a carboxylic group was introduced on the fused silica slide. This was accomplished according to a protocol published by Thompson *et al.*, [27] who modified a silica surface with terminal carboxylic groups for the later immobilization of the enzyme urease. For this purpose, the scientists first introduced an amino group to the silica slide which was subsequently treated with glutaric anhydride.

For the introduction of an amine group on the surface of the fused silica femtoliter array, the silanizing agent APTES (8) (3-Aminopropyl)triethoxysilane was applied. In accordance to the silanization protocol (A), previously applied for the introduction of clickable silanes on the fused silica surface (chapter 5.2.1), the activated femtoliter array was incubated in a 2%-solution of (8) in toluene under reflux and anaerobic conditions for several hours (Figure 4.19 A).

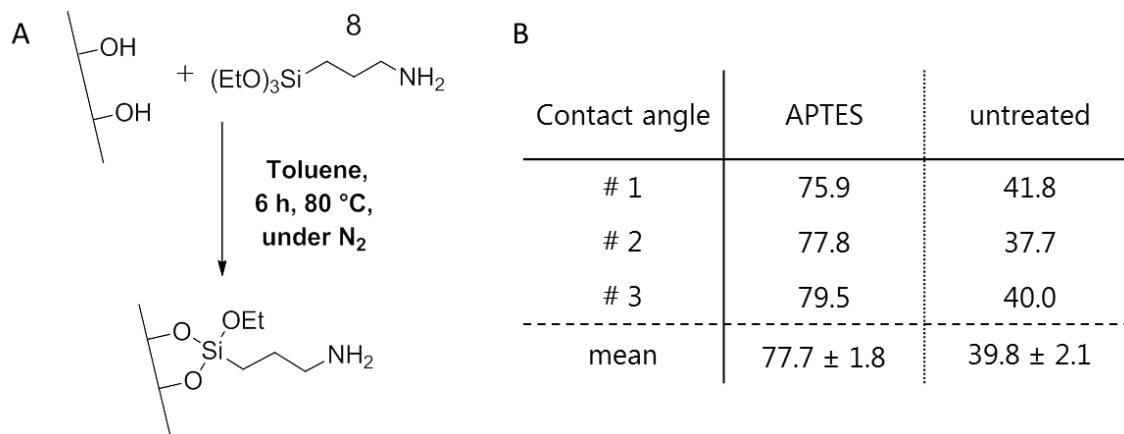


Figure 4.19 Introduction of APTES (8) on the fused silica femtoliter array. (A) The silanization reaction was performed in toluene under reflux and anaerobic conditions for six hours. (B) The contact angles were measured with DI water in three independent measurements for fused silica slides treated with APTES as well as for untreated slides. Additionally, the mean contact angle of all three measurements is stated. The increase in average contact angle after silanization confirms the successful introduction of the silane on the femtoliter array surface.

The success of the silanization process was verified by examination of the resulting surface contact angles. Untreated, dry fused silica slides that had previously been cleaned in piranha acidic solution, with subsequent incubation in distilled water, were used as a reference. Goniometric analysis provided a mean contact angle of $39.8^{\circ} \pm 2.1$ for the unmodified glass slides. For slides functionalized with (8), an elevated average contact angle of $77.7^{\circ} \pm 1.8$ was recorded (Figure 4.19 B). The acidic cleaning process yielded a hydrophilic fused silica surface with relatively low water contact angles for the unmodified slide. [33] Upon silane deposition, a distinct increase in hydrophobicity, accordingly in contact angle is observed. This result is in good agreement with literature reports [29, 33] and confirms the presence of APTES (8) on the fused silica surface.

In the next step, the silanized slide was treated with glutaric anhydride, according to the protocol by Thompson *et al.*, [27] resulting in a carboxylated array surface. The carboxylic group was then activated using DCC and NHS as shown in Figure 4.3. Finally, the slide was incubated with the target antibody, resulting in the formation of a stable peptide bond between the carboxylated femtoliter array surface and the primary amine groups of the protein.

The successful introduction of the antibody on the surface of the fused silica fL-array was confirmed in a test experiment (Figure 4.20). For this purpose, the target antibodies were labeled with fluorescein and covalently linked to the activated carboxylic groups on the slide surface. The attachment of the antibodies to the surface of the wells was monitored by wide-field fluorescence microscopy. In a reference experiment, identical fluorescein-labeled antibodies were applied. However, no DCC/ NHS-mediated activation of the carboxylic groups was performed. Thus, the formation of a peptide bond between slide surface and protein was prevented, resulting in the wash-off of the antibodies.

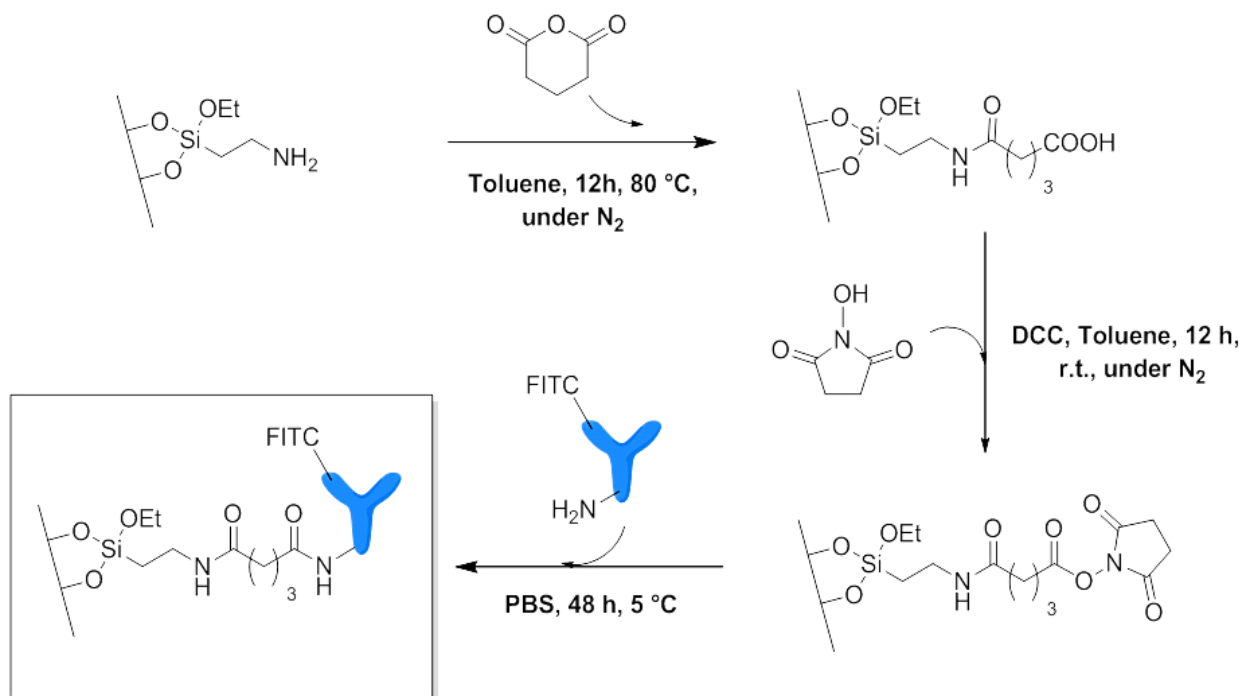


Figure 4.20 Test experiment to confirm the introduction of the antibody on the surface of the fL-array. In a first step, the amine functionalized slide was treated with glutaric anhydride to generate a carboxylic surface. On the TS, the carboxylic groups were activated using DCC and NHS and afterwards bond to the primary amine groups of a fluorescein-labeled antibody. The NC was incubated with the labeled antibody without prior carboxyl activation. Thus, no peptide bonds should form.

Figure 4.20 depicts the outcome of the test experiment. The relative fluorescence intensity of the blind, the test slide and the negative control are demonstrated. The test slide displays a significantly higher average fluorescence intensity signal (2.80 ± 0.25) than the negative control (1.49 ± 0.15). This finding is in agreement with the expected experiment outcome and confirms the specific attachment of the fluorescein-labeled antibody to the activated carboxylic groups on the femtoliter array surface.

The remaining fluorescence signal recorded for the negative control was attributed to an insufficient bound-free separation. As previously discussed in chapter 5.2.3, the dimensions of a femtoliter may result in an inefficient washing process. The

slides were cleaned by repeated washing steps with different solvents. In the process, the cleaning solution was repeatedly pipetted onto the array and flushed through the wells by frequent up- and down pipetting. For future experiments some additional cleaning steps, as discussed in chapter 5.2.3, should be considered in order to optimize bound-free-separation.

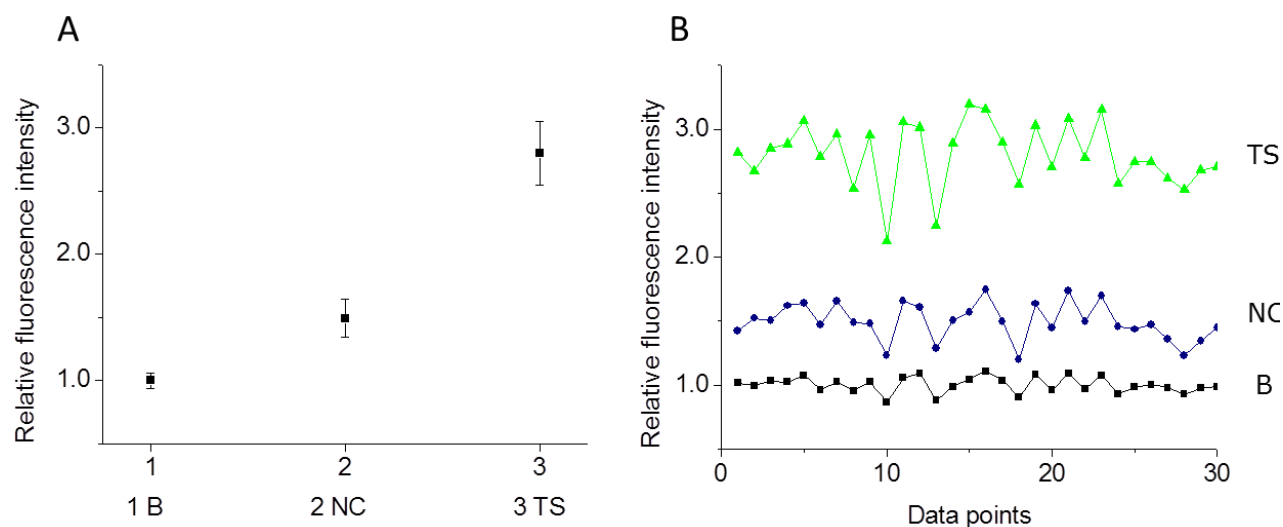


Figure 4.21 (A) Mean relative fluorescence intensity of the blind (B) (1.00 ± 0.06), the negative control (NC) (1.49 ± 0.15) and the test slide (TS) (2.80 ± 0.25) recorded from 30 randomly picked ROI (mean and standard deviation (error bars) are depicted). (B) The fluctuation of the fluorescence signal over the entire wafer surface is displayed.

In summary, the specific binding of antibodies to the fused silica femtoliter well surface by using well-established and simple peptide chemistry, was demonstrated. This allows for the development of ultrasensitive immunological assays with enzymatic signal amplification and digital concentration readout.

5.3. Materials and Methods

5.3.1. General Specifications

NMR Spectroscopy. ^1H - and ^{13}C -NMR spectra were recorded on an Avance 300 NMR-spectrometer from Bruker Bio Spin (www.bruker-biospin.com). Chemical shifts (δ) are given in parts per million (ppm) using solvent signals as the reference. Coupling constants (J) are reported in Hertz (Hz). Splitting patterns are designated as s (singlet), d (doublet), t (triplet), q (quartet), m (multiplet), dd (doublet of doublet). (NMR-spectra can be found in the Appendix, Figure 7.3.6).

Mass Spectroscopy. Mass spectroscopy was performed by the Central Analytics Department at the University of Regensburg. Mass spectra were acquired on a Thermoquest Finnigan TSQ (LC-ESI) mass spectrometer (Thermo Scientific, www.thermo.com) or an Agilent 6540 (HR-ESI) mass spectrometer (Agilent Technologies Inc., www.agilent.com).

IR Spectroscopy. ATR-IR spectroscopy was performed with an Excalibur FTS 3000 Spectrometer (Bio-rad, www.bio-rad.com) equipped with a Specac Golden Gate Diamond Single Reflection ATR-System (www.specac.com). (IR-spectra can be found in the Appendix, Figure 7.3.1).

UV-VIS and Emission Spectra. UV-VIS spectra were acquired with a Cary 50 Bio UV-visible spectrophotometer from Varian (Agilent Technologies Inc.). Measurements were performed in standard quartz cuvettes. Emission spectra were recorded on a Jasco FP6300 luminescence spectrometer equipped with a 150-W continuous wave Xenon lamp as the excitation source. Spectra were recorded in standard or semi micro fluorescence cuvettes. Microplate measurements were acquired on a Fluostar Optima microtiter plate reader (BMG labtech, www.bmg-labtech.com) equipped with a high energy xenon flash lamp.

Contact Angle Measurement. Contact angle measurements of the silanized fused silica slides were performed by Albert Hutterer at the faculty of microsystem techniques of the OTH (Ostbayerische Technische Hochschule Regensburg, Germany). Contact angles were measured with deionized (DI) water on a Drop Shape Analyzer - DSA25 (Kruess, www.kruss.de). The contact angle was determined on the smooth surface at the fringe area of the fused silica slide next to the femtoliter array. Reported values represent an average of three measurements per specimen.

Fluorescence Microscopy. A detailed description of the applied fluorescence microscope as well as the explicit experimental microscope settings, information on the applied buffers and details on image processing and data analysis can be found in chapter 2.3.3.

Femtoliter Arrays. All functionalization experiments were performed with femtoliter arrays that were microstructured into the surface of a fused silica wafer by photolithography and anisotropic reactive ion etching as described in chapter 2.2.1.

Incubation Chamber. The design of the applied incubation chamber was inspired by a similar design developed by Michael Thaller in his master thesis. [74] The chamber consisted of an array holder plate with a rectangular immersion in the center where the fused silica slide was located (Figure 4.7). On top of the fused silica slide an aluminum T-piece with an integrated cylindrical incubation chamber could be fastened in a way that the incubation chamber lay centrally over the array. Upon tightening of two screws at either end of the T-piece, the chamber was locked on the bottom plate with help of a rubber ring embedded in the bottom of the T-piece. The incubation chamber was sealed with help of a Teflon stamp to prevent evaporation during incubation. After application, the chamber was disassembled and the individual components were cleaned by ultrasonication, first in distilled water and subsequently in acetone.

5.3.2. Introduction of Peptides using Click Chemistry

Buffers and Reagents. Dilutions and washing steps were mainly performed with phosphate buffered saline (PBS: 2.7 mM KCl, 2 mM KH_2PO_4 , 137 mM NaCl, 10 mM Na_2HPO_4 , pH 7.4) containing varying amounts of bovine serum albumin (BSA, Sigma-Aldrich) and Tween 20 (Sigma-Aldrich). Stock solutions of 0.5 mg/mL streptavidin-5-FAM (Strep-FAM, AnaSpec, www.anaspec.com) in 1:1 PBS/glycerol (Sigma-Aldrich), 1.0 mg/mL streptavidin- β -galactosidase conjugate (Strep-Gal, Life Technologies, www.lifetechnologies.com) in 1:1 30 mM TEA (pH 7.6)/glycerol and 100 mM resorufin- β -D-galactopyranoside (RGP, Iris Biotech GmbH) in DMSO were aliquoted and stored at -20°C . Tris(3-hydroxypropyltriazolylmethyl)amine (THPTA, 95 %) and aminoguanidine hydrochloride ($\geq 98\%$) were purchased from Sigma Aldrich and applied without further purification.

Unless otherwise stated, all other chemicals and solvents were purchased from Sigma-Aldrich, Merck and ABCR. They were of analytical grade and used without further purification.

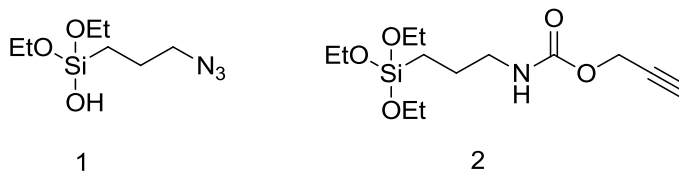
Clickable Silanes 1 and 2

Figure 4.22 Chemical structures of the clickable silanes (1) (3-azidopropyl)diethoxy(hydroxyl)silane and (2) O-(propargyloxy)-N-(triethoxysilylpropyl)urethane.

(3-Azidopropyl)triethoxysilane (1) was synthesized from (3-chloropropyl)triethoxysilane according to a protocol described by Daniela Achatz in her Diploma thesis. [75]

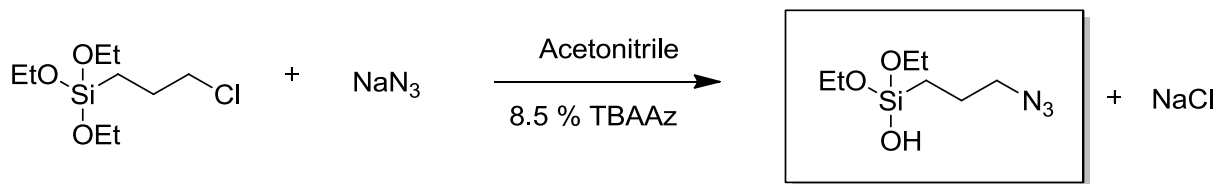


Figure 4.23 Synthesis of (3-azidopropyl)diethoxyhydroxylsilane from (3-chloropropyl)triethoxysilane

To a solution of 5.0 g (20.8 mmol, 1 eq.) (3-chloropropyl)triethoxysilane (Sigma-Aldrich) in 20 mL acetonitrile 1.64 g (25 mmol, 1.2 eq.) sodium azide (Sigma-Aldrich) were added. 0.5 g (1.77 mmol, 8.5 mol-%) tetrabutylammoniumazide (TBAAz, ABCR, www.abcr.de) were added and the mixture was stirred under reflux for 70 h. The generated sodium chloride was filtered off and the solvent was removed on a rotary evaporator. The residue was dissolved in 150 mL DCM and washed three times with 20 mL double distilled water. The organic phase was dried over Na_2SO_4 . The drying agent was filtered off and the solvent was removed on a rotary evaporator yielding the product in form of a colorless liquid.

$^1\text{H-NMR}$ (CDCl_3): $\delta = 3.75$ (q, 4H, $J = 7.0$ Hz), 3.20 (t, 2H, $J = 7.0$ Hz), $1.71 - 1.58$ (m, 2H), 1.16 (t, 6H, $J = 7.0$ Hz), $0.66 - 0.54$ (m, 2H)

(The recorded ^1H -spectrum (Appendix, Figure 7.3.6) is in accordance with the spectrum stated in literature. [75])

ATR-IR (neat): $\nu = 2096, 2889, 2928, 2976 \text{ cm}^{-1}$

O-(Propargyloxy)-*N*-(triethoxysilylpropyl)urethane (2) was purchased from ABCR (www.abcr.de) and used without further purification.

Clickable Dyes 3 and 4

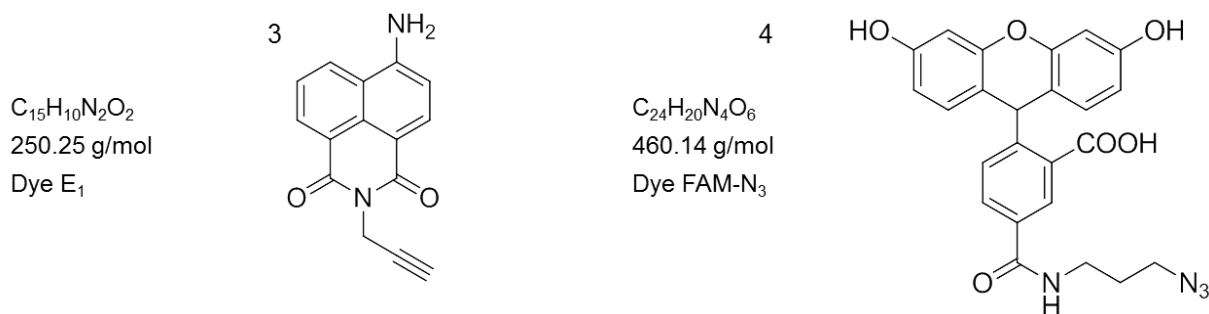


Figure 4.24 Chemical structure of the clickable dyes (3) (Dye E₁) and (4) (5-fluorescein-Azide, FAM-N₃, Jena Bioscience, www.jenabioscience.com).

The clickable naphthalic anhydride dye “E₁” (3) was synthesized from 4-amino-1,8-naphthalic anhydride according to a protocol published by Kele *et al.* in 2009. [76]

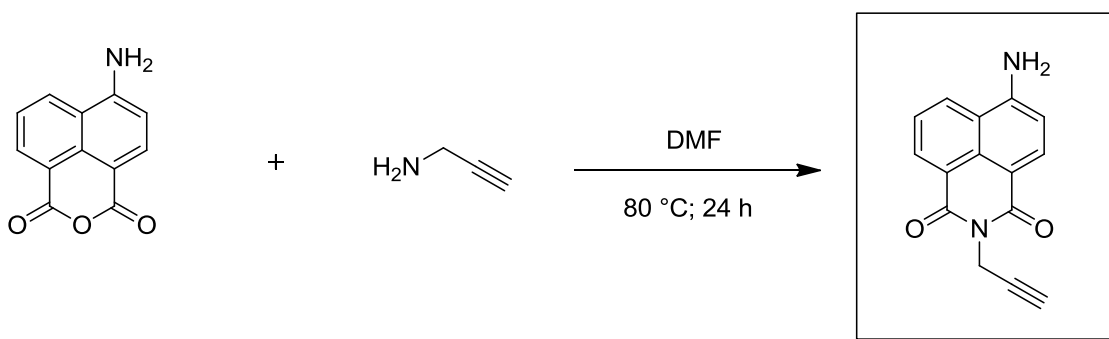


Figure 4.25 Synthesis of the clickable naphthalic anhydride dye “E₁” (3) from 4-amino-1,8-naphthalic anhydride

A mixture of propargylamine (0.51 mL, 8 mmol, 2 eq.) and 4-amino-1,8-naphthalic anhydride (0.853 g, 4 mmol, 1 eq.) was heated at 80 °C overnight in DMF under stirring (Figure 4.26 A). After cooling, the solution was poured into 200 mL of ice-cold distilled water (Figure 4.26 B). The precipitate was filtered, washed with double distilled water and acetone and dried *in vacuo* to yield a yellow solid (Figure 4.26 C).

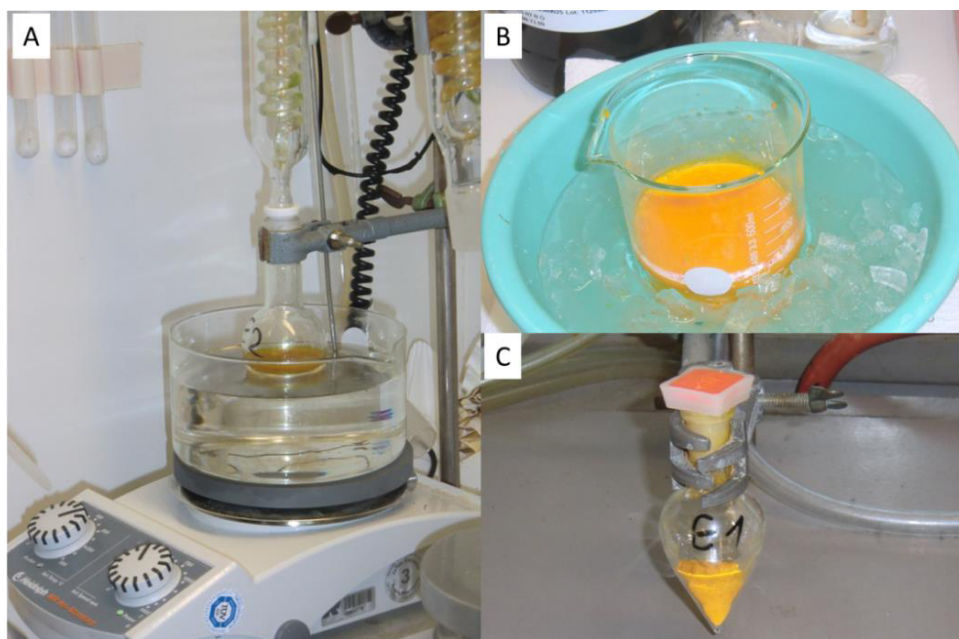


Figure 4.26 Synthesis of the clickable naphthalic anhydride dye “E₁” (3) from 4-amino-1,8-naphthalic anhydride. (A) The reaction mixture was refluxed overnight. (B) The solution was poured into 200 mL of ice-cold water. (C) After washing and drying a yellowish solid was yielded.

¹H-NMR (CDCl₃): δ = 8.65 (dd, 1H, J_1 = 1.0 Hz, J_2 = 7.3 Hz), 8.46 (d, 1H, J = 8.2 Hz), 8.13 (dd, 1H, J_1 = 1.0 Hz, J_2 = 8.4 Hz), 7.68 (dd, 1H, J_1 = 7.4 Hz, J_2 = 8.4 Hz), 6.90 (d, 1H, J = 8.2 Hz), 4.95 (d, 2H, J = 2.5 Hz), 2.17 (t, 1H, J = 2.5 Hz)

(The recorded ¹H-spectrum (Appendix, Figure 7.3.6) is in accordance with the spectrum stated in literature. [76])

ESI-MS (m/z): MH⁺ calculated: 251.1; found: 251.1

5-Fluorescein-Azide (4) (FAM-N₃, Jena Bioscience, www.jenabioscience.com) was diluted in DMSO (1 mg/mL), aliquoted and stored at -20 °C.

Clickable Peptides

The clickable peptides (molecular structure and characterization of all applied peptides: (Appendix, Figure 7.3.3) were synthesized in the group of Dr. Niels Röckendorf at the Leibniz-Research Center in Borstel. The peptides were generated from the amino acid building blocks by standard solid-phase peptide synthesis on a polystyrene solid support. They were characterized by Electrospray Ionization Mass Spectrometry (ESI-MS) and Elemental Analysis.

Femtoliter Array Functionalization.

Silanization. Prior to silanization, the clean glass slide was oxidized in Piranha solution (1:3 ratio of 30 % H₂O₂ and conc. H₂SO₄) for 15 min, washed with distilled water and dried under nitrogen.

Method A. The surface of the fused silica femtoliter array was silanized similar to a protocol published by Kallury *et al.* in 1992. [27]

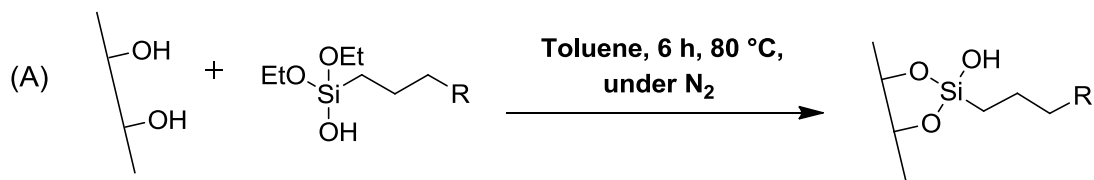


Figure 4.27 *Method A:* Surface silanization of fused silica slides in toluene under reflux according to Kallury *et al.*

For silanization the glass slide was positioned in a round bottom Schlenk flask which was flushed with nitrogen. A 2 % solution of silane (1) or (2) in toluene was pipetted on top of the slide. The reaction mixture was refluxed at 80 °C for approximately 5 h.

Subsequently, the flask was allowed to cool; the silanized slide was removed and washed thoroughly with dry acetone ($\geq 99.9\%$). Finally, the slide was baked for 60 min at $100\text{ }^{\circ}\text{C}$ in a drying cupboard.

Method B. In an alternative silanization reaction the fused silica slides were treated according to silanization protocols published by Rissin *et al.* [30] and Karrasch *et al.* [31]

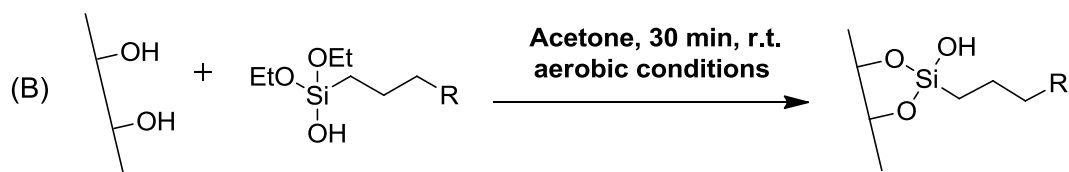


Figure 4.28 *Method B:* Surface silanization of fused silica slides in acetone at room temperature

For silanization the glass slide was positioned in a clipped snap-cap vial and covered with a 2 %-solution of the respective silane in acetone ($\geq 99.9\%$). The reaction mixture was incubated in the open vial for 30 min at room temperature. Afterwards, the slide was removed and washed thoroughly with dry acetone ($\geq 99.9\%$). Finally, the slide was baked in a drying cupboard at $100\text{ }^{\circ}\text{C}$ for 60 min.

Click Coupling Reactions. Click coupling reactions and initial washing steps were performed in the incubation chamber. The silanized slide was loaded into the holder plate, array-side up. Subsequently, the T-piece was fixed on top of the slide. After loading, the chamber was sealed with help of a Teflon stamp.

Coupling of Clickable Dyes. The click reaction was performed in water/DMSO mixtures (1:1 to 1:4, v/v) by adding CuSO_4 and ascorbic acid. The cycloaddition was accelerated by the addition of catalytic quantities of triethylamine (Et_3N). In a standard procedure

200 μL of the clickable dye solution (0.1 to 0.5 mg/mL) were pipetted on top of the femtoliter array. Thereafter, 5 μL of a 20 mM aqueous solution of copper sulfate, 5 μL of a 0.1 M solution of sodium ascorbate and 3 μL Et_3N were added. For the negative control slide no CuSO_4 was added. The reaction solution was mixed and incubated overnight at r.t. under mild shaking. After incubation, the slide was washed in the incubation chamber in several steps (distilled water, DMSO, distilled water). The slide was then removed from the incubation chamber, washed again with DMSO, water and acetone and finally air-dried. Functionalized slides were stored in the dark. The fluorescence intensity was recorded by fluorescence microscopy from slides filled with 5 μL of PBS.

Coupling of Clickable Peptides – Classical Click Reaction. The click reaction was performed in double distilled water by adding CuSO_4 and ascorbic acid. The cycloaddition was accelerated by the addition of catalytic quantities of Et_3N . In a standard procedure, 250 μL of the clickable peptide solution (10 μM - 100 μM) were pipetted on the femtoliter array. 5 μL of a 20 mM aqueous solution of CuSO_4 , 5 μL of a 0.1 M solution of sodium ascorbate and 3 μL Et_3N were added. The reaction solution was mixed and incubated overnight at 4 $^\circ\text{C}$ under mild shaking. The supernatant solution was removed and the array was washed several times with water and DMSO. The slide was then removed from the chamber, washed again with DMSO and water and finally air-dried. Peptide-functionalized slides were stored at 4 $^\circ\text{C}$.

Coupling of Clickable Peptides – Advanced Protocol. The click reaction was performed in double distilled water by adding CuSO_4 and ascorbic acid as well as the supplementary reagents THPTA and aminoguanidine hydrochloride. The silanized, fused silica slide was fixed in the incubation chamber. 100 μL of the clickable peptide (10 μM in H_2O) were pipetted on the femtoliter array. 10 μL of a THPTA solution in water (10 mM), 10 μL aqueous aminoguanidine solution (100 mM), 10 μL of a 100 mM sodium ascorbate solution, 2 μL of an aqueous CuSO_4 solution (20 mM) and 68 μL double distilled water

were added, yielding a total reaction mixture of 200 μL . The solution was mixed by repeated up-and down pipetting and subsequently incubated overnight at 4 $^{\circ}\text{C}$ under mild shaking. Afterwards, the supernatant solution was removed and the array was washed several times with PBST (PBS/0.05 % Tween 20) and water.

Streptavidin- β -Galactosidase Binding. Prior to incubation with the Strep-Gal conjugate the peptide-functionalized array was blocked with a solution of 1 % polyvinylpyrrolidone (PVP, mol wt 10 000, Sigma Aldrich) in PBS: The silica slide was fixed in the incubation chamber, which was loaded with 250 μL of 1% PVP. The array was incubated for 1 h at 4 $^{\circ}\text{C}$ under mild shaking. Afterwards the blocking solution was removed and the array was washed several times with PBST. The blocked silica slide was fixed in the incubation chamber and covered with 200 μL of a 0.56 $\mu\text{g}/\text{mL}$ Strep-Gal solution in PBS containing 0.05 mg/mL BSA and 0.005 % Tween 20. The array was incubated for 3 h at 4 $^{\circ}\text{C}$ under mild shaking. Afterwards, the enzyme solution was removed; the slide was washed repeatedly with PBST and water and finally air-dried. The functionalized slide was stored at 4 $^{\circ}\text{C}$. The fluorescence intensity was recorded by fluorescence microscopy. Prior to the measurements 5 μL of PBS was pipetted on the test slide and the negative control. 5 μL of a 0.56 $\mu\text{g}/\text{mL}$ Strep-Gal solution were enclosed in an unmodified fused silica femtoliter array for the positive control.

Control Experiment: Comparison of the Classical Click Reaction and the Advanced Protocol. The control experiment was performed in a clear, flat bottom 96-well microtiter plate (MTP, Nunc, www.nuncbrand.com). The activity of Strep-Gal was observed in parallel in three different environments: (1) buffer only, (2) conditions of the classical click reaction and (3) conditions of the advanced click protocol. All reaction conditions were monitored in triplicate in three adjacent MTP wells. Each well confined a total volume of 100 μL PBS, containing 1 mM MgCl_2 , 0.05 mg/mL BSA and 0.005 % Tween 20,

as well as (1) 100 μM RGP and 0.056 $\mu\text{g/mL}$ Strep-Gal; (2) 400 μM CuSO_4 , 2 mM sodium ascorbate, 1 % (v/v) Et_3N , 100 μM RGP and 0.056 $\mu\text{g/mL}$ Strep-Gal; (3) 200 μM CuSO_4 , 5 mM sodium ascorbate, 5 mM aminoguanidine hydrochloride, 1 mM THPTA, 100 μM RGP and 0.056 $\mu\text{g/mL}$ Strep-Gal. The reaction was started by the addition of Strep-Gal. After mixing, image acquisition was started within 2 min after enzyme addition. The generation of the fluorescent product resorufin was monitored every 30 s over a time course of 10 min.

5.3.3. HRP Modification for Application in Click Reactions

Buffers and Reagents. Lyophilized, salt free peroxidase from horseradish (HRP, type XII, 250-330 units/mg) and 1H-imidazole-1-sulfonyl azide were purchased from Sigma-Aldrich. A 20 mM stock solution of Amplex Red (Life Technologies) in DMSO was split into aliquots and stored at -20 °C. Substrate turnover experiments with HRP and N₃-HRP were performed in phosphate buffered saline (PBS: 2.7 mM KCl, 2 mM KH₂PO₄, 137 mM NaCl, 10 mM Na₂HPO₄, pH 7.4) with an addition of 0.05 mg/mL BSA (Sigma-Aldrich) and 0.005 % (w/v) Tween 20 (Sigma-Aldrich). Unless otherwise stated, all other chemicals and solvents were purchased from Sigma-Aldrich, Merck and ABCR. They were of analytical grade and used without further purification.

Diazo-transfer Reaction. The diazo-transfer reaction was performed similar to protocols published by Goddard-Borger *et al.* [65] and van Dongen *et al.* [66]. To a solution of HRP in double distilled water (200 µL, 2.5 mg/mL, 1 eq.) 100 µL of an aqueous solution of K₂CO₃ (2 mg/mL) and 25 µL of CuSO₄·5H₂O solution in double distilled water (1 mg/mL) were added. An aqueous solution of 1H-imidazole-1-sulfonyl azide (15 µL, 2 mg/mL, 1.75 eq.) was added and the solution was incubated overnight at r.t. under mild shaking (600 rpm). Afterwards, the reaction mixture was transferred to an Amicon centrifugal filter unit (Millipore™) with a cutoff of 3 kDa. The mixture was centrifuged to dryness. The supernatant was redissolved in double distilled water (500 µL) and centrifuged again. In total five washing steps were performed. The clean product was redissolved in double distilled water (200 µL) and analyzed by ESI-TOF-MS.

ESI-MS (m/z):	M(native HRP):	43174.86 Da
	M(N ₃ -HRP):	calculated: 43278.82 (for four transfer reactions)
		found: 43278.82

Substrate Turnover Experiment with HRP and N₃-HRP. HRP and N₃-HRP were investigated in parallel in the wells of a transparent, flat bottom 96-well MTP (Nunc). The activity of both enzymes was monitored in triplicate in three adjacent wells. HRP/N₃-HRP (approximately 36 pM) were incubated with 250 μM Amplex Red and various concentrations of H₂O₂ in a total volume of 100 μL. Measurements were taken every 30 seconds on a Fluostar Optima MTP reader ($\lambda_{\text{ex}} = 544 \text{ nm}$, $\lambda_{\text{em}} = 590 \text{ nm}$). Substrate turnover rates were calibrated by comparison with the fluorescence intensities of resorufin standard solutions (The resorufin calibration curve can be found in the Appendix, Figure 7.3.7). The enzymatic rates were standardized, with the maximum substrate turnover rate of native HRP at 1 mM H₂O₂ as 100%.

5.3.4. Immobilization of Antibodies via Peptide Chemistry

Buffers and Reagents. 3-Aminopropyl-triethoxysilane (APTES, ≥ 98 %), glutaric anhydride (95 %), Fluorescein isothiocyanate (FITC, ≥ 90 %), N-Hydroxysuccinimide (NHS, 98 %), Sephadex (G-25) and γ -Globuline from bovine blood (≥ 99 %) were purchased from Sigma Aldrich. N,N'-Dicyclohexylcarbodiimide (DCC, 99 %) was purchased from Merck. Labeling of antibodies was performed in phosphate buffered saline (PBS: 2.7 mM KCl, 2 mM KH_2PO_4 , 137 mM NaCl, 10 mM Na_2HPO_4 , pH 7.4). When applied in washing steps, PBS was complemented with 0.5 % Tween 20 (PBST, Sigma-Aldrich). Unless otherwise stated, all other chemicals and solvents were purchased from Sigma-Alrich, Merck and ABCR. They were of analytical grade and used without further purification.

Femtoliter Array Functionalization.

The surface functionalization of the fused silica femtoliter array was done similar to a protocol published by Kallury *et al.* in 1992. [27]

Silanization. Prior to silanization, the clean glass slide was incubated in methanol and concentrated H_2SO_4 for 20 min respectively, washed with distilled water and dried under nitrogen. The glass slide was positioned in a round bottom Schlenk flask which was flushed with nitrogen. A 2 % solution of APTES in toluene was pipetted on top of the slide. The reaction mixture was refluxed at 80 °C for approximately 5 h. Subsequently, the flask was allowed to cool; the silanized slide was removed and washed thoroughly with methanol. Finally, the slide was baked for 60 min at 100 °C in a drying cupboard.

Introduction of the Carboxylic Group. The silanized slide was positioned in a round bottom Schlenk flask which was flushed with nitrogen. A solution of 0.3 g glutaric anhydride in 15 mL toluene was pipetted on top of the array. The reaction mixture was

refluxed overnight at 80 °C. The flask was allowed to cool down. The carboxylated slide was removed, washed thoroughly with ethanol and finally dried under nitrogen.

Carboxyl Activation. The terminal carboxylic groups were activated by NHS-ester formation in the presence of DCC. For this purpose the glass slide was positioned in a round bottom Schlenk which was flushed with nitrogen. A solution of DCC (20 mg) and NHS (40 mg) in 10 mL THF was pipetted on top of the slide. The reaction mixture was incubated at room temperature overnight under nitrogen. Finally, the activated slide was washed thoroughly with ethanol and air-dried.

Antibody Binding. For characterization, the activated femtoliter array was covered with a solution of the FITC-labelled bovine γ -globuline in double distilled water (0.01 mg/ml – 0.1 mg/mL). The mixture was left to react for 48 h at 4 °C. Afterwards, the slide was recovered and washed thoroughly with PBST and double distilled water.

Antibody Labeling. For γ -globulin labeling, 100 μ L of a 1 mg/mL antibody solution in PBS (pH 8.0) was combined with 7.5 μ L FITC in DMSO (0.5 mg/mL) and incubated for approximately 1 h at 37 °C in a thermomixer (900 rpm, Eppendorf, www.eppendorf.de). The FITC-labeled antibodies were purified by size exclusion chromatography in a 10 mL Pierce centrifuge column (www.piercenet.com) packed with Sephadex G-25, using PBS (pH 7.4) as the running buffer. The collected fractions were concentrated using commercial Amicon Centrifugal filter units (MilliporeTM, www.merckmillipore.de) with an exclusion size of 30 kDa to yield a final solution of 1 mg/mL FITC- γ -globulin in PBS.

5.4. Conclusion

Large arrays of homogeneously arranged ultra-small reaction chambers in combination with enzymatic signal amplification enable the digital readout of low target concentrations in complex samples (chapter 4). [13, 15, 77, 78] The foundation for the application of fused silica femtoliter arrays in single molecule bioassays is the introduction of various biomolecules on the surface of the fused silica wells. For this purpose popular synthesis strategies, such as click chemistry and common peptide chemistry were applied. The stable and covalent attachment of the biomolecules to the femtoliter array surface was verified by fluorescence microscopy.

In chapter 5.2.4, it is described how any type of protein can successfully be linked to a fused silica surface using basic peptide chemistry. Yet, the application of peptide chemistry has some drawbacks that may render alternative binding techniques such as click chemistry more beneficial. The NHS-ester activation of carboxylic groups is an effective way to form peptide bonds. However, the hydrolysis of the NHS-ester will always compete with the formation of the peptide bond. The hydrolysis rate increases with buffer pH, and peptide-binding is less efficient, if the protein concentration is low. In contrast, the CuAAC reaction is unsusceptible towards pH changes. Independent of reaction conditions, it is fast, quantitative, and biorthogonal. [9-12] Nevertheless, the click chemistry approach held its challenges. In order to successfully apply click chemistry in single molecule analysis, the biotoxic side-effects of the common CuSO_4 /sodium ascorbate mediated reaction had to be considered and suppressed. In this way, an effective protocol for the Cu-mediated immobilization of biomolecules to the surface of the fused silica femtoliter arrays could be developed.

The successful immobilization of different biomolecules on the fused silica surface of femtoliter wells using either click or peptide chemistry clears the way for the development of a wide range of different, ultra-sensitive biological assays.

5.5. References

1. Kolb, H.C., M.G. Finn, and K.B. Sharpless, *Click Chemistry: Diverse Chemical Function from a Few Good Reactions*. Angew. Chem. Int. Ed., **2001** (40): 2004.
2. Kolb, H.C. and K.B. Sharpless, *The growing impact of click chemistry on drug discovery*. Drug. Discov. Today, **2003** (8): 1128.
3. Huisgen, R., *1,3-Dipolar Cycloadditions - Past and Future*. Angew. Chem. Int. Ed., **1963** (2): 565.
4. Huisgen, R., *Kinetics and Mechanism of 1,3-Dipolar Cycloadditions*. Angew. Chem. Int. Ed., **1963** (2): 633.
5. Huisgen, R., *Concerted Nature of 1,3-Dipolar Cycloadditions and Question of Diradical Intermediates*. J. Org. Chem., **1976** (41): 403.
6. Tornøe, C.W., C. Christensen, and M. Meldal, *Peptidotriazoles on solid phase: [1,2,3]-triazoles by regiospecific copper(I)-catalyzed 1,3-dipolar cycloadditions of terminal alkynes to azides*. J. Org. Chem., **2002** (67): 3057.
7. Rostovtsev, V.V., L.G. Green, V.V. Fokin, and K.B. Sharpless, *A stepwise Huisgen cycloaddition process: Copper(I)-catalyzed regioselective "ligation" of azides and terminal alkynes*. Angew. Chem. Int. Ed., **2002** (41): 2596.
8. Himo, F., T. Lovell, R. Hilgraf, V.V. Rostovtsev, L. Noodleman, K.B. Sharpless, and V.V. Fokin, *Copper(I)-catalyzed synthesis of azoles. DFT study predicts unprecedented reactivity and intermediates*. J. Am. Chem. Soc., **2005** (127): 210.
9. Prescher, J.A. and C.R. Bertozzi, *Chemistry in living systems*. Nat. Chem. Biol., **2005** (1): 13.
10. Kurpiers, T. and H.D. Mootz, *Bioorthogonal Ligation in the Spotlight*. Angew. Chem. Int. Ed., **2009** (48): 1729.
11. Baskin, J.M. and C.R. Bertozzi, *Bioorthogonal click chemistry: Covalent labeling in living systems*. QSAR Comb. Sci., **2007** (26): 1211.
12. Sletten, E.M. and C.R. Bertozzi, *Bioorthogonal Chemistry: Fishing for Selectivity in a Sea of Functionality*. Angew. Chem. Int. Ed., **2009** (48): 6974.
13. Rissin, D.M., D.R. Fournier, T. Piech, C.W. Kan, T.G. Campbell, et al., *Simultaneous Detection of Single Molecules and Singulated Ensembles of Molecules Enables Immunoassays with Broad Dynamic Range*. Anal. Chem., **2011** (83): 2279.

14. Rissin, D.M., C.W. Kan, T.G. Campbell, S.C. Howes, D.R. Fournier, *et al.*, *Single-molecule enzyme-linked immunosorbent assay detects serum proteins at subfemtomolar concentrations*. Nat. Biotechnol., **2010** (28): 595.
15. Rissin, D.M., C.W. Kan, L. Song, A.J. Rivnak, M.W. Fishburn, *et al.*, *Multiplexed single molecule immunoassays*. Lab Chip, **2013** (13): 2902.
16. Kan, C.W., A.J. Rivnak, T.G. Campbell, T. Piech, D.M. Rissin, *et al.*, *Isolation and detection of single molecules on paramagnetic beads using sequential fluid flows in microfabricated polymer array assemblies*. Lab Chip, **2012** (12): 977.
17. Breitmaier, E. and G. Jung, *Organische Chemie: Methoden der Peptidsynthese*. 6th ed (**2005**): Georg Thieme Verlag.
18. Neises, B. and W. Steglich, *4-Dialkylaminopyridines as Acylation Catalysts .5. Simple Method for Esterification of Carboxylic-Acids*. Angew. Chem. Int. Ed., **1978** (17): 522.
19. Nakajima, N. and Y. Ikada, *Mechanism of amide formation by carbodiimide for bioconjugation in aqueous media*. Bioconjugate Chem., **1995** (6): 123.
20. Merrifield, R.B., *Solid phase peptide synthesis. I. The synthesis of a tetrapeptide*. J. Am. Chem. Soc., **1963** (85): 2149.
21. Phaner-Goutorbe, M., V. Dugas, Y. Chevolot, and E. Souteyrand, *Silanization of silica and glass slides for DNA microarrays by impregnation and gas phase protocols: A comparative study*. Mat. Sci. Eng. C-Mater., **2011** (31): 384.
22. Gauthier, M.A., M.I. Gibson, and H.A. Klok, *Synthesis of Functional Polymers by Post-Polymerization Modification*. Angew. Chem. Int. Ed., **2009** (48): 48.
23. Achatz, D.E., F.J. Heiligtag, X.H. Li, M. Link, and O.S. Wolfbeis, *Colloidal silica nanoparticles for use in click chemistry-based conjugations and fluorescent affinity assays*. Sens. Actuators, B, **2010** (150): 211.
24. Achatz, D.E., G. Mezo, P. Kele, and O.S. Wolfbeis, *Probing the activity of matrix metalloproteinase II with a sequentially click-labeled silica nanoparticle FRET probe*. ChemBioChem, **2009** (10): 2316.
25. Kallury, K.M.R., P.M. Macdonald, and M. Thompson, *Effect of Surface-Water and Base Catalysis on the Silanization of Silica by (Aminopropyl)Alkoxysilanes Studied by X-Ray Photoelectron-Spectroscopy and C-13 Cross-Polarization Magic-Angle-Spinning Nuclear-Magnetic-Resonance*. Langmuir, **1994** (10): 492.

26. Muller, R., A. Eidt, K.A. Hiller, V. Katzur, M. Subat, *et al.*, *Influences of protein films on antibacterial or bacteria-repellent surface coatings in a model system using silicon wafers*. *Biomaterials*, **2009** (30): 4921.
27. Kallury, K.M., W.E. Lee, and M. Thompson, *Enhancement of the thermal and storage stability of urease by covalent attachment to phospholipid-bound silica*. *Anal. Chem.*, **1992** (64): 1062.
28. Asbach, B., M. Kolb, M. Liss, R. Wagner, and M. Schaferling, *Protein microarray assay for the screening of SH3 domain interactions*. *Anal. Bioanal. Chem.*, **2010** (398): 1937.
29. Howarter, J.A. and J.P. Youngblood, *Optimization of silica silanization by 3-aminopropyltriethoxysilane*. *Langmuir*, **2006** (22): 11142.
30. Rissin, D.M. and D.R. Walt, *Digital readout of target binding with attomole detection limits via enzyme amplification in femtoliter arrays*. *J. Am. Chem. Soc.*, **2006** (128): 6286.
31. Karrasch, S., M. Dolder, F. Schabert, J. Ramsden, and A. Engel, *Covalent binding of biological samples to solid supports for scanning probe microscopy in buffer solution*. *Biophys. J.*, **1993** (65): 2437.
32. Nakazawa, J. and T.D. Stack, *Controlled loadings in a mesoporous material: click-on silica*. *J. Am. Chem. Soc.*, **2008** (130): 14360.
33. Cras, J.J., C.A. Rowe-Taitt, D.A. Nivens, and F.S. Ligler, *Comparison of chemical cleaning methods of glass in preparation for silanization*. *Biosens. Bioelectron.*, **1999** (14): 683.
34. Sawoo, S., P. Dutta, A. Chakraborty, R. Mukhopadhyay, O. Bouloussa, and A. Sarkar, *A new bio-active surface for protein immobilisation via copper-free 'click' between azido SAM and alkynyl Fischer carbene complex*. *Chem. Commun.*, **2008**: 5957.
35. Simon, A., T. Cohen-Bouhacina, M.C. Porte, J.P. Aime, and C. Baquey, *Study of two grafting methods for obtaining a 3-aminopropyltriethoxysilane monolayer on silica surface*. *J. Colloid. Interf. Sci.*, **2002** (251): 278.
36. Etienne, M. and A. Walcarius, *Analytical investigation of the chemical reactivity and stability of aminopropyl-grafted silica in aqueous medium*. *Talanta*, **2003** (59): 1173.
37. Bhatia, S.K., J.L. Teixeira, M. Anderson, L.C. Shriver-Lake, J.M. Calvert, *et al.*, *Fabrication of surfaces resistant to protein adsorption and application to two-dimensional protein patterning*. *Anal. Biochem.*, **1993** (208): 197.
38. Kurth, D.G. and T. Bein, *Surface-Reactions on Thin-Layers of Silane Coupling Agents*. *Langmuir*, **1993** (9): 2965.

39. Petri, D.F.S., G. Wenz, P. Schunk, and T. Schimmel, *An improved method for the assembly of amino-terminated monolayers on SiO₂ and the vapor deposition of gold layers*. *Langmuir*, **1999** (15): 4520.
40. Flink, S., F.C.J.M. van Veggel, and D.N. Reinhoudt, *Functionalization of self-assembled monolayers on glass and oxidized silicon wafers by surface reactions*. *J. Phys. Org. Chem.*, **2001** (14): 407.
41. Mader, H.S., M. Link, D.E. Achatz, K. Uhlmann, X. Li, and O.S. Wolfbeis, *Surface-modified upconverting microparticles and nanoparticles for use in click chemistries*. *Chemistry*, **2010** (16): 5416.
42. Sivakumar, S., P.R. Diamente, and F.C. van Veggel, *Silica-coated Ln³⁺-Doped LaF₃ nanoparticles as robust down- and upconverting biolabels*. *Chemistry*, **2006** (12): 5878.
43. Bagwe, R.P., L.R. Hilliard, and W. Tan, *Surface modification of silica nanoparticles to reduce aggregation and nonspecific binding*. *Langmuir*, **2006** (22): 4357.
44. Liebherr, R.B., T. Soukka, O.S. Wolfbeis, and H.H. Gorris, *Maleimide activation of photon upconverting nanoparticles for bioconjugation*. *Nanotechnology*, **2012** (23): 485103.
45. Vandenberg, E.T., L. Bertilsson, B. Liedberg, K. Uvdal, R. Erlandsson, H. Elwing, and I. Lundstrom, *Structure of 3-Aminopropyl Triethoxy Silane on Silicon-Oxide*. *J. Colloid. Interf. Sci.*, **1991** (147): 103.
46. Weber, P.C., D.H. Ohlendorf, J.J. Wendoloski, and F.R. Salemme, *Structural origins of high-affinity biotin binding to streptavidin*. *Science*, **1989** (243): 85.
47. Chaiet, L. and F.J. Wolf, *The Properties of Streptavidin, a Biotin-Binding Protein Produced by Streptomyces*. *Arch. Biochem. Biophys.*, **1964** (106): 1.
48. Fry, S.C., *Oxidative scission of plant cell wall polysaccharides by ascorbate-induced hydroxyl radicals*. *Biochem. J.*, **1998** (332 (Pt 2)): 507.
49. Wang, Q., T.R. Chan, R. Hilgraf, V.V. Fokin, K.B. Sharpless, and M.G. Finn, *Bioconjugation by copper(I)-catalyzed azide-alkyne [3 + 2] cycloaddition*. *J. Am. Chem. Soc.*, **2003** (125): 3192.
50. Hong, V., S.I. Presolski, C. Ma, and M.G. Finn, *Analysis and optimization of copper-catalyzed azide-alkyne cycloaddition for bioconjugation*. *Angew. Chem. Int. Ed.*, **2009** (48): 9879.
51. Baker, W.L., J. Goode, and L. Cooper, *Estimation of Hydrogen-Peroxide Formed and Residual Ascorbate in the Copper Catalyzed Oxidation Reaction of Ascorbate at Ph-7*. *Mikrochim. Acta*, **1992** (106): 143.

52. Liu, P.Y., N. Jiang, J. Zhang, X. Wei, H.H. Lin, and X.Q. Yu, *The oxidative damage of plasmid DNA by ascorbic acid derivatives in vitro: the first research on the relationship between the structure of ascorbic acid and the oxidative damage of plasmid DNA*. Chem. Biodiversity, **2006** (3): 958.
53. Liu, Y.H., G. Sun, A. David, and L.M. Sayre, *Model studies on the metal-catalyzed protein oxidation: Structure of a possible His-Lys cross-link*. Chem. Res. Toxicol., **2004** (17): 110.
54. Levengood, M.R., C.C. Kerwood, C. Chatterjee, and W.A. van der Donk, *Investigation of the substrate specificity of lactacin 481 synthetase by using nonproteinogenic amino acids*. ChemBioChem, **2009** (10): 911.
55. Nagaraj, R.H., D.R. Sell, M. Prabhakaram, B.J. Ortwerth, and V.M. Monnier, *High correlation between pentosidine protein crosslinks and pigmentation implicates ascorbate oxidation in human lens senescence and cataractogenesis*. Proc. Natl. Acad. Sci. U. S. A., **1991** (88): 10257.
56. Chan, T.R., R. Hilgraf, K.B. Sharpless, and V.V. Fokin, *Polytriazoles as copper(I)-stabilizing ligands in catalysis*. Org. Lett., **2004** (6): 2853.
57. Kohmura, Y. and T. Katsuki, *Asymmetric allylic oxidation of cycloalkenes using a tridentate tris(oxazoline) ligand as a chiral auxiliary*. Tetrahedron Lett., **2000** (41): 3941.
58. Gornall, A.G., C.J. Bardawill, and M.M. David, *Determination of serum proteins by means of the biuret reaction*. J. Biol. Chem., **1949** (177): 751.
59. Lottspeich, F., J.W. Engels, and A. Simeon, *Bioanalytik*. 2nd ed (**2006**): Spektrum
60. Lowry, O.H., N.J. Rosebrough, A.L. Farr, and R.J. Randall, *Protein measurement with the Folin phenol reagent*. J. Biol. Chem., **1951** (193): 265.
61. Agard, N.J., J.A. Prescher, and C.R. Bertozzi, *A strain-promoted [3 + 2] azide-alkyne cycloaddition for covalent modification of biomolecules in living systems*. J. Am. Chem. Soc., **2004** (126): 15046.
62. Baskin, J.M., J.A. Prescher, S.T. Laughlin, N.J. Agard, P.V. Chang, *et al.*, *Copper-free click chemistry for dynamic in vivo imaging*. Proc. Natl. Acad. Sci. U. S. A., **2007** (104): 16793.
63. Chang, P.V., J.A. Prescher, E.M. Sletten, J.M. Baskin, I.A. Miller, *et al.*, *Copper-free click chemistry in living animals*. Proc. Natl. Acad. Sci. U. S. A., **2010** (107): 1821.
64. Welinder, K.G., *Covalent structure of the glycoprotein horseradish peroxidase (EC 1.11.1.7)*. FEBS Lett., **1976** (72): 19.

65. Goddard-Borger, E.D. and R.V. Stick, *An efficient, inexpensive, and shelf-stable diazotransfer reagent: imidazole-1-sulfonyl azide hydrochloride*. *Org. Lett.*, **2007** (9): 3797.
66. van Dongen, S.F., R.L. Teeuwen, M. Nallani, S.S. van Berkel, J.J. Cornelissen, R.J. Nolte, and J.C. van Hest, *Single-step azide introduction in proteins via an aqueous diazo transfer*. *Bioconjugate Chem.*, **2009** (20): 20.
67. Berglund, G.I., G.H. Carlsson, A.T. Smith, H. Szoke, A. Henriksen, and J. Hajdu, *The catalytic pathway of horseradish peroxidase at high resolution*. *Nature*, **2002** (417): 463.
68. Veitch, N.C., *Horseradish peroxidase: a modern view of a classic enzyme*. *Phytochemistry*, **2004** (65): 249.
69. Rodriguez-Lopez, J.N., M.A. Gilabert, J. Tudela, R.N. Thorneley, and F. Garcia-Canovas, *Reactivity of horseradish peroxidase compound II toward substrates: kinetic evidence for a two-step mechanism*. *Biochemistry*, **2000** (39): 13201.
70. Valderrama, B., M. Ayala, and R. Vazquez-Duhalt, *Suicide inactivation of peroxidases and the challenge of engineering more robust enzymes*. *Chem. Biol.*, **2002** (9): 555.
71. Rondelez, Y., G. Tresset, K.V. Tabata, H. Arata, H. Fujita, S. Takeuchi, and H. Noji, *Microfabricated arrays of femtoliter chambers allow single molecule enzymology*. *Nat. Biotechnol.*, **2005** (23): 361.
72. Gorris, H.H. and D.R. Walt, *Mechanistic aspects of horseradish peroxidase elucidated through single-molecule studies*. *J. Am. Chem. Soc.*, **2009** (131): 6277.
73. Ehrl, B.N., R.B. Liebherr, and H.H. Gorris, *Single molecule kinetics of horseradish peroxidase exposed in large arrays of femtoliter-sized fused silica chambers*. *Analyst*, **2013** (138): 4260.
74. Thaller, M., *Master-Thesis: Vesicle-Based Chemosensors for the Application in Femtoliter Arrays*. Institute for Analytical Chemistry, Chemo- and Biosensors, **2012**. University of Regensburg.
75. Achatz, D.E., *Diploma Thesis: Fluorescent Silica Nanoparticles for Click Labeling of Proteins*. Institute for Analytical Chemistry, Chemo- and Biosensors, **2008**. Universität Regensburg.
76. Kele, P., X. Li, M. Link, K. Nagy, A. Herner, *et al.*, *Clickable fluorophores for biological labeling-with or without copper*. *Org. Biomol. Chem.*, **2009** (7): 3486.
77. Song, L., D.W. Hanlon, L. Chang, G.K. Provuncher, C.W. Kan, *et al.*, *Single molecule measurements of tumor necrosis factor alpha and interleukin-6 in the plasma of patients with Crohn's disease*. *J. Immunol. Methods*, **2011** (372): 177.

78. Wilson, D.H., D.W. Hanlon, G.K. Provuncher, L. Chang, L. Song, *et al.*, *Fifth-generation digital immunoassay for prostate-specific antigen by single molecule array technology*. *Clin. Chem.*, **2011** (57): 1712.

6. Summary

6.1. In English

The aim of this thesis was the analysis of individual enzyme molecules in large arrays of homogeneously arranged femtoliter-sized reaction chambers. The implementation of single molecule technologies in bioanalytical research provides us with new insights into the basic principles of life, revealing interesting details of biomolecular interactions. Thus, different conformational states or enzymatic subpopulations that were hidden in conventional bulk experiments are disclosed. Large arrays of homogeneous microwells are a convenient and versatile platform for monitoring the activity of many individual enzyme molecules in parallel. Entrapment of individual enzyme molecules in femtoliter-sized reaction chambers spares surface immobilization and allows for a kinetic investigation of enzymes free in solution. Additionally, the high degree of parallelization enables the investigation of a statistically representative enzyme population.

The first part of this work discusses the implementation of a novel, optimized setup for single enzyme molecule analysis in large, homogeneous arrays of femtoliter-sized reaction chambers. The generation, characterization and application of two different types of arrays etched into the surface of fused silica slides or molded in PDMS is presented. The gradual improvement of the applied experimental setup is described, considering aspects, such as tight array sealing, photobleaching, signal readout and non-specific adsorption. Ultimately, an optimized setup was achieved that enabled highly sensitive and accurate single enzyme molecule experiments. The effectivity of the designed setup was verified in the single molecule investigation of the model enzyme β -galactosidase. Several hundred enzyme molecules were individualized in the wells of both femtoliter arrays and their individual substrate turnover recorded over time by fluorescence microscopy. A broad activity distribution within the probed β -galactosidase

population was detected for both experiments in fused silica and PDMS femtoliter arrays, which is in good agreement with previous reports.

In the next chapter, the femtoliter array setup was employed to gain a single molecule perspective on the mechanisms that drive the evolution of new enzyme activity. For this purpose we investigated and compared the kinetics of wild-type and *in vitro* evolved β -glucuronidase (GUS) at the single molecule level. Several hundred GUS molecules were individualized in the wells of fused silica femtoliter arrays and their individual substrate turnover rates observed in parallel by fluorescence microscopy. Individual GUS molecules exhibited distinct, long-lived activity states, whereas their mean activity was consistent with classical Michaelis-Menten kinetics. In comparison to the wild-type enzyme, the partially evolved variant (also called generalist) displayed a much broader activity distribution, indicating a higher conformational plasticity. This finding was confirmed by circular dichroism. The broader conformational heterogeneity of the partially evolved GUS indicates a functional division of work between individual molecules in a population of generalists, which are characterized by their promiscuous activity with many different substrates.

Finally, the established femtoliter array platform was introduced to a different, more recent application: Large arrays of homogeneously arranged microwells in combination with enzymatic signal amplification enable the digital readout of target concentrations way below the detection limit of conventional assays. In context of this thesis, the applicability of fused silica femtoliter arrays for digital concentration readout was demonstrated in a proof of principle experiment with β -galactosidase. Subsequently, the surface of fused silica arrays was modified to enable their application in bioanalytical assays. Biomolecules such as peptides or antibodies were covalently linked to the surface of the fused silica wells, using either click chemistry or common peptide chemistry. Thus, the foundation for the future application of fused silica femtoliter arrays in ultra-sensitive bioassays with digital concentration readout was laid.

6.2. In German

Ziel dieser Arbeit war die Untersuchung individueller Enzymmoleküle in großen Arrays aus homogen angeordneten Kammern im Femtoliter-Maßstab. Die Etablierung von Einzelmolekültechniken in der bioanalytischen Forschung eröffnet uns neue Erkenntnisse zu den grundlegenden Prozessen des Lebens. Faszinierende Details zu intermolekularen Wechselwirkungen werden sichtbar gemacht und Protein-Konformationen oder Subpopulationen aufgedeckt, die in konventionellen Bulk-Experimenten verborgen geblieben sind. Der Einsatz großer Arrays aus homogen angeordneten Mikrokavitäten ist eine exzellente und vielseitige Methode zur gleichzeitigen Analyse einer großen Anzahl individueller Enzyme. Der Einschluss einzelner Enzymmoleküle in individuellen Gefäßen erübrigt eine Oberflächenimmobilisierung und erlaubt eine direkte Untersuchung frei in Lösung. Zusätzlich ermöglicht der hohe Grad an Parallelisierung die Analyse einer statistisch repräsentativen Enzympopulation.

Im ersten Teil dieser Arbeit wird die Entwicklung eines neuen, optimierten Systems zur Einzelenzymmoleküldetektion in homogenen Arrays aus Femtolitergefäßen diskutiert. Dabei wird zunächst die Herstellung und Charakterisierung zweier unterschiedlicher Array-Typen, gefertigt in Quarzglas beziehungsweise PDMS, vorgestellt. Anschließend wird die schrittweise Optimierung des experimentellen Aufbaus erläutert, wobei wesentliche Punkte, wie ein dichter Array-Verschluss, Fotobleichen, Signal-Auslesung und unspezifische Bindung berücksichtigt wurden. Auf diese Weise konnte ein optimiertes System entwickelt werden, das die Durchführung von hochempfindlichen Einzelenzymmessungen ermöglicht. Die Funktionsfähigkeit des entwickelten Systems wurde anhand einer Einzelmolekülanalyse des Modellenzym β -Galactosidase sichergestellt. Einige hundert Enzymmoleküle wurden in den einzelnen Kammern beider Arrays isoliert und ihr jeweiliger Substratumsatz mit Hilfe eines Fluoreszenzmikroskops aufgezeichnet. Dabei wurde für beide Arraytypen - und in guter Übereinstimmung mit

früheren Ergebnissen - eine breite Verteilung der Enzymaktivitäten innerhalb der β -Galactosidase-Population festgestellt.

Im zweiten Teil der Arbeit wurden Femtoliterarrays aus Quarzglas eingesetzt, um die Mechanismen der Enzymevolution aus dem Blickwinkel der Einzelmolekülanalytik zu betrachten. Für diesen Zweck wurde die Kinetik einer Wildtyp- und einer *in vitro* entwickelten β -Glucuronidase (GUS) auf der Einzelmolekülebene untersucht und verglichen. Mehrere hundert GUS Moleküle wurden in den Kammern eines Quarzglas Arrays isoliert und ihr jeweiliger Substratumsatz parallel mittels Fluoreszenzmikroskopie beobachtet. Individuelle GUS Moleküle wiesen unterschiedliche, langlebige Aktivitätszustände auf, wobei ihre mittlere Aktivität mit der klassischen Michaelis-Menten-Kinetik übereinstimmte. Im Vergleich zum Wildtyp-Enzym, zeigte die Mutante (oder Generalist) eine deutlich breitere Aktivitätsverteilung, was auf eine stärkere strukturelle Plastizität hindeutet. Dieses Ergebnis konnte durch eine Circular dichroismus Studie bestätigt werden. Die stärkere strukturelle Heterogenität der GUS Mutante deutet auf eine funktionelle Arbeitsteilung zwischen den einzelnen Individuen der Population hin.

Im letzten Kapitel dieser Arbeit, wurde der Quarzglas Femtoliter-Array für eine andere, aktuelle Anwendung der Einzelenzymdetektion eingesetzt: Arrays homogener angeordneter Femtoliter-Kammern in Kombination mit enzymatischer Signalverstärkung ermöglichen das digitale Auslesen von Analytkonzentrationen deutlich unterhalb der Nachweisgrenze konventioneller Assays. Im Rahmen dieser Arbeit wurde zunächst die Eignung des Quarzglas-Femtoliter Arrays für die digitale Konzentrationsbestimmung demonstriert. Anschließend wurde die Oberfläche, der Arrays derart modifiziert, dass sie in bioanalytischen Assays zur Anwendung kommen können. Unter Verwendung von Click-Chemie oder gewöhnlicher Peptid-Chemie wurden Biomoleküle wie Peptide oder Antikörper kovalent an der Oberfläche der winzigen Quarzglasgefäße immobilisiert. Auf diese Weise wurde die Grundlage für eine Anwendung der Femtoliter-Arrays in hochempfindlichen Assays mit digitaler Konzentrationsbestimmung geschaffen.





7. Appendix

7.1. Analysis of Single β -Galactosidase in Femtoliter Arrays

Figure 7.1.1

Schematic representation of the photolithographic chrome mask for the fabrication of femtoliter arrays of the type D_4P_6 , where D defines the well diameter and P the distance from border to border between two adjacent wells. The femtoliter arrays produced with help of the chrome mask have a well-radius of about $2\ \mu\text{m}$ and an average well-depth of $3.5 \pm 0.1\ \mu\text{m}$.

The photolithographic chrome mask was designed and fabricated by Florian Götz and Albert Hutterer from the Faculty of Microsystem Engineering, University of Applied Sciences, Regensburg.

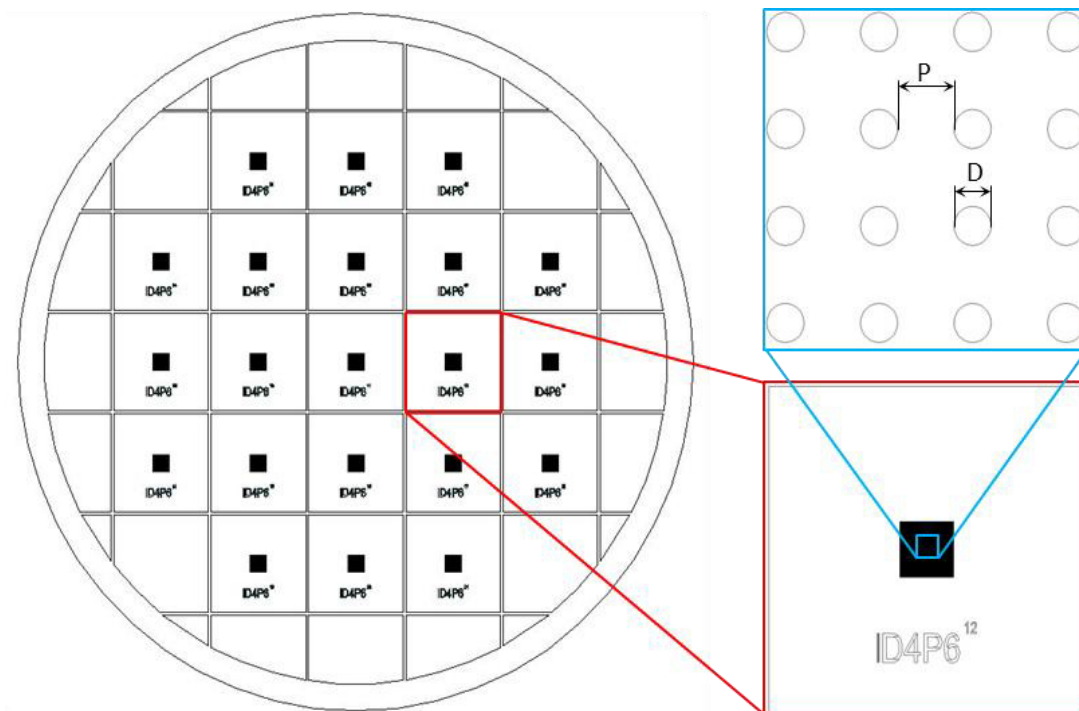


Figure 7.1.2

Schematic representation of the custom-built casting equipment for PDMS array molding: The casting form (beige) consists of a solid bottom plate (110 mm in diameter) equipped with four M4 threads and a cover ring (outer diameter: 110 mm, inner diameter: 90 mm). For PDMS-array generation, the silicon template (grey) with the integrated SU-8 femtoliter well structures (yellow) is clamped into the casting form and fixed with help of four M4x10 screws. The casting form is placed on a leveled surface and the degassed, liquid PDMS (blue) is poured on the master template. After curing the PDMS sheet with integrated femtoliter arrays is removed from the casting form and ready for application in single molecule experiments.

The casting equipment was designed by Albert Hutterer from the Faculty of Microsystem Engineering, University of Applied Sciences, Regensburg. The form was designed with the CAD Software Autodesk Inventor (www.autodesk.de). The design was transferred to the 3D printer Objet Connex 500 (www.stratasys.com) and generated from VeroWhite+ /RGD83 primary material.

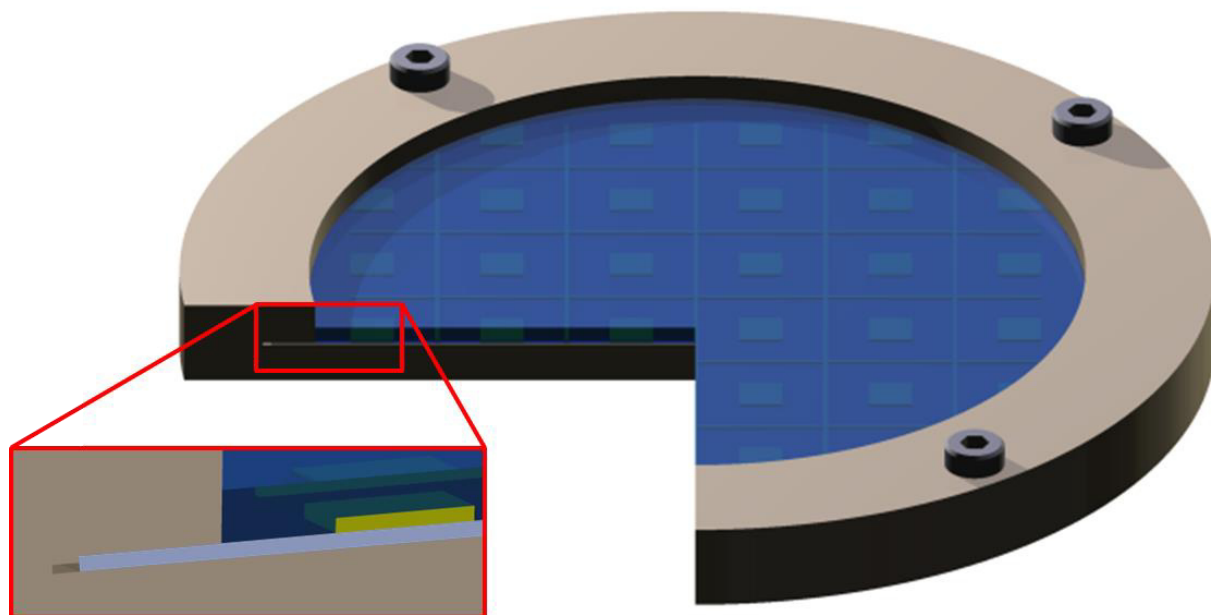


Figure 7.1.3

Features of the topographic structure introduced on PDMS gaskets, measured by profilometry (P16+ profilometer, LOT-Oriel). The mean roughness ($R_a = 225$ nm), and the maximum deflections ($P_{Peak} = +572$ nm, and $P_{Valley} = -942$ nm) were determined.

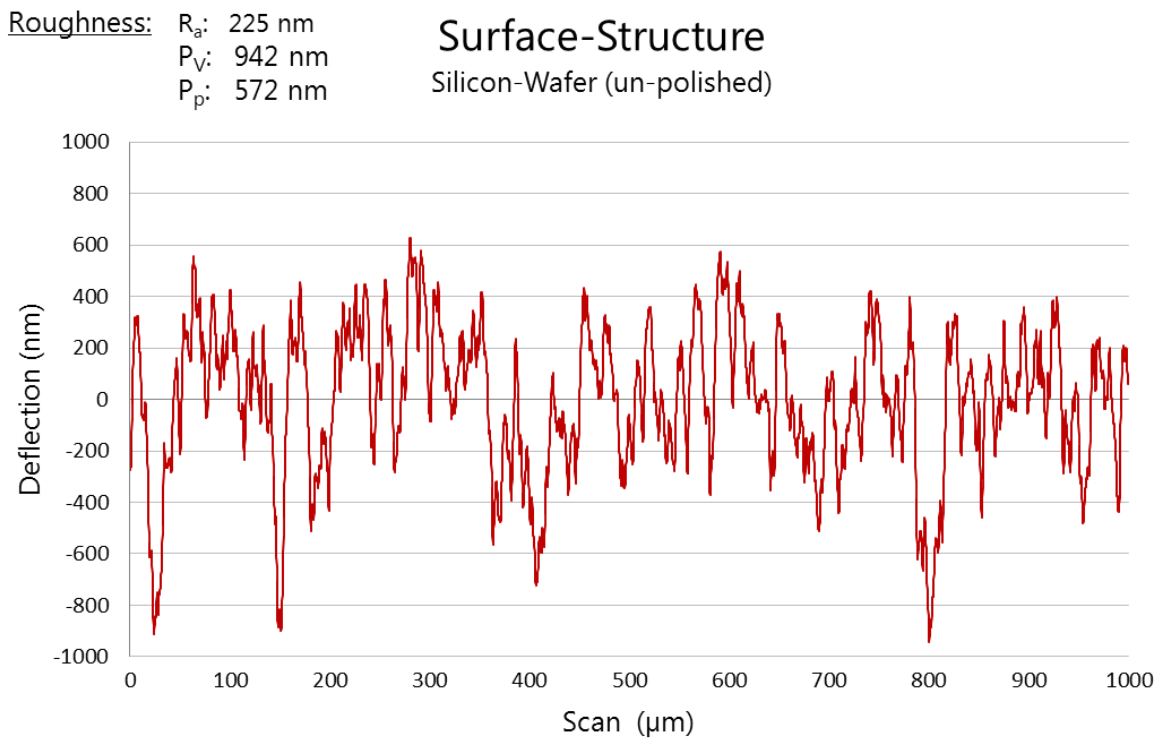


Figure 7.1.4

Kinetics of single β -galactosidase molecules in blocked and unblocked femtoliter reaction chambers: [1] The average kinetic response from individual enzymes isolated in reaction chambers without BSA/Tween 20 blocking was significantly lower than for blocked reaction chambers. This result confirms that surface passivation prior to experimentation is essential for single enzyme molecule measurements in femtoliter arrays. The diagram was reprinted from reference [1] with permission from ACS, © 2008.

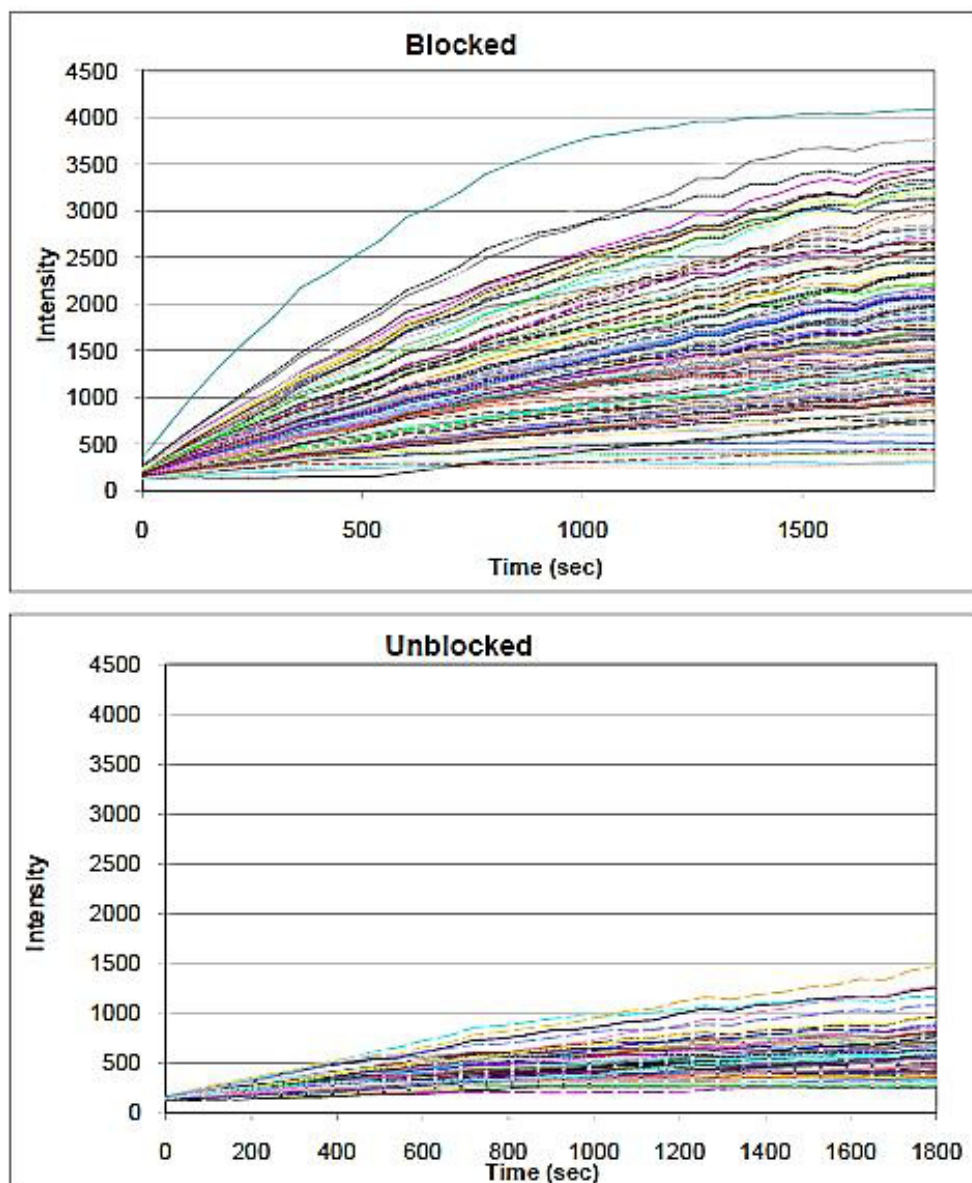


Figure 7.1.5

Schematic representation of the quaternary structure of β -galactosidase from *Escherichia coli*: Each monomer (A-D) of the homotetrameric enzyme unites five well-defined structural domains. The active site is formed primarily by the third, central domain, but also includes critical catalytic residues from other domains. Schematic representation reprinted with permission from [2], ©2012.

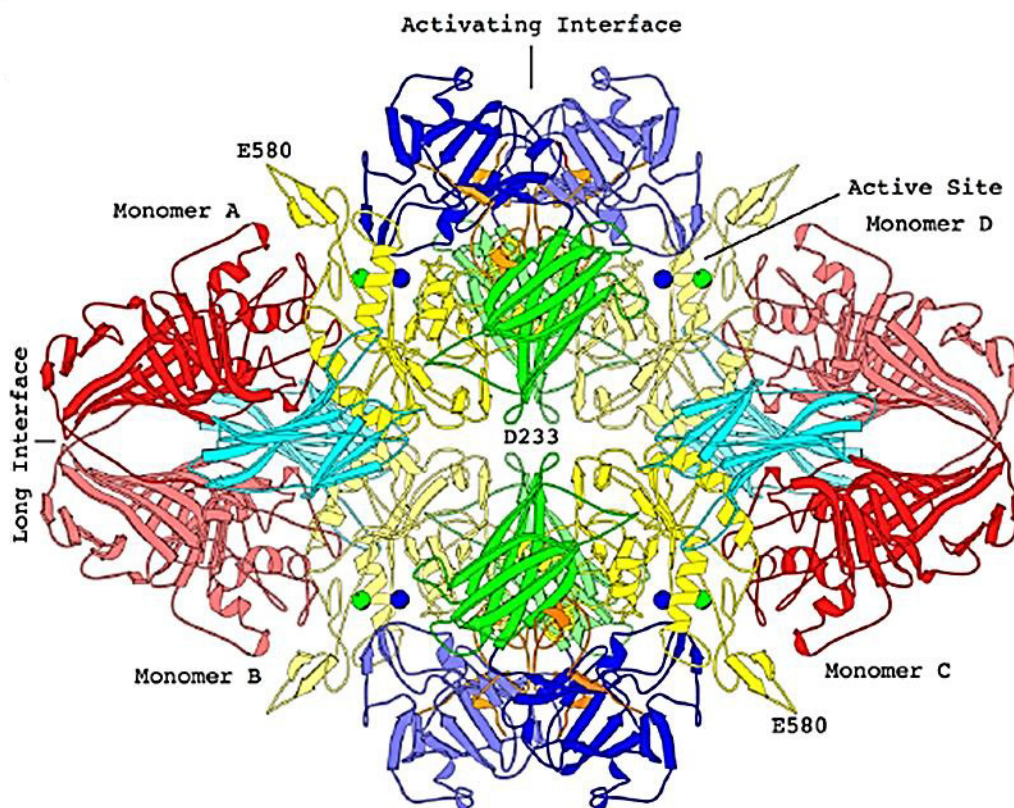


Figure 7.1.6

Calibrating the fluorescence intensity of resorufin standard solutions in fused silica (A) and PDMS femtoliter wells (B). A linear regression (black line) was applied to the data points (A) Mean and standard deviation of the fluorescence intensity in fused silica chambers: $y = 12.9 x$. (B) Mean and standard deviation of the fluorescence intensity in PDMS wells: $y = 14.3 x$.

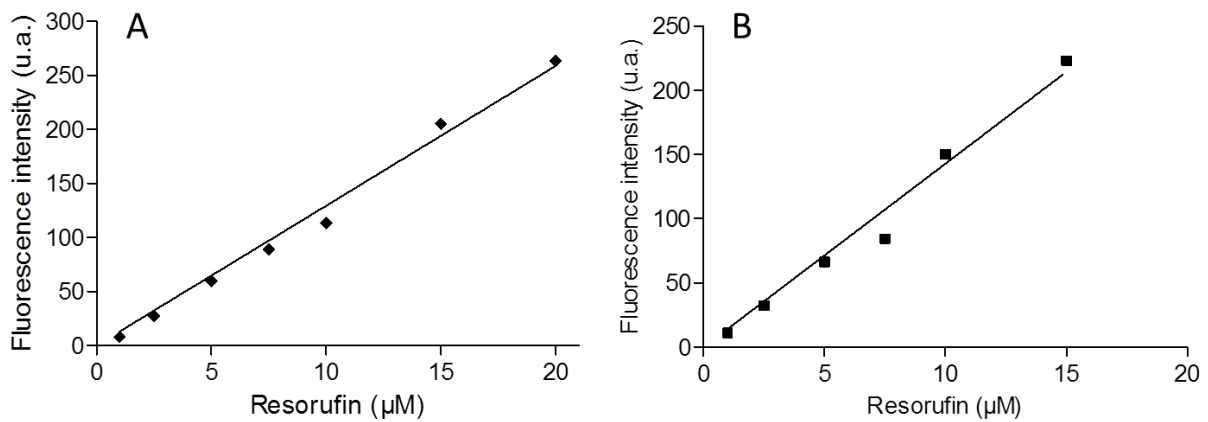
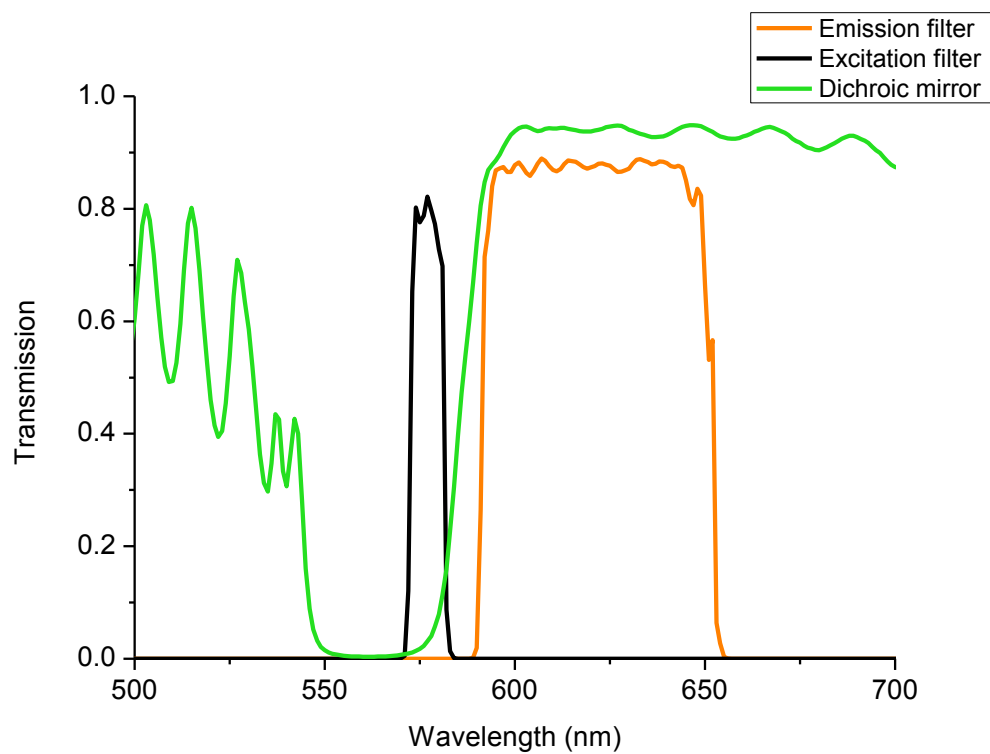


Figure 7.1.7

Filter spectra of the 41034 – Rhodamine X / Resorufin filter cube from Chroma Technology consisting of three interference filters: A HQ570/20x bandpass excitation filter (transmission spectrum in black), a Q585lp longpass dichroic mirror (transmission spectrum in green), separating excitation and emission light, and a HQ620/60m bandpass emission filter (emission spectrum in orange).



7.2. Single Molecule Perspective on Evolution

Figure 7.2.1

Matsumura and Ellington converted the native substrate specificity of wild-type GUS to β -galactosidase activity by *in vitro* evolution within a few steps of mutation and screening. [3] Figure 7.2.1 displays the activities of some of the partially evolved variants, identified by Matsumura and Ellington during the *in vitro* evolution process. Schematic representation reprinted from [3] with permission from Elsevier, © 2001.

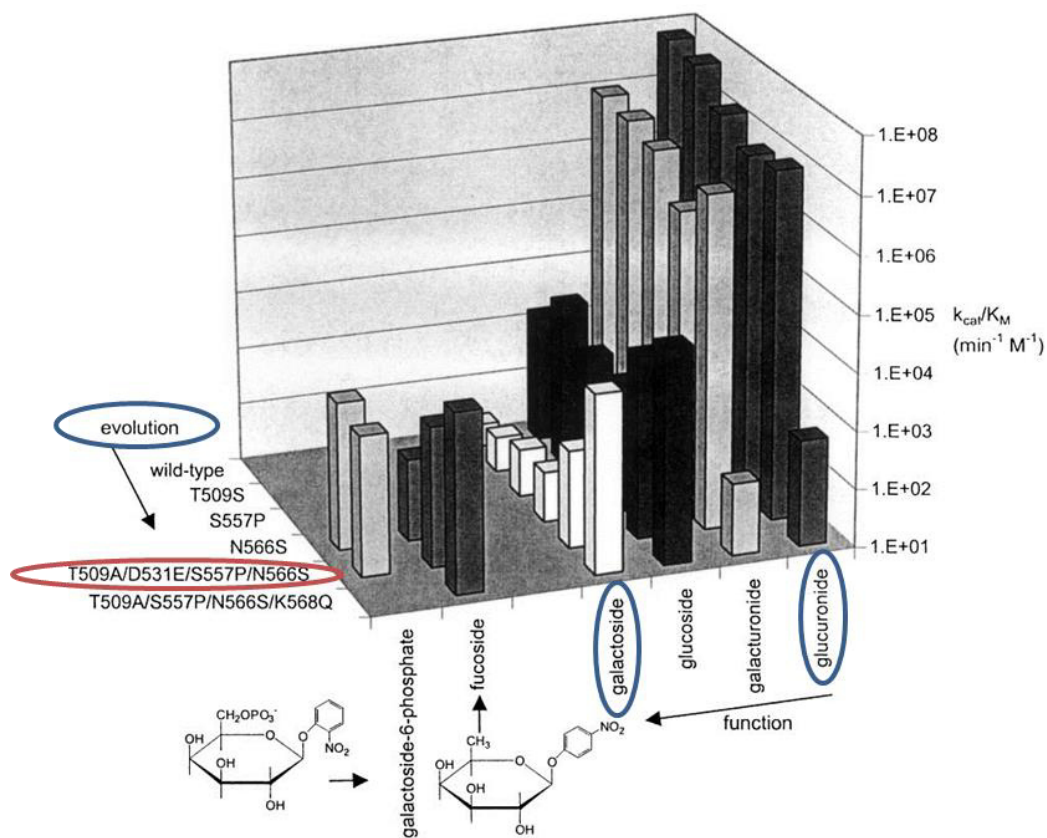


Figure 7.2.2

SDS-page analysis of enzyme purification: The expressed enzymes were purified by nickel chelate affinity chromatography, followed by size exclusion chromatography. Increasing amounts of the purified proteins (wild-type GUS: 3-12 μg , partially evolved GUS variant: 5-20 μg as determined by Bradford assay) were loaded onto the gel. The mass of the bands in each sample indicates the size of the monomer (68 kDa) in the tetrameric enzyme (273 kDa).

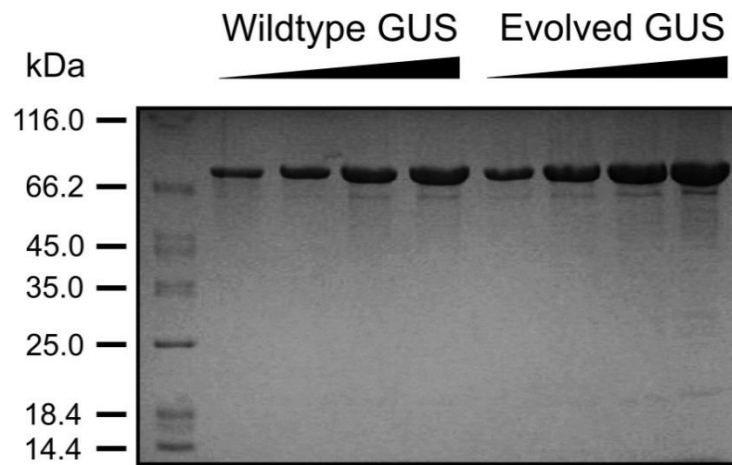


Table 7.2.1

The kinetic parameters of wildtype and evolved GUS were investigated in bulk solution with (a) the chromogenic substrate *para*-nitrophenyl glucuronide (*p*NP-G) (in (1) GUS buffer (50 mM sodium phosphate, pH 7.0, 5 mM β -mercaptoethanol, 1 mM EDTA) and (2) PBS buffer (2.7 mM KCl, 2 mM KH_2PO_4 , 137 mM NaCl, 10 mM Na_2HPO_4 , pH 7.4) respectively) and (b) the fluorogenic substrate resorufin β -D-glucuronide (ReG). The standard error of the non-linear regression to the Michaelis-Menten equation is shown for K_M and k_{cat} .

GUS	Substrate	Buffer	K_M (μM)	k_{cat} (s^{-1})	k_{cat}/K_M ($\text{s}^{-1}\text{M}^{-1}$)
Wildtype GUS	<i>p</i> NP-G	GUS	117 ± 14	104 ± 2.2	8.9×10^5
	<i>p</i> NP-G	PBS	163 ± 24	93 ± 3.5	5.7×10^5
	ReG	PBS			1.6×10^6
T509A/D531E/S557P/N566S	<i>p</i> NP-G	GUS	629 ± 80	52 ± 1.8	8.3×10^4
	<i>p</i> NP-G	PBS	1260 ± 214	50 ± 3.5	4.0×10^4
	ReG	PBS			9.3×10^4

The kinetic parameters of wild-type and evolved GUS were determined by Max Renner in the context of a research project at the group of Prof. Reinhard Sterner, institute for biophysics and physical biochemistry, University of Regensburg.

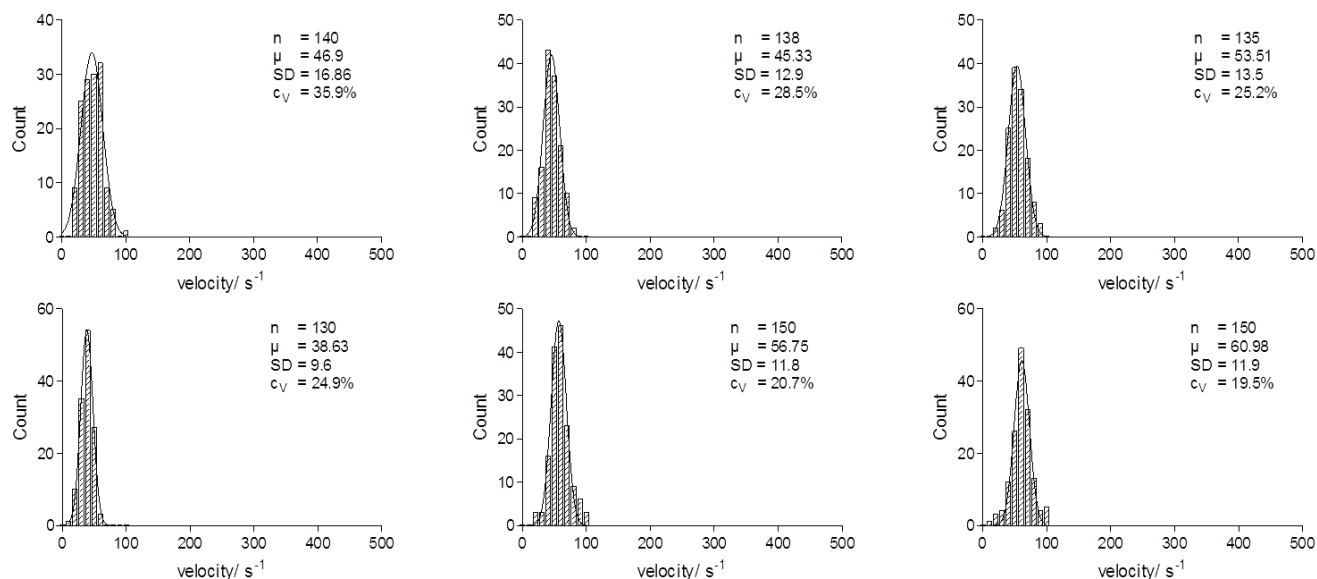
Video 7.2.1

The catalytic hydrolysis of ReG to highly fluorescent resorufin was monitored simultaneously in more than 100 wells that contained a single GUS molecule by wide-field fluorescence microscopy. The Video on the supplementary CD depicts a small section of the array and demonstrates the signal increase in individual wells over 300 seconds.

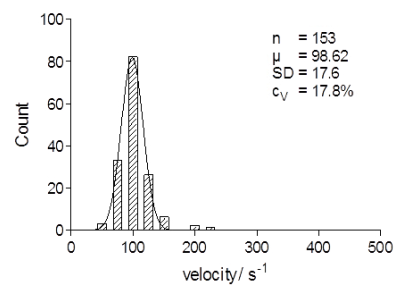
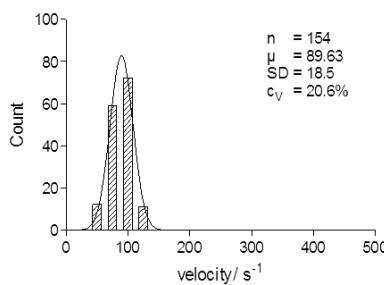
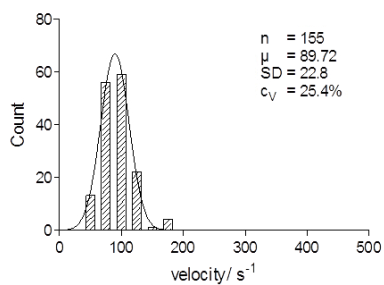
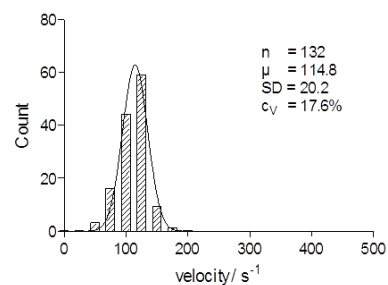
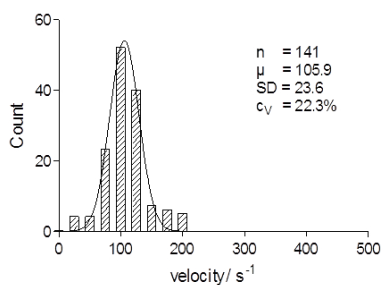
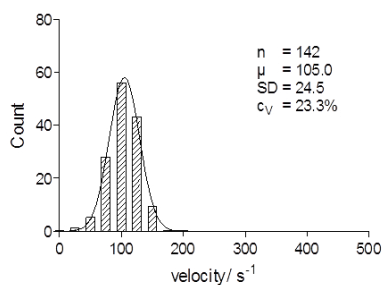
Figure 7.2.3

The substrate turnover rates of several hundred single wild-type GUS molecules, monitored at different ReG concentrations, are assembled as histograms. Each histogram displays one out of six independent measurements per substrate concentration, recorded over a time course of 5 minutes.

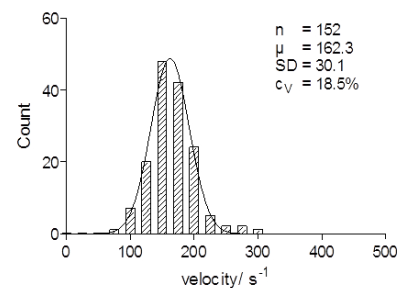
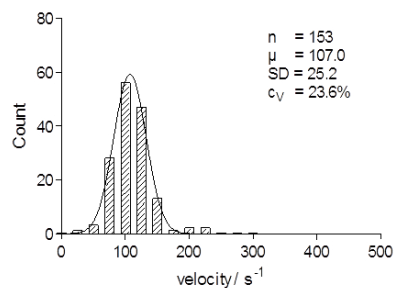
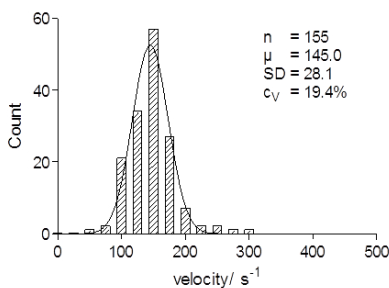
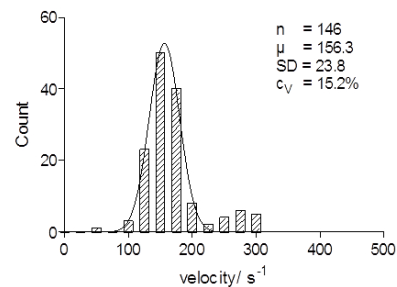
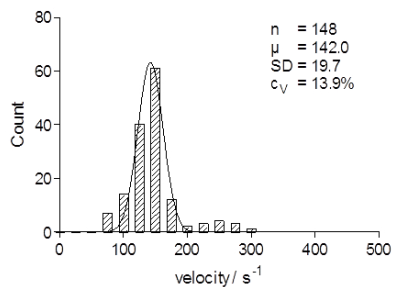
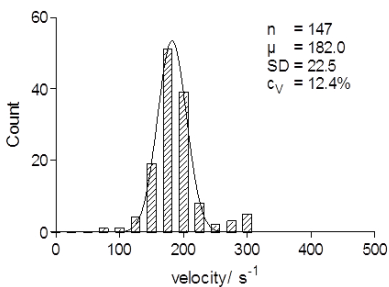
(1) At 12.5 μM ReG:



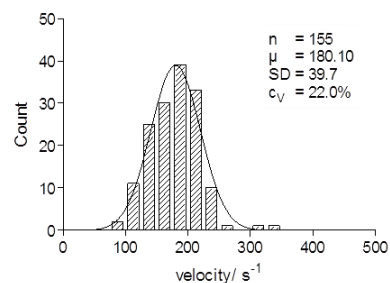
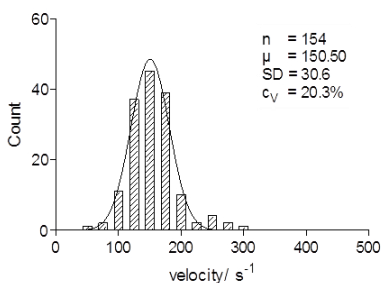
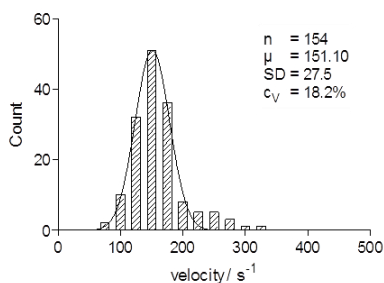
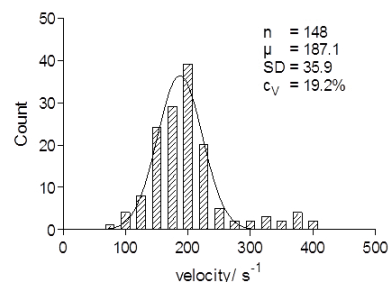
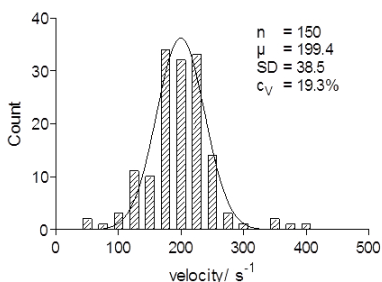
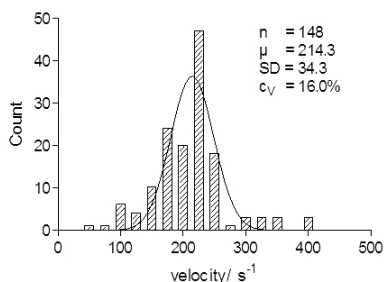
(2) At 25 μM ReG:



(3) At 50 μM ReG:



(4) At 100 μM ReG:



(5) At 150 μM ReG:

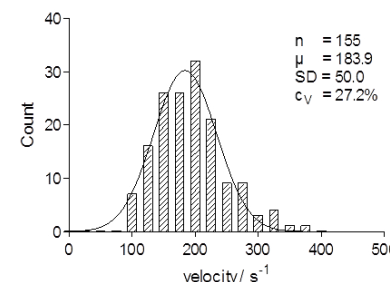
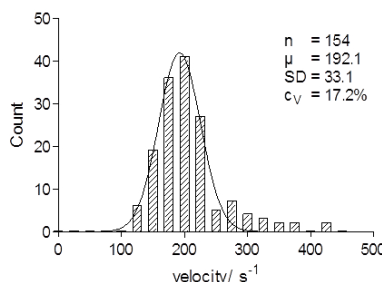
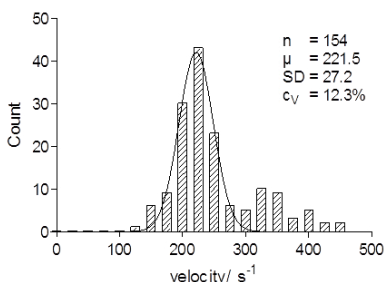
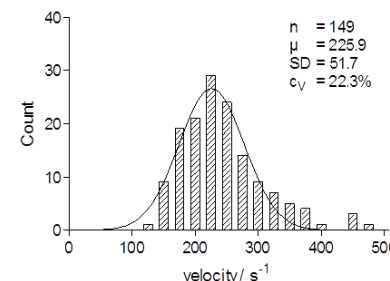
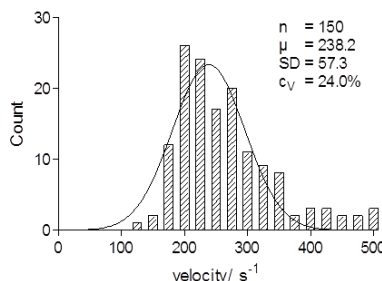
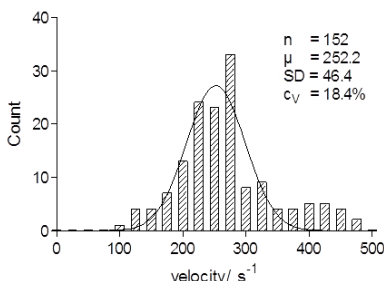


Table 7.2.2

Survey of the substrate turnover rates of several hundred single wild-type GUS molecules, monitored at different ReG concentrations in six independent measurements in fused silica femtoliter arrays;

	Mean Velocity \pm SD		Coefficient of Variation	
Wildtype	252.2 \pm 46.4	221.5 \pm 27.2	18.4 %	12.3 %
150 μ M	238.2 \pm 57.3	192.1 \pm 33.1	24.0 %	17.2 %
# (1-6)	225.9 \pm 51.7	183.9 \pm 50.0	22.3 %	27.2 %
	219.0 \pm 44.3		20.2 %	
Wildtype	214.3 \pm 34.3	151.1 \pm 27.5	16.0 %	18.2 %
100 μ M	199.4 \pm 38.5	150.5 \pm 30.6	19.3 %	20.3 %
# (1-6)	187.1 \pm 35.9	180.1 \pm 39.7	19.2 %	22.0 %
	180.4 \pm 34.4		19.2 %	
Wildtype	182.0 \pm 22.5	145.0 \pm 28.1	12.4 %	19.4 %
50 μ M	142.0 \pm 19.7	107.0 \pm 25.2	13.9 %	23.6 %
# (1-6)	156.3 \pm 23.8	162.3 \pm 30.1	15.2 %	18.5 %
	149.1 \pm 24.9		17.2 %	
Wildtype	105.0 \pm 24.5	89.7 \pm 22.8	23.3 %	25.4 %
25 μ M	105.9 \pm 23.6	89.6 \pm 18.5	22.3 %	20.6 %
# (1-6)	114.8 \pm 20.2	98.6 \pm 17.6	17.6 %	17.8 %
	100.6 \pm 21.2		21.2 %	
Wildtype	46.9 \pm 16.9	38.6 \pm 9.6	35.9 %	24.9 %
12.5 μ M	45.3 \pm 12.9	56.8 \pm 11.8	28.5 %	20.7 %
# (1-6)	53.5 \pm 13.5	61.0 \pm 11.9	25.2 %	19.5 %
	50.4 \pm 12.8		25.6 %	

Figure 7.2.4

At a 100 μM substrate concentration, the mean activity of the partially evolved variant is about five times lower than the average wild-type GUS activity. The low activity of the generalist results in relatively weak fluorescence intensities retrieved from individual femtoliter chambers, which may increase the background noise. To account for the noise in the fluorescence measurements, the activity distribution of the partially evolved variant was not only compared to wild-type GUS analyzed at 100 μM ReG, but also at 12.5 μM ReG. Under these conditions, wild-type GUS shows a similarly weak fluorescence increase as wild-type GUS and a slightly broader activity distribution (CV = 26 %) compared to higher substrate concentrations (CV \approx 20 %). The generalist, however, displays the broadest activity distribution (CV = 34 %) compared to wild-type GUS irrespective of the substrate concentration (Figure 9.2.4 A). The coefficients of variation (CV = μ/σ), calculated from six independent single molecule experiments, of both wild-type and partially evolved GUS, were compared using a t-test to determine the significance (Figure 9.2.4 B). The difference in the activity distribution between wild-type GUS and generalist was significant (WT at 100 μM ReG: $p \leq 0.0001$; WT at 12.5 μM ReG: $p \leq 0.02$).

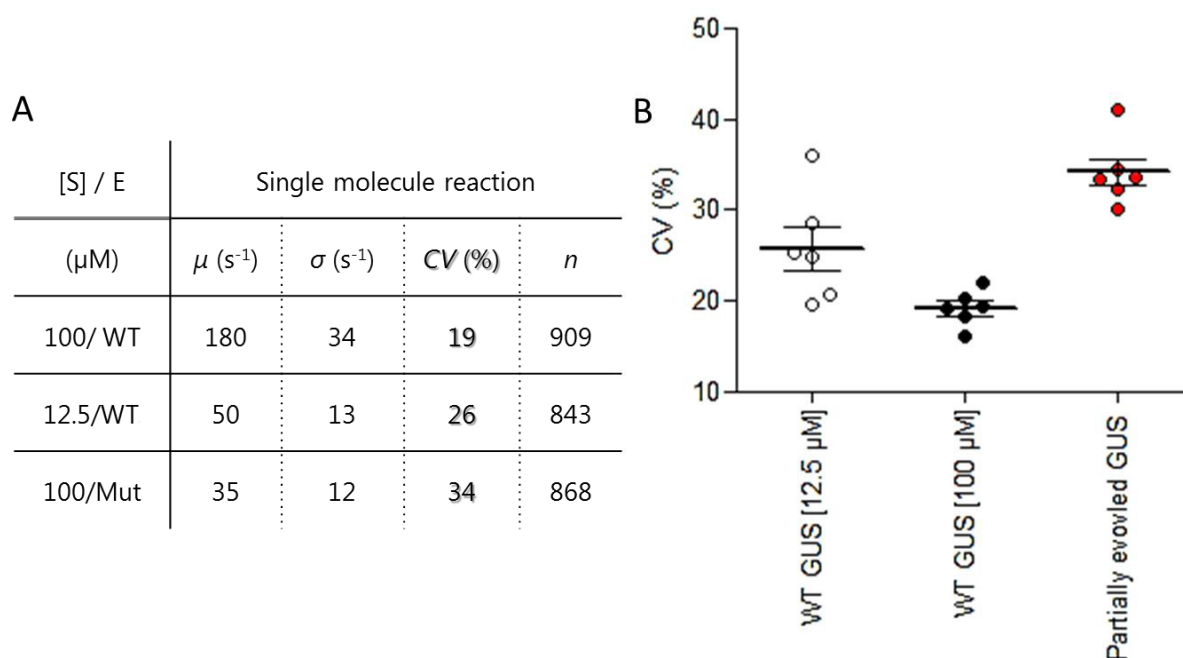
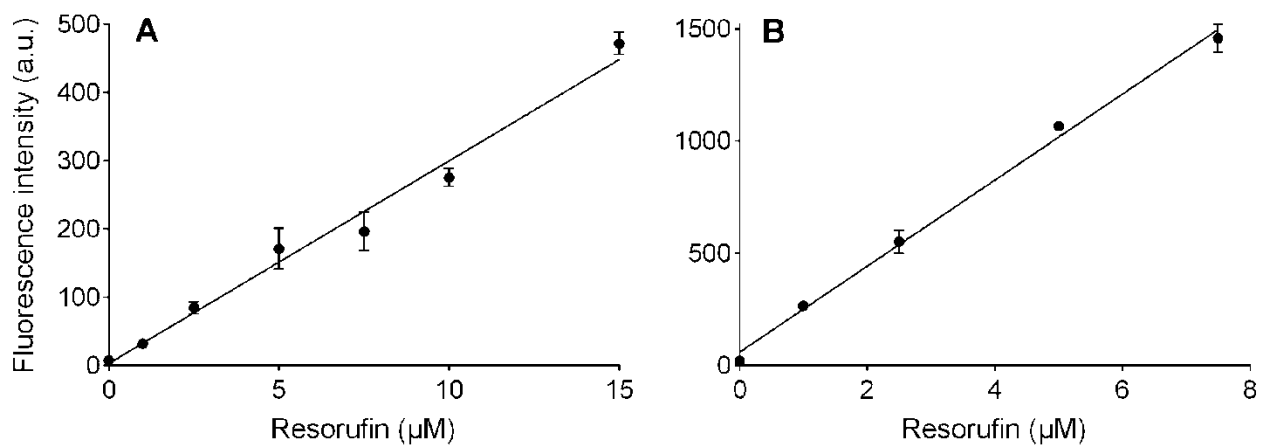


Figure 7.2.5

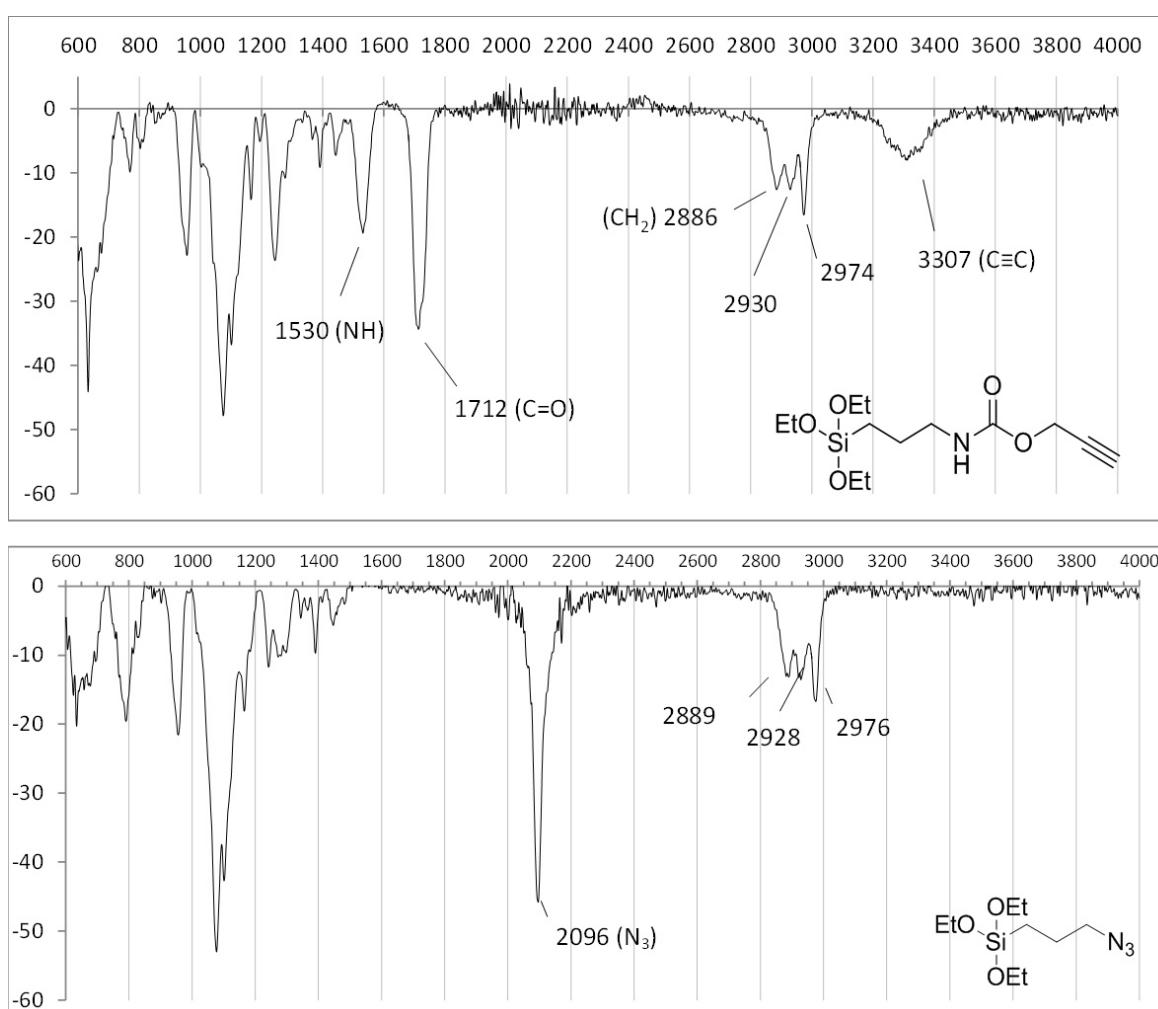
Calibration curve of the fluorescence intensity of resorufin standard solutions in femtoliter chambers (A) and in microtiter plate wells (B). A linear regression (black line) was applied to the data points (A) (mean and standard deviation of the fluorescence intensity in ten femtoliter chambers): $y = 29.7x + 3$ and (B) (mean and standard deviation of the fluorescence intensity in three wells): $y = 192x + 59$.



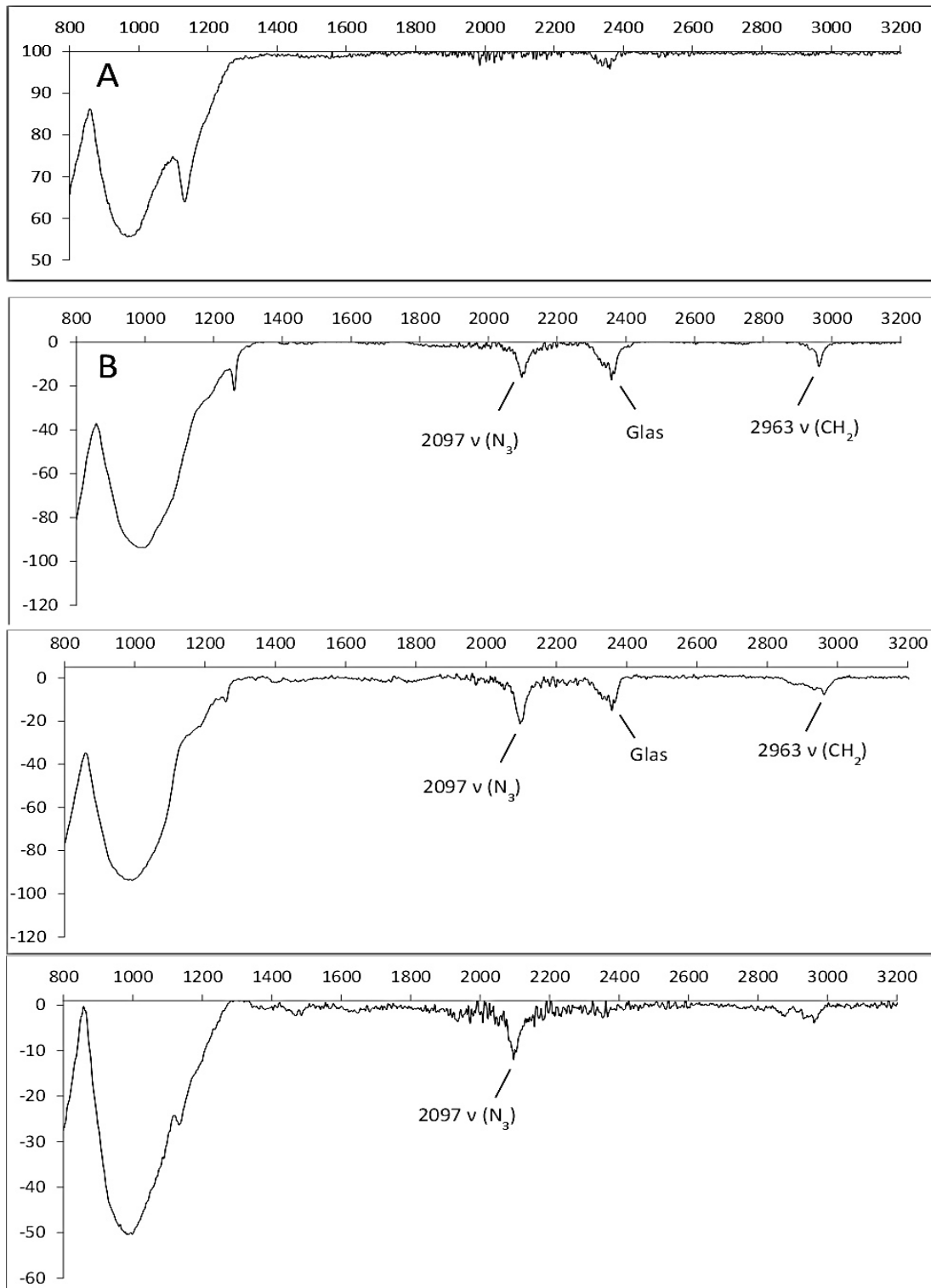
7.3 Femtoliter Arrays for Concentration Analysis

Figure 7.3.1

(a) IR-spectra of the clickable silanes 1 ((3-Azidopropyl)diethoxy(hydroxyl) silane) and 2 (O-(Propargyloxy)-N-(triethoxysilylpropyl)urethane) applied for the functionalization of the fused silica surface of the femtoliter wells to make them applicable for click chemistry.



(b) IR-spectra of (A) the unmodified fused silica slide and (B) three slides modified with the clickable silane (1).



(c) IR-spectra of (A) the unmodified fused silica slide and (B) three slides modified with the clickable silane (2).

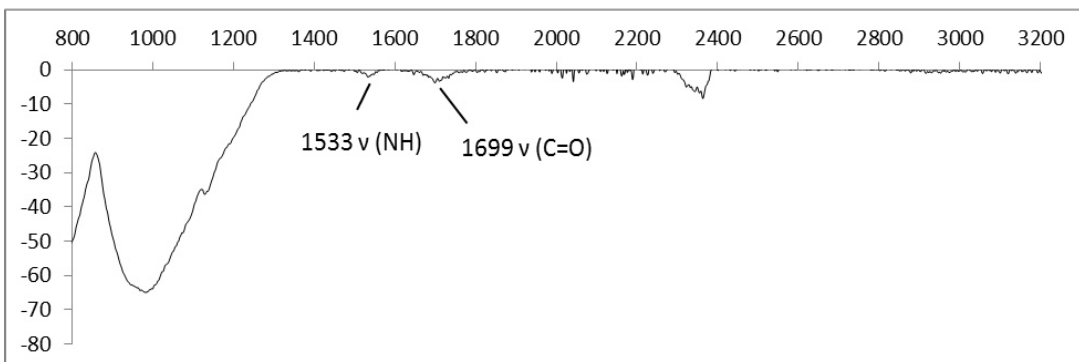
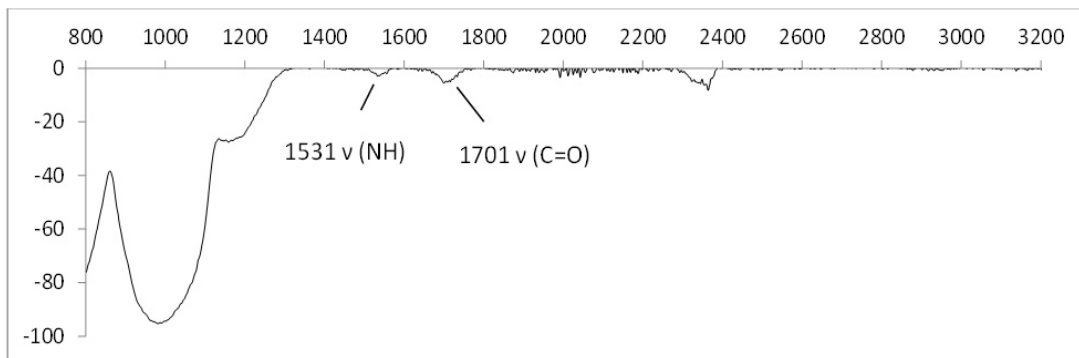
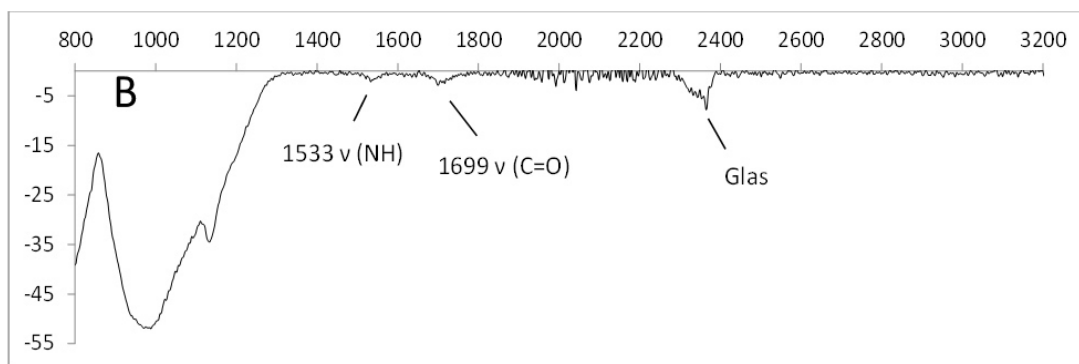
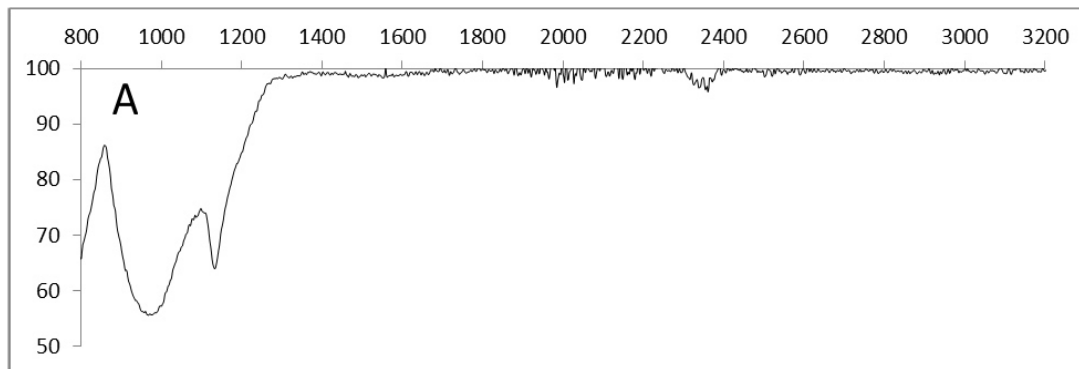
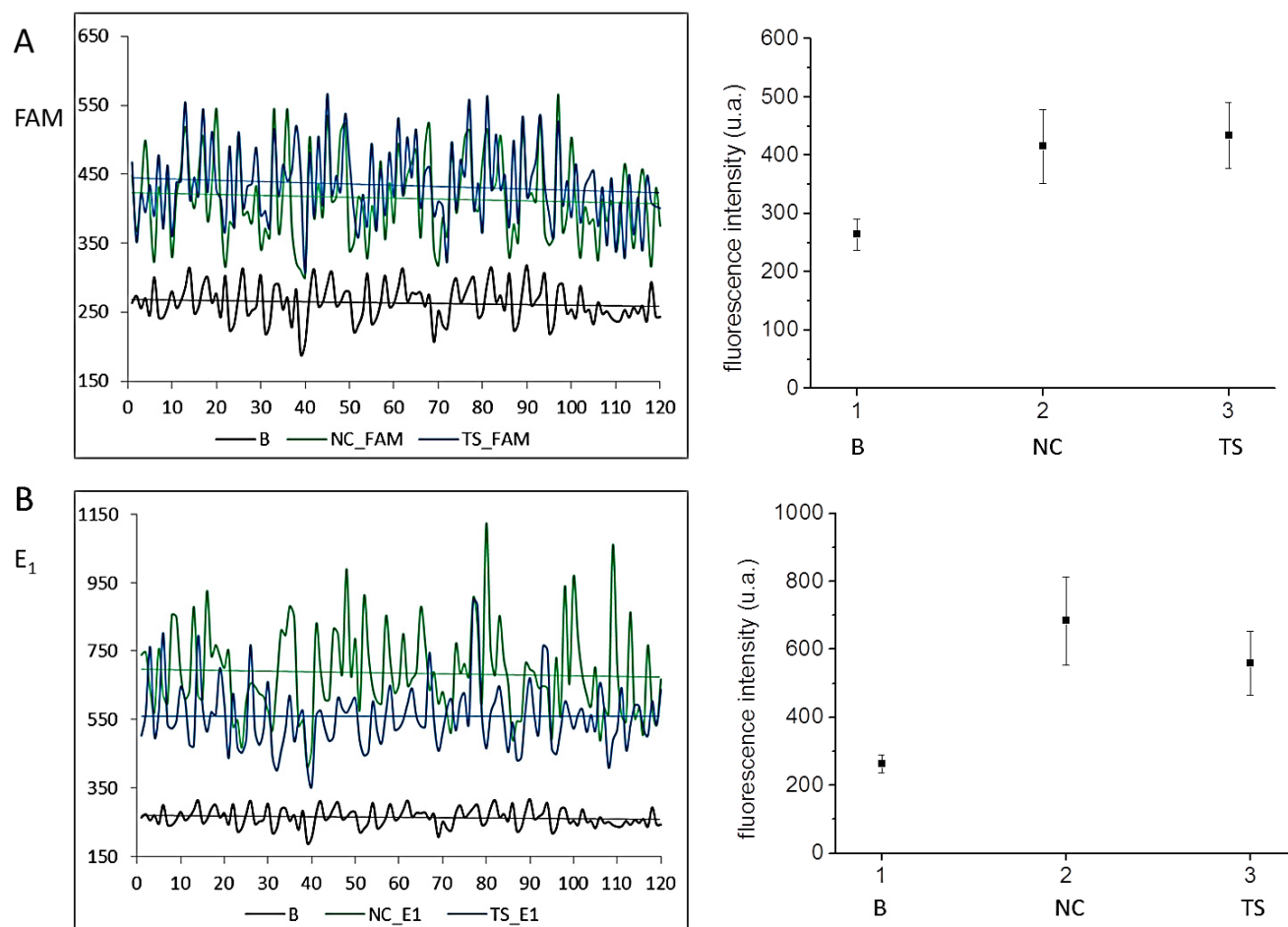


Figure 7.3.2

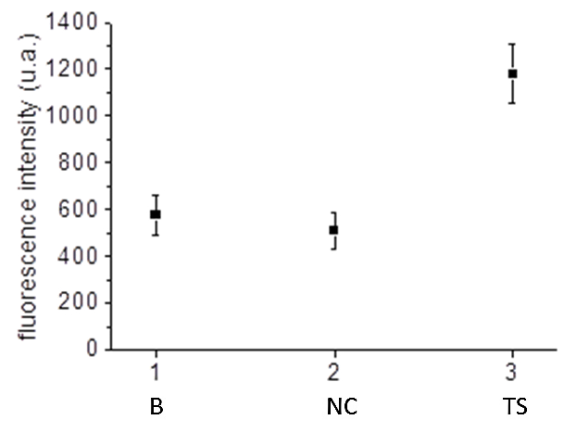
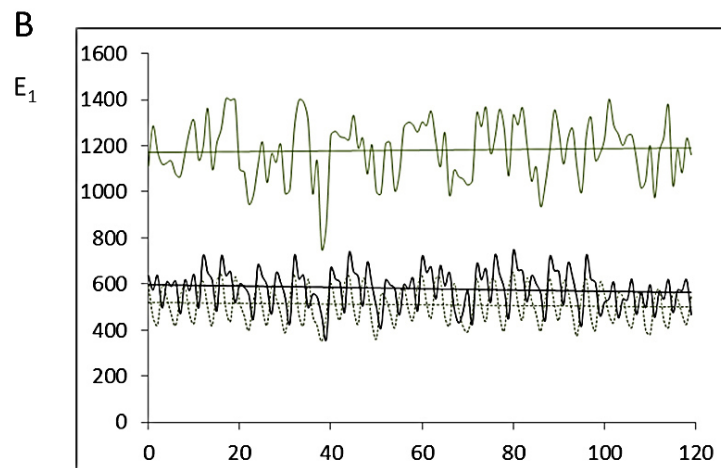
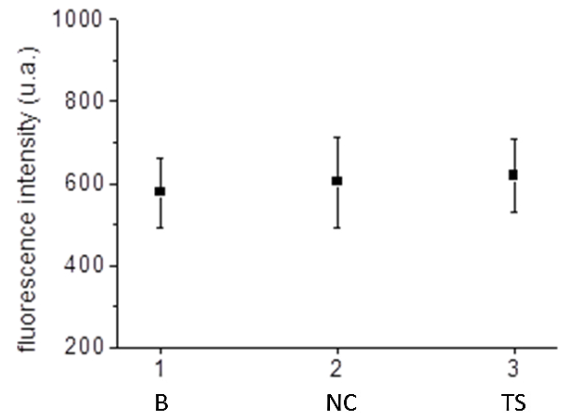
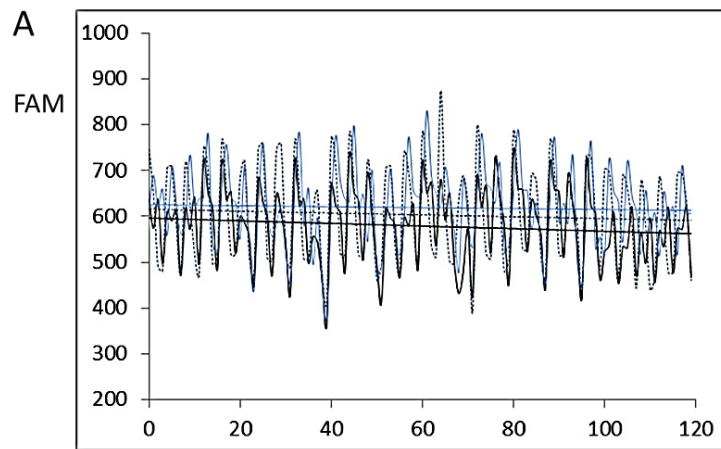
Fluorescence intensity spectra of fused silica femtoliter arrays with (A) alkyne- or (B) azido-modified surfaces that were functionalized with the clickable fluorescent dyes (3) and (4) according to method (B): in acetone at room temperature. For measurement evaluation 120 random regions of interest (ROI) were picked of the B, NC and TS, their fluorescence signal recorded (left) and averaged (right).

Slides functionalized with method (B) did yield greatly differing results:

Measurement (1)



Measurement (2)



Measurement (3)

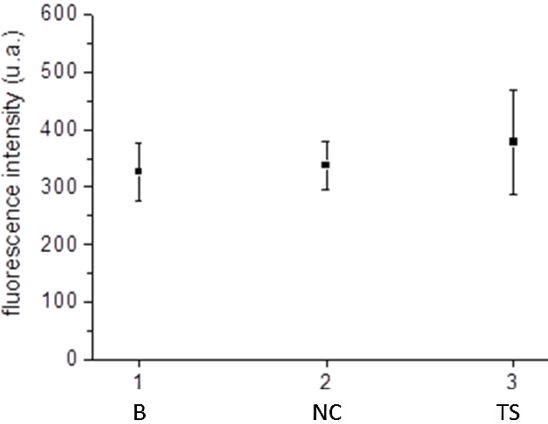
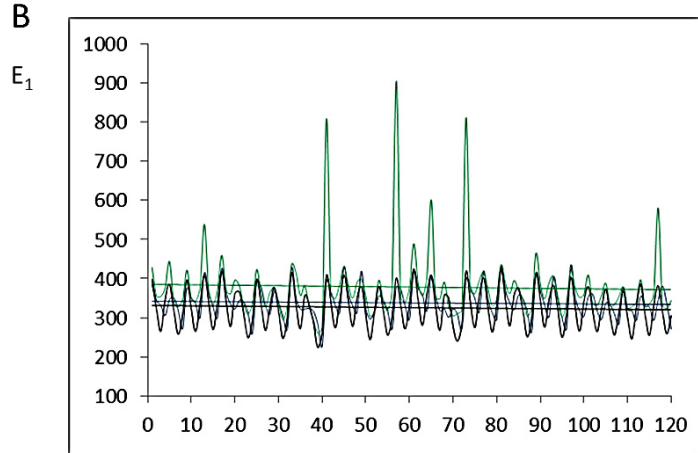
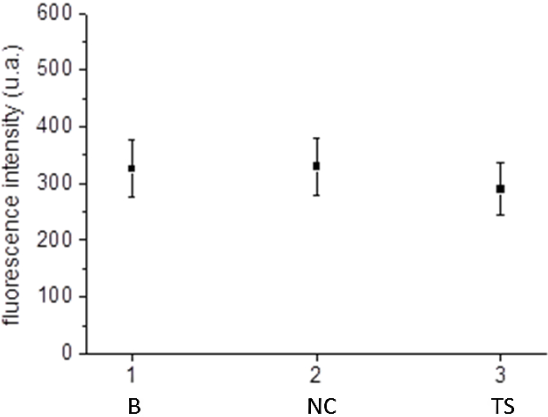
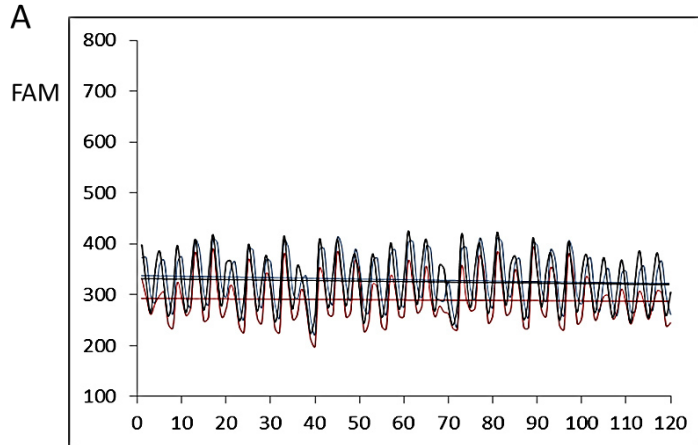
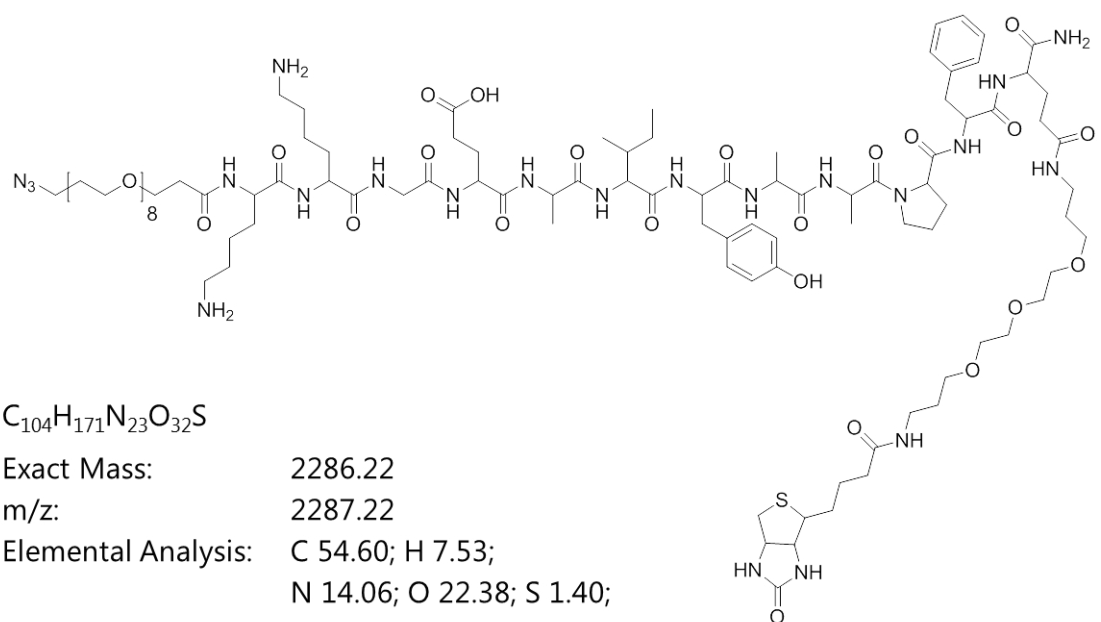
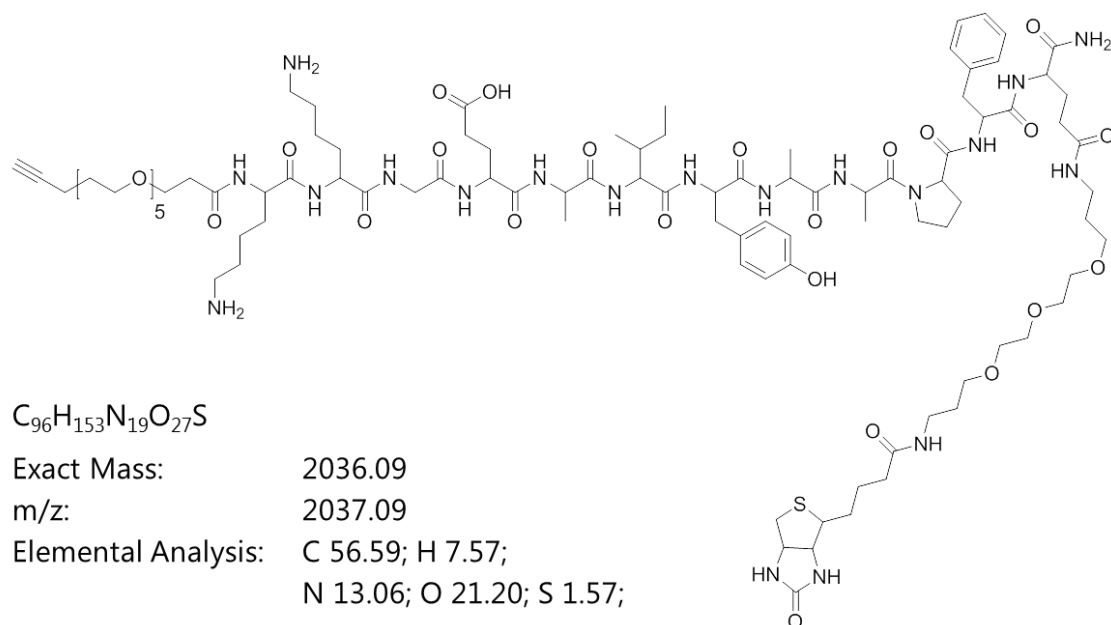


Figure 7.3.3

Chemical structure of the clickable peptides applied in this thesis.

(1) Peptides with biotin-label:



(2) Peptides without biotin-label:

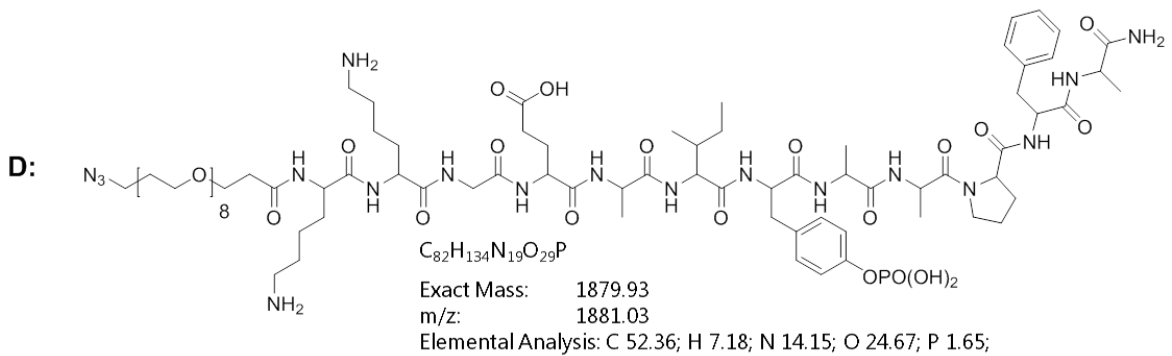
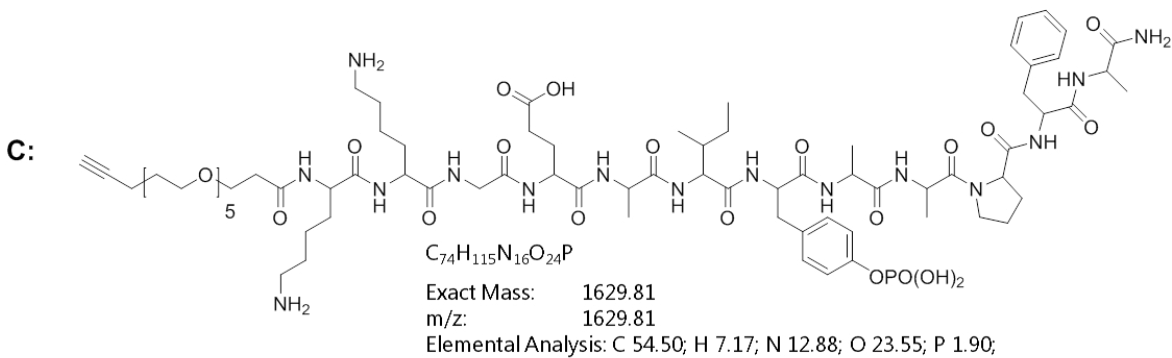
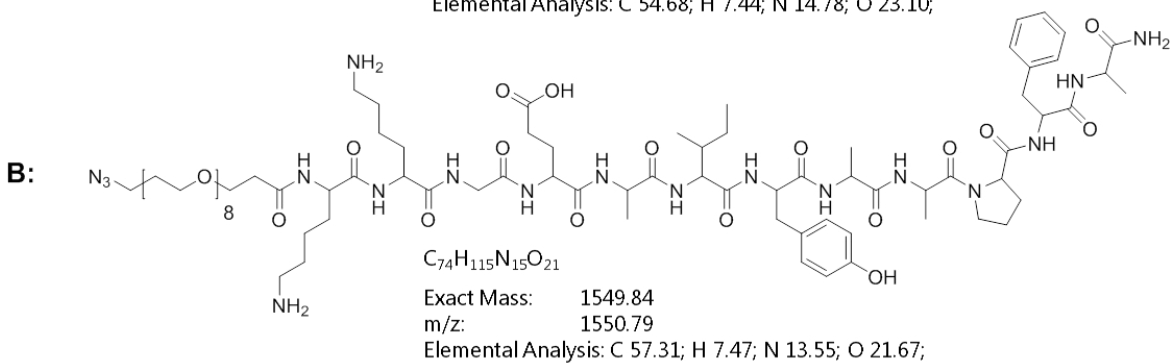
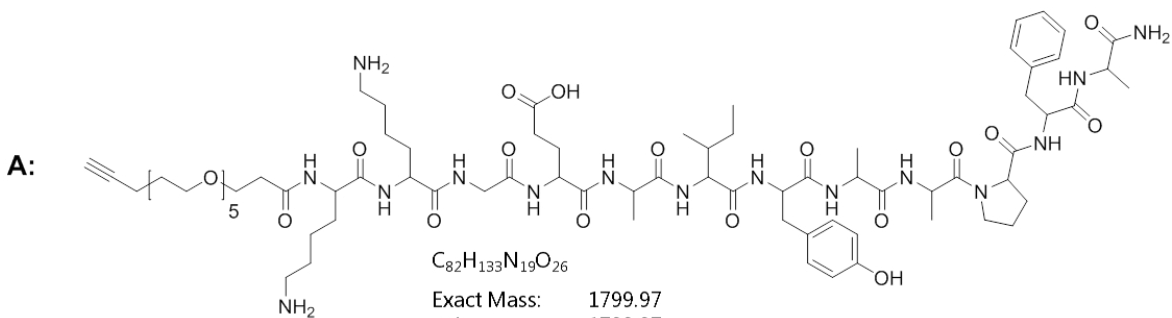
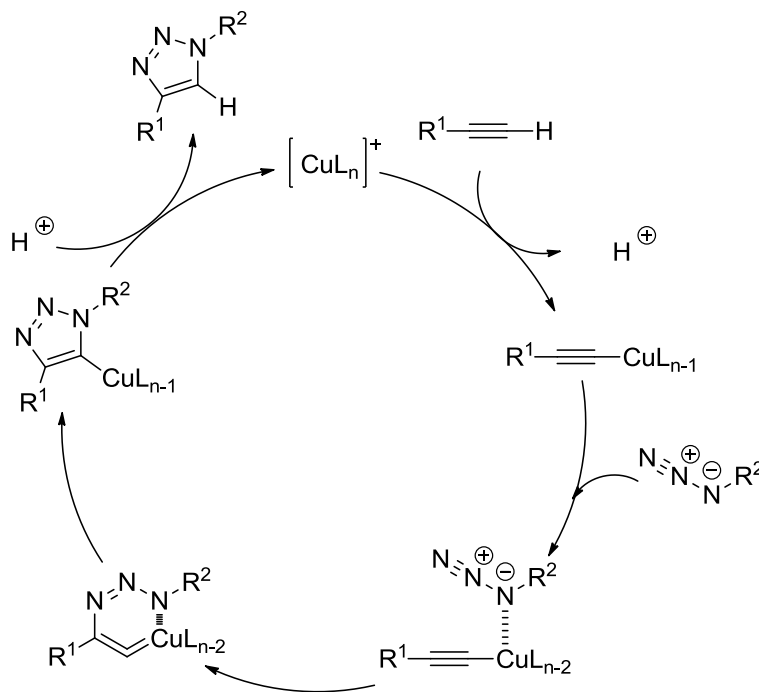
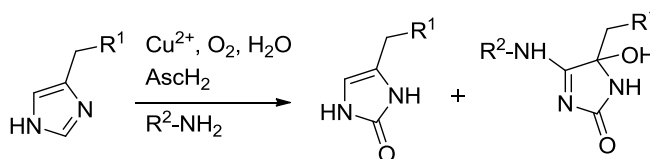
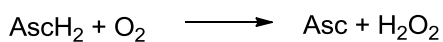
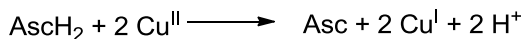


Figure 7.3.4

(A) Proposed catalytic cycle for the Cu(I) catalyzed [2+3]-cycloaddition, where L stands for a random ligand. [4, 5]



(B) Application of Cu(II) in combination with sodium ascorbate for the catalysis of bioconjugation reactions may entail negative side-effects such as the generation of hydrogen peroxide via a superoxide radical or other reactive oxygen species that lead to the oxidation and/or cleavage of biomolecules.



(C) Dehydroascorbate and other ascorbate byproducts can covalently modify amino acid side-chains resulting in adduct formation, crosslinking and protein precipitation [6]

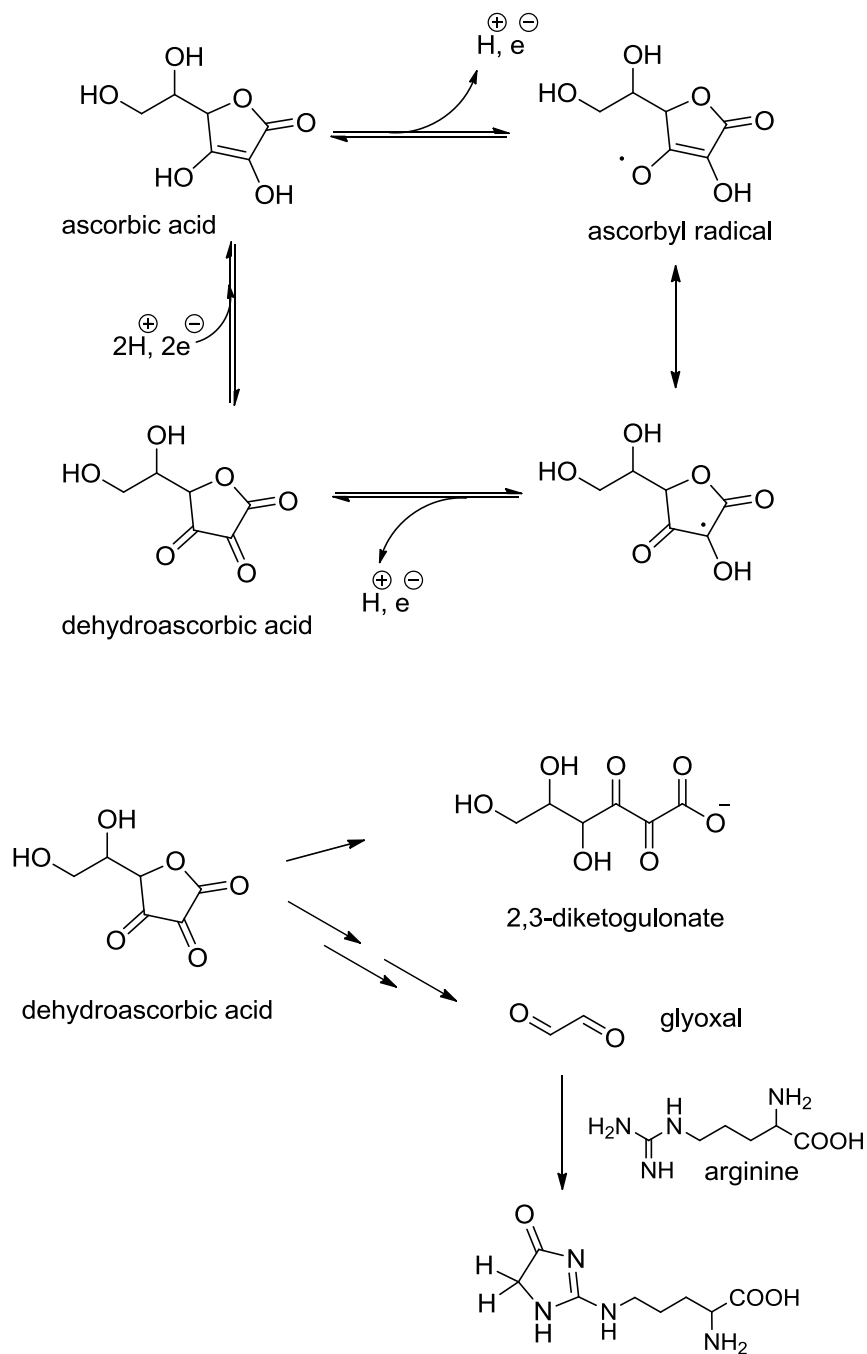


Figure 7.3.5

ESI-MS spectra of (A) native HRP and (B) azido-HRP. The increase in molecular weight between HRP (43175 Da) and N₃-HRP (43279 Da) equates to the conversion of an average of four amine-groups to azide-groups per HRP molecule.

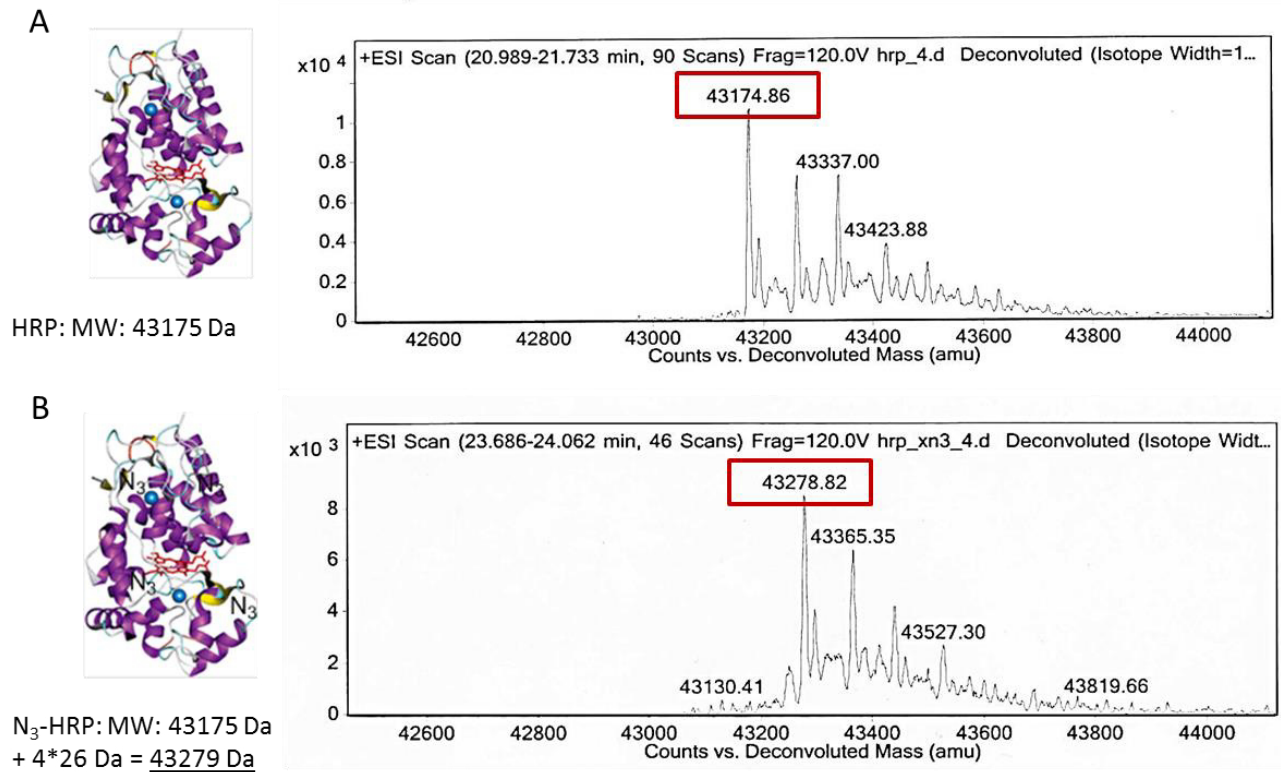
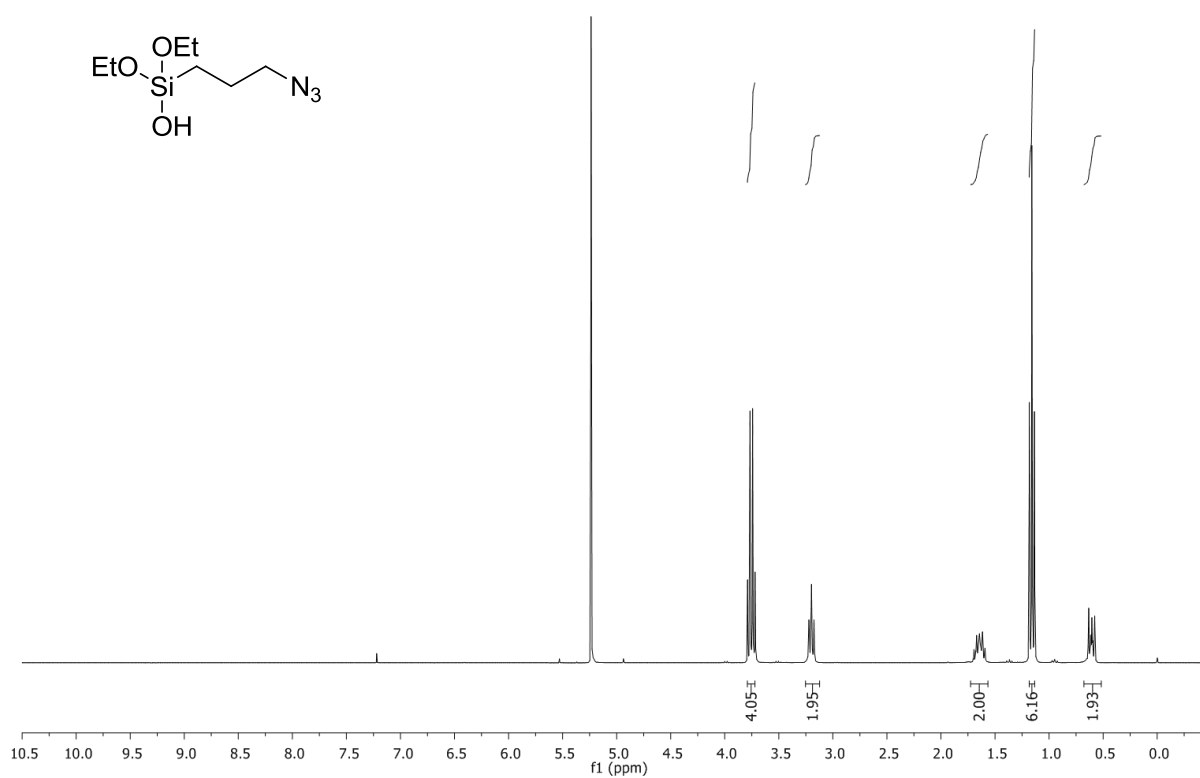


Figure 7.3.6

NMR-spectra of:

(a) 3-(Azidopropyl)diethoxy(hydroxyl)silane (clickable silane 1)

$^1\text{H-NMR}$ (300 MHz, CDCl_3): δ : 3.75 (q, $J = 7.0$ Hz, 4H), 3.20 (t, $J = 7.0$ Hz, 2H), 1.71 – 1.58 (m, 2H), 1.16 (t, $J = 7.0$ Hz, 6H), 0.66 – 0.54 (m, 2H).



(b) Clickable dye E₁ (3)

¹H-NMR (CDCl₃): δ = 8.65 (dd, 1H, J₁ = 1.0 Hz, J₂ = 7.3 Hz), 8.46 (d, 1H, J = 8.2 Hz), 8.13 (dd, 1H, J₁ = 1.0 Hz, J₂ = 8.4 Hz), 7.68 (dd, 1H, J₁ = 7.4 Hz, J₂ = 8.4 Hz), 6.90 (d, 1H, J = 8.2 Hz), 4.95 (d, 2H, J = 2.5 Hz), 2.17 (t, 1H, J = 2.5 Hz)

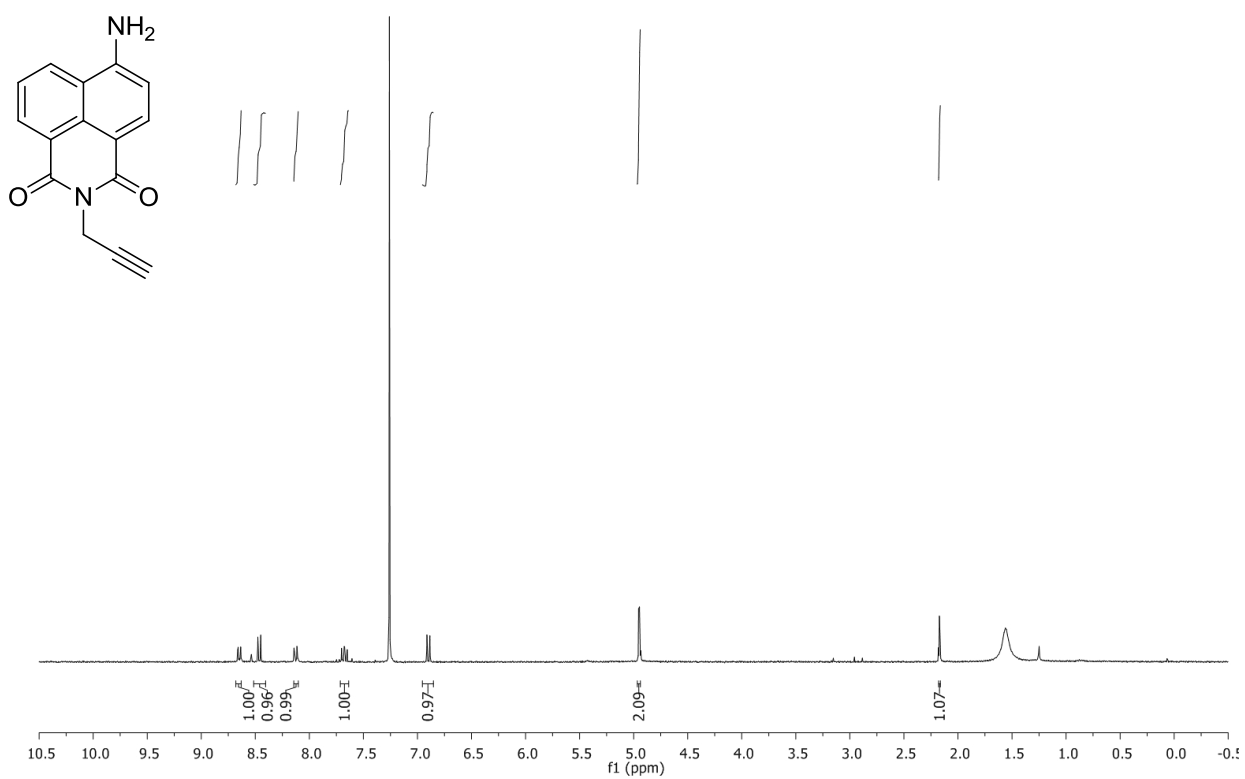
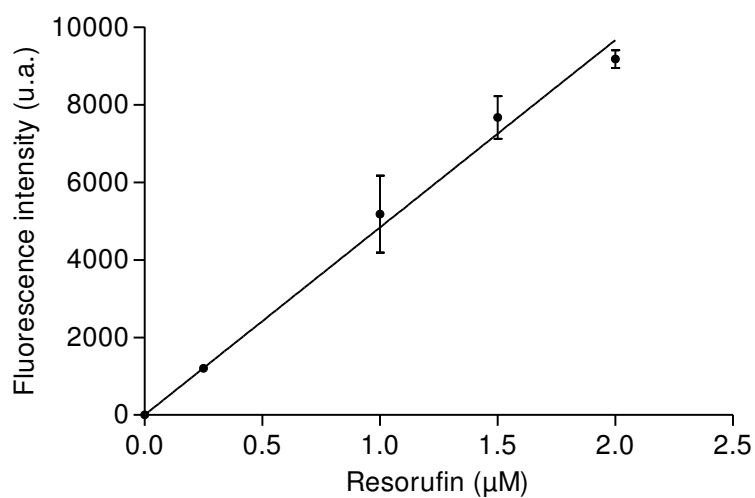


Figure 7.3.7

HRP substrate turnover rates were calibrated by comparison with the fluorescence intensities of resorufin standard solutions.

Calibration curve for the fluorescence intensity of resorufin standard solutions in microtiter plate wells: A linear regression was applied to the data points (mean and standard deviation of the fluorescence intensity in three MTP wells): $y = 4832$ (black line).



7.4 References

1. Rissin, D.M., H.H. Gorris, and D.R. Walt, *Distinct and long-lived activity states of single enzyme molecules*. J. Am. Chem. Soc., **2008** (130): 5349.
2. Juers, D.H., B.W. Matthews, and R.E. Huber, *LacZ beta-galactosidase: structure and function of an enzyme of historical and molecular biological importance*. Protein Sci., **2012** (21): 1792.
3. Matsumura, I. and A.D. Ellington, *In vitro evolution of beta-glucuronidase into a beta-galactosidase proceeds through non-specific intermediates*. J. Mol. Biol., **2001** (305): 331.
4. Rostovtsev, V.V., L.G. Green, V.V. Fokin, and K.B. Sharpless, *A stepwise Huisgen cycloaddition process: Copper(I)-catalyzed regioselective "ligation" of azides and terminal alkynes*. Angew. Chem. Int. Ed., **2002** (41): 2596.
5. Himo, F., T. Lovell, R. Hilgraf, V.V. Rostovtsev, L. Noodleman, K.B. Sharpless, and V.V. Fokin, *Copper(I)-catalyzed synthesis of azoles. DFT study predicts unprecedented reactivity and intermediates*. J. Am. Chem. Soc., **2005** (127): 210.
6. Liu, P.Y., N. Jiang, J. Zhang, X. Wei, H.H. Lin, and X.Q. Yu, *The oxidative damage of plasmid DNA by ascorbic acid derivatives in vitro: the first research on the relationship between the structure of ascorbic acid and the oxidative damage of plasmid DNA*. Chem. Biodiversity, **2006** (3): 958.

7.5 Lab Course on Single Enzyme Analysis in PDMS Femtoliter Arrays

Femtoliter Arrays for Single Molecule Analysis and Digital Concentration Readout

1. Introduction

The development of new technologies for the analysis of single enzyme molecules has considerably increased our understanding of biochemical processes, as the observation of single enzyme molecules uncovers subpopulations and kinetic details that remain hidden in traditional ensemble experiments. For example, single enzyme molecules exhibit a broad distribution of individual activities due to different protein conformations, which is known as static heterogeneity. A large number of single enzyme molecules are required to investigate the static heterogeneity within an enzyme population. However, most single molecule techniques only enable the investigation of a single or few molecules at a time.

In contrast, so-called femtoliter arrays consist of tens of thousands reaction chambers each defining a volume of approximately $50 \mu\text{m}^3$ (fL) (equals the size of a yeast cell). Femtoliter arrays are suitable for isolating and analysing hundreds of individual enzyme molecules simultaneously. A highly diluted enzyme solution together with a large excess of a fluorogenic substrate is enclosed in the femtoliter cavities. In chambers containing a single enzyme molecule, the activity is determined by the enzymatic turnover of the substrate into a fluorescent product. The resulting fluorescence increase is monitored using a fluorescence microscope equipped with a sensitive camera.

In addition to basic research, the detection of single molecules by means of the enzymatic turnover of a fluorogenic substrate can also be used in bioanalysis. In this case, the focus is not on the kinetics of a single enzyme molecule. Instead, the enzyme is used as a reporter for another bioanalyte as described in lab 1 (heterogeneous immunoassay). Due to an enzymatic amplification step, analytes may be detected with high sensitivity. In a conventional ELISA the reaction volume in the chambers is typically about 100 μL . This detection volume is much too high for detecting single molecules of an analyte in presence of the correspondingly high background resulting from autofluorescence, Raman scattering, unspecific binding of the reporter molecule etc. However, if the volume is decreased by a factor of 10^{10} like in the femtoliter chambers, a single molecule ELISA may be established. For a sandwich ELISA, the surface of the chambers would be coated with a capture antibody that specifically binds to a bioanalyte like e.g. a serum protein. Next, a second antibody that is conjugated to an enzyme and also binds to the analyte is added. As one enzyme molecule will be bound per analyte the signal created by the enzyme molecule can be used for the detection of a single molecule.

In a single molecule ELISA, the analyte concentration is determined simply by counting the “active” chambers (chambers that light up due to substrate turnover). In contrast to a conventional (analogue) ELISA, the signal will never fall below the detection limit. Instead, the number of active chambers decreases when the analyte is diluted. Thus, this approach is also called “digital” ELISA.

1.1 Isolation of single enzyme molecules

In this lab we use femtoliter arrays moulded in PDMS (polydimethylsiloxan) that consist of 62500 uniform cylindric wells (diameter 4 μm ; depth 3.8 μm), see fig. 3.1. Each reaction chamber defines a volume of approx. 50 fL.

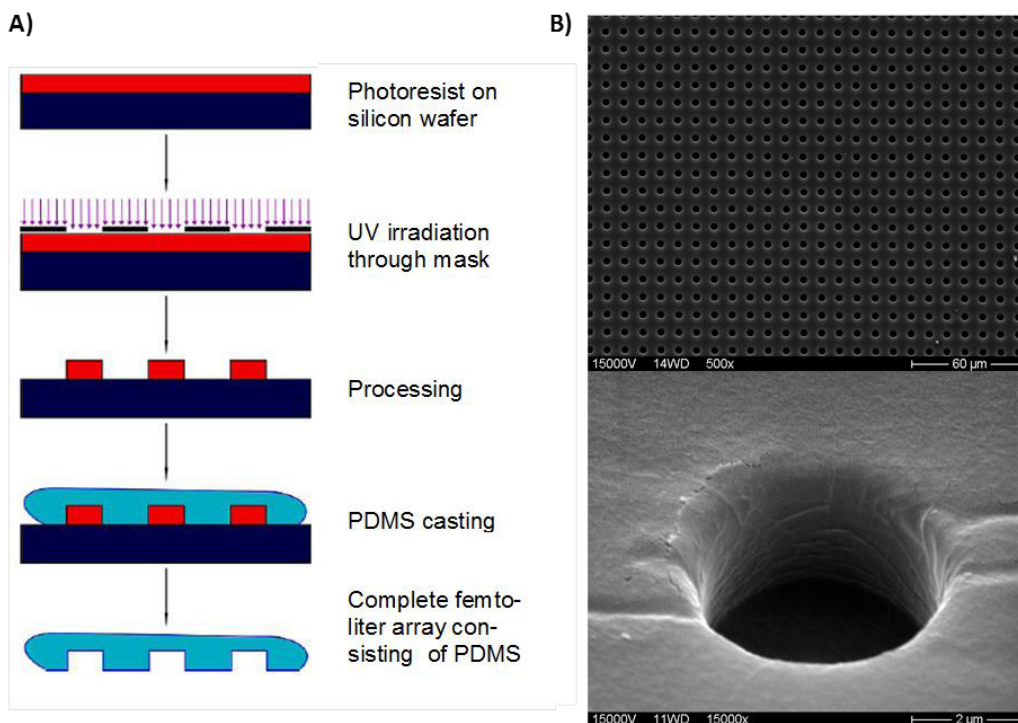


Fig. 3.1: A) Preparation of a wafer of femtoliter arrays moulded in PDMS by soft lithography (Institute for Microsystems technology, Hochschule Regensburg; compare lab 4.2.2 „Elastomeric stamps and casting molds“). A silicon wafer is coated by a layer 3 μm -strong layer of the photoresist SU-8 and irradiated with UV light through a mask. The photoresist is cured by irradiation. Non-hardened photoresist is removed in a washing step. Afterwards, liquid PDMS is cast into the silicon mould and polymerized at 90 $^{\circ}\text{C}$. The dry PDMS foil with the incorporated femtoliter array is pulled off the wafer. Arrays are cut out on demand.

B) Scanning electron microscopic (SEM) picture of a femtoliter array of PDMS and a single reaction chamber.

As it is not possible to deposit one single enzyme molecule into each chamber of the femtoliter array a highly diluted enzyme solution is spread on the femtoliter array that distributes randomly in the chambers. An enzyme concentration c of 36 pM distributed in a volume V of 50 fL yields on average one enzyme molecule per chamber (ratio: μ): $\mu = c \times V \times N_A$. The actual number v of enzyme molecules per reaction chamber can be calculated by the Poisson distribution (eq. 1) that, in general, describes the probability of a small number of events in a large number of trials. In our case, the probability $P_{\mu}(v)$ that exactly v enzyme molecules are present in a distinct femtoliter chamber is given by

$$P_{\mu}(v) = e^{-\mu} \frac{\mu^v}{v!} \quad (1)$$

For an average occupancy of one enzyme molecule per chamber, some chambers will remain empty, but there are also some that contain two or more enzyme molecules. However, chambers containing more than one enzyme have to be avoided to allow a conclusion on the single enzyme kinetics. Thus, the enzyme solution is further diluted to 1.8 pM ($\mu = 0.05$) such that most of the chambers stay empty ($P_{0.05}(0) = 0.951$) and only approximately 5 % of the chambers contain a single enzyme molecule only ($P_{0.05}(1) = 0.048$). The probability that a chamber hosts more than one enzyme molecule is marginally low ($P_{0.05}(\geq 2) = 0.0012$). This assures that with high probability the substrate turnover in the active chambers will be caused by a single enzyme molecule. If only 5 % of 62500 femtoliter chambers in an array are occupied there are still hundreds of single enzyme reactions that can be observed in parallel.

1.2 Enzyme kinetics of β -galactosidase

In the lab we will isolate single enzyme molecules of β -galactosidase from *E. coli* in the femtoliter chambers. With a molar mass of 464 kDa it is a very large protein that is always present as a homotetramer with four catalytically active sites. This model enzyme hydrolyses glycosidic bonds of β -galactopyranosides like, for example, the fluorogenic substrate resorufin- β -D-galactopyranoside. This substrate is non-fluorescent; however, after hydrolysis of the glycosidic bond resorufin is liberated yielding a strong increase of fluorescence (fig. 3.2).

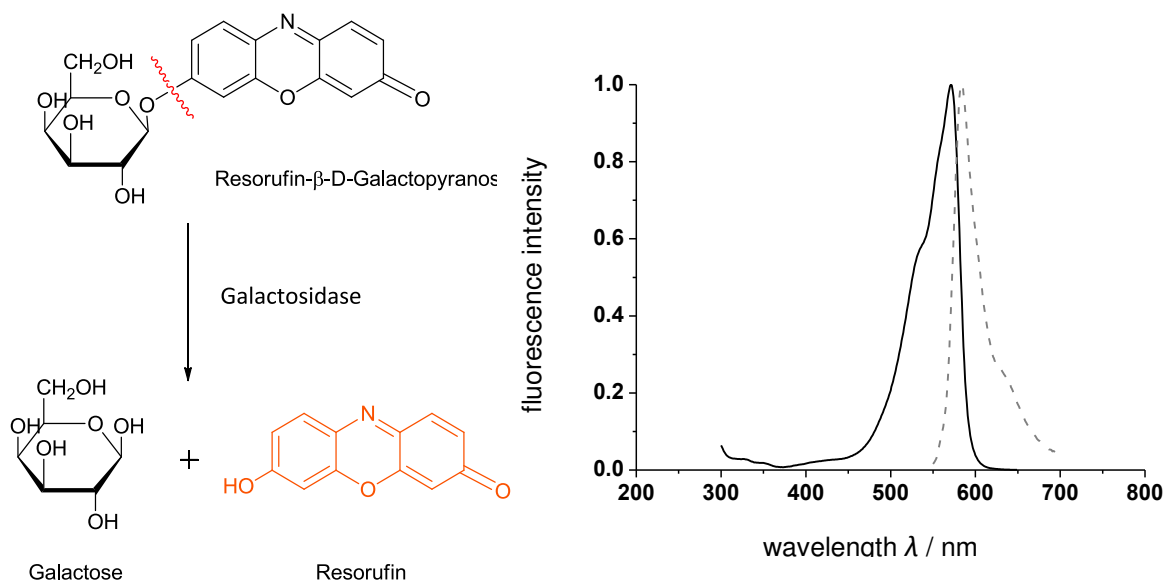


Fig. 3.2: A) Hydrolytic cleavage of the fluorogenic substrate resorufin- β -D-galactopyranoside by β -galactosidase yields the strongly fluorescent resorufin

B) Excitation- and emission spectrum of resorufin. Resorufin is excited at $\lambda_{exc} = 572$ nm and emits at $\lambda_{em} = 583$ nm.

The enzyme β -galactosidase is well suited for single molecule analysis as it is both stable and shows a high turnover rate of up to 1000 substrate molecules per second. The fluorogenic substrate is present in the chambers in large excess (100 μ M; or approx. 5 million molecules) compared to the single β -galactosidase molecules. Consequently, single β -galactosidase molecules produce enough fluorescent product within a short time that can be detected via fluorescence microscopy. The increase in fluorescence in those chambers that contain an enzyme molecule will be recorded under the fluorescence microscope by a sensitive camera and analysed afterwards. The enzyme kinetics can be described generally by the model of Michaelis and Menten (2) as shown in the short excursion in the manual for lab 1 (*“Homogeneous immunoassay for the detection of biotin”*).



The substrate resorufin- β -D-galactopyranoside binds reversibly to the free enzyme (galactosidase) forming the enzyme-substrate-complex. Next, the substrate may either dissociate (k_{-1}) or will be transferred to product (k_2) liberating the free enzyme and the fluorescent resorufin. Under steady-state conditions, the concentration of the enzyme-substrate-complex remains constant due to continuous formation and decay while substrate and product concentration decrease or increase, respectively with time. The rate of product formation depends on both the rate constant k_2 and the concentration of the enzyme-substrate-complex: $d[\text{P}]/dt = [\text{ES}] \times k_2$

A single enzyme molecule is not in a steady-state in a traditional sense because the enzyme is either present as a complex with the substrate or free in solution. However, as an integrated fluorescence signal for many subsequent substrate turnover cycles for a single enzyme molecule is measured the same picture is obtained as by observing many enzyme molecules simultaneously in a classical ensemble reaction.

1.3 Fluorescence microscopy

Fluorescence microscopy is most frequently employed for single molecule studies due to its high sensitivity. If the background is reduced to a large extent (e.g. by total internal reflection microscopy (TIRF)) and a sensitive camera is employed even single fluorophore molecules can be observed. Fluorescence microscopy is very sensitive because photons emitted by a single fluorophore can be detected with a maximum efficiency of 10 % if a high resolution objective (high numerical aperture) is used. Each fluorophore undergoes up to 10^6 excitation cycles before it photobleaches, which is enough to observe it for a certain time.

In our case, such a high sensitivity will not be required as hundreds of fluorophores will be produced per second by the single enzyme molecule in occupied chambers. Thus, a conventional wide-field microscope is sufficient to observe the enzyme molecules. Approximately 5000 reaction chambers of the femtoliter array lie within the focus and can hence be observed simultaneously by the inverse fluorescence microscope. In an inverse microscope the microscope stage is the highest point. Thus the object - in this case the femtoliter array - is well accessible. The array is placed on the microscope stage and is illuminated from below (fig. 3.3). A mercury vapour lamp serves as the excitation source. Only

wavelengths suitable for the excitation of resorufin ($\lambda = 577 \pm 10$ nm) pass through an excitation filter. The monochromatic light is reflected onto the object by a dichroic mirror. Such dichroic mirrors or beam splitters have a so-called critical wavelength: light of shorter wavelength will be reflected while longer wavelengths pass the mirror. The mirror is chosen to have its critical wavelength between the maxima of excitation and emission. Thus, the excitation light is reflected and guided to the object, while the long-wave fluorescence light (here: $\lambda \geq 585$ nm) passes the mirror and reaches the eye through the emission- or barrier filter and the ocular.

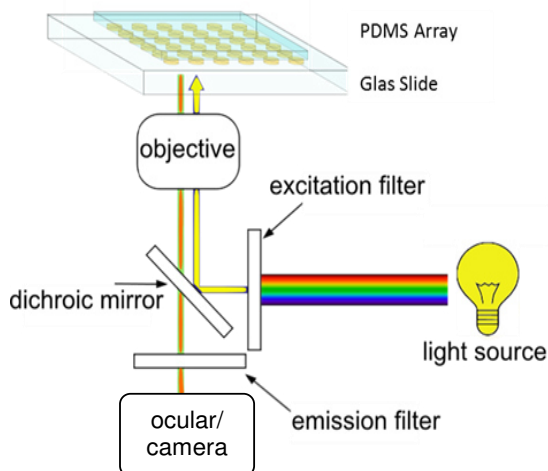


Fig. 3.3: Light path in an inverse epifluorescence microscope.

An almost complete separation of excitation and emission is mandatory for obtaining a good image. Excitation filter, beamsplitter and barrier filter are combined in a filter cube which can be exchanged easily to investigate different fluorophores. The fluorescence intensity of the femtoliter chambers is recorded by a digital camera and analysed by the software on a PC.

2. Scope of the lab

The activity of the enzyme β -galactosidase and its activity distribution within the enzyme population is to be determined by single enzyme analysis. A dilution of the enzyme with $c = 1.8$ pM (equals a ratio of enzyme molecules to reaction chambers of 1:20) in combination with the substrate resorufin- β -D-galactopyranoside is enclosed into a femtoliter array moulded in PDMS and the production of the fluorescent product resorufin is observed over time. The fluorescence intensity of the single chambers is monitored with a fluorescence microscope and documented on a PC.

Next a digital concentration determination in the femtoliter array is to be performed using two different enzyme concentrations. An enzyme concentration of 1.8 pM and 0.36 pM will be applied and the number of chambers containing an enzyme molecule will be estimated. The observed enzyme concentration is calculated using the Poisson distribution and compared with the actual concentration.

3. Experimental

3.1 Preparation

Solutions:

- PBS buffer: 4 g NaCl, 1.9 g Na₂HPO₄ × 7 H₂O, 0.1 g KCl, 0.1 g KH₂PO₄; 500 mL containing 10 mM MgCl₂, 0.05 mg/mL BSA and 0.005% Tween 20
- Resorufin stock solution: 10 mM in DMSO
- Substrate stock solution: 5 mM resorufin-β-*D*-galactopyranoside in DMSO
- Enzyme stock solution: 2 μM β-*D*-galactosidase in DMSO

Before starting the experiment, an array of approximately 4 × 4 mm in size is cut out of the PDMS foil with a scalpel. The glass slides for sealing (1.5 × 1.5 cm) have already been cleaned with piranha solution prior to the lab and are ready for use.

The dry PDMS array is put on the glass slide in the microscope mount. An initial focussing on the array surface is done through the ocular and the screen by aid of the assistant. The z-direction of the microscope table is noted.

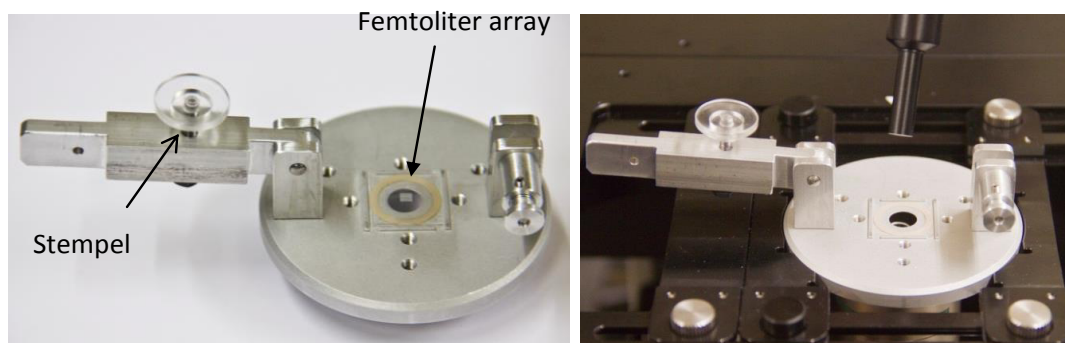


Fig. 3.4: Microscope mount to fasten the femtoliter array on the fluorescence microscope

3.2 Microscope setting

The images acquisition is set to:

Exposure time:	200 ms
Gain:	4
Optical filter:	ND 8
Recording interval:	every 30 sec

3.3 Calibration of fluorescence intensity

The following dilutions are prepared from the 10 mM resorufin stock solution:

0 μM 2.5 μM 5 μM 7.5 μM

Take a new PDMS array and pipette 8-10 μL of resorufin solution onto the array. Carefully remove excess fluid with the pipette and seal the array using a clean glass slide as instructed by the assistant.

Adjust the slide onto the microscope mount and close it. Apply a pressure of about 3.5 cNm by use of the torque screw driver. Focus once more. Finally, turn off the light and start the measurement in the dark.

Measure the other resorufin concentrations accordingly. Clean the glass slides for 15 min in the ultrasonic bath between measurements and the PDMS replace the array by a new one.

The procedure described above has to be carried out uninterruptedly and precisely. For measuring the galactosidase activity it will be essential that all preparation steps are completed within two minutes and the fluorescence measurement is started within this time period. Only in this case the substrate turnover and the increase in product concentration can be monitored from the beginning.

The experimental steps are trained during the calibration, so that the single steps during the enzyme measurement can be done smoothly and within the given two minute period.

3.4 Single enzyme measurements

First, the stock solutions of the enzyme and the substrate are diluted to the desired concentrations.

Take care: The substrate has to be protected from light to prevent photobleaching!

Substrate stock solution:	5 mM
Working concentration:	100 μM

β -Galactosidase:	
Stock solution:	2 μM
Working concentration:	1.8 pM or 0.36 pM

The enzyme reaction in the array shall be performed using a substrate concentration of 100 μM and an enzyme concentration of 1.8 pM (measurement 1) or 0.36 pM (measurement 2), respectively. The final dilution is obtained when enzyme and substrate are mixed:

5 μL enzyme solution + 20 μL substrate solution.

The reaction starts as soon as substrate and enzyme are joined. From this moment on the reaction should be monitored within 2 min under the microscope. This requires all necessary materials (PDMS array, cleaned glass slide, torque spanner adjusted correctly) to be prepared and ready for use. Immediately before the experiment combine 20 μL of the respective enzyme solution and 80 μL of the 125 μM substrate solution in a separate Eppendorf cup. Apply the solution to the array and close it. Mount the glass slide, focus and start the measurement. Four image sections are monitored in parallel for 15 min.

4. Data analysis

4.1 Selection of chambers by definition of ROIs (“region of interest“)

The definition of ROIs is done during the lab, as a special software is required that is installed on the PC in the lab. The tools for data analysis can be found behind the icon „Measurement“ – „Simple ROI editor“.

Use the selection tools to define five chamber- and two background ROIs for each measurement of the resorufin standards. For the activity measurements with an enzyme concentration of 1.8 pM choose 25 ROIs of chambers that show an increase in fluorescence and five background ROIs, i.e. chambers with no increase in fluorescence. The fluorescence intensities will be determined automatically by the software and written in a file after pressing the icon „perform measurement“. The data will be exported to Excel and converted by the program *Converter.jar*.

Create a jpg-file of a suitable picture of both measurements with enzyme concentrations of 1.8 and 0.36 pM as instructed by the assistant.

4.2 Drawing a resorufin calibration curve

Calculate the mean and the standard deviation of five data points of each resorufin standard concentration and plot the fluorescence intensity against the concentration. Draw a calibration curve by linear regression and determine its slope (m_{kal}).

4.3 Determination of the activity of single β -galactosidase molecules

Correct the fluorescence intensities by background subtraction of the mean of 5 background chambers from the time course of the 25 selected single enzymes. Plot the corrected fluorescence intensities versus time and calculate the initial slopes by linear regression. Next, determine the turnover rates (number of substrate molecules N cleaved per time) of the single enzyme molecules in a reaction volume of $V = 48$ fL ($V = 3.8 \mu\text{m} \times (2 \mu\text{m})^2 \times \pi$) using the slope of the calibration curve (m_{kal}) and the respective slope of the fluorescence intensities (m_{exp}).

$$\text{Turnover rate} = \frac{\Delta c (\text{resorufin})}{\Delta t} \cdot V \cdot N_{\text{A}} = \frac{m_{\text{exp}}}{m_{\text{kal}}} \cdot V \cdot N_{\text{A}}$$

4.4 Determination of the activity distribution in a β -galactosidase population

Visualize the distribution of enzyme activities within the population by a histogram. Next, determine the Gaussian distribution by nonlinear regression of the histogram (see excursion: Establishing a histogram using QtiPlot). Extract the standard deviation (σ) and the mean turnover rate (χ_c) as regression parameters of the Gaussian distribution and calculate the variation coefficient (c_v) of the activity distribution:

$$c_V = \frac{\sigma}{\chi_c}$$

Which information regarding the static heterogeneity of the β -galactosidase population can be obtained from the coefficient of variation?

4.5 Digital concentration readout of the enzyme concentration

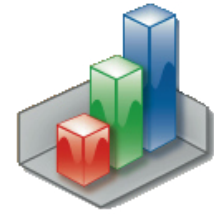
Count the occupied (= fluorescent) chambers of the femtoliter array that were filled with a solution of 1.8 pM or 0.36 pM β -galactosidase. Determine the enzyme concentration from the ratio of occupied chambers to the total number of reaction chambers (3500 in the visible area of the array). Note that the number of occupied chambers depends linearly on the enzyme concentration for high dilutions (number of enzyme molecules \ll number of chambers) according to the Poisson distribution (2).

number of occupied wells	0.10	0.05	0.02	0.01	...
enzyme concentration (pM)	3.6	1.8	0.72	0.36	...

What is the difference between the concentrations determined by counting compared to the initially applied concentration? What might be the reasons for this difference?

Supplement: Creating a histogram using QtiPlot

QtiPlot is a professional tool for scientific data analysis and visualization comparable to Origin, SigmaPlot



Installation:

QtiPlot is free for members of the University of Regensburg and may be downloaded from the Rechenzentrum, either via the F-drive:

F:\Q\QtiPlot or the RZ-Homepage:

<http://www.uni-regensburg.de/Einrichtungen/RZ/Benutzer/Allgemein/PCSI/index.phtml> .

(status 01.03.2012)

1. Installation of Python 2.6.2 (Calculation script for QtiPlot for data ananalysis);
2. Installation of QtiPlot 0.9.8

Tutorials and documentation for QtiPlot may be found following the links on the RZ-homepage.

Rechenzentrum der Universität Regensburg

Home RZ → Benutzer → Allgemeine Dienstleistungen → Softwareindex → Alphabetischer Index

Benutzer Webmaster | Besucher & Gäste | Workgroupmanager | Systembetreuer

PC Softwareindex - Alphabetischer Index

7 A B C D E F G H I J K L M N O P Q R S T U V W X

QtiPlot CIP

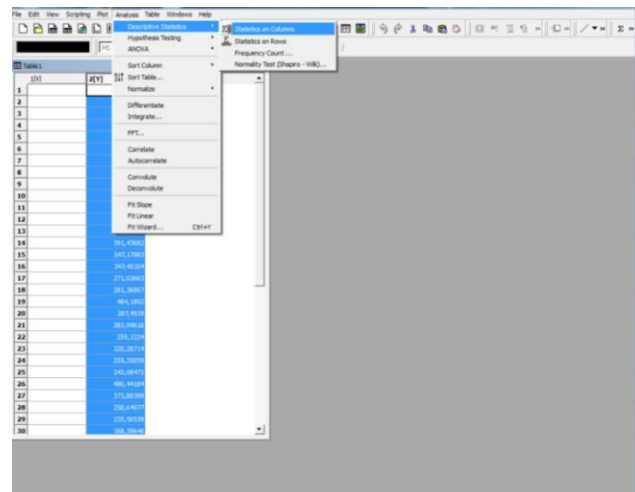
Funktion: Datenvisualisierung
Kategorie: Datenvisualisierung
Beschreibung: Programm zur Visualisierung speziell naturwissenschaftlicher Daten
Hinweise: Python in der Version 2.6.2 wird für Windows benötigt. Für Mac OS wird entweder Python 2.5 (Mac OS X 10.4 or later) oder Python 2.6 (Mac OS X 10.6 or later) benötigt.
Aktualisierungen: 0.9.8.10
Plattform: Win32, WinVista32, Win7
Verzeichnis: F:\Q\QtiPlot
Lizenz: GNU
Letzte Änderung: 07.02.2012

Dokumentation: [QtiPlot User Guide](#)
[Online Dokumentation](#)
Verweise: [QtiPlot Home Page](#)

Download: Windows
 QtiPlot 0.9.8.10 Setup, 16.1 MB
 Python 2.6.2 Setup, 13.8 MB

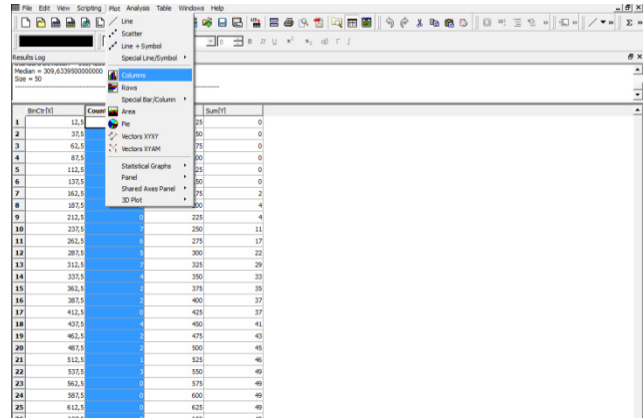
Creating a histogram of the activity distribution of galactosidase:

- Open a table and copy the calculated turnover rates into column (Y)
- Highlight the column and click on. *Analysis > Descriptive Statistics > Frequency Count*
- Perform a Frequency Count starting with Minimum 0 to Maximum 800; Step Size 25

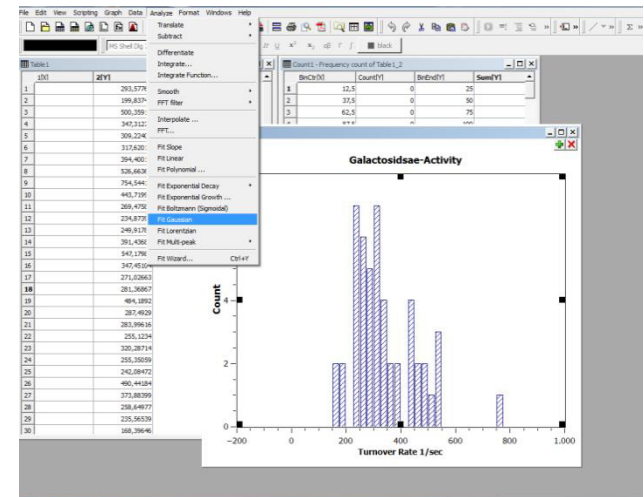


Appendix

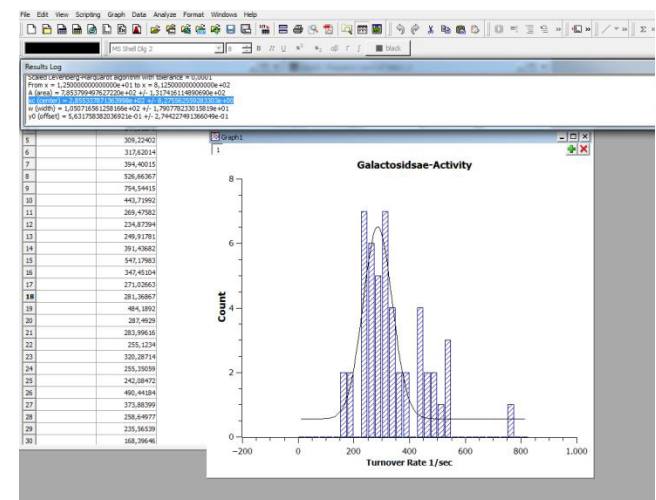
- A new table will be opened with four columns; highlight the column *Count (Y)*;
- Chose > *Plot > Columns*;
- The histogram will appear in a „raw“ format



- Finish the diagram: Captions; axes; 20 % spacing between the bars, etc. to optimise the layout of the histogram;
- Click on the histogram;
- Choose > *Analyse > Fit Gaussian*



- A Gaussian fit of the histogram will appear
- Simultaneously an analysis window „Results-Log“ pops up; here you will find the mean activity χ_c of the enzyme determined by the Gaussian fit, as well as the width (w) of the distribution;
- The standard deviation σ of the activity distribution is defined as $w/2$;



7.6 Abbreviations

Ala	alanine
Apo	apochromatic
APTES	(3-Aminopropyl) triethoxy-silane
ATP	adenosine triphosphate
ATR	attenuated total reflection
Asn	asparagine
Asp	aspartic acid
bp	bandpass
B	blind
BSA	bovine serum albumin
CCD	charge-coupled device
CCMV	cowpea chlorotic mottle virus
CD	circular dichroism
CE	capillary electrophoresis
CMOS	complementary metal-oxide semiconductor
CV	coefficient of variation
cm	centimeter (10^{-2} meter)
cNm	centinewtonmeter
COP	cyclic olefin polymer
CuAAC	Cu(I)-catalyzed azide-alkyne cycloaddition
DCC	dicyclohexylcarbodiimide
DCM	dichloromethane
DI	deionized
DMAP	dimethylaminopyridine
DMF	dimethylformamide
DMSO	dimethyl sulfoxide
DNA	desoxyribonucleic acid
<i>E. coli</i>	<i>Escherichia coli</i>
EDTA	ethylenediaminetetraacetic acid
ELISA	enzyme-linked immunosorbent assay
eq	equation

Appendix

eq.	equivalent
ESI	electrospray ionization
Et ₃ N	triethylamine
FAM	fluorescein amidite
FDG	fluorescein-di-β-D-galactopyranoside
FITC	fluorescein isothiocyanate
fL	femtoliter (10 ⁻¹⁵ liter)
FRET	fluorescence resonance energy transfer
Gal	β-Galactosidase
Gln	glutamine
Glu	glutamic acid
GUS	β-glucuronidase
His	histidine
HMDS	hexamethyldisilazane
hPa	hectopascal
HRP	horseradish peroxidase
IC	internal conversion
IPTG	isopropyl-β-D-thiogalactopyranosid
IR	infrared
ISC	intersystem crossing
ISFET	ion-sensitive field-effect transistor
kDa	kilodalton
kV	kilovolt
<i>lac</i>	lactose
LB	Luria-Bertani
LDH-1	lactate dehydrogenase
LED	light-emitting diode
LIF	laser-induced fluorescence
lp	longpass
Lys	lysine
min	minute(s)
mJ	millijoule (10 ⁻³ joule)
mm	millimeter (10 ⁻³ meter)
ms	millisecond (10 ⁻³ seconds)

MS	mass spectrometry
MM	Michaelis-Menten
μg	microgram (10^{-6} gram)
μm	micrometer (10^{-6} meter)
μM	micromolar (10^{-6} mol/liter)
MTP	microtiter plate
MW	molecular weight
NA	numeric aperture
NAD	nicotinamide adenine dinucleotide
NC	negative control
ND	neutral density
NHS	<i>N</i> -hydroxysuccinimide
nL	nanoliter (10^{-9} liter)
nm	nanometer (10^{-9} meter)
NMR	nuclear magnetic resonance
NpBHC	<i>N-p</i> -bromobenzylamino-hydroxymethyl-cyclopentanetriol
MCS	multiple cloning site
MS	mass spectrometry
Mut	mutante
OD	optic density
PAGE	polyacrylamide gel electrophoresis
PBS	phosphate buffered saline
PC	positive control
PDMS	poly(dimethylsiloxane)
PGMEA	propylene glycol monomethyl ether acetate
PEG	polyethylene glycol
pL	picoliter (10^{-12} liter)
pM	picomolar (10^{-12} mol/liter)
<i>p</i> NP	<i>para</i> -nitrophenyl
ppm	parts per million
Pro	proline
PVP	polyvinylpyrrolidone
ReG	resorufin-β-D-glucuronide

Appendix

RGP	resorufin- β -D-galactopyranoside
RIA	radioimmunoassay
RNA	ribonucleic acid
ROI	region of interest
rpm	revolutions per minute
r.t.	room temperature
sccm	standard cubic centimeter per minute
sCMOS	scientific complementary metal-oxide semiconductor
SD	standard deviation
SDS	sodium dodecyl sulfate
SEC	size exclusion chromatography
SEM	scanning electron microscopy
Ser	serine
Strep	streptavidine
TAE	tris-acetate-EDTA
TBAAz	tetrabutylammoniumazide
THF	tetrahydrofuran
THPTA	tris(3-hydroxypropyltriazolylmethyl)amine
Thr	threonine
TIRF	total internal reflection fluorescence
TOF	time of flight
TRIS	tris(hydroxymethyl)aminomethane
TS	test slide
u.a.	units arbitrary
UV	ultraviolet
VIS	visible
VR	vibrational relaxation
W	watt
WT	wild-type
zL	zeptoliter (10^{-21} liter)
% (v/v)	volume per volume
% (w/v)	weight per volume

8. Curriculum Vitae

Raphaela Barbara Liebherr

Born on September 14, 1986 in Sonthofen (Allgäu), Germany

Education

- 10/2011 – 04/2015 **PhD Thesis** at the Institute of Analytical Chemistry, Chemo- and Biosensors: Prof. Joachim Wegener (University of Regensburg)
“Single-Enzyme Analysis in Femtoliter-Arrays”
- 10/2009 - 09/2011 **Master of Science** Chemistry (1.2)
(University of Regensburg and Turku University, Finland)
Master Thesis: *“Thiol-Chemistry on Upconverting Nanoparticles”* (1.0)
Institute of Analytical Chemistry, Chemo- and Biosensors: Prof. Otto S. Wolfbeis (Regensburg)
Institute of Biotechnology: Prof. Tero Soukka (Turku)
- 10/2006 – 09/2011 **Bachelor of Science** Chemistry (1.3)
(University of Regensburg and University of Aberdeen, Scotland)
Bachelor Thesis: *“Synthesis and NMR-spectroscopic characterization of HMNP-complexes”* (1.0)
Institute of Organic Chemistry: Prof. Ruth Gschwind
- 09/1993 – 06/2006 **University Entrance Diploma** (Gymnasium Sonthofen) (1.0)

International Experience

- 09/2008 – 03/2009 Academic Studies and Research Training at the University of Aberdeen, Scotland, in the context of the ERASMUS-program 2008/09
- 06/2011 – 07/2011 Visiting Scientist at the Institute of Biotechnology, Turku University, Finland

Advanced Education/ Certificates

11/2013	Introduction in Business studies for Chemists GDCh-Education
10/2012	Strategic and successful communication in management VCI-Education
Language Skills	German (native), English (fluent), French (good, („ <i>Diplôme d'études en langue française</i> “ (DELF); <i>1er degré</i>)), Spanish (basics)

Awards/ Honors

03/2012 – 02/2014	Doctoral Scholarship of the Fund of the Chemical Industries
11/2013	Boehringer Ingelheim Fund “Stiftung für medizinische Grundlagenforschung” Travel Grant
06/2010	Final Degree Award of the University Regensburg awarded by the “Dr. Alfons-Paulus-Stiftung”
06/2009 – 09/2011	Scholarship of the “Studienstiftung des Deutschen Volkes”
06/2006	“ <i>Appolinaire-Award</i> ” of the Robert-Bosch-Stiftung for extraordinary achievements in the subject French
06/2006	“ <i>Dr. Werner Röhrs Award</i> ” for outstanding achievements in the final secondary school examinations (Abitur)

Interests

Music (Violin), Travelling, Alpine Sports

9. List of Publications and Presentations

9.1 Master Thesis

Liebherr R.B., *Thiol-Chemistry on Upconverting-Luminescent-Nanoparticles (UCLNPs)*, (2011), Institute for Analytical Chemistry, Chemo- and Biosensors, University of Regensburg.

9.2 Papers

(* authors contributed equally)

*Liebherr R.B., *A. Hutterer, M.J. Mickert, F.C. Vogl, A. Beutner, A. Lechner, H. Hummel and H.H. Gorris, *Three-in-one enzyme based assay on single molecule detection in femtoliter arrays*, **2015**, submitted.

Liebherr R.B. and H.H. Gorris, *Enzyme Molecules in Solitary Confinement*, *Molecules*, **2014**, (19): 14417, doi: 10.3390/molecules190914417.

Liebherr R.B., M. Renner and H.H. Gorris, *A Single Molecule Perspective on the Functional Diversity of in Vitro Evolved beta-Glucuronidase*, *J. Am. Chem. Soc.*, **2014** (136): 5949, doi: 10.1021/ja412379p.

Ehrl B.N., R.B. Liebherr and H.H. Gorris, *Single molecule kinetics of horseradish peroxidase exposed in large arrays of femtoliter-sized fused silica chambers*, *Analyst*, **2013** (138): 4260, doi:10.1039/c3an00809f.

Liebherr R.B., B.N. Ehrl, A. Hutterer, H. Hummel and H.H. Gorris, *Enzyme – Individualität statt Konformität*, *Analytik News*, **2013** (31): published online: www.analytik-news.de/Fachartikel/2013/31.html.

Gorris H.H. and R.B. Liebherr, *Fokus auf das einzelne Individuum im Ensemble*, *Blick in die Wissenschaft*, **2013** (27): 24, www.universitaetsverlag-regensburg.de/artikel_7978.ahtml.

Liebherr R.B., T. Soukka, O.S. Wolfbeis and H.H. Gorris, *Maleimide-activation of photon-upconverting nanoparticles for bioconjugation*, *Nanotechnology*, **2012** (23): 485103, doi:10.1088/0957-4484/23/48/485103.

9.3 Abstracts for Selected Posters and Talks

A Single Molecule Perspective on Enzyme Evolution, Liebherr R.B., M. Renner, M. Mickert and H.H. Gorris, 20th Single Molecule Workshop Picoquant, Berlin, Germany, 2014. (Poster)

Analyzing Enzymes on a Single Molecule Scale, Liebherr R.B. and H.H. Gorris, 13th Conference on Methods and Applications of Fluorescence (MAF), Genoa, Italy, 2013. (Poster)

Discovery of Enzyme Features by Single Molecule Analysis in Femtoliter Arrays, Liebherr R.B. and H.H. Gorris, GDCh-Wissenschaftsforum CHEMIE, Darmstadt, Germany, 2013. (Poster)

Nachweis und Charakterisierung von Biomolekülen auf der Einzelmolekül-Ebene, Liebherr R.B. and H.H. Gorris, 8. Deutsches Biosensor Symposium, Wildau, Germany, 2013. (Talk)

Analyzing single enzyme molecules and single lipid vesicles in femtoliter arrays, Liebherr R.B., F.C. Vogl, B.N. Ehrl, M. Thaller and H.H. Gorris, 18th Single Molecule Workshop Picoquant, Berlin, Germany, 2012. (Talk)

Analysis of Individual Enzyme Molecules in Femtoliter Arrays, Liebherr R.B., F.C. Vogl and H.H. Gorris, 8th ISC Modern Analytical Chemistry, Prague, Czech Republic, 2012. (Talk)

Photon-upconverting nanoparticles for ratiometric encoding and bioconjugation, Gorris H.H., R.B. Liebherr, S.M. Saleh, R. Ali and O.S. Wolfbeis, 12th Conference on Methods and Applications of Fluorescence (MAF), Strasbourg, France, 2011. (Poster)

DANKSAGUNG

Mein erster Dank geht an PD Hans-Heiner Gorris für die Bereitstellung des interessanten Themas, die intensive Betreuung, die gründliche Korrektur der vorliegenden Arbeit, sowie die ausführlichen wissenschaftlichen Diskussionen.

Des Weiteren gilt mein Dank allen Professoren des Instituts für Analytische Chemie für Ihre Unterstützung in wissenschaftlichen und anderen Belangen. Insbesondere bedanken möchte ich mich bei Prof. Joachim Wegener für seine Betreuung und die Übernahme des Amtes des Erstgutachters. Prof. Antje Bäumner und Prof. Otto Wolfbeis danke ich für die guten Arbeitsbedingungen am Institut und ihr stetes Interesse an meiner Arbeit. Vielen Dank ebenfalls an meinen dritten Prüfungsbeauftragten Prof. Burkhard König und an Prof. Frank-Michael Matysik für die Ausübung des Prüfungsvorsitzes.

Den Mitarbeitern des Lehrstuhls von Prof. Helmut Hummel beziehungsweise Prof. Alfred Lechner der Technischen Hochschule Regensburg danke ich für Ihre umfassende Mithilfe bei der Durchführung meiner Doktorarbeit. Insbesondere gilt mein Dank Florian Götz für die Entwicklung der Femtoliter Arrays und Albert Hutterer für die Anfertigung und detaillierte Charakterisierung verschiedenster Arraysysteme, für die Vermessung von Kontaktwinkeln, Aufnahme von REM-Messungen und insbesondere seine Offenheit für alle neuen, zum Teil aufwändigen und zeitintensiven Ideen.

Danke auch an Dr. Jochen Lampel und Prof. Günther Bernhard für Ihre Unterstützung in Fachfragen zu Gerätedetails des Fluoreszenzmikroskops und zur Mikroskopie im Allgemeinen. Prof. Douglas Craig danke ich für sein Interesse an meiner Arbeit und den wissenschaftlichen Austausch zu alternativen Einzelmolekültechniken.

Mein Dank geht an den Lehrstuhl für Biophysik und physikalische Biochemie von Prof. Reinhard Sterner für die Unterstützung bei der Untersuchung von Evolutionsmechanismen. Insbesondere vielen Dank an Monika Meier und Max Renner für die Exprimierung, Reinigung und Charakterisierung des Glucuronidase Wildtyps und der Mutante und an Klaus-Jürgen Tiefenbach für die Aufnahme der CD-Spektren.

Vielen Dank an die Feinmechaniker der Universität Regensburg für die gewissenhafte und geduldige Umsetzung immer neuer Ideen und Anregungen zur Verbesserung der Array-Fixierung. Vielen Dank auch an die Mitarbeiter der Zentralen Analytik für die Durchführung mehrerer Messungen.

Bei Andrea Beutner und Lucia Birner bedanke ich mich für die im Rahmen ihrer Bachelorarbeiten durchgeführten Messungen. Des Weiteren danke ich allen jetzigen und ehemaligen Mitarbeitern unserer Arbeitsgruppe für die gute Zusammenarbeit und das sehr angenehme Gruppenklima. Insbesondere bedanken möchte ich mich bei Franziska Vogl, Benno Ehrl und Matthias Mickert für ihren Beitrag zu meiner Arbeit. Vielen Dank an Andreas Sedlmeier für seine Unterstützung bei der Anfertigung von Schemazeichnungen, für seine Freundschaft und sein offenes Ohr bei allen großen und kleinen Problemen in der Chemie und des Alltags. Ganz besonders möchte ich mich außerdem bei all meinen lieben, hilfsbereiten Laborgefährten bedanken.

Dr. Daniela Achatz danke ich dafür, dass sie mich als Analytik-Neuling unter Ihre Fittiche genommen hat, mir vieles gelernt und gezeigt hat und mir eine super erste Laborgefährtin war. Dr. Robert Meier danke ich für viele wichtige Tipps, Ratschläge und praktische Hilfestellungen sowie amüsante Gespräche. Dr. Heike Mader danke ich für das Korrekturlesen dieser Arbeit, dafür, dass sie mich bei der Herberg-Suche in ihr Büro aufgenommen hat und mir eine wertvolle Büronachbarin und Freundin war.

Den Sekretärinnen sowie allen technischen Angestellten, insbesondere Barbara Goricnik, Gisela Hierlmeier, Gisela Emmert, Nadja Hinterreiter, Angelika Stoiber und Joachim Rewitzer danke ich für ihre Hilfsbereitschaft in allen chemischen Dingen und vielen anderen Fragen des Alltags. Nicole Guber danke ich für die unzähligen Kopien, Faxe oder Briefe, die über ihren Schreibtisch liefen, für ihre Unterstützung in vielen, vielen alltäglichen Dingen, für ihre Anteilnahme und ihre Freundschaft.

Ich danke allen Mitgliedern des Instituts für Analytische Chemie, Chemo- und Biosensorik für das gut Arbeitsklima, die unterhaltsamen Mittags- und Kaffeepausen und unzähligen Geburtstagskuchen oder sonstige Leckereien.

Meiner Tante Edeltraud Bach und meinem Onkel Dr. Bernhard Bach danke ich für ihr Interesse an meiner Arbeit, ihre Anteilnahme an meinem Leben und ihre jahrelange treue Unterstützung.

Meinen Geschwistern Tamara, Manuel und Norbert und meinen Eltern Brigitte und Heinrich Liebherr möchte ich dafür danken, dass ich mich mit Problemen immer an sie wenden kann und stets mit offenen Armen empfangen werde.

Zuletzt und ganz besonders möchte ich mich bei Matthias Knorn bedanken für das Korrekturlesen dieser Arbeit, für wertvolle Hilfestellungen bei organisch-chemischen Fragestellungen und für so viele andere Dinge ...

Eidesstattliche Erklärung

Ich erkläre hiermit an Eides statt, dass ich die vorliegende Arbeit ohne unzulässige Hilfe Dritter und ohne Benutzung anderer als der angegebenen Hilfsmittel angefertigt habe; die aus anderen Quellen direkt oder indirekt übernommenen Daten und Konzepte sind unter Angabe des Literaturzitats gekennzeichnet.

Weitere Personen waren an der inhaltlich-materiellen Herstellung der vorliegenden Arbeit nicht beteiligt. Insbesondere habe ich hierfür nicht die entgeltliche Hilfe eines Promotionsberaters oder anderer Personen in Anspruch genommen. Niemand hat von mir weder unmittelbar noch mittelbar geldwerte Leistungen für Arbeiten erhalten, die im Zusammenhang mit dem Inhalt der vorgelegten Dissertation stehen.

Diese Arbeit wurde bisher weder im In- noch im Ausland in gleicher oder ähnlicher Form einer anderen Prüfungsbehörde vorgelegt.

Ort, Datum

Unterschrift